Durham E-Theses

Synthesis of fluorinated organic compounds for use as additives in Lithium-Ion Batteries

WALTON, JOSHUA,JAMES

How to cite:

Use policy

A Thesis Entitled

Synthesis of fluorinated organic compounds for use as additives in Lithium-Ion Batteries

By

Joshua James Walton

A candidate for the degree of Doctor of Philosophy

Department of Chemistry, Durham University

2019

"Think positive – you can and you will"

Sylvia Eddies

Abstract

Lithium-ion Batteries (LIBs) are an important facet of modern society. They are the subject of much research interest due to the increased demand for electric vehicles and their prevalent use in portable electronics, such as mobile phones and laptops. There are many ways in which battery performance can be improved, once such route is through the use of electrolyte additives. This project, in collaboration with Sony and Murata Manufacturing, focuses on electrolyte additives that affect the formation of the solid electrolyte interphase layer (SEI), a film that forms upon and protects electrodes.

To this end, a series of dicarbonyl derivatives, such as dialkyl 2-fluoromalonate, were prepared through direct fluorination or transesterification reactions and subjected to LIB analysis for viability as use as additives. None of these compounds improve battery performance, but a mechanism of additive decomposition was proposed based on the findings. This included radical based reduction of a carbonyl and the elimination of the ester alkyl group.
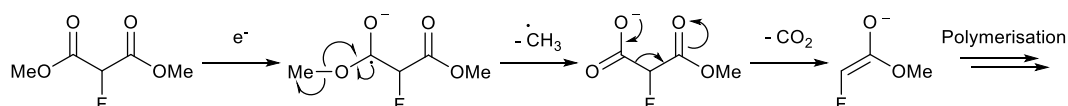

Based on this mechanism, new targets were identified; substituted dialkyl malonates that would stabilise the alkyl radical formation, and methyl fluoro cyano esters which would combine dialkyl 2-fluoromalonates and cyano containing compounds, such as succinonitrile, which have been shown to be beneficial to battery operation. These compounds were synthesised through alkylation reactions, such as substitution or Michael addition, and were monodecarboxylated using the Krapcho decarboxylation. Difluorinated targets were synthesised by a free radical addition reaction of ethyl 2-bromo-2,2-difluoroacetate and a Michael acceptor.

A ketone target was synthesised through addition of acrylonitrile to hydrolysis conditions of ethyl 2-fluoroacetoacetate. Longer alkyl backbone compounds were synthesised from methyl acetoacetate and the substitution reaction with the desired bromo-cyano-alkyl. Following this, fluorination was undertaken using Selectfluor™ and decarboxylation

using the Krapcho decarboxylation. Finally, an alkene based compound was synthesised through the Wittig reaction of the ketone product.

These compounds were subjected to LIB analysis in Murata Manufacturing, Atsugi, Japan, and were assessed based on capacity retention and cell swelling. No compound improved upon the reference cell, a cell with no additive other than 1% vinylene carbonate (VC), but the majority improved the swelling inhibition. An interesting trend was observed between additive structure and degree of swelling inhibition; the longer the alkyl backbone chain of methyl fluoro cyano esters, the increased swelling inhibition. The mechanism of decomposition was probed using a variety of different analytical techniques and three processes were postulated.

$$(1)$$

$$(2)$$

$$(3)$$
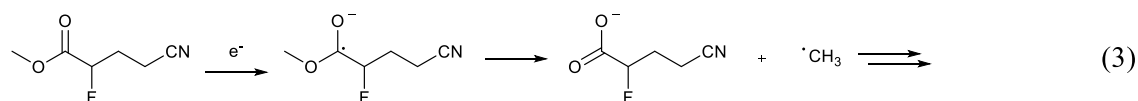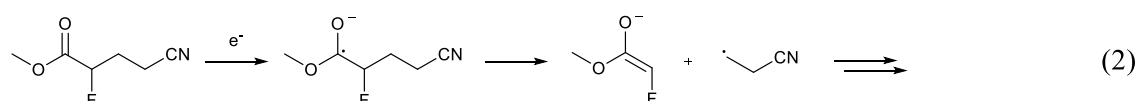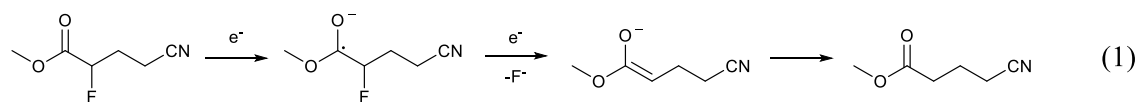
Process (1) is the process promoted in longer chained compounds, and is thought to be the process that is beneficial to cell swelling inhibition, through layering and prevention of CO_2 generation. Processes (2) and (3) are thought to be detrimental to cell operation. The overall most beneficial additive synthesised for battery operation was methyl 7-cyano-2-fluoroheptanoate (**118**).
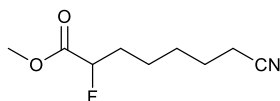
Acknowledgements

Firstly I have to thank Professor Graham Sandford who supervised, mentored and supported my work throughout this PhD. His kindness and availability throughout the project was immeasurably helpful. Keep chiselling homeslice.

The support I received from my industrial sponsors have been more than I could have asked for and I have to express great thanks to Takumi Hiasa particularly, who patiently answered my many, many questions about batteries. In addition to this, thanks have to go to Kazumasa Takeshi, Qiaoshu Hu and Hitoshi Katakura for making me feel so welcome on my placements at Murata Manufacturing.

Also, thanks must go to the guys at Sony MSL who helped me enormously at the start of this project. Thanks to Clemens Wall, Nadejda Krasteva and Gabriele Nelles.

The research in this project would not have been possible without the incredible work of the support staff of the analytical services within Durham. Thanks have to go to Alan, Catherine and Juan in NMR, Dave and Pete in mass spectrometry and Dima in crystallography.

I'd like to thank everyone that worked in the office throughout the entirety of this project. This includes Mark Fox, Etienne, Ben, Neshat, Tucker, Hector, Estelle, Kevin, Dan, Anne, Zahide, Ellis, Jonny, Kiera, Ned, Abi, Rob, Sophie and Lawrence. Special thanks have to go to Alex and Marcus, who have been through the lot with me. Additionally, I'd like to express gratitude specifically to Tony, Bear and Darren, who taught me a lot throughout my time in the lab.

I have to thank my Mam and Dad who helped shape me into the person I am today and for politely asking what it is I do, even though they don't really understand. I couldn't have done it without them. Thank you also Grandma Sylvia, you've helped a lot.

And finally, Laura.

Abbreviations

ASAP	Atmospheric solid analysis probe
b.p.	Boiling point
CE	Coulombic efficiency
COSY	Correlation spectroscopy
DAST	Diethylaminosulfur trifluoride
DMC	Dimethyl carbonate
DMSO	Dimethyl sulfoxide
DEC	Diethyl carbonate
EC	Ethylene carbonate
EI	Electron ionisation
EIS	Electrical Impedance Spectroscopy
Eq	Equivalent
EtOAc	Ethyl acetate
FEC	Fluoroethylene carbonate
GCMS	Gas chromatography mass spectrometry
h	Hour
IPA	*iso*-Propyl alcohol
IR	Infrared

LIB	Lithium-ion Battery
LiBOB	Lithium bis(oxalate) borate
NMR	Nuclear Magnetic Resonance
PC	Propylene carbonate
Ref	Reference cell
SEI	Solid electrolyte interphase layer
SN	Succinonitrile
THF	Tetrahydrofuran
TLC	Thin Layer Chromatography
Tosic acid	*para*-Toluenesulfonic acid
TREAT.HF	Triethylamine trihydrofluoride
UV	Ultraviolet
VC	Vinylene carbonate

Contents

Chapter 1

Lithium-ion batteries and organofluorine chemistry

1.1   Background

The invention of the battery can be dated back to the work of Volta in 1800, which, perhaps somewhat ironically from a modern viewpoint, predates the work of Faraday and, arguably, the first practical use of electricity by 20 years.[1] In modern society, batteries have been established as a fundamental part of life, from the lead-acid batteries used in cars to the Lithium-Ion batteries (LIBs) found in mobile phones, laptops and electric vehicles.

Specifically, LIBs have developed massively since their first commercial release in 1991, with varying material use and cell structure. The high energy density and cycleability of the battery has led to an increasing market size, projected to be $92 billion globally in 2024, due to use in mobile phones and increasing demand in the electric car sector.[2] Due to greater pressure to minimise greenhouse emissions, a significant drive in the automotive industry is towards electric vehicles which is reflected in various grants awarded by governments, such as €500 million in Germany for the development of LIBs.[3]
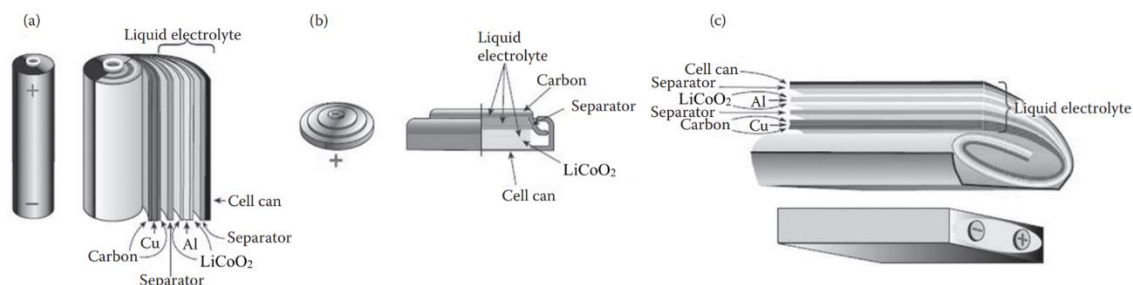
Figure 1 - Different examples of battery schematics; (a) a cylindrical cell, (b) a coin cell and (c) a pouch cell[4]

Due to greater power demands placed upon newer models of mobile phones and the change of view that batteries are no longer replaceable and are a permanent component within a phone, LIB research is a widely active field. Through new innovations, it is hoped that enhancing the battery will allow for more advanced features on newer phones whilst allowing a longer product lifespan.

Also of significant interest is the safe operation of Lithium-Ion Batteries. Famously, the largest safety recall in the history of consumer electronics (at the time) occurred in 2006 when Dell recalled 4.1 million notebook batteries due to a manufacturing defect.[5] More recently, Samsung also recalled more than 2.5 million smartphones in 2016 due to a manufacturing fault causing the positive and negative electrodes within the phone to come into contact and short circuit.[6]

This literature review aims to demonstrate how LIBs function and the use of fluorinated materials in battery design, particularly the impact upon electrolyte systems.

1.2   Development of Lithium-Ion Batteries

1.2.1   The first battery

Volta is commonly credited with creating the first battery, referred to as a Voltaic pile, which consisted of layers of zinc, brine-soaked cardboard (or cloth) and copper, which behave as the anode, electrolyte, separator and cathode of a cell, respectively. On the anode, where oxidation takes place on discharge, the zinc metal yields two electrons (Equation 1) and dissolves into the electrolyte solution to form zinc chloride. On the copper electrode, the influx of electrons causes the electrolysis of water in the electrolyte, releasing hydrogen gas (Equation 2) and producing sodium hydroxide.[7] The net effect of these two reactions (Equation 3) is the creation of an electric potential, which can be varied by changing the number of combined layers.

$$Zn \rightarrow Zn^{2+} + 2e^- \tag{1}$$

$$2H_2O + 2e^- \rightarrow H_2 + 2OH^- \tag{2}$$

$$Zn + 2NaCl + 2H_2O \rightarrow H_2 + ZnCl_2 + 2NaOH \tag{3}$$
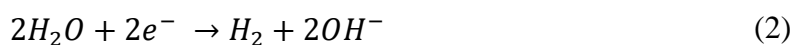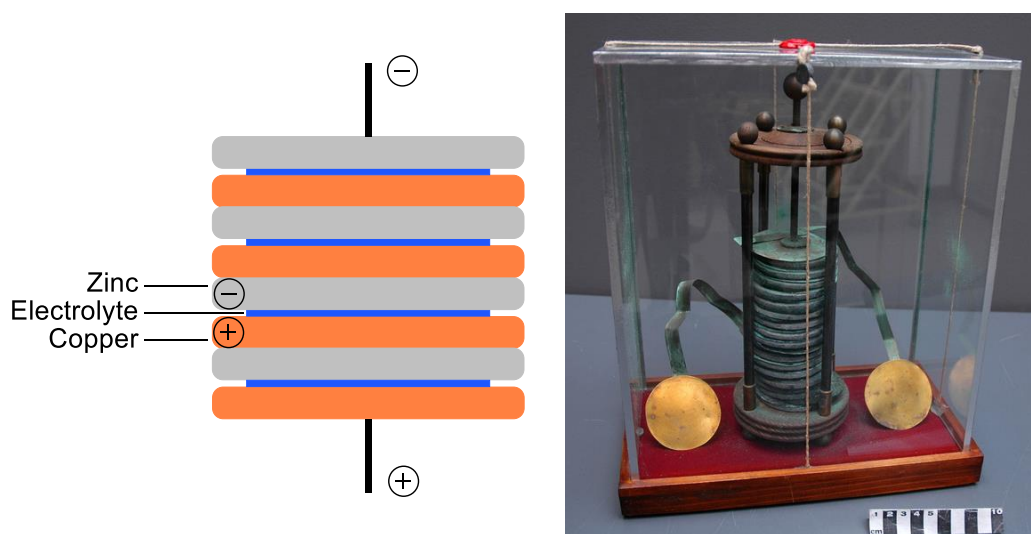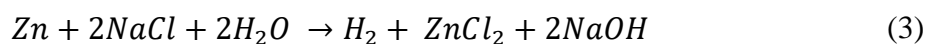
Figure 2 - (Left) schematic of voltaic pile, (right) photo of voltaic pile replica[8]

Whilst very basic in design and only producing a small voltage (1.1 V), this discovery was significant in the field of chemistry. It provided a reliable and steady current which, within the next eight years, led to the isolation of elemental potassium, sodium, barium, calcium, strontium and magnesium via electrolysis.[9, 10]

After Volta's discovery, many variations and advances were realised but, until 1859, all batteries were single use and the components had to be replaced when the reaction inside the cells was complete.

1.2.2   First rechargeable battery

The first rechargeable battery was made by Gaston Planté using a lead-based battery system. These batteries consisted of two sheets of lead separated by cloth soaked in a solution of 10% sulfuric acid in water. When a potential is first placed over the cell, one electrode reacts with water to form a layer of lead oxide, liberating hydrogen (Equation 4). On the other electrode, lead oxide, which is pre-formed on the surface through contact with air, is reduced producing water and pure lead (Equation 5). In this charged state, completion of the circuit causes both electrodes to react with the sulfuric acid present to produce lead sulfate and water (Equation 6) with one electrode being reduced and the

other oxidised. By applying a potential over the cell again, the reaction can be reversed, making the cell rechargeable.[11]

$$Pb + 2H_2O \rightarrow PbO_2 + 2H_2 \tag{4}$$

$$PbO_2 + 2H_2 \rightarrow Pb + 2H_2O \tag{5}$$

$$PbO_2 + Pb + 2H_2SO_4 \rightarrow 2\ PbSO_4 + 2H_2O \tag{6}$$
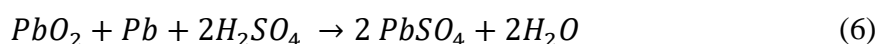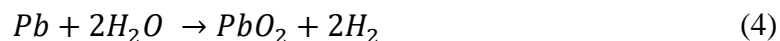
This type of battery was improved further by Camille Faure who used a lead grid lattice with lead oxide pressed upon it to form a plate which could be stacked to increase the power of the battery. Faure patented his designs, which were easier to produce in bulk and led to the wide-spread use of batteries.[12] The lead-acid battery is relatively heavy and has relatively low power compared to other batteries, but is stable and robust. Consequently, this type of lead-acid battery, with small changes in material and the use of additives, is used regularly to this day in systems in which weight is not a major consideration, such as cars or back-up power supplies.

The development of rechargeable batteries led to the source of some confusion within the field with regards to nomenclature; which electrode is the cathode/anode if both give and accept electrons depending on charge or discharge? The convention adapted was that the terms were used when the battery is providing work and, therefore, discharging. Thus, the anode (or negative electrode) throughout the rest of this thesis shall be referred to as the electrode which is oxidised on discharge and the cathode (or positive electrode) is the electrode which is reduced on discharge.

1.2.3   The development of intercalation based batteries

Up until the turn of the 20th century, the lead-acid battery was the only rechargeable system but both Thomas Edison and Waldemar Jungner both independently developed the nickel based battery, the former using iron and the latter using cadmium. These batteries were not only the second rechargeable battery types but the first to utilise an alkaline solution as the electrolyte. The positive electrode consists of nickel oxide hydroxide that is reduced on discharge to form nickel hydroxide (Equation 7), the

negative electrode consists of cadmium which is oxidised on discharge to form cadmium hydroxide (Equation 8) and the electrolyte was a solution of potassium hydroxide. The full cell (Equation 9 shows discharge) can be recharged by passing a potential over the cell, generating the starting materials.[13]

$$NiOOH + H_2O + e^- \rightarrow Ni(OH)_2 + {}^-OH \tag{7}$$

$$Cd + 2\ {}^-OH \rightarrow Cd(OH)_2 + 2e^- \tag{8}$$

$$2NiOOH + Cd + 2H_2O \rightarrow 2Ni(OH)_2 + {}^-OH \tag{9}$$
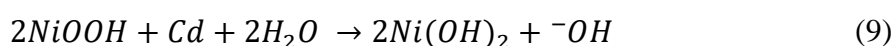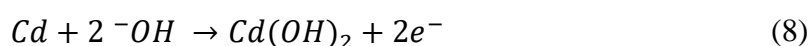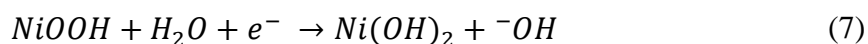
This battery can be charged quickly, perform well at low temperature and has high-rate capabilities. These properties meant that nickel batteries, for a long time, were the only available battery for power tools and early portable devices. The key part of this cell is the nickel oxide hydroxide electrode reversibly inserts protons into the electrode's layers of nickel oxide. The storage of hydrogen in the electrode of a cell prompted research into nickel-metal hydride cells.

In the 1970's, patents were filed by Daimler-Benz protecting the use of an alloy of metal hydrides (the metal residing from groups 3, 4 or 5) and another metal (nickel, copper, silver, iron and chromium-nickel steel) as the negative electrode in a cell, nickel being the most common.[14] The positive anode remains the nickel oxide hydroxide electrode and undergoes the same reaction as expressed in Equation 7. The negative electrode reacts in a similar way to the nickel-cadmium battery; the metal hydride reacts with a hydroxide ion, on discharge, to produce the oxidised metal and water (Equation 10). The net reaction on discharge is the migration of hydride from the positive to the negative electrode (Equation 11).

$$MH + {}^-OH \rightarrow M + H_2O + e^- \tag{10}$$

$$NiOOH + MH \rightarrow Ni(OH)_2 + M \tag{11}$$
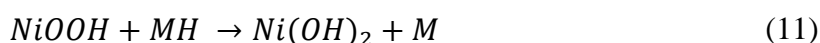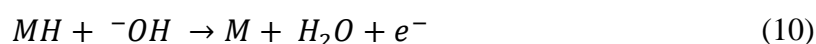
Whilst having a larger energy density, the metal hydride cell has some substantial drawbacks; usage at high temperatures and cycling with heavy electrical loads significantly reduces the lifespan of the battery.[15] Another drawback concerning the use of protons as the transfer agent in batteries is that the electrolyte has to be in aqueous solution to facilitate the migration. This ultimately limits the voltage window of the battery to be equal to or less than 1.5V.[16]

1.2.4   Lithium-Ion batteries

The drawbacks to the initial batteries listed in the previous section led to research into the use of lithium as a material with a high energy density which could potentially give a more stable battery. Research began at the start of the 20th century but it wasn't until the 1970's that the first non-rechargeable lithium based batteries came onto the market. Lithium-Ion batteries have an electrolyte consisting of organic compounds such as liquid dimethyl or diethyl carbonates into which lithium salts can readily dissolve and this allows a much higher voltage window compared to aqueous electrolyte media.[16]

1   **2**   **3**   **4**
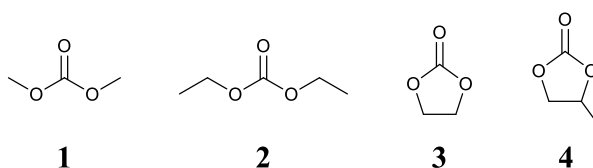
Figure 3 – Electrolyte solvents for LIBs; dimethyl carbonate **1**, diethyl carbonate **2**, ethylene carbonate **3** and propylene carbonate (PC) **4**

Original Lithium-Ion batteries consisted of a lithium metal electrode which, upon discharge, released lithium ions into the electrolyte (Equation 12). The opposing electrode consisted of a layered titanium sulfide which, upon discharge, intercalated the lithium in-between the layers of TiS_2 (Equation 13). In addition to this, the electrolyte consisted of dimethyl carbonate **1** (DMC), diethyl carbonate **2** (DEC) and a lithium salt to carry the charge. Also, the electrolyte, contained a small amount of ethylene carbonate **2** (EC) "additive" which, upon discharge created a passivation layer (known as a solid electrolyte interphase layer or SEI; see section 1.4) on the lithium anode to protect the electrodes from degradation. The overall reaction on discharge within the cell is the migration of lithium ions from the anode to the cathode with the release of energy (Equation 14).[17]

$$Li \rightarrow Li_{1-x} + xLi^+ + xe^- \tag{12}$$

$$TiS_2 + xLi^+ + xe^- \rightarrow Li_xTiS_2 \tag{13}$$

$$Li + TiS_2 \rightarrow Li_{1-x} + Li_xTiS_2 \tag{14}$$
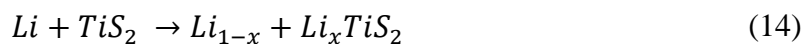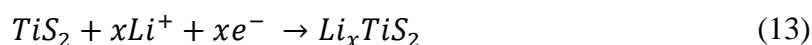
Lithium batteries were initially sold charged as single use batteries due to issues that arise from repeated charging; the SEI formed allows lithium ions to pass through on discharge, whilst on charging the lithium ions can start to plate on the SEI instead of re-intercalating into the electrode. This leads to the formation of dendrites and can cause internal short-circuiting. As such lithium metal was not developed further as a material for batteries but is still used in half cells as a measure to compare different experimental electrodes and additives.[16]

Further development into the use of lithium within batteries was pioneered by Goodenough who recognised that oxides would provide the potential for larger batteries based on lower energy 2p orbital bands being available as opposed to the 3p orbitals available in sulfur. This idea explored lithium extraction from layered lithium metal oxides ($LiMO_2$) for use in batteries and, through this work, lithium cobalt oxide ($LiCoO_2$) and lithium nickel oxide ($LiNiO_2$) were found to give reversible lithium extraction reactions.[18] At the same time it was found that lithium intercalation into graphite could be achieved reversibly without the formation of dendrites.[19]

The combination of these two discoveries led to the first rechargeable Lithium-Ion Battery being created and patented in 1985.[20] The battery was assembled in a discharged state, with graphite on one electrode and lithium cobalt oxide on the other and, upon charging, there is migration of lithium ions from $LiCoO_2$ to graphite (Figure 4). On discharge, the intercalated-graphite anode releases lithium ions into the solution and oxidises back to graphite (Equation 15). Concurrently, the lithium cobalt oxide cathode is reduced as it intercalates the lithium ions from the electrolyte (Equation 16). The full cell reaction (Equation 17) was facilitated by an electrolyte that consists of a mixture of ethylene carbonate and dimethyl carbonate with a soluble lithium based salt, such as $LiPF_6$.

$$Li_xC \rightarrow C + xe^- + xLi^+ \tag{15}$$

$$Li_{1-x}CoO_2 + xe^- + xLi^+ \rightarrow LiCoO_2 \tag{16}$$

$$Li_{1-x}CoO_2 + Li_xC \rightarrow LiCoO_2 + C \tag{17}$$
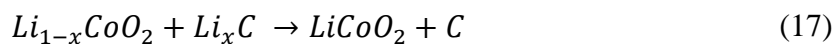
This battery was first commercialised by Sony in 1991 and has since been developed into the basis for powering most portable electronic devices used in modern society. Since then lithium-ion batteries have been developed to improve upon or increase the usability of the battery including switching to other carbonate systems such as propylene carbonate **4** (PC), the use of additives in the electrolyte or, in a emerging technology, changing the liquid electrolyte altogether to a solid polymer based system.
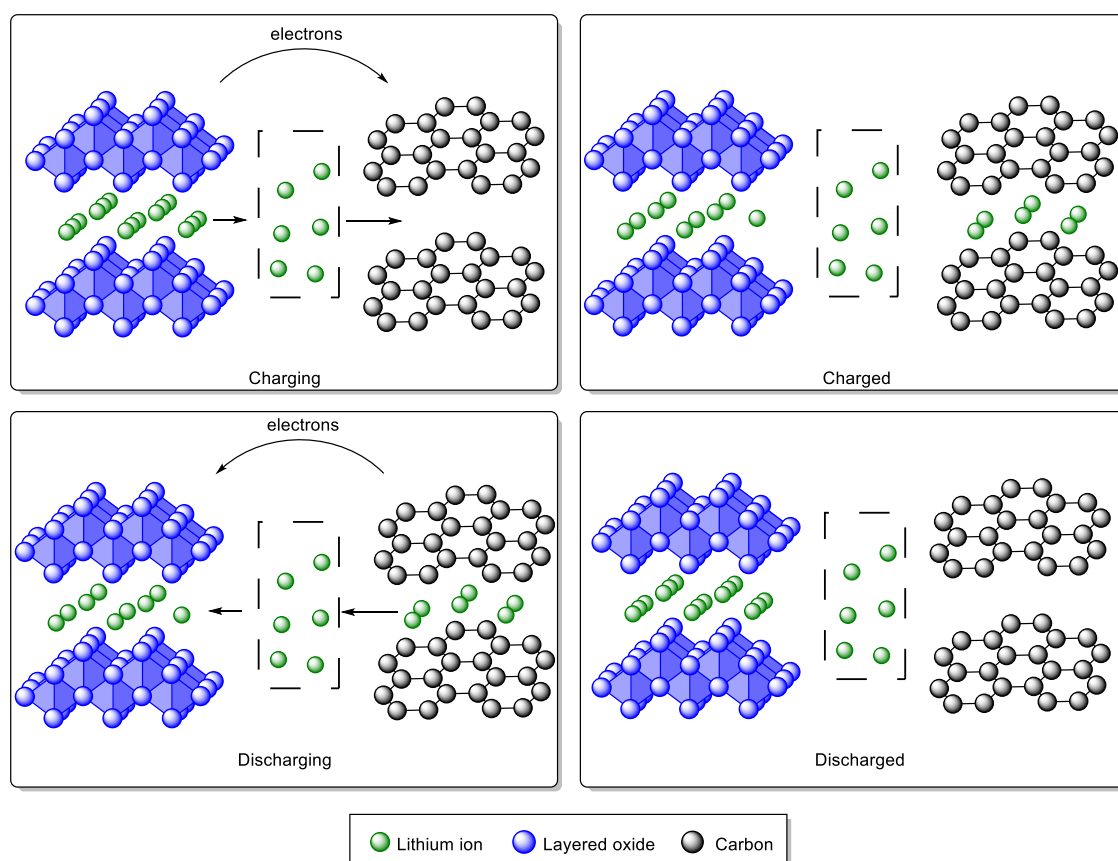

Figure 4 - Structure of a standard Lithium-Ion cell; on charge the lithium ions migrate from the layered oxide to the graphite electrode and on discharge, the reverse reaction occurs

One avenue of further study into battery materials is to replace graphite as the anode. Graphite has a maximum capacity for the amount of lithium intercalation of Li_xC with $0 \leq x \leq 1/6$. Consequently, other anode materials are being investigated, such as silicon based electrodes which could provide a higher stability with regards to lithium consumption but these unfortunately struggle with a large expansion upon charging (~300%).[16]

1.3   Electrolyte additives

A large area of active study within the scientific community is towards the development of more effective electrolyte additives for increasing overall performance of Lithium-Ion Batteries. Additives have an array of different uses and are the most economic and effective methods of improving the Lithium-Ion Battery as "drop-in" materials. Despite only contributing to no more than 5% of the electrolyte by weight, they have a pronounced effect on the stability of the components as well as decreasing the degradation and increasing the safety of the battery after repeated cycling.[21] The major categories of electrolyte additives used in Lithium-Ion Batteries are outlined and briefly explained below.

1.3.1   Cathode protection

The cathode, typically $LiCoO_2$, is susceptible to degradation from two potential sources, water or other impurities, and the irreversible oxidation of solvents found in the electrolyte. Lithium-ion batteries are typically prepared in dry conditions, so degradation from water occurs when side reactions occur within the cell. Although not fully understood, production of water within a cell via the oxidation of the carbonate solvents found within the electrolyte by oxygen released from the cathode has been proposed. The water and carbon dioxide generated would then be able to undergo a side reaction with lithium hexafluorophosphate to produce hydrofluoric acid which, at high concentrations, could start to dissolved the cathode material.[22]

Consequently, one of the most popular types of additives to protect the cathode are based around scavenging or preventing the generation of water or acid derivatives within the battery. One such strategy to achieve this was patented in 1998 which utilises butylamine (or other amine based compounds) dissolved in the electrolyte or placed within the

cathode material to react with any acids generated and, therefore, prevent decomposition of the electrode.[23] Another additive for preventing degradation of the cathode was based on organosilicon compounds containing an N-Si bond, such as *N,N*-diethylamino trimethyl-silane **5**. Nitrogen to silicon bonds are particularly sensitive to attack from water or a hydrogen halide, liberating an amine and a silicon based compound (Figure 5).[24] The resulting amines are inert with regards towards further chemistry within the battery with the exception of complexing PF_5 molecules that are within the electrolyte, lowering the Lewis acidity of these molecules and providing stability to the SEI by preventing attack of the surface.[21]

5
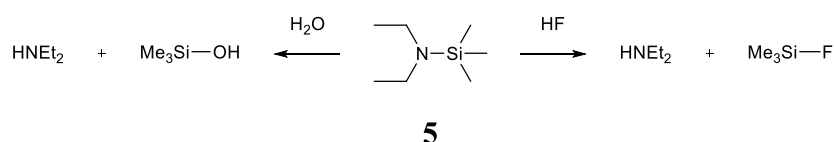
Figure 5 - *N,N*-diethylamino trimethyl-silane **5** as a water and hydrofluoric acid scavenger to protect the cathode

1.3.2   LiPF$_6$ stabiliser additives

The lithium hexafluorophosphate electrolyte that is most commonly used in LIBs can also decompose within the battery due to the salt equilibrium (Equation 18).

$$LiPF_6 \rightleftharpoons LiF + PF_5 \tag{18}$$

The phosphorus pentafluoride species can react with common organic electrolyte solvents as well as destabilise any solid electrolyte interphase (SEI) layer that may be present. As well as reducing the amount of $LiPF_6$ available to mediate the electrochemical reactions of the cell, the LiF produced disrupts the SEI in addition to causing production of PF_5 gas which increases the battery volume posing a potential safety hazard by swelling.

One suggested method of inhibiting this process is simply by using Le Chatelier's principle; with the addition of LiF, the equilibrium is pushed further towards the lithium hexafluorophosphate side of the equation and, hence, reduces the concentration of phosphorus pentafluoride present. It's also noteworthy that the quantities of lithium fluoride required to get a pronounced effect are also small; a concentration of 0.18% LiF in a $LiCoO_2$-graphite cell with an electrolyte of 1:1 EC:DEC, 1 molar $LiPF_6$, showed a

reduction of volume expansion by 15%. As stated above however, much higher concentrations than this would cause negative effects due to LiF disruption of the SEI. [25]
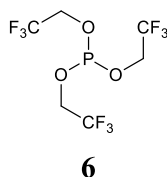

6

Figure 6 - *Tris*-[2,2,2-trifluoroethyl]-phosphite **6**

An alternative method of preventing the problems listed above is tempering of the reactivity of the phosphorus pentafluoride molecule by the addition of a small amount of a weak Lewis-base. This strategy entails some degree of caution, however, because if the PF_5 molecule is stabilised too much, this will drive the equilibrium to decrease the concentration of lithium hexafluorophosphate in the electrolyte. For example, small amounts of *tris*-[2,2,2-trifluoroethyl]-phosphite **6** have been found to form a weak 1:1 complex with phosphorus pentafluoride which is reflected in the increased stability of the electrolyte.[26]

1.3.3   Safety protection agents

Another category of additives found in batteries are those which aim to improve the safety of the battery under extremes of operation. The majority of hazardous behaviour of batteries can be attributed to runaway reactions that occur at high potentials and two approaches can be taken to tackle these issues; protection from overcharging and the prevention of fire.

One strategy to prevent hazards occurring is through the use of a shuttle additive which, at the extremes of the potential of the cell, are oxidised at the positive electrode and then diffuse to the negative electrode upon which the additive is reduced again. Through this action, the maximum potential of a cell can be mediated and overcharging is limited and for example, 2,2'-bipyridyl **7** and 1,10-phenanthroline **8** to iron complexes have been used.[27]
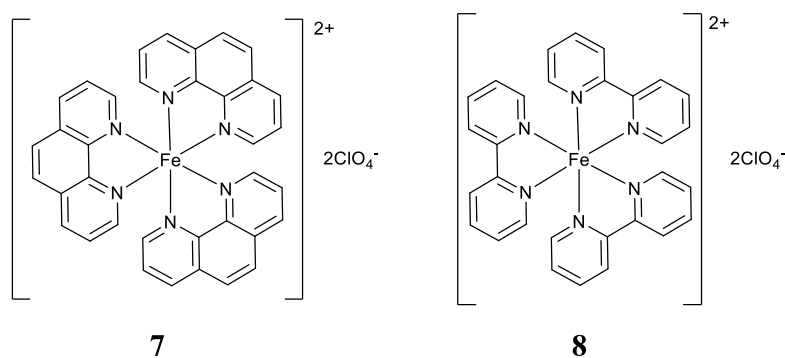
7   **8**

Figure 7 – Structures of the 2,2'-bipyridyl **7** and 1,10-phenanthroline **8** iron complexes which can be used as shuttle additives in Lithium-Ion Batteries

However, the draw back to iron complexes are the conditions required; the reaction must be highly reversible, the shuttle additive must have good solubility in the electrolyte solvent and the oxidation window must be just above the cathode full-charge potential. These are very specific demands which are not easily attainable and with regards to the above example, the shuttle voltage is 3.8-3.9 V which is slightly below the requirements of typical commercial LIB systems (4 V-4.5 V).[27]

Due to these drawbacks, another method of preventing overcharging that may be utilised is the use of a so-called "shutdown" additive. The premise of this strategy is that at high potentials the additives polymerise on the cathode blocking the electrochemical reaction whilst also releasing a gas which can activate a device to switch off the current. A good example is the use of xylene, which dissolves readily in the electrolyte solvent, forms a strong polymerised layer on the cathode at the extremes of the potential and has minimal influence on the cycling behaviour of the battery.[28]

The strategy for fire retardation generally tends to be via using radical scavenging agents which would terminate chain reactions that are responsible for the combustion of any gas phase products liberated in the cell. One such example for a flame retardant additive is hexamethoxycyclotriphosphazene **9** (Figure 8) which was shown to reduce the self-heat rate of the battery to a third of its original value.[29]

MeO, N, OMe
MeO—P, P—OMe
N, N
P
MeO OMe
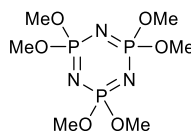
9

Figure 8 – Hexamethoxycyclotriphosphazene **9**

1.4   Solid electrolyte interphase layers (SEI)

Quite possibly the most important additives found within batteries are those which are designed to form a solid electrolyte interphase layer on the surface of an electrode. These layers provide protection for the electrode and prevent degradation through redox reactions, help prolong battery lifetimes and improve the stability of the battery over repeated cycles. It is also worth noting that the composition of SEI's is a highly debated subject due to difficulties in normalising all conditions amongst different research groups as well as difficulties in extracting detailed information on the SEI without causing damage to the layer.[30]

1.4.1   Understanding SEIs

Solid electrolyte interphase layers are coatings formed on an electrode when the battery is first charged and are typically beneficial to the whole electrochemical system. On the first charge of the lithium-ion battery, typically, the negatively polarised graphite electrode causes some of the electrolyte to irreversibly decompose to form a passive layer of both organic and inorganic products. In an ideal system, this layer is sufficiently passive to prevent the un-impeded migration of lithium ions after repeated charges whilst preventing further side reactions from occurring with both the electrode and the electrolyte.[30] Upon first charging there is an irreversible charge loss due to the consumption of electrolyte solvent and the formation of an SEI and, therefore, is a common indicator that an SEI has formed.[31]

The shelf-life of a lithium-ion battery is determined by how well the lithium ions can be prevented from diffusing through the battery when there is no electrical work placed upon the battery. As such, the shelf-life of the battery is also dependent on the SEI formed and the ability of the layer to passivate the electrodes.[32]

In addition to increasing the kinetic stability of the cell, the solvent molecules can, without the presence of the SEI, co-intercalate alongside the lithium ions causing a large increase in the volume of the battery (~150%) as well as reducing the lithium storage capacity.[33] The co-intercalation of solvent, particularly PC, is often irreversible and can cause exfoliation of the graphite electrode.[34] An effective SEI prevents this occurring and protects the anode.
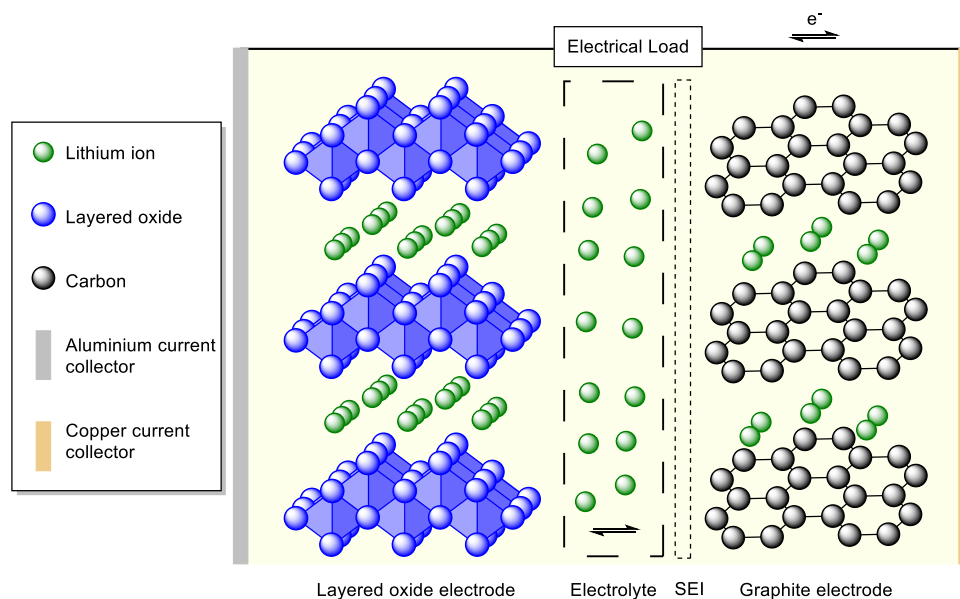
Figure 9 – Schematic of a LIB, with the position of a typical SEI protecting the anode

The ideal SEI would have a high conductivity of lithium ions but a very low electronic conductivity whilst adhering strongly to the electrode that it is formed upon. The formation of this SEI layer should be fast which, in practice, requires the potential for the SEI formation to be energetically more favourable than the intercalation potential of the electrodes. The SEI should be a uniform and dense layer evenly spread over the electrode whilst containing good passivating agents that are insoluble in the electrolyte.[30] In addition to this, a high degree of flexibility in the SEI would allow the structure to remain intact despite any chemical side reactions that could occur on the electrode over the lifetime of the battery.[35]

1.4.2   Factors affecting SEI formation

There are many factors behind what creates the SEI within a battery and it is a combination of several properties that dictates the quality of the SEI formed. Arguably the most obvious characteristic which will dictate the type of layer that is formed is the surface upon which the SEI is formed.

It was shown, using graphite as the example electrode, that the shape, crystal structure and specific surface area of the electrode are all crucial in the synthesis of SEI's. It also stands to reason that the number and nature of defects in the electrode also play a defining role in the type of SEI that is formed; generally edges on crevices of the electrode produce SEI's with a high inorganic content whilst long, flat graphene sheets produced SEI's with a high organic content.[36] It is worth noting, however, that highly ordered structures of graphite, whilst potentially yielding a more desirable and organic-rich SEI also have greater susceptibility to co-intercalation by the solvent.[37]

To this end, attempts have been made to try and activate the surface of the electrodes to improve the SEI that is formed. Both oxidation, via nitric acid and ammonium persulfate,[38] and reduction, via butyl-lithium solution[39], were attempted upon the surfaces of electrodes but both met with mixed results. The former produced a battery which had an increased reversible capacity and a lower irreversible capacity loss which is thought to be a result of an etched surface.[38] The latter formed a thicker SEI which reduced the irreversible capacity loss but was also brittle and susceptible to damage over the battery's lifetime.[39]

The second most significant contributor to the quality of the SEI layer formed is the electrolyte solution which makes up the majority of the composition of the layer. As such, the solvent systems used for LIB systems has a large impact on the properties of the SEI; using different systems in the solvent produces different salts and different layers. For example, ether based solvents produce lithium alkoxides[37], carbonates produce lithium carbonates[37] and methyl formate produces lithium formate in SEI's.[40] At higher concentrations of carbonate systems, such as **3** and **4**, the major reduction products are $(CH_2OCO_2Li)_2$ or $ROCO_2Li$ whilst at lower concentrations it is lithium carbonate. Using ethylene carbonate as an example, two mechanisms have been proposed for solvent

reduction (Figure 10). The lithium carbonate salt tends to lead to a less stable SEI formed and a higher degree of gas generation whereas the $(CH_2OCO_2Li)_2$ salts form a more compact and stable layer[41] and are generally more desirable. Also, as a practical example of the difference between surface sites in SEI formation, Li_2CO_3 is generally produced in cracks or on edges of the surface of the electrode whilst the organic product is produced on the graphite sheets.[42]
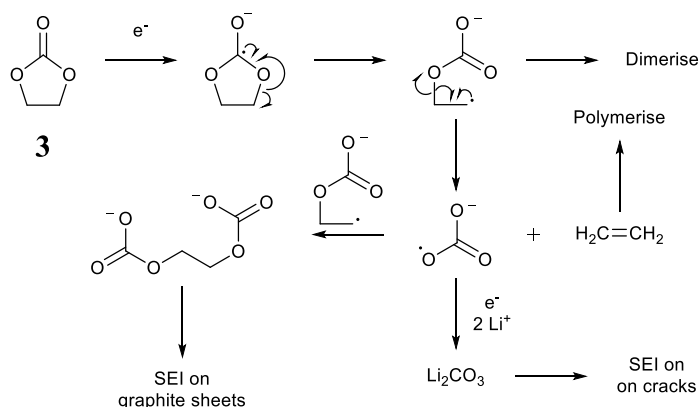

Figure 10 - Two mechanisms for the decomposition of **3** into its SEI products[41]

The final major factor which can affect SEI formation is the additives which are placed within the electrolytes of batteries in efforts to manipulate the formation of the SEI and these are discussed below.

1.4.3   SEI morphology modifier

The previous section described the importance of the morphology and attempts to treat the surface of the electrode to improve the SEI formed. Another strategy is the use of additives which may improve the layer *in-situ*. Within the SEI formed, it is often the inorganic products such as LiF that lead to a brittle and ineffective layer. One of the compounds used to counteract this via complexation of LiF is *tris*(pentafluorophenyl) borane which forms a 1:1 complex with the lithium fluoride salt. When used in 0.1 - 0.2 M concentrations, an improvement to the cycleability and capacity retention is observed. The drawback of this strategy is that LiF may be removed from the electrolyte as opposed to the SEI which pushes the equilibrium of the lithium hexafluoride salt (Equation 18) to produce a higher quantity of highly reactive PF_5.[43]

An alternative strategy has been attempted using alkali metals to form an SEI based on different inorganic compounds, such as $NaClO_4$ in an EC-DEC Lithium-Ion Battery which formed a uniform and lower resistance layer when compared to the layer without the additive.[44]

1.4.4   Reduction type additive

Reduction type additives work on the principle that they are reduced before the electrolyte solvent starts to decompose and deactivate the catalytic activity of the electrode preventing it from sustaining damage from other chemical reactions. Through this method there should be an increased stability to the SEI and a lesser degree of gas production. This type of battery additive can be broadly split into two groups; polymerisable monomers and reducing agent additives.

The former is typically a small organic compound with at least one double bond within it. Perhaps the most useful example of this type of compound is vinylene carbonate (VC) **10** which is widely used as an additive.
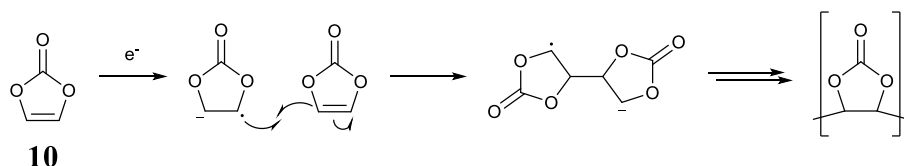

10

Figure 11 - Mechanism for the polymerisation of vinylene carbonate

Within a Lithium-Ion Battery, the VC reacts with the anode material, preferentially to the electrolyte solvent, and undergoes rapid polymerisation. This reaction results in a thinner SEI with lower concentrations of inorganic salts within the layer.[45] The SEI formed reduces the irreversible capacity loss on first cycle, increases battery stability and decreases surface impedance of the graphite in comparison to the corresponding cell without the additive.[46]

Whilst VC is possibly the most famous of these types of compounds, there are a wide range of polymerisable monomer reduction type additives. They are particularly desirable as they only require one electron reduction to start the propagation and formation of the SEI. The effectiveness of these types of additives and the subsequent layer formed are

affected by the solubility of the resulting polymer, the degree to which the layer adheres to the electrode as well as the efficiency of electrically-induced polymerisation.[21]

Reducing agent type additives work to assist SEI formation by adsorbing onto the catalytic active sites on the electrode surface. It then logically follows that the effectiveness of such processes is proportional to the affinity of the functional groups on the additives for the active sites. There is a large prevalence of sulfur containing compounds which is consistent with sulfur behaving as a catalyst poison for many other catalysts.

For example, polysufide containing systems (S_n^{2-}) are found to benefit both the graphite electrode and the lithium source in a PC electrolyte based battery. The graphite electrode showed longer-life cycleability and lower self-discharge whilst lithium sources showed much less dendrite formation.[47] Unfortunately these sulfur type compounds also suffer from redox-shuttle type reactions (see section 1.3.3) so the viability of these systems is drastically lowered.
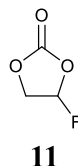
11

Figure 12 – Fluoroethylenecarbonate (FEC) **11**

Other types of reducing agent type additives are halogenated based species such as halogenated carbonates and lactones. An example can be found in fluoroethylene carbonate **11** (FEC) which has a dual action towards creating a beneficial SEI. Upon first charge in a cell, the fluoroethylene carbonate loses HF to form vinylene carbonate which then behaves as a polymerisable additive (as shown above).[48] The resulting HF then stabilises the battery by either reaction with lithium carbonate salts or formation of LiF. The former includes reactions which results in a more uniform SEI surface which helps prevent dendrite formation[49] whereas the latter, as discussed above, helps push the equilibrium towards lithium hexafluorophosphate.[45]

1.4.5 Reaction type additives

Reaction type additives behave differently to reduction type additives in that they do not undergo an electrochemical based reaction; they either react by scavenging electrons from partially reduced solvent molecules or combine with the reaction products of electrochemical reactions of the solvent. Since the additives are not reduced electrochemically, the potential for the formation of the SEI is similar to that of the potential for the solvent reduction in these types of batteries.

One of the earliest examples of a reaction type additive is carbon dioxide. The CO_2 molecule inserts into lithium based salt products of solvent reduction by reacting with reduced ethylene carbonate to produce the salt **12**. This then forms part of the SEI giving a more stable layer and reduces the amount of irreversible capacity loss.[50]
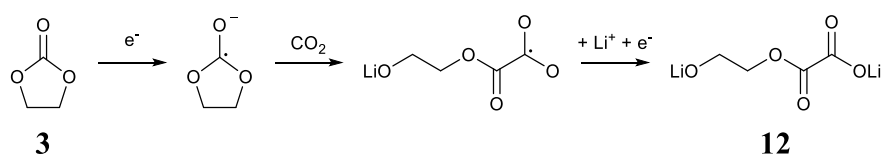

Figure 13 - Mechanism of CO_2 scavenging radicals within a battery electrolyte to form a more stable SEI[50]

The problems associated with this type of additive, however, is the low solubility of CO_2 in the organic solvent and the high pressures that could arise. This was somewhat addressed with the use of dialkyl pyrocarbonate as this is an *in-situ* provider of carbon dioxide.[51] Further complications arise due to the production of gas within a cell which can lead to swelling and, in turn, a potential hazard to battery safety.

Another example of a multi-purpose reaction type additive is 4-fluorophenyl isocyanate **13** which has three mechanisms of action. The isocyanate stabilises the SEI with respect to the electrode through stabilising interactions with polar chemisorbed groups on the graphite as well as scavenging any water that may be in the electrolyte. Finally, the isocyanate group can act as a weak Lewis acid to deactivate the highly reactive PF_5 group in the electrolyte. It was shown that 4-fluorophenyl isocyanate protects PC decomposition, improved cyclic stability and has limited impact on the other characteristics of the battery.[52]
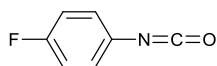
13

Figure 14 - Structure of 4-fluorophenyl isocyanate

Boron based compounds have also been of significant interest in this area as they were found to increase both low temperature performance and rate capability whilst also stabilising the SEI. Perhaps the most well-known of these types of compounds is lithium bis(oxalate) borate (LiBOB) **14**. This salt, originally intended to replace LiPF$_6$ as the main electrolyte salt, was found to improve the performance of LIBs when used at the additive level, suppressing PC decomposition and stabilising the SEI despite repeated cycling. It was found that boron to oxygen based compounds are present in the SEI in such batteries prompting the suggestion that LiBOB reacts with typical products found in the SEI to form oligomers, such as **15** and **16**.[53]
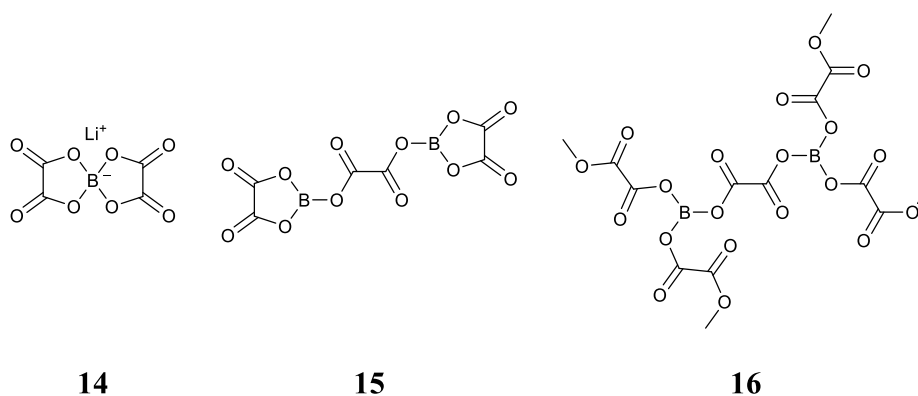
14   **15**   **16**

Figure 15 – **14** the additive, and **15** and **16**, two examples of the oligomers that can form between LiBOB and the LIB solvent[53]

1.4.6   Nitriles in LIBs

If there is a particular electron-withdrawing group within the additive molecular structure, such as a halogen or nitrile moiety, this can result in a more electrophilic additive which can be more easily reduced. Allyl cyanide **17** is one such additive which works by polymerisation after reduction of the vinyl moiety. This polymerised structure then forms a thin layer which protects the graphite anode within a LIB.[54]
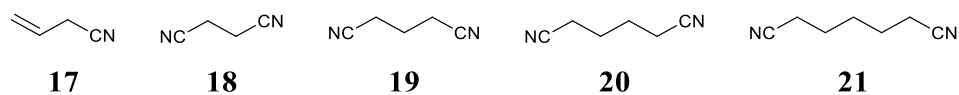
Figure 16 - Some examples of LIB additives that contain nitriles

Further nitrile-containing additives that are of significant interest include succinonitrile (SN) **18**[55] and other longer chained di-nitriles; glutaronitrile **19**,[56] adiponitrile **20**[55,57] and pimelonitrile **21**.[55] These compounds provide a large improvement to the battery; they reduce the irreversible capacity loss but, perhaps more interestingly, they significantly reduce gas generation within the cell, with SN showing the most pronounced effect. This was originally attributed to chemisorption of the nitrile compounds onto the lithium cobalt oxide cathode, but, despite the exact mechanism being unknown, SN has also been shown to decompose oxidatively forming an interphase layer and providing protection from high-potential oxidation reactions of the solvent.[58]

1.4.7   Synthesis and use of fluorinated organic compounds in LIBs

Commonly seen throughout modern batteries is the frequent use of fluorinated compounds; from fluorinated lithium salts to the use of fluoro-organic compounds as additives within the electrolyte. The unique properties of fluorine allow for this; high electronegativity and strong C-F bonds formation allow for tune-ability of compounds used in batteries. The former results in lower reduction potentials of certain compounds, ideal for reduction type additives, whilst the latter allows the use of highly fluorinated systems for protection or binding within the batteries operating environment.
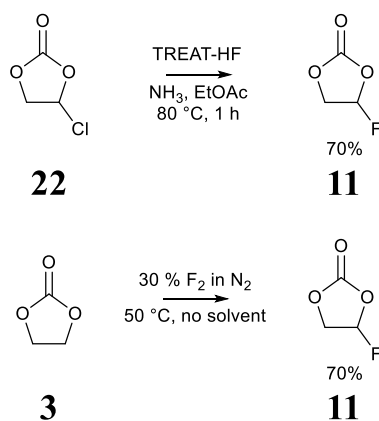

Figure 17 - Synthetic strategies for the synthesis of fluoroethylene carbonate

FEC **11**, described above in 1.4.4, can be simply synthesised from chloro-ethylene carbonate **22** using halogen exchange with triethylamine HF (TREAT-HF)[48, 59] or direct fluorination of ethylene carbonate using fluorine gas (Figure 17).[60] The additive works efficiently by facilitating the elimination of HF on the first charge of the battery and polymerising the remaining VC molecule forming a thin and stable SEI.[48]
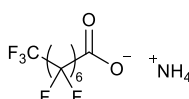

23

Figure 18 - Ammonium perfluorocaprylate

Another fluororganic compound used as an additive in LIBs is ammonium perfluorocaprylate **23**, which is relatively simple to synthesise from the perfluorinated octanoic acid and ammonia to form the salt. The additive adsorps onto the anode and undergoes reduction to form a layer consisting of native additive, reduction products and LiCO$_3$. This SEI is thin, prevents the solvent decomposition and minimises internal resistance of the battery.[61]

24   **25**   **26**
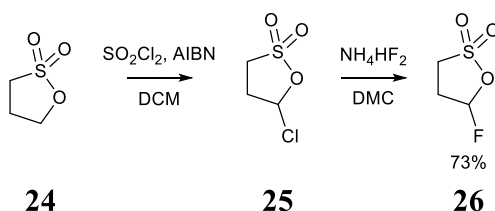
Figure 19 - Synthesis of **26**

1,3-Propane sultone is an effective additive because reduction of the compound forms Li$_2$SO$_3$ and (RSO$_3$Li)$_2$ salts,[62] the presence of which in the SEI allows for much greater ionic conductivity.[63] 3-Fluoro-1,3-propane sultone **26** improves upon this by enhancing the anodic stability and, therefore, allows an improved SEI formation.[64] **26** can be prepared in a method patented by LG via chlorination of **24** to form the chloro-sultone **25** and then halogen exchange using ammonium bifluoride.[65]

1.4.8 Use of fluoromalonate diesters within LIBs

Fluoromalonate diester is a highly versatile building block in fluoroorganic chemistry and provides a pathway for conveniently placing fluorine atoms within complex organic structures (see later sections). Recently there has been examples of turning this molecule towards use within LIBs, of which this thesis also explores. Two examples are discussed below.
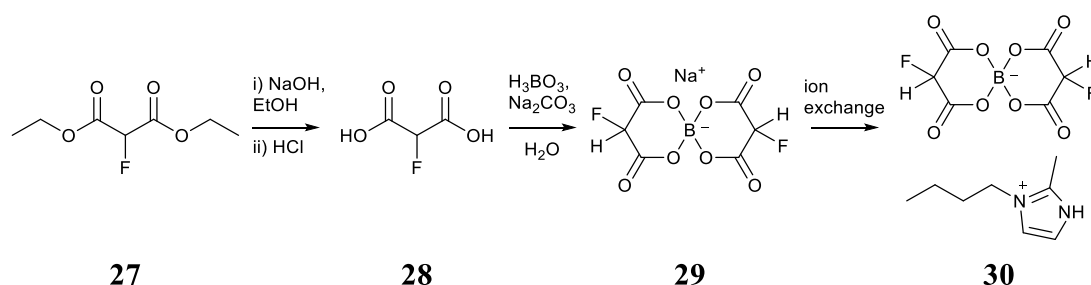

Figure 20 - Synthetic strategy for the synthesis of bis(fluoromalonato)borate ionic liquid

The *bis*(fluoromalonato)borate ionic liquid **30** was developed initially as an alternative electrolyte but also allows battery improvement when used as an additive.[66] It can be synthesised from diethyl 2-fluoromalonate **27** by hydrolysis followed by reaction with boric acid and base giving the sodium salt **29**. After ion exchange with the corresponding imidazolium bromide, **30** can be isolated by filtering away the sodium bromide and removing the solvent. Under battery conditions, **30** was shown to take part in SEI formation producing a layer that improves cyclic stability and protects graphite from PC exfoliation.
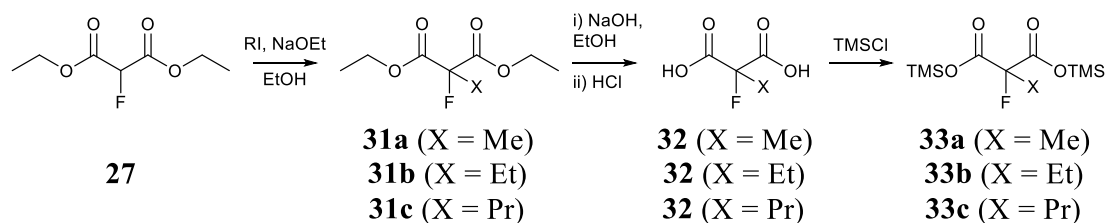

Figure 21 – Synthesis of **33** family of additives

A series of fluoro-malonate-derivative type additives was prepared via the alkylation of **27** using alkyl iodides and base, after which the malonic acid was prepared by hydrolysis.

Reaction with trimethyl silyl chloride gave the desired series of additives.[67] In particular, *bis*(trimethylsilyl) 2-fluoro-2-methyl-malonate **33a** works particularly well as a reductive additive via mechanisms similar to previously mentioned additives. Upon first charge, HF is eliminated and the remaining compound can react and be incorporated into the SEI, resulting in a thinner layer that protects the battery from detrimental side reactions.[68]

This thesis describes the synthesis and application of small fluorinated molecules such as fluoro-diketones, fluoro-diester and fluoro-ketoester systems as additives in lithium-ion battery electrolytes building upon the literature described above. Consequently, a discussion on the field of organofluorine chemistry follows with emphasis on reactions of fluorodicarbonyl systestems of relevance to this project.

1.5   Organofluorine chemistry

1.5.1   Background

The field of organofluorine chemistry is of significant interest due to the unique properties of the fluorine atom; it is the most electronegative element and C-F bonds are not prevalent in nature. In fact, only about a dozen naturally occurring fluorinated species have been found and, as such, the field can be considered entirely man-made.[69]

The origin of the field can be traced back to the work of Henri Moissan and the first isolation of elemental fluorine. This was achieved by passing an electrical current over a mixture of potassium bifluoride and dry hydrogen fluoride separating out hydrogen and fluorine gases at the different electrodes.[70] Such was the impact and difficulty of this discovery that his efforts merited the Nobel prize in 1906 which was awarded to Moissan as the sole recipient.[71]

Despite many attempts to do so, the high electronegativity and reactivity of fluorine means that even today there are no current viable methods to produce fluorine gas chemically and electrolysis remains the major means of production.[72, 73] Through this process, over 17 thousand metric tonnes of fluorine gas are produced worldwide every year for a variety of uses in many different sectors.[74]

The development of the use of fluorine was limited after its discovery due to the highly corrosive nature of the compound, and so advances in the field stalled until the late 1930's

when large scale production began for the production of $U^{235}F_6$. This demand pushed forward methodologies for the safer production and handling of fluorinated materials which in turn led to the development of organofluorine chemistry.[73]

Fluorine has now become prevalent in modern lifestyles, from being present in electronic devices, to surface coatings on cookware, to water-resistant clothing. The extreme properties of the atom have been useful to materials chemistry, but there is increasing prevalence in fine chemicals; half of all blockbuster pharmaceuticals contain fluorine.[75]

1.5.2   Properties of fluorine

Fluorine owes its reactive nature to its electronic configuration; $1s^2 2s^2 2p^5$. The shell structure is close to the nuclei of the atom and the atom gains significant electronic stabilisation from accepting an electron, dominating the chemistry of the atom and giving it the Pauling value of $\chi = 4$.[76, 77] This high electronegativity, perhaps counter-intuitively, results in a strong bond of fluorine to carbon due to the formation of large partial charges and the resulting ionic-type coulombic interaction between the two atoms.[78]

Another side effect of the large electronegativity of fluorine is the highly contracted nature of the atom and the bond it forms with carbon. Its atomic radii is close to that of hydrogen and the bond length between carbon and fluorine is the closest to that of carbon to hydrogen. This has obvious consequences for the behaviour and conformation of fluorinated organic compounds and plays a part in their interactions with other molecules.

Table 1 - The Van der Waals radii[79] and C-X bond lengths of some common elements[80]

	H	C	N	O	F	Cl
Van Der Waals radii / Å	1.20	1.70	1.55	1.52	1.47	1.75
Bond lengths to carbon / Å	1.06 – 1.10	1.42 – 1.57	1.33 – 1.54	1.40 – 1.49	1.32 – 1.43	1.71 – 1.85
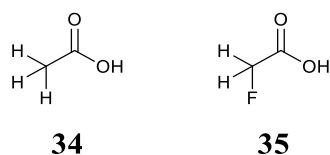
Figure 22 - Acetic acid **34** and fluoroacetic acid **35**

Consequently, due to fluorine being sterically similar to hydrogen, it can behave as a bioisostere for hydrogen within compounds and can be incorporated into biological systems similar to a proton while drastically changing the chemistry. The classic example of this is fluoroacetic acid **35**; whilst acetic acid **34** is regularly used in food, **35** stops the Kreb's cycle by preventing an elimination of water and causing a build-up of fluorocitrate **39** and, as a result, is a potent toxin.[81]
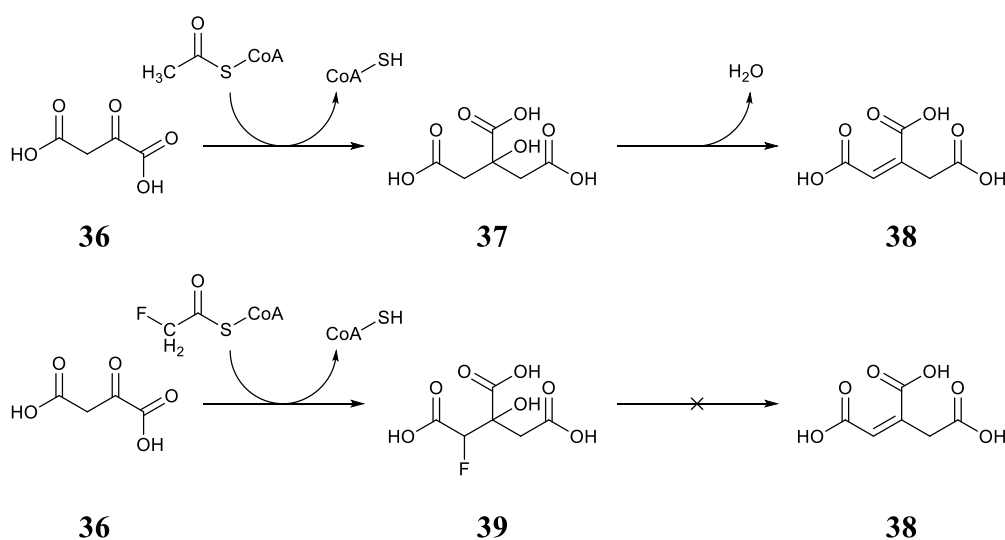
Figure 23 – (Top) Kreb's cycle mechanism from oxoacetate **36** to *cis*-aconitate **38**, (below) the prescence of fluorine blocks the cycle

The highly electronegative nature of fluorine has pronounced effects on the electronic nature of a compound which is reflected in the changes in pK_a. The increasing number of fluorine atoms within a compound can cause greater stability of the conjugate base through inductive effects.

34	35	40	41
4.76	2.59	1.34	0.52
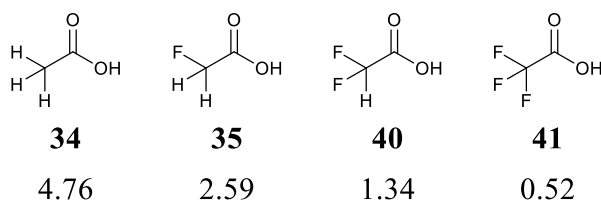
Figure 24 - Structures of increasingly fluorinated acetic acid and their pK$_a$s[82]

On a similar note, the converse is true for bases. The highly electronegative nature of the fluorine atom causes stability in an electron rich compound, such as a base, and destabilises the conjugate acid and causes a reduction in basicity of compounds.
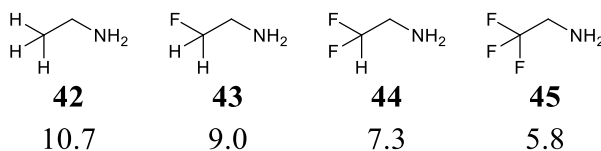

42	43	44	45
10.7	9.0	7.3	5.8

Figure 25 - Structures of increasingly fluorinated bases and their pK$_a$s[83]

Due to the strong electronic effects of fluorine, the presence of fluorine atoms within a molecule can cause drastic changes to the lipophilicity of a compound. Typically, within a saturated alkyl chain, the presence of a fluorine causes a decrease in lipophilicity, whereas when adjacent to a polar group, electron density is withdrawn and lipophilicity is increased.[84]

1.5.3   Strategies for fluorination

The synthesis of organofluorine compounds are of significant interest in the research community since they are sparse within Nature. The origin of all fluorinating reagents is from fluorspar, CaF_2, which is converted to hydrofluoric acid by reactions with conc. sulfuric acid. After this, much development has occurred over the years to create a whole host of different fluorinating materials, for both discovery and manufacture. The reagents for incorporating fluorine into compounds can be broadly split into two groups depending on the fluorinating reagent used; nucleophilic or electrophilic fluorination (Figure 26).[85]

An important consideration for the fluorination of a compound is also the point at which fluorination takes place; ideally a compound could be fluorinated as and when desired

within a synthetic sequence. Due to the harsh reaction conditions and typically unselective nature of fluorination reactions, the point of fluorination is broadly divided into two catagories; early and late stage fluorination. The former consists of fluorination of smaller "building-block" molecules and incorporating into a larger structure with successive reactions. The latter typically requires milder fluorinating reagents or compounds with limited positions available for fluorination. Due to considerations of substrate, cost and green metrics, early-stage fluorination is the major method of fluorination within manufacture whereas late-stage is typically used in discovery processes.[86]
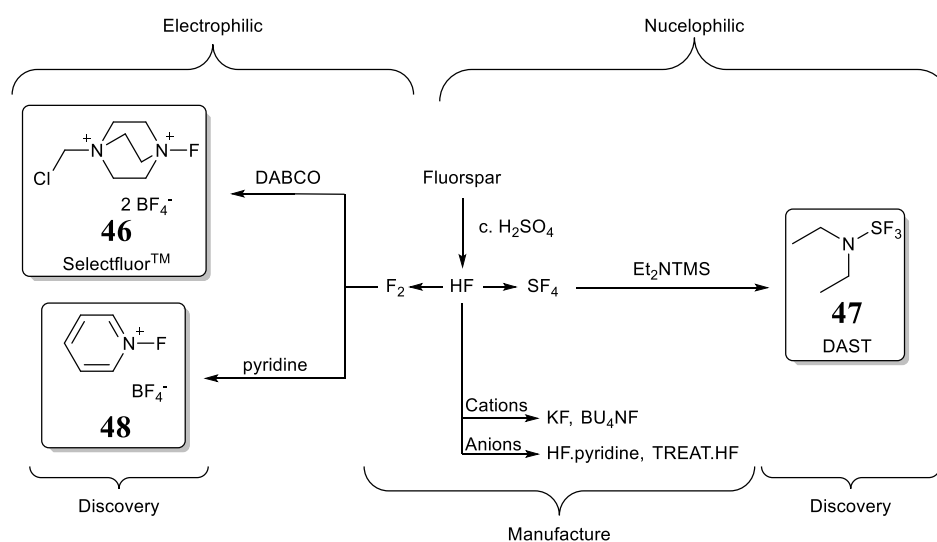
Figure 26 - Sources of fluorinating agents[85]

1.5.3.1 Nucleophilic fluorination

The simplest nucleophilic fluorinating reagent, "F-" is HF due to the reagent being the source of all other fluorinating reagents and is, therefore often considered for manufacturing processes where possible. The major drawbacks of this reagent are its highly corrosive nature along with a severe risk to health.[87]

One such field that the HF is prominent is the refrigeration business, due to the development of new generation of typically heavily-fluorinated refrigerants which have low global warming potential. The generation of chloro- and fluorinated aliphatic compounds is of significant interest, and the use of HF in the synthesis of these compounds is prevalent. One such example is the addition of HF across the chlorinated

alkene **49**, in the presence of catalytic tantalum pentafluoride, which generates 1,1,2,-trichloro-1-fluoro-ethane **50**. The extent of fluorination and substitution can be tuned by a change of catalyst and reaction conditions.[88]
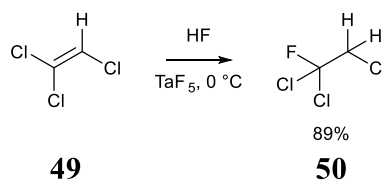

Figure 27 - An example of using HF synthetically

Whilst being a cheap reagent, the highly corrosive and volatile nature of HF can be tapered somewhat using Olah's reagent; a dilution of anhydrous HF with 30% pyridine (PPHF).[89]
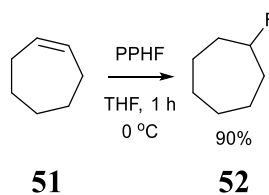

Figure 28 - Fluorination using Olah's reagent[89]

Late stage fluorination has obvious attractions, however; the ability to synthesise the non-fluorinated analogue and selectively fluorinate at a site would simplify the use of fluorinating reagents in organic synthesis. The main drawback with this strategy is the current reagents used for late stage fluorination are typically very expensive, have poor atom economy which results in a large generation of waste.

A famous laboratory scale reagent for such reactions is diethylaminosulfur trifluoride (DAST) **47**. The reagent typically works by substitution of alcohols within compounds to produce the fluorinated product or higher oxidation levels of alcohols to generate poly-fluorinated compounds. Much like the other previously described reagents, DAST is also a hazardous material due to the production of HF when in contact with water.[90]
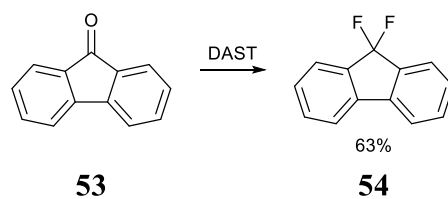
Figure 29 - An example of the use of DAST[90]

1.5.3.2 Electrophilic fluorination

Electrophilic fluorination strategies proceed using "F+" reagents and the most famous and widely used is Selectfluor[TM]. This compound is popular due to it being a solid, relatively selective and bench-stable. There are a myriad of examples of this reagent being used due to its commercial availability and versatility but drawbacks of the compound are the large amount of waste that is generated from the reactions since fluorine constitutes 5% by weight of the reagent.
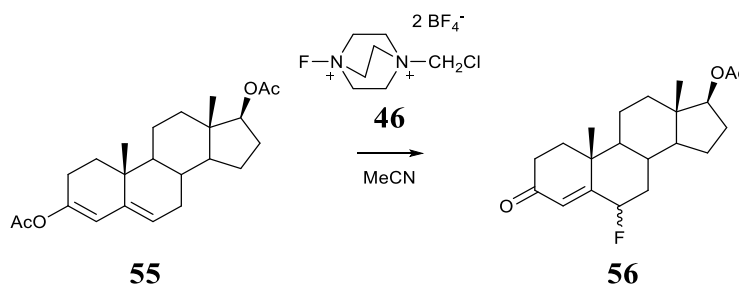
Figure 30 - Selective fluorination of testosterone enol diacetate using Selectfluor[91]

The most simple electrophilic fluorination strategy is direct fluorination using elemental fluorine gas. Similar to HF, this reagent is a highly corrosive gas meaning that storage and use can be difficult. In addition to this, reactions with F_2 are extremely exothermic and can lead to explosions if used without caution. The development of micro-reactors, coolers, appropriate solvents and flow controllers has allowed the use of fluorine gas in a safe and dependable manner. Perhaps the most famous example of this strategy historically is the synthesis of fluorouracil, one of the first fluorine-containing pharmaceuticals.
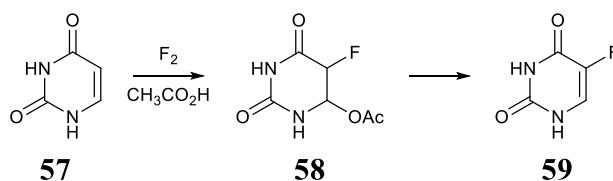
Figure 31 – Synthesis of 5-fluorouracil via direct fluorination[92]

1.5.4   Dialkyl 2-fluoromalonate esters

Diakyl 2-fluoromalonate has been previously discussed with regards to its use as an additive within a LIB, but the uses of the molecule spread much further. Due to the highly functionalised nature of the molecule, it can be readily used in building-block syntheses for generating fluorinated materials. Due to the importance of the molecule to the thesis, a small literature review follows and further details are contained in a recent review from Durham.[93]

1.5.4.1 Synthesis of 2-fluoromalonate derivatives

Historically there have been many different methods used by different groups to synthesise 2-fluoromalonate, the first of which was developed in the 1950's. Ethyl fluoroacetate **60** was added to a suspension of sodium hydride to deprotonate the α-hydrogen after which ethyl chloroformate was added dropwise and left to reflux overnight giving **27**.[94] Alternatively, a recent patent describes a similar process, through the use of DMC **1**, sodium methoxide and dropwise addition of **61** to give a higher yield of the methyl diester **62** with 98.5% purity.[95]
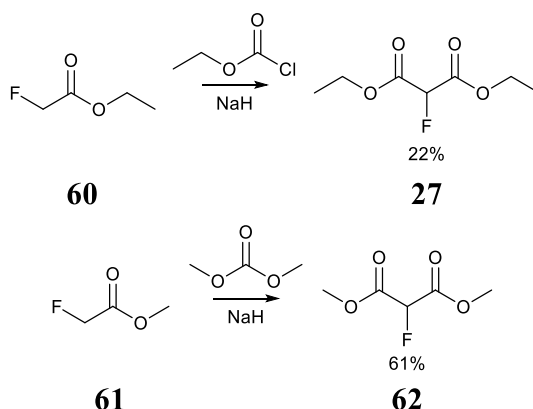
Figure 32 – (Above) The mechanism of the first synthesis of diethyl 2-fluoromalonate[94], (below) recently patented method of synthesis of **62**

Another method was patented by Bayer via halogen exchange using HF. The reaction simply consists of refluxing diethyl chloromalonate **63** and HF dissolved in trimethylamine at 110 °C for 15 hours and gives the product in 84% yield.[96]
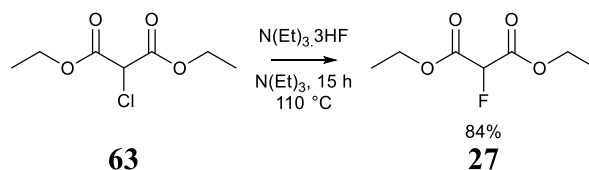

Figure 33 - Bayer's synthesis of **27**

A recent publication describes a different method of nucleophilic fluorination using HF through the use of diazomalonates **64**. By dropwise addition of **64** into neat HF, the diazomalonate is protonated, followed by rapid attack of a fluoride ion, eliminating nitrogen gas. The focus of the paper is on the generation of the cationic intermediate but reports high yields with good selectivity of monofluorinated product.[97]

64a (R = Me)   **62** (R = Me, 82%)
64b (R = Et)   **27** (R = Et, 84%)
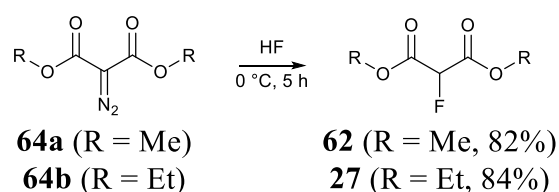
Figure 34 - Synthesis of dialkyl 2-fluoromalonates from dialkyl 2-diazo-malonates

Perhaps a more appealing method of synthesis, especially on larger scale, is the direct fluorination approach. The first approach devised using this method was achieved by directly fluorinating the trimethylsilyl-malonate derivative **65** which forces the malonate into the enol form. This yielded the product in moderate yields which could not be improved due to the large amount of difluorinated product formed.[98]
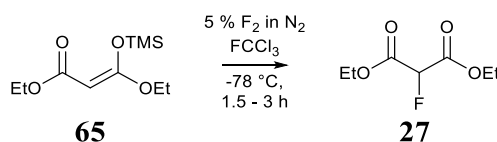
Figure 35 - First direct fluorination strategy used for the synthesis of dialkyl 2-fluoromalonate[98]

These results were improved upon with the work undertaken in Durham which utilised fluorine gas in the presence of a hydrated copper nitrate salt which acts as a catalyst. The malonate coordinates with the copper which encourages enolisation. This reaction was optimised to give excellent yields, minimalizing the generation of the difluorinated side product, giving high purity material without the need of further purification.[99] Limitations of this method are the possibility of fluorination on the alkyl side chain when the alkyl chains are not a methyl or ᵗbutyl groups.
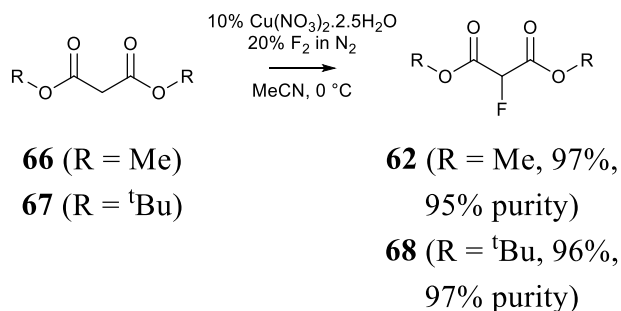
Figure 36 - Direct fluorination using fluorine gas and copper catalyst[99]

In addition to this, flow processes were developed for the synthesis of fluoromalonate for the use in up-scaled reactions. The problems associated with this method were fluorinations occurring on the side chains of the malonate system which decreased yield and proved problematic with regards to separation. This problem was overcome by the direct fluorination of Meldrum's acid **69** which could then could be separated easily and converted into the dialkyl ester upon stirring with the corresponding alcohol.[100]
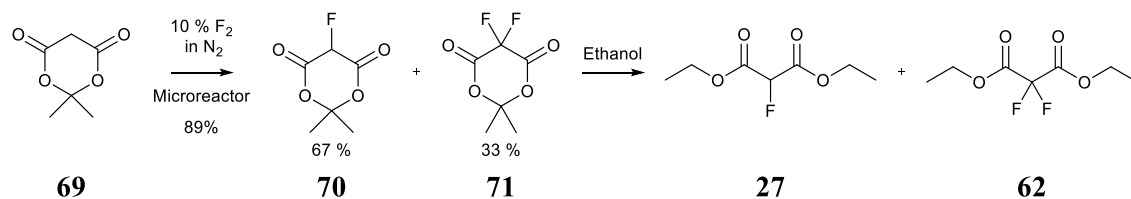
Figure 37 - Synthetic pathway for the flow synthesis of fluoromalonate via Meldrum's acid[100]

The different processes towards synthesising fluoromalonate come with advantages and disadvantages, especially depending on scale of use. Whilst fluorine gas is a highly reactive material that requires expensive equipment, the low atom economy is appealing to large scale industrial processes. Similarly, fluoroacetate, as previously discussed, is acutely toxic and provides problems of its own when preparing the synthesis.

1.5.4.2 Reactions of dialkyl 2-fluoromalonate esters

Diakyl 2-fluoromalonate is a multi-functional molecule which can be easily varied and changed with simple reactions and the chemistry was recently comprehensively reviewed[93]. Some recent literature reports only are described here to compliment the review. The diester moiety along with the acidic proton in the β-position affords a wide scope of chemistry, from both nucleophilic attack and a variety of carbonyl/enolate chemistry.

As to be expected, there are a myriad of examples of using di-alkyl 2-fluoromalonate to react with carbon electrophiles at the enolic site. One such example which showcases this, along with the use of fluoromalonate as a building-block type compound, is the synthesis of the carboxypeptidase U inhibitor **74**. Deprotonation using base, such as sodium hydride, gives the sodium malonate anion which can undergo S_N2 attack of alkyl halides.
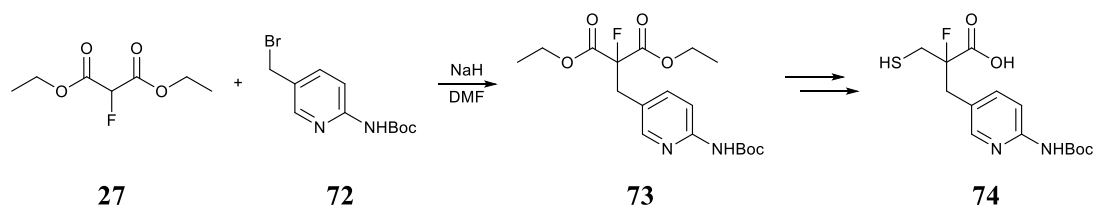

Figure 38 - Synthetic strategy for incorporating the fluorine into **74** using diethyl 2-fluoromalonate

Also, the synthesis of chiral systems has been explored through Michael addition reactions in the presence of a chiral catalyst. A recent publication has shown that the asymmetrical Michael addition shown in Figure 39 can be achieved in high yield and selectivity when undertaken in the presence of **76** and methyl acrylate.[101]
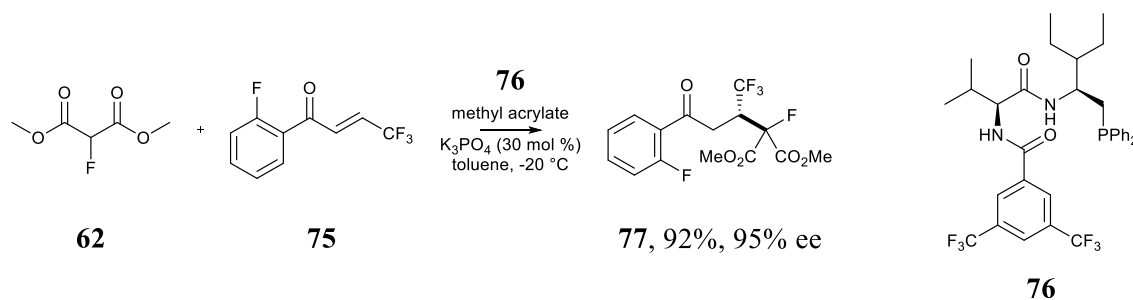

Figure 39 – Dimethyl 2-fluoromalonate in asymmetrical Michael addition

The diester moieties provide sites for a variety of different nucleophilic attacks and the reactivity of these ester groups can be tuned by varying the alkyl chains or functional group interconversion to the corresponding acid or acyl chloride. One example of utilising this strategy for the synthesis of complex structures is through the reaction of malonates with benzamidine **78** to generate the chloro-fluoro-phenylpyrimidine **80**, which are precursors to biologically active systems.[102]
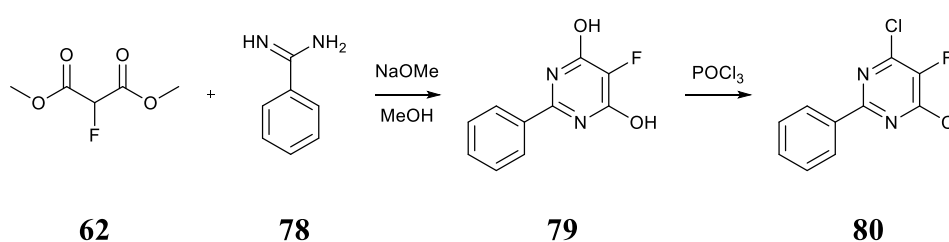
Figure 40 - Synthesis of fluorophenylpyrimidines **80** from fluoromalonate[102]

Another recent publication shows the versatility of dimethyl 2-fluoromalonate as a nucleophile in Mannich-type reactions. The reactions were demonstrated to show high yields, even with fused ring or sterically demanding structures.[103]
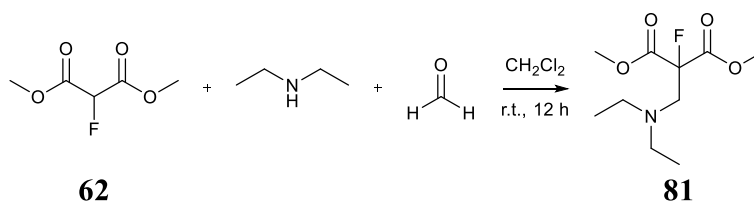
Figure 41 - Dimethyl 2-fluoromalonate can undergo Mannich-type reactions

A succinct example combining both nucleophilic and electrophilic attack on fluoromalonate can be seen in the use of diethyl 2-fluoromalonate in the synthesis of ethyl 3-fluoro-2-oxo-1,2,3,4-tetrahydroquinoline-3-carboxylate **84**. The diethyl 2-fluoromalonate is deprotonated with sodium hydride and reacted with 2-nitrobenzyl bromide. The resulting compound is then reduced and the amine group then attacks one of the ester groups to yield the fluorinated heterocycle.[104]
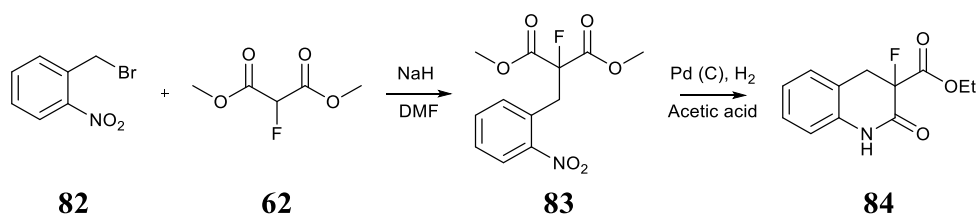
Figure 42 - The functionality of 2-fluoromalonate **62** is demonstrated in the synthesis of **84**[104]

1.5.5   Alkyl 2-fluoroacetoaceate

Another small fluorinated dicarbonyl compound that is of interest, and is available for a building-block strategy, is alkyl 2-fluoroacetoacetate. Another dicarbonyl compound, the chemistry is similar to that of fluoromalonate; the only minor changes are the higher degree of enol content which often increases reactivity when used as a nucleophile.

1.5.5.1 Synthesis of 2-fluoroacetoacetate

The strategies historically employed for synthesising ethyl 2-fluoroacetoacetate therefore closely follow that of fluoromalonate; the first reported synthesis required the use of ethyl fluoroacetate and acetyl chloride (Figure 43). But the method struggles from the similar issue of high levels of toxicity due to fluoroacetate.[94]
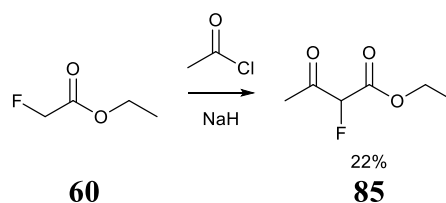
Figure 43 - First reported synthesis of **85**

Similarly, **85** can be synthesised from the chloro-substituent **86** and subjected to halogen exchange using TREAT.HF in acetonitrile. This is described in the same Bayer patent as the previously mention fluoromalonate synthesis, and the benefits of this strategy include the lack of difluorinated side product produced, but requires the use of corrosive HF.[96]
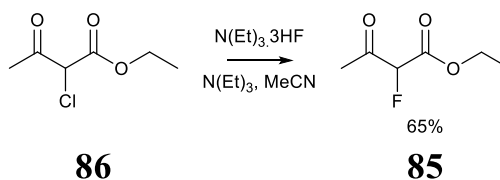
Figure 44 - Bayer synthesis of **85**[96]

The first recorded use of fluorine gas for the synthesis of **85** was using the trimethylsilyl enol ether **87**.[105] By locking the compound into the enol form, this minimalizes the amount of difluoro-impurity produced. The yield of 46% was improved upon in a later paper from Durham using microreactors and formic acid as a solvent; 99% conversion was reported with an isolated yield of 73%.[106]
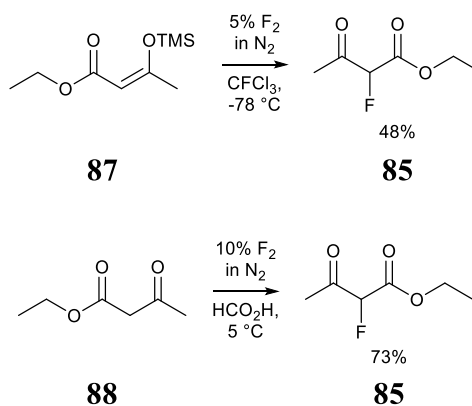
Figure 45 – (Above) first process using F_2,[105] (below) improved method from Durham[106]

A recent publication describes an alternative synthesis of **85** that hasn't been replicated for fluoromalonate using hypervalent iodine. This "apparent" electrophilic fluorination uses 10 equivalents of TREAT.HF with a slight excess of the iodine reagent to give the mono-fluorinated compound **85** as the major product.[107]
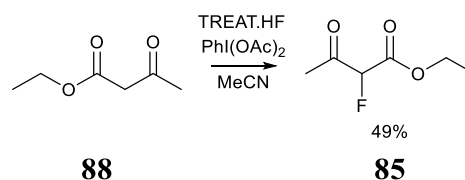

Figure 46 - Synthesis of **85** via hypervalent iodine chemistry

1.5.5.2 Reactions of 2-fluoroacetoacetate

Due to the structural similarity of 2-fluoroacetoacetate and 2-fluoromalonate, reactions are understandably very similar. The key difference is the unsymmetrical nature of alkyl 2-fluoroacetoacetate and no obvious leaving group on the ketone moiety.

The reaction of ethyl 2-fluoroacetoacetate **85** with acetimidine results in the formation of the fluorinated pyrimidine **89**. After attack of the amine at the ester, and subsequent elimination of ethoxide, cyclisation and elimination gives the final compound.
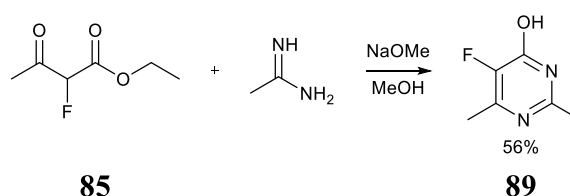

Figure 47 - Synthesis of **89** from ethyl 2-fluoroacetoacetate

Recent publications also describe Pechmann condensation type reactions that generate fluorinated heterocycles from fluoroacetoacetate. Acid-catalysed transesterification reaction, cyclisation and eventual elimination of water gives the fluorocoumarin derivative.[108]
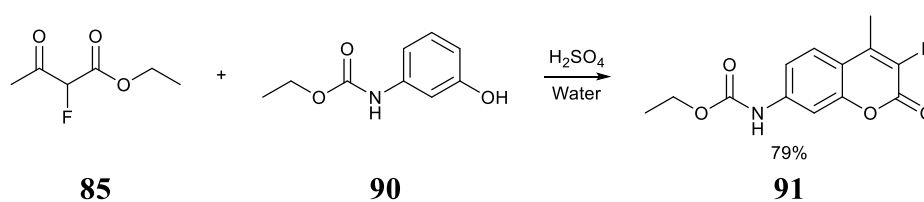
Figure 48 - Pechmann condensation using ethyl 2-fluoroacetoacetate

When used as a nucleophile, ethyl 2-fluoroacetoacetate can be used in Michael addition reactions. One example generates ethyl 2-fluoroacetoacetate **85** *in situ* and then followed by a Michael addition and Robinson annulation to generate the larger, complex fluorinated compound **93**. The presence of chiral catalyst **92** also resulted in high levels of enatiomeric excess and diastereromeric ratio.[109]
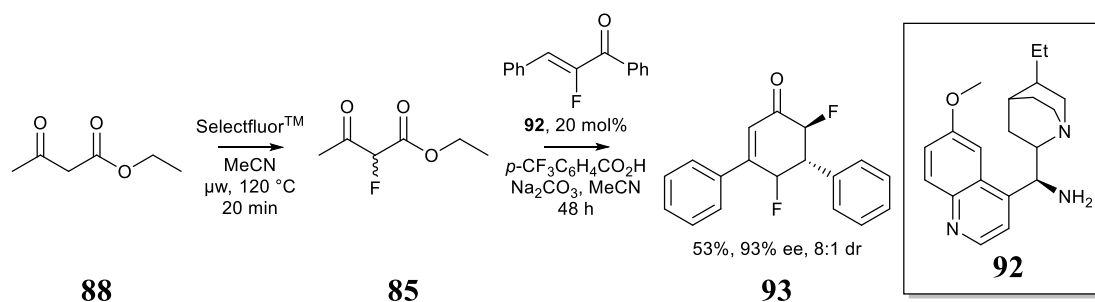

Figure 49 - A one pot synthesis using ethyl 2-fluoroacetoacetate to generate complex fluorinated compounds

1.6   Conclusion

Lithium-ion batteries dominate modern society due to their high energy density, higher potentials and their comparatively better cycleability. The batteries are used in many facets of modern society and their continuing improvement is important for future technologies and clean energy generation. The areas in which the battery can be improved upon are the subject of intense commercial interest around the world, especially towards additives. Additives can have a multitude of purposes within the battery but the ones with the most pronounced affect are those that shape and effect the solid electrolyte interphase layer that is formed within the battery. These layers are responsible for the protection of the electrodes, ensuring shelf-life and improving the stability of the overall cell.

One potential such avenue for new additives for lithium-ion batteries are small fluorinated organic compounds and several systems, including dialkyl 2-fluoromalonate derivatives, have been explored for use as additives in LIBs which will be discussed within this thesis.

Chapter 2

Fluoromalonate derivatives as battery electrolytes

2.1   Aims

As discussed in the introduction chapter, fluoromalonate derivatives have been used as additives in LIB electrolytes. The aim for this project is to develop the use of fluoromalonate derivatives for electrolyte additives to assess how differing structural features affect LIB performance.

R = Me, Et, ^{i}Pr, ^{t}Bu,
CH$_2$CF$_3$, CH$_2$CH$_2$CF$_2$CF$_3$
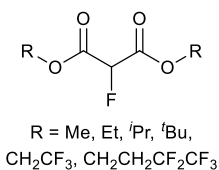
In the first instance, variation to the ester alkyl group will be probed. Through the comparison of primary, secondary and tertiary alkyl esters to probe electronic and steric effects upon additive performance. In addition to this, the effect of fluorinated side chains will be studied to see what, if any, electron withdrawing or donating effects have upon battery performance.

R$_3$ = alkylation or Michael
addition products
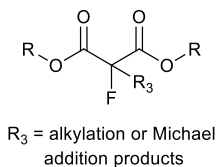
The effect of functionalisation at β-position of the fluoromalonate additive upon LIB performance was will be investigated, through the generation of compounds via Michael addition and alkylation reactions.

To effectively probe the effects of these structural changes, non-fluorinated compounds shall also be tested as control samples. As compound isolation and purification for LIB testing was the main aim of this project, yields of reactions were not of particular importance and therefore full reaction optimisation was not always undertaken once sufficient material for LIB analysis had been collected.

2.2   Project information

The results discussed within this project can be split into two categories; the synthetic strategies towards the preparation of target additives and the results of subsequent battery testing. This first chapter will describe the work that was undertaken in collaboration Sony MSL based in Stuttgart. The synthesis was undertaken in Durham and the battery analysis, unless specified, was undertaken by the author in Sony Materials Sciences Laboratories (MSL) in Stuttgart, in collaboration with scientists from Sony whilst on placement for two periods of two weeks.

2.3   Additive synthesis and purification

2.3.1   Control compounds

At the outset of this project, certain non-fluorinated compounds were purchased and purified to be control substrates and allow comparisons of how different functional groups perform in LIB battery testing. Compounds **66, 88, 94, 95 and 96** were all purified by vacuum distillation to high purity by ^{1}H and ^{19}F NMR spectroscopy and GCMS analysis.
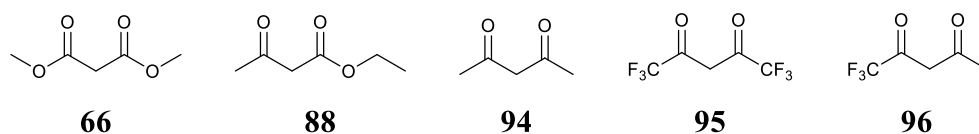

Figure 50 - Dicarbonyl structures purchased for battery testing

2.3.2   Fluorination of dimethyl malonate

Dimethyl 2-fluoromalonate **62** was required for testing as a battery electrolyte additive and also as the starting material for the synthesis of families of related systems. Fluorination of dimethylmalonate was carried out using the literature process optimised at Durham.[99]
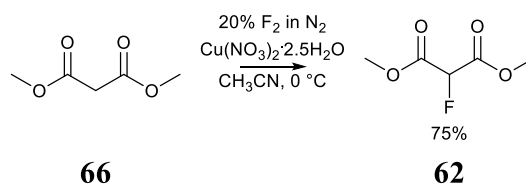
Figure 51 - Synthesis of dimethyl 2-fluoromalonate[99]

This reaction was repeated several times throughout the project on large scale (approximately 40 g) and routinely gave a high yield of monofluorination product **62**. To ensure high purity for battery analysis, purification was carried out using Fischer spahltrohr microdistillation equipment.

2.3.3   Transesterification reactions

To access compounds to allow investigations into the effect of alkyl side chains upon additive battery performance, transesterification reactions were undertaken. It was hoped that a general method could be developed to allow a wide scope of different products without the need of direct fluorination. As is seen in the literature, fluorination of dialkyl malonates, with the exception of dimethyl malonate and di-*tert*-butyl malonate, often lead to side-chain fluorination side products and consequently, transesterification of dimethyl 2-fluoromalonate was thought to be a better synthetic approach.[110]

2.3.3.1 Diethyl 2-fluoromalonate

The first reaction attempted was the simplest transesterification possible, starting with **62** (dimethyl 2-fluoromalonate) to generate **27** (diethyl 2-fluoromalonate). The reaction was first attempted using *p*-toluenesulfonic acid (tosic acid) as the acid catalyst and, after 9 hours of refluxing in ethanol at 90 °C, the reaction mixture was concentrated and worked-up.
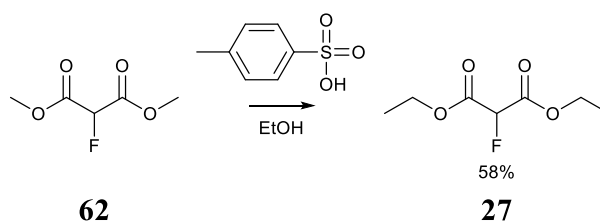
Figure 52 - Reaction scheme for the synthesis of **27**

The crude product showed a 99%+ conversion with trace amounts of tosic acid and therefore the reaction mixture was vacuum distilled to provide **27** in 58% yield. The spectroscopic data was consistent with that of literature values.[110]

2.3.3.2 Transesterification reactions using 2,2,2-trifluoroethanol

Analogous transesterification reactions of **62** and **66** were attempted using 2,2,2-trifluoroethanol. The two reactions were set up using the same conditions as the previously successful transesterification reaction described above; refluxing at 90 °C in the presence of tosic acid catalyst and excess alcohol and the reaction monitored by GCMS.

66, (X = H)   **97**, (X = H)
62, (X = F)   **98**, (X = F)
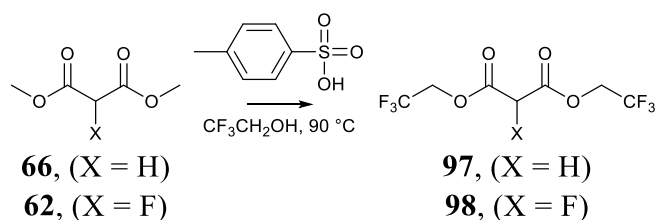
Figure 53 – Tosic acid catalysed reaction scheme for synthesis of **97** and **98**

This showed partial conversion in both reactions; the presence of three peaks in the gas chromatogram corresponding to the starting material, the mono-substituted and di-substituted products, but the reaction could not be driven further.

Consequently, a second strategy for transesterification using basic conditions was attempted by adding sodium to the trifluoroethanol to form the corresponding sodium salt and, thereby, enhancing the nucleophilic strength. However, this reaction was also unsuccessful due to the formation of many side-prodcuts.

66, (X = H)   **97**, (X = H)
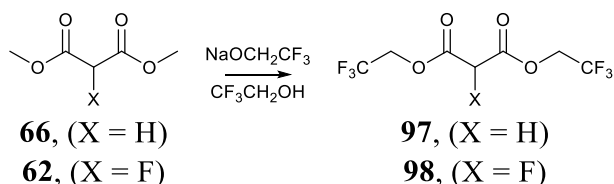**62**, (X = F)   **98**, (X = F)

Figure 54 – Reaction scheme of basic synthesis of **97** and **98**

The synthesis of the bis(2,2,2-trifluoroethyl) malonate **97** was finally achieved by carrying out the reaction in an inert atmosphere, starting from malonic acid **99** as opposed to the ester and using a different solvent with only approximately five times the excess of the 2,2,2-trifluoroethanol, adapting literature conditions.[111]
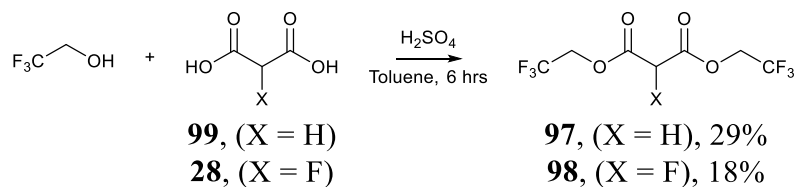

Figure 55 – Synthesis of **97** and **98**

The reaction gave successful conversion to the diester product and, after purifying via vacuum distillation, gave bis-(2,2,2-trifluoroethyl) malonate **97** in a 29% yield.
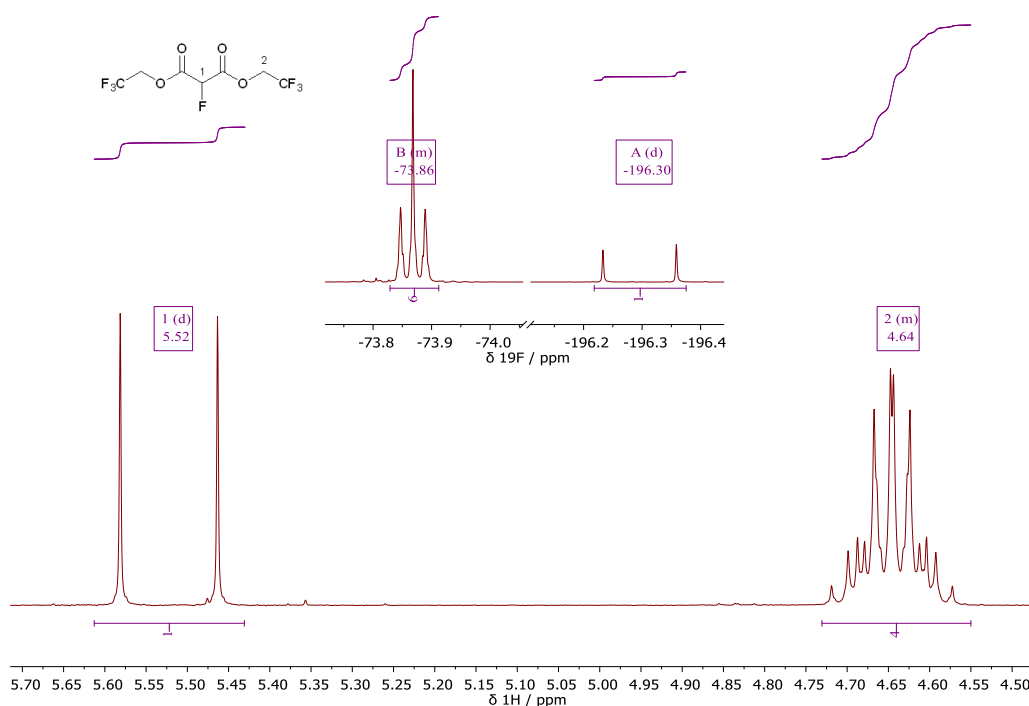
Figure 56 - ^{1}H NMR spectrum of **98**, (inset) ^{19}F NMR spectrum of **98**

With the success of this reaction, a similar process was attempted using fluoro-malonic acid **28** which was prepared from diethyl 2-fluoromalonate **27** using lithium hydroxide in water and ethanol following literature conditions.[112] This successfully yielded bis(2,2,2-trifluoroethyl) 2-fluoromalonate **98** in 18% yield. The yields and reaction conditions

reflect the poor nucleophilic nature of 2,2,2-trifluoroethanol but sufficient material could be isolated for LIB analysis.

2.3.3.3 Transesterification reaction using 3,3,4,4,4-pentafluorobutanol

Following on from the successful transesterification using 2,2,2-trifluoroethanol, similar reactions were attempted using 3,3,4,4,4-pentafluorobutanol.
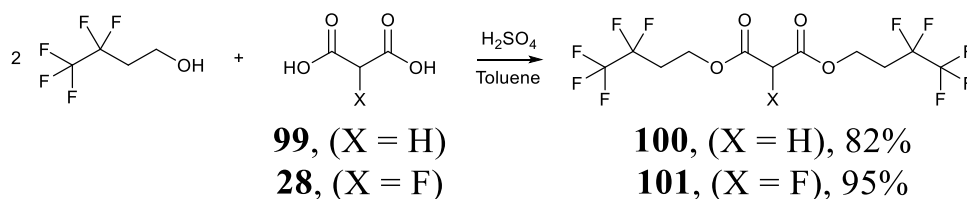

Figure 57 - Reaction scheme for the transesterification reaction using 4,4,4,3,3-pentafluorbutanol

This reaction was attempted using fluoromalonic acid and malonic acid concurrently and was successful providing, after purification by vacuum distillation, bis(3,3,4,4,4-pentafluorobutyl) 2-fluoromalonate in 95% yield and bis(3,3,4,4,4-pentafluorobutyl) malonate in 82% yield respectively. The higher yield of these transesterifications using 3,3,4,4,4-pentafluorobutanol compared to 2,2,2-trifluoroethanol reflect the higher nucleophilicity of the former system due to the presence of CH_2 groups between the perfluorinated part of the molecule and the nucleophilic oxygen site.
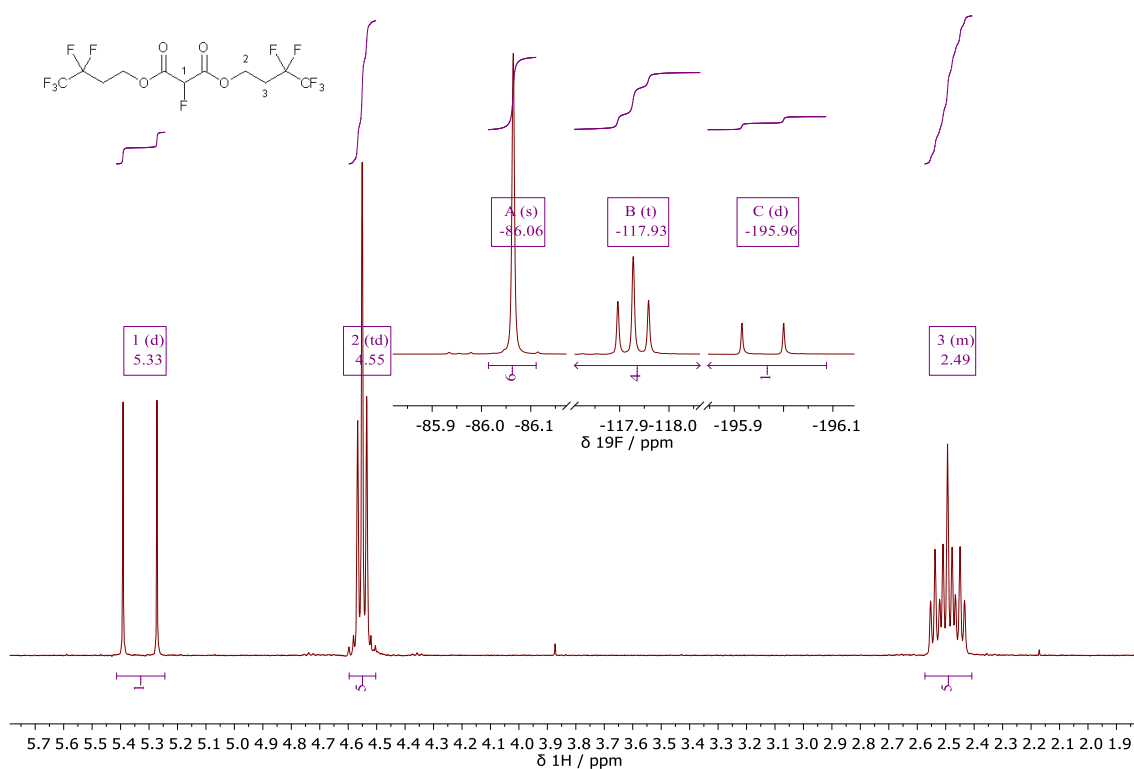
Figure 58 - ^{1}H NMR spectrum of **101**, (inset) ^{19}F MR spectrum of **101**

2.3.4   Michael addition reaction

Dimethyl 2-(2-cyanoethyl)-2-fluoromalonate was synthesised from dimethyl 2-fluoromalonate via a Michael addition using acrylonitrile. Following a literature procedure from Durham,[113] the reaction was undertaken on a small scale using dimethyl 2-fluoromalonate and an excess of acrylonitrile.
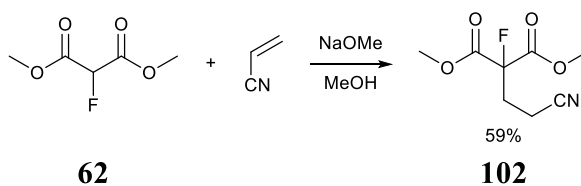

Figure 59 - Synthesis of dimethyl 2-(2-cyanoethyl)-2-fluoromalonate[113]

Reaction conditions had to be screened, by variation of temperature, reaction time and reagent ratios, to give a product mixture which contained minimal side products. Eventually, purification by vacuum distillation yielded pure dimethyl 2-(2-cyanoethyl)-2-fluoromalonate **102** which was consistent with spectroscopic literature values.[113]

2.3.5   Trifluoromethylation reactions

The electrophilic trifluoromethylating reagent chosen for the attempted synthesis of the β-substituted trifluoromethylated malonate system was an Umemoto reagent (Figure 60).[114] These compounds are (trifluoromethyl)-dibenzoheterocyclic salts with the trifluoromethyl group bonded to a positively charged sulfur, selenium or tellurium atom.
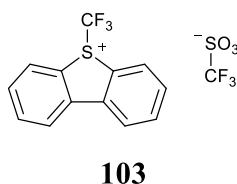

103

Figure 60 - Structure of the Umemoto reagent used in the trifluoromethylation reactions

Adapting literature conditions,[114] dimethyl malonate was deprotonated by sodium hydride in THF and added to the Umemoto reagent. The reaction mixture was stirred at room temperature for 21 hours but the reaction showed no product by ^{19}F NMR.

66   **104**
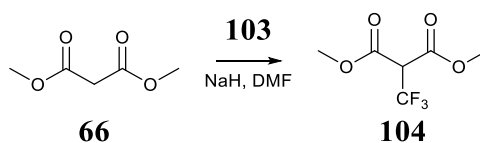
Figure 61 - Reaction scheme for the trifluoromethylation of dimethyl malonate

Repeats of the reaction only showed small amounts of product present by ^{19}F NMR spectroscopy. It was hypothesised that the formation of a trifluoromethyl group adjacent to an acidic proton allowed the decomposition of the compound via the elimination of HF. To prevent this degradation pathway, the reaction was adapted by using dimethyl 2-methyl malonate.

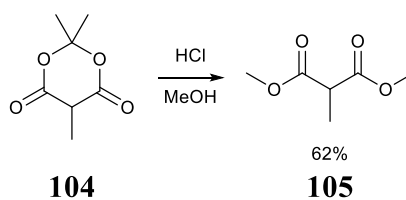**104**   **105**

Figure 62 - Synthesis of **105**

Dimethyl 2-methyl malonate **105** was prepared from a sample of 2,2,5-trimethyl-1,3-dioxane-4,6-dione (methyl Meldrum's acid) **104** by dissolving the starting material in methanol with a couple of drops of catalytic hydrochloric acid. This was stirred under reflux for 6 hours until 100% conversion was achieved, as monitored by ^{1}H NMR. After work-up, the sample was purified by vacuum distillation to give a 99%+ purity product in a 62% yield.

Trifluoromethylation of dimethyl 2-methyl malonate was followed by ^{19}F NMR but despite numerous repeats, only a complex mixture of products was observed. Similar systems in the literature produced only modest yields and this approach was abandoned given the possible instability in LIB devices.[114]

2.3.6   Fluoro-Meldrum's acid synthesis

The synthesis of Meldrum's acid **69** was attempted to develop conditions to synthesise the fluorinated analogue. A literature procedure was followed, starting with malonic acid **99**.[115]
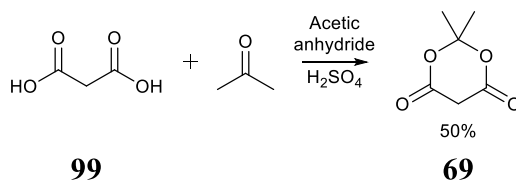
Figure 63 - Synthesis of Meldrum's acid

Stirring **99** and acetic anhydride at 0 °C, concentrated sulfuric acid was added followed by the dropwise addition of acetone and left to stir for 2.5 hours. The reaction mixture was then left in the fridge overnight which precipitated pure white crystals of Meldrum's acid in 50% yield.

The literature conditions were then adapted for the use of 2-fluoromalonic acid **28** but no products were observed by ^{19}F NMR after the same reaction conditions.
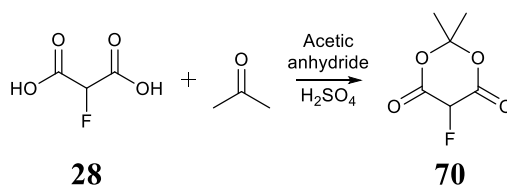
Figure 64 - Synthetic strategy for the synthesis of fluoro-Meldrum's acid

The reaction conditions were changed to try detect the product but every attempt resulted in no isolated product. A different strategy was undertaken using Selectfluor[TM] and fluorinating Meldrum's acid.
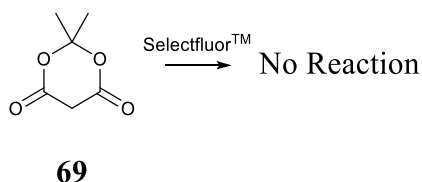

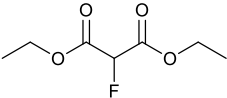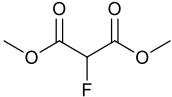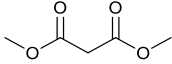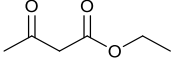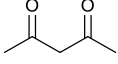Figure 65 - The second synthetic strategy for the synthesis of **70**
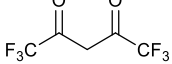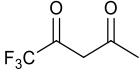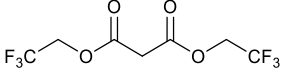
However, stirring **69** (Meldrum's acid) with Selectfluor[TM] in acetonitrile without base showed no product by ^{19}F NMR spectroscopy, despite high enol content of the starting material. The use of sodium hydride, Selectfluor[TM] and THF also showed no product. Finally, conditions listed in a patent were followed multiple times,[116] using dry acetonitrile at -40 °C showed the presence of a small amount of product by ^{19}F NMR which could not be isolated.
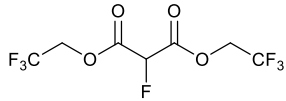
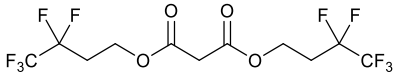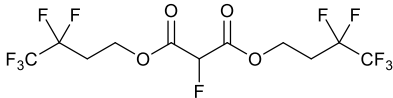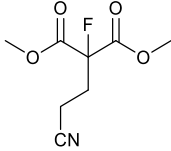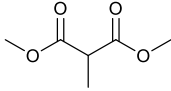Whilst examples of making fluoro-Meldrum's acid *in* situ are reported, the isolation of the compound is not reported in the literature. The viability of these compounds within LIBs, given their instability, is questionable and, as such, attempts to synthesise these compounds were abandoned.

2.3.7   Compounds analysed

In total, 13 compounds were analysed as LIB additives as listed in Table 2

Table 2 - A summary of the samples assessed for LIB additive analysis

Sample Name	Sample Number	Sample Structure
Diethyl 2-fluoromalonate	**27**	
Dimethyl 2-fluoromalonate	**62**	
Dimethyl malonate	**66**	
Ethyl acetoacetate	**88**	
Acetylacetone	**94**	
Hexafluoro-acetylacetone	**95**	
1,1,1-trifluoro-2,4,-pentadione	**96**	
Bis(2,2,2-trifluoroethyl) malonate	**97**	

Bis(2,2,2-trifluoroethyl) 2-fluoromalonate	**98**	
Bis(4,4,4,3,3-pentafluorobutyl) malonate	**100**	
Bis(4,4,4,3,3-pentafluorobutyl) 2-fluoromalonate	**101**	
Dimethyl 2-(2-cyanoethyl)-2-fluoromalonate	**102**	
Dimethyl 2-methyl malonate	**105**	

2.4   Electrochemical testing

The tests were undertaken using EL-CELL cells at Sony MSL laboratories, which collect data on each independent electrode, as well as the overall cell. The data was obtained from cycling the cells to full charge and complete discharge. In each of these tests, a reference cell (labelled "Ref") is made which measures battery performance without an additive.

2.4.1   Introduction

The type of battery structure used to undertake these tests were split cells (Figure 66) consisting of a glass fibre separator which is soaked in the electrolyte. On one side of the separator is the anode which has a copper current collector with graphite on the side facing the separator. On the other side, is the cathode which has lithium cobalt oxide facing the separator, placed upon an aluminium current collector (Figure 67 and Figure 68). Finally,

there is a lithium metal ring around the outside of the separator which can be used as a reference during electrochemical testing. The split cells are useful for initial tests as the layered materials can be separated after battery tests to allow studies of the electrode surfaces.
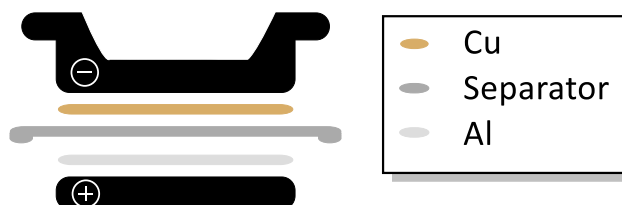

Figure 66 – Basic arrangement of the split cell
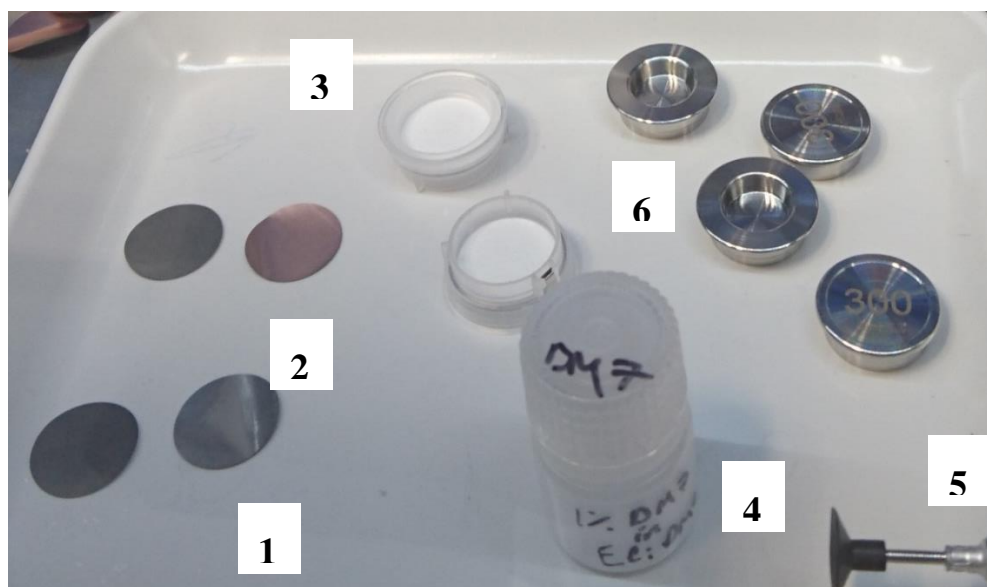
Figure 67 – The components of a split cell used for initial battery tests at Sony MSL; 1 the aluminium-backed, lithium cobalt oxide electrode; 2 the copper-backed, graphite electrode; 3 the glass wool separator with lithium reference; 4 the electrolyte with 1% additive by volume; 5 the base of the cell which holds the aluminium electrode in place; 6 the cap of the cell which is placed on top of the copper electrode and held down with an internal spring inside the cell

Figure 68 – The assembly of the split cell; 1 the aluminium electrode within the separator and the base on top; 2 the copper electrode within the separator; 3 the cell within the base with the top placed upon it; 4 the EL-CELLS fully assembled within the climate controlled testing chamber
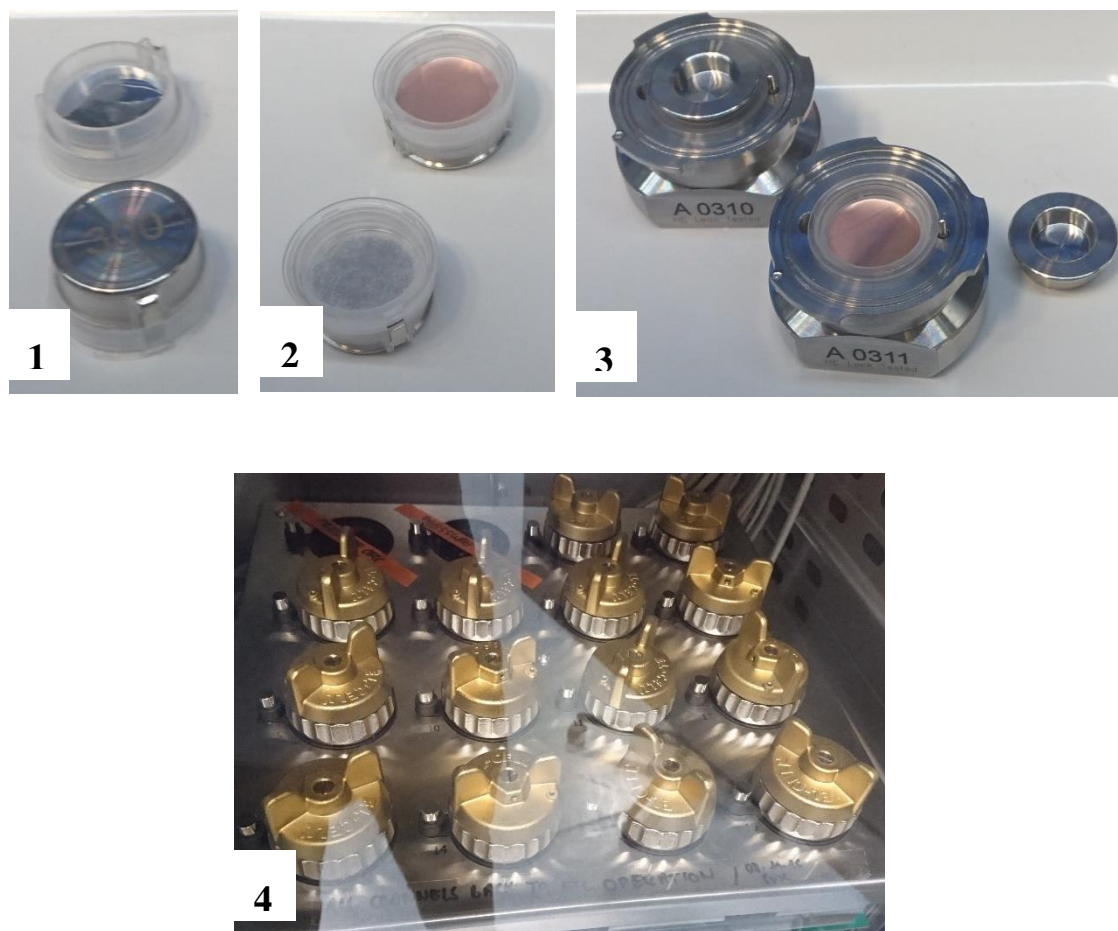
The cells consisted of a lithium cobalt oxide cathode, graphite anode and the electrolyte. The electrolyte consisted of 1 molar $LiPF_6$ in a 3:7 ratio of ethylene carbonate and dimethyl carbonate solution with 1% by volume of additive.

At this stage of the project, compounds were being tested for all functionality within a LIB, therefore various aspects of battery performance were analysed. The additives were assessed for rate capability, cyclic stability, capacity retention, coulombic efficiency and Electrical Impedance Spectroscopy. Each experiment includes a brief explanation of the technique and referenced to an electrolyte solution that did not contain any additive, labelled Ref. The data is then collectively cross-referenced in 2.4.8.

2.4.2   Rate capability

The rate capability is a measure of power density and is studied, in these tests, when subjected to different C-rates. The C-rate is a measure of how quickly a battery is charged or discharged with regards to its maximum capacity and normalised to one hour (i.e. 1C means the battery is discharged or charged within one hour).

Throughout these tests, the first charges and discharges are performed at slower rates to ensure the most efficient intercalation of the lithium ions in the cell. It is worth noting, however, that the rate at which discharging occurs typically has a larger effect on the capacity of a cell in comparison to the charging.
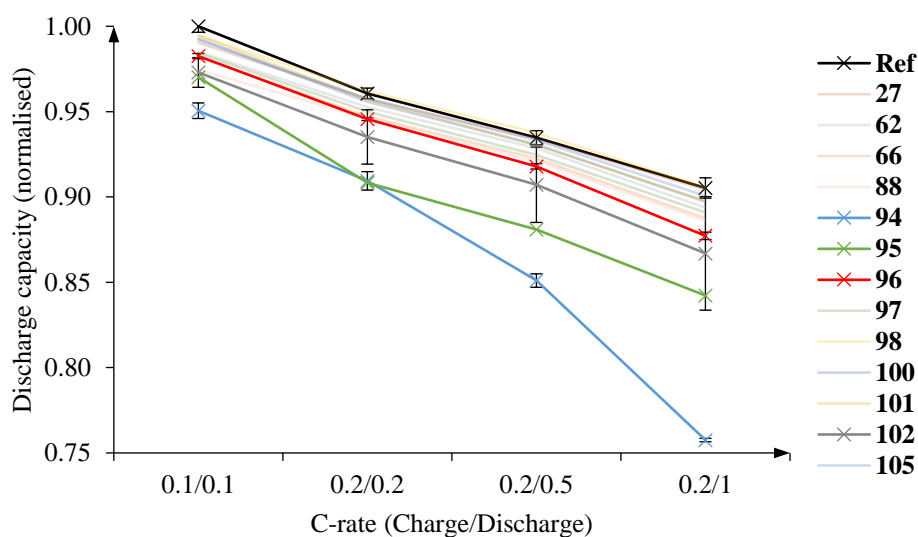

Figure 69 - Rate capacity tests of the graphite//LCO cells

The data suggests that most additives have a small detrimental effect on the rate capabilities compared to the reference sample, with the exception of four samples **94, 95, 96** and **102** which were significantly worse. Diketone **94** is the most detrimental to battery

capacity.

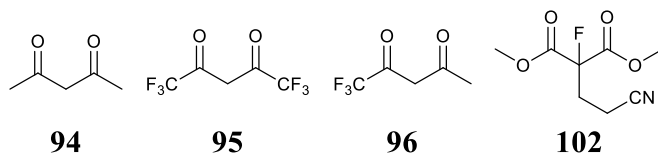**94**   **95**   **96**   **102**

Figure 70 - Additives which perform the most poorly in the rate capacity tests

It's interesting to note that all the diketone compounds tested performed to a lower standard than the esters. In addition to this, the only compound that is di-substituted in the β-position performed marginally worse in comparison to other compounds.

2.4.3   Cyclic stability

The cyclic stability tests are a continuation of the rate capability tests. This shows the average discharge capacity for each cycle and is a measure of how well the battery can perform practically. To get a more accurate understanding of the long term performance of these additives within LIBs, a much longer experiment is required, typically using different types of cells, such as coin cells. Despite this, tests of 15 cycles give an early indication of performance. The first five cycles were run using variable conditions (described in the experimental) and after this, each charge and discharge cycle is 1C.
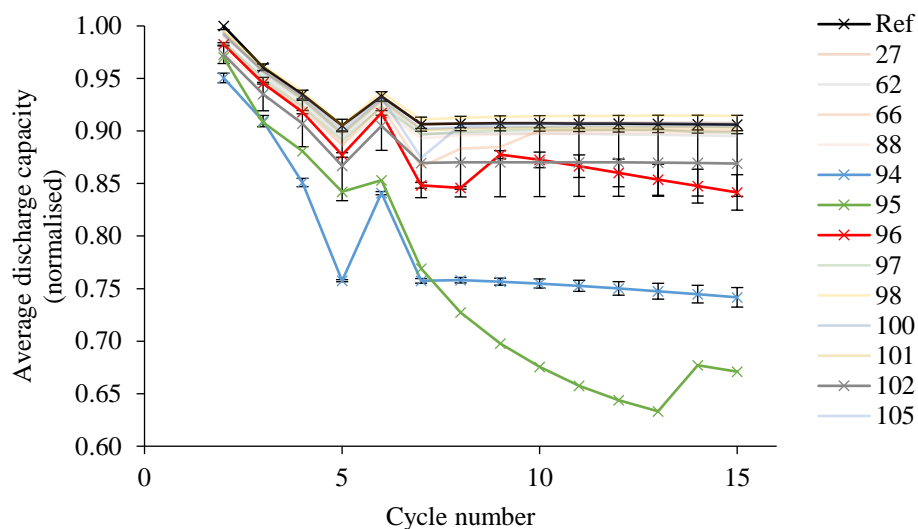
Figure 71 - Cyclic stability tests of the split cells

The tests (Figure 71), whilst showing irregularity in the first 6 cycles because of the previously mentioned, differing charging and discharging cycles, all show that most of the samples performed similarly to the reference cell, with the exception of **94**, **95, 96** and **102**. This result is perhaps unsurprising given the rate capability tests, but suggests that these compounds are, indeed, having a negative effect on the battery system. Longer lasting effects upon battery life cannot be drawn upon these results alone, since only 15 cycles were assessed, which is significantly smaller than that of a practical LIB lifespan. However, **94**, **95, 96** and **102** can be dismissed as useful additives at this early stage.

2.4.4   Capacity retention

Capacity retention is found by measuring the percentage of the capacity stored by the battery after 15 cycles, compared to the first. This value is also a measure of how little the battery degrades through repeated cycling.
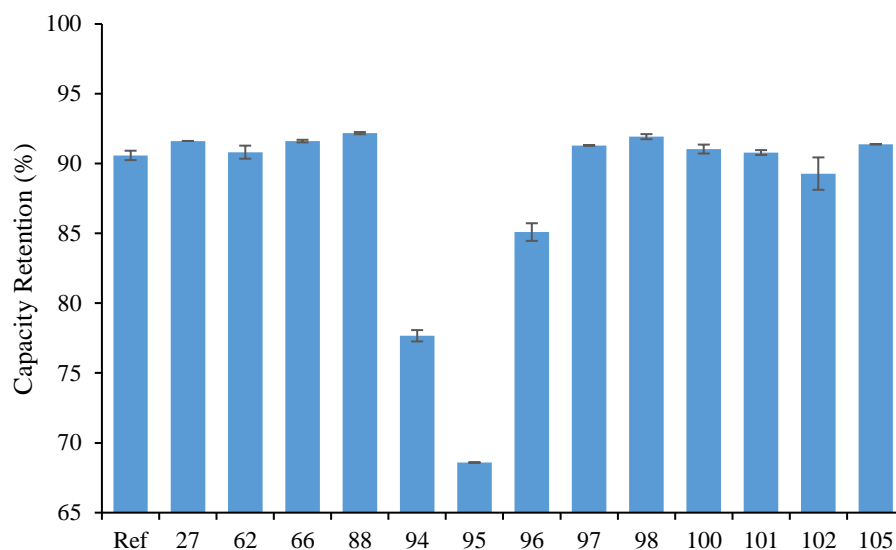
Figure 72 - The capacity retention of the split cells

The results of these tests are mostly in agreement with the cyclic stability tests with respect to **94**, **95** and **96** which perform worse than the other additives. The **102** doped battery, despite performing badly in the cyclic stability tests, is comparable to the reference with regards to capacity retention. Some additives performed slightly better than the reference, namely **27**, **66**, **88**, **98** and **105** whilst the remaining samples are comparable.

2.4.5   Coulombic efficiency

The coulombic efficiency (CE) is the ratio between the charge capacity of the battery and discharge capacity of the battery after full charge. Typically, coulombic efficiency is an indicator of the degree of side reactions that occur within a cell; the lower the efficiency on the first cycle, the more side reactions are occurring. The coulombic efficiency of a cell typically increases with each successive cycle and a higher value reflects better reversibility of lithium ion insertion within a cell.
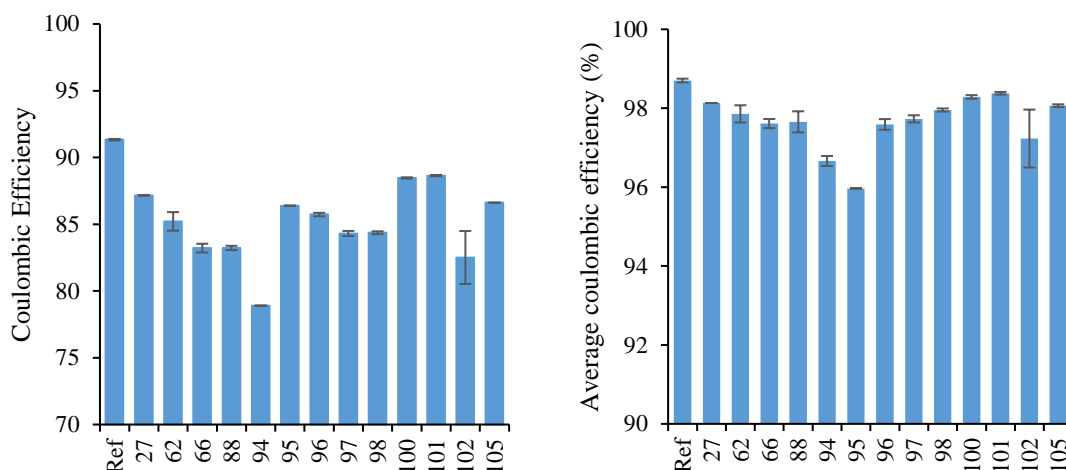
Figure 73 - Coulombic efficiency of the first cycle of the split cells (left) and the average coulombic efficiency (right)

The coulombic efficiency of the graphite cells was found to be lower than the reference cell on first charge which is consistent to that expected and due to degradation of the additives to potentially form an SEI. Importantly, the average coulombic efficiency of the cells after fifteen cycles was comparable to the reference values, showing good reversibility of lithium ion insertion in these cells.

2.4.6   dQ/dV with respect to voltage

When voltage of a LIB is plotted against the charge, it gives a characteristic curve yielding information about the voltage output with respect to the level of charge in the battery. The derivative of this graph, however, reveals information about chemical changes within the cell, from side reactions to phase transitions. By comparison to a reference cell side reactions can be indicated, hinting towards SEI formation.
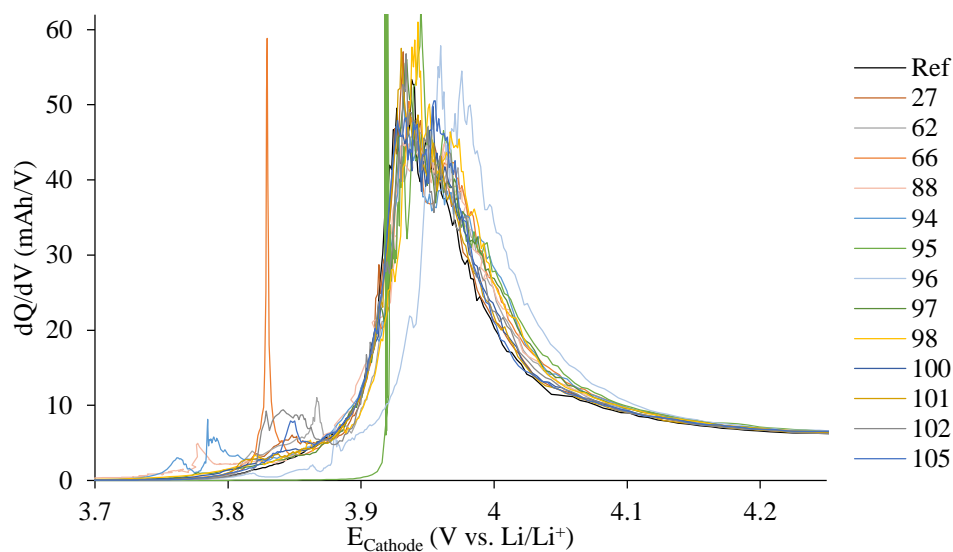
Figure 74 - dQ/dV plotted against the potential of the cathode of the first charge of all samples
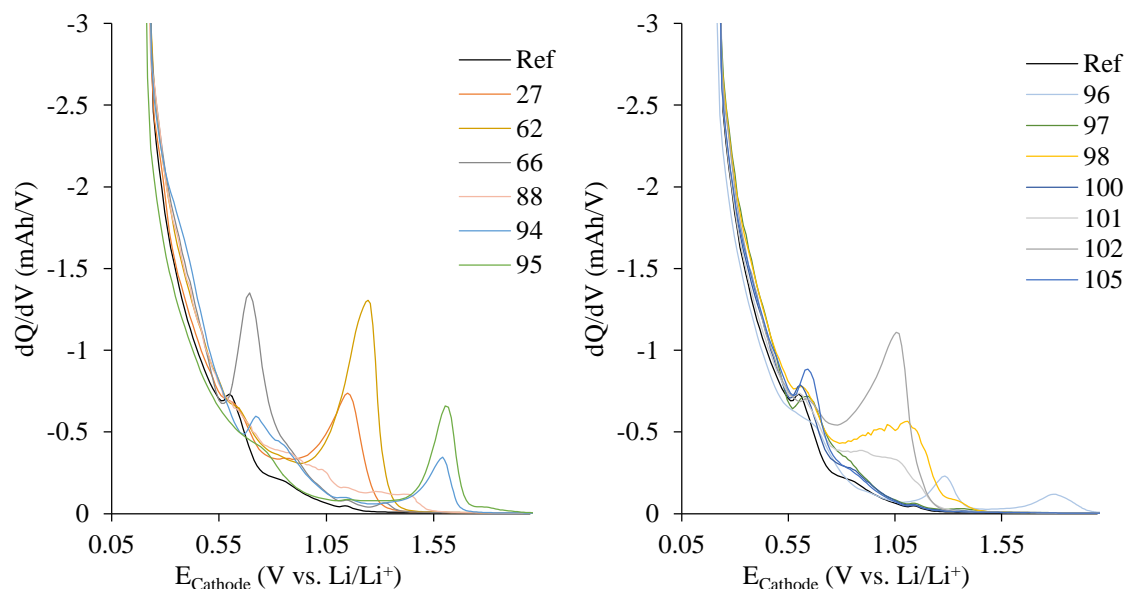

Figure 75 – Expansion of dQ/dV plotted against the potential of the cathode over the first charge of all samples

The results of the cell cathodes are in agreement with the major oxidation reaction in the cell; the lithium de-intercalating from the lithium cobalt oxide. In addition to this reaction there are other oxidative side reactions occurring in the cells that contain additives.

An expansion of the potential centred around 3.85 V show that all samples differ from the reference in this region, likely due to formation of an SEI. Interestingly, samples **97**, **98**, **100** and **101** (fluorinated dialkyl malonates), show a somewhat muted degree of

reaction in comparison to other additives, as shown by smaller oxidation peaks of these samples.
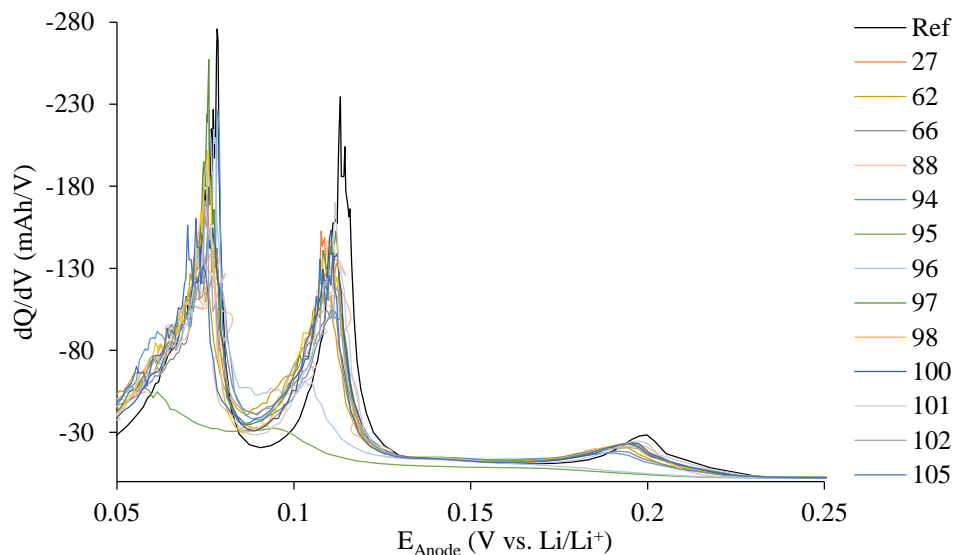

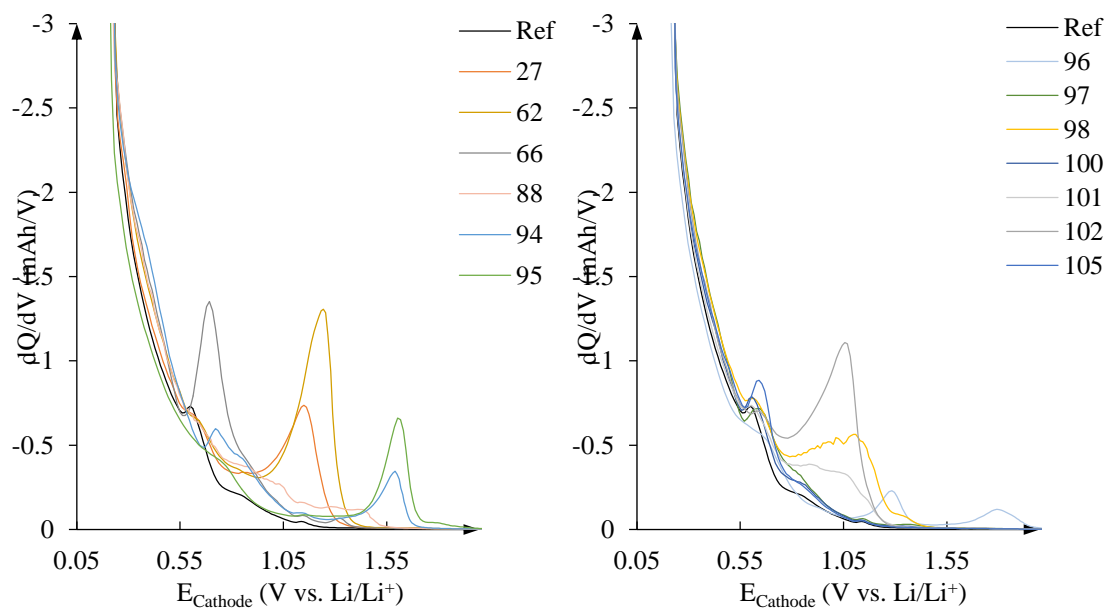Figure 76 – dQ/dV plotted against the potential of the anode of the first charge of the split cells

Figure 77 - dQ/dV plotted against the potential of the anode of the first charge of the split cells

In general, the anodes of the split cell tests show a good agreement with regards to the main reduction peaks; the intercalation of the lithium ions into the graphite sheets. The

exceptions to this are **95** and **96** which show suppressed peaks, the precise reason for which is not clear.

Interestingly, there are additional peaks at a higher potential, suggesting that additional reduction reactions are occurring. Whilst appearing more pronounced in some cases, all samples show the presence of these peaks. These are not present in the control sample, suggesting reactions of the additive upon the anode, probably leading towards the formation of the SEI.

The plots of both the cathode and anode show no further reactions after the discharge of the cell, reinforcing the hypothesis that reactions of the additives are contributions to SEI formation.

2.4.7   Electrical impedance spectroscopy

In an ideal system, placing a current with a potential results in resistance. In real world applications, the assumptions of Ohm's law, such as resistance being independent of frequency and current and voltage being in phase, don't apply and so the more general term impedance is used.

Electrical impedance spectroscopy (EIS) shows the impedance of a system by placing a sinusoidal potential over a cell and measuring the current produced. Since potential and current are dependent, the current produced is also sinusoidal. It has the same frequency of the potential but having a phase difference. Using Ohm's law, expressing both potential and current as a function of time, the impedance can be found using Equation 19, where ϕ is the phase shift and Z_0 is the magnitude. Using Euler's relationship (Equation 20), it's possible to express both the current and potential as complex functions which simplifies to the complex expression of impedance (Equation 21). Plotting the imaginary parts of this equation against the real parts of the equation, known as a Nyquist plot, can hint towards processes within a cell and, despite some debate over the exact processes, can indicate the formation of a SEI within a cell.

$$Z = \frac{E_t}{I_t} = \frac{E_0 sin(\omega t)}{I_0 sin(\omega t + \phi)} = Z_0 \frac{sin(\omega t)}{sin(\omega t + \phi)} \tag{19}$$

$$e^{ix} = cos\,x + isin\,x \tag{20}$$

$$Z = \frac{E_t}{I_t} = \frac{E_0 e^{i\omega t}}{I e^{i\omega t} e^{-i\phi}} = Z_0 e^{i\phi} = Z_0(cos\,\phi + i\,sin\,\phi) \tag{21}$$
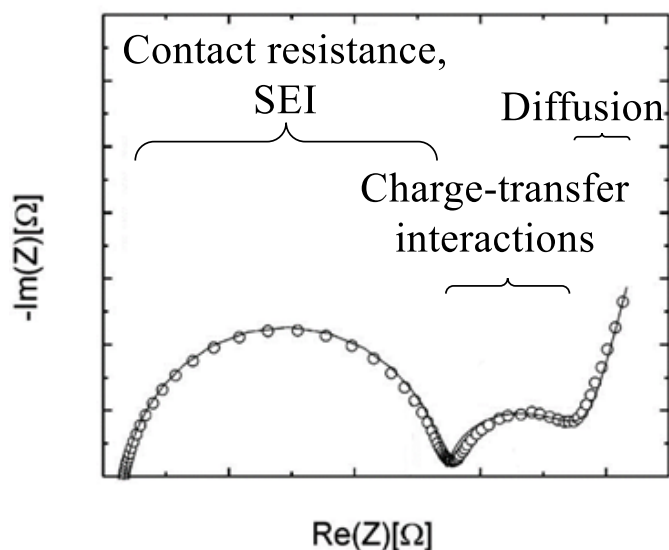

Figure 78 - Typical Nyquist plot of a lithium-ion battery[117]

The plot generated gives no information about the frequency of the experiment but gives information on the processes that take place independent of it. The different regions of the plot give different information about the impedance within a cell. The slope on the right hand side of the graph is impedance due to diffusion of lithium ions within a cell. The hump in the middle of the line is typical of charge transfer-type interactions, such as lithium ions leaving the electrolyte solution. The hump on the left hand side is impedance caused by contact resistance such as lithium ions having to pass through an SEI. The gap between the curve and the y axis is attributed to Ohmic losses which are internal resistance, intrinsic to all real cells. Comparison of these graphs can hint as to what happens within a cell at different times of its charge cycle.

An EIS is taken before the previously mentioned tests and after the full experiment consisting of 15 cycles. The **102** sample gave results which were not reproducible and, therefore, has been omitted from these discussions.
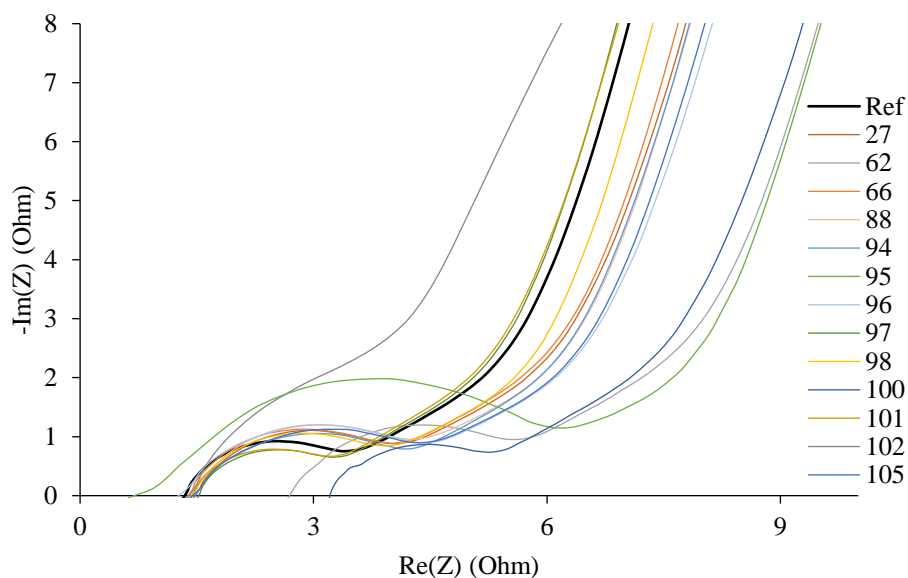

Figure 79 - EIS of all cells before any charging or discharging

The graphite cell tests show that most samples, before the experiment, show similar curves to the reference.
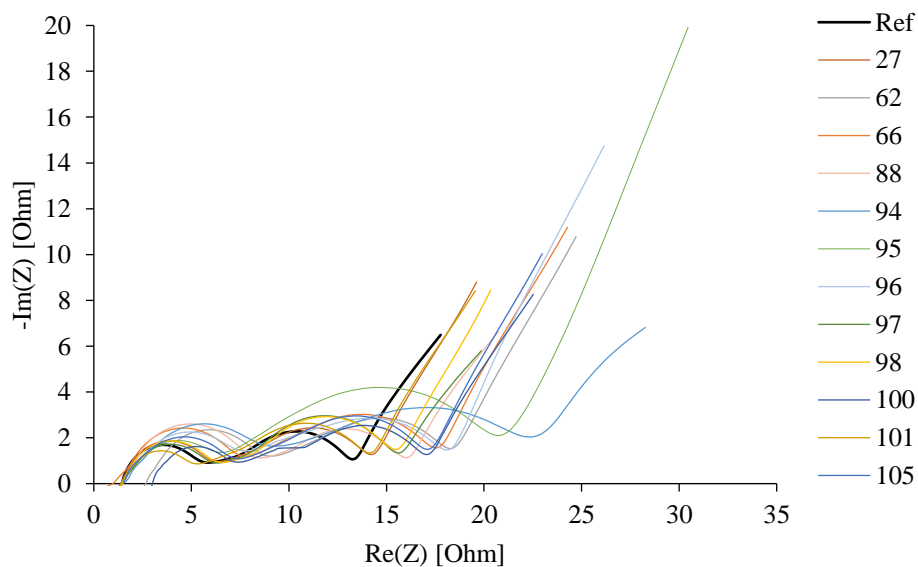

Figure 80 - EIS of full cells after cycling

After the graphite cells were cycled, all samples showed an increased impedance when compared to the reference which can be attributed to the formation of a SEI.

Figure 81 – EIS of cells anode after cycling
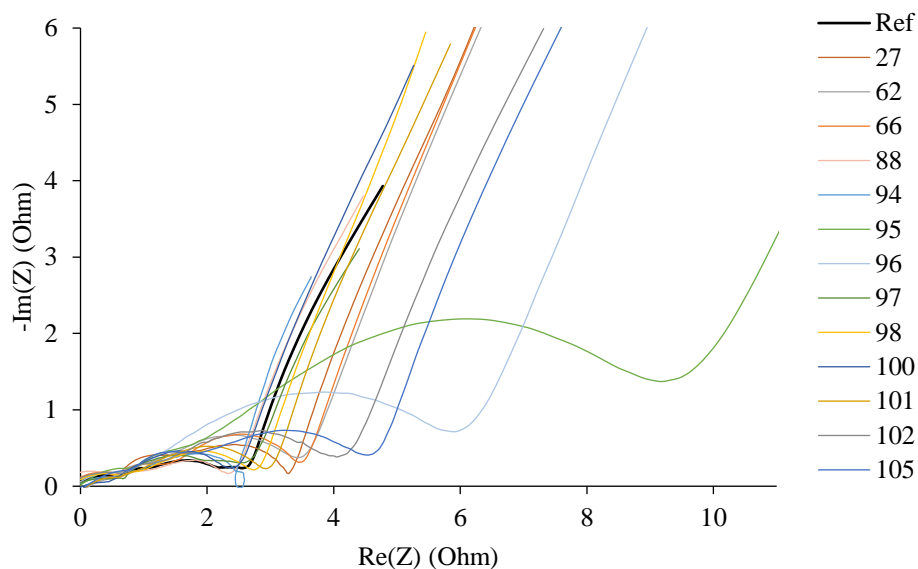
The anodes of the graphite cells showed mixed results with respect to the reference. Three samples show a reduction in impedance when compared to the reference, namely **88**, **94** and **100**, and three other samples are comparable; **97**, **98** and **101**. The remaining samples are all above the reference; samples **62**, **95**, **96** and **105** all significantly so.
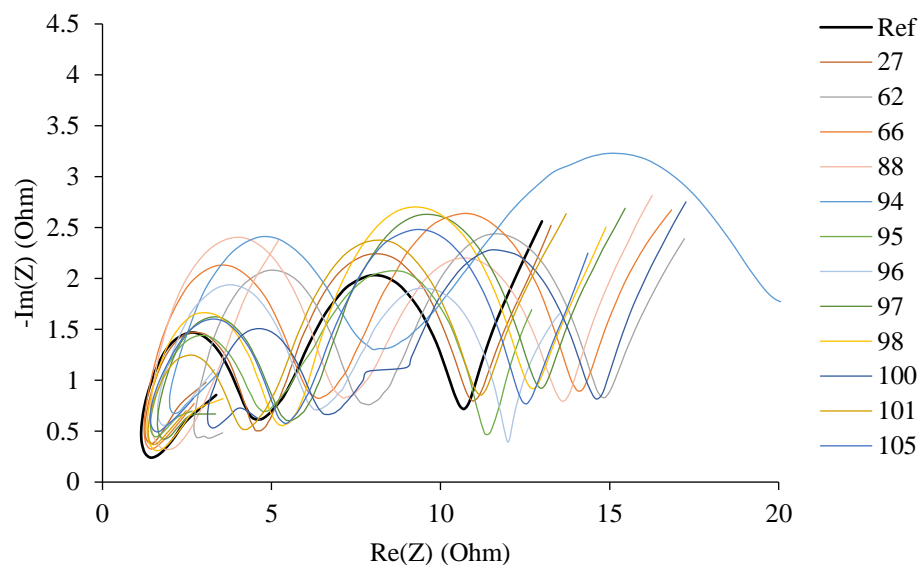
Figure 82 - EIS of graphite cells cathode after cycling

The EIS of the cathode after cycling shows an increase of the impedance for all samples, with **94** and **102** showing a much stronger increase. The reason for this increase is attributed to the formation of an SEI in all cases, although the reason for the larger increase of **94** and **102** cannot be drawn from this information alone.

2.4.8   Battery tests comparison

Due to the difficult nature of definitively understanding the processes that occur within a cell during charge and discharge, the exact impact and chemical processes that an additive undergoes within a cell is difficult to access. Looking at each test, no sample improved upon the reference sample, with some samples causing notable detrimental changes to the battery performance.

Despite this, trends can be found to probe which structural features in an additive are beneficial to a cell. In an attempt to do so, base numerical values have been attributed to the tests from previous sections and cross examined in Table 3. The cells have been given a visual gradient colour comparison, showing the most favourable value as green and the most detrimental values are shown in red.
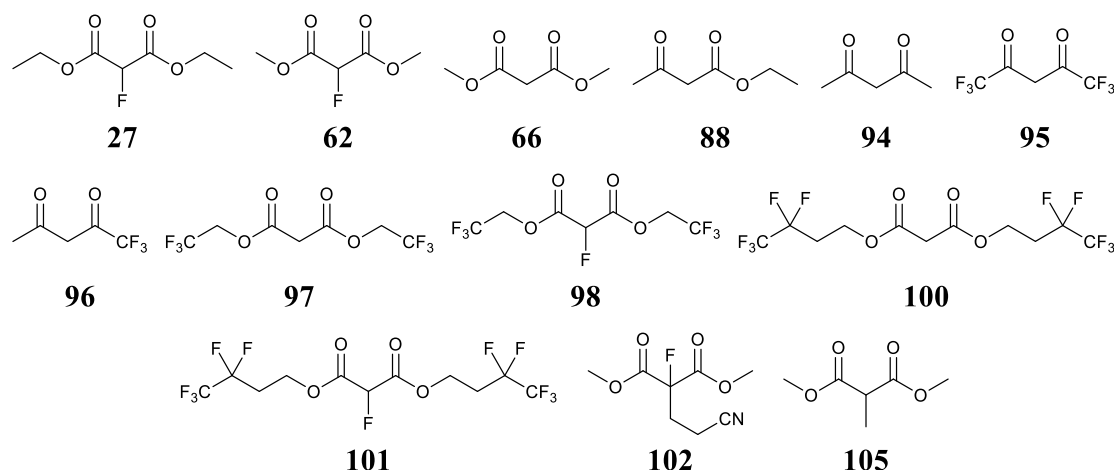
Figure 83 – All of the additives which underwent battery tests in graphite cells.

Table 3 - Cell performance with additives

	Ref	27	62	66	88	94	95	96	97	98	100	101	102	105
CE cycle 1 (%)	91.33	87.16	85.21	83.21	83.23	78.90	86.39	85.73	84.31	84.36	88.47	88.64	82.51	86.61
Average CE cycle 1-15 (%)	98.70	98.13	97.86	97.61	97.65	96.66	95.97	97.59	97.73	97.95	98.28	98.38	97.23	98.06
Discharge capacity 1st cycle (normalised)	1.000	0.990	0.985	0.982	0.975	0.950	0.971	0.82	0.985	0.994	0.993	0.994	0.974	0.992
Discharge capacity after 15 cycles (normalised)	0.905	0.907	0.894	0.900	0.898	0.739	0.665	0.836	0.898	0.914	0.904	0.903	0.869	0.907
Capacity retention after 15 cycles (%)	90.59	91.62	90.82	91.61	92.18	77.67	68.59	85.10	91.30	91.93	91.04	90.79	89.28	91.38
Ohmic resistance (cycled)	1.36	1.29	2.51	0.57	1.38	1.61	1.40	1.46	1.32	1.34	2.90	1.38	1.41	1.51
Internal resistance at 1khz (cycled)	5.67	6.10	8.59	7.34	7.84	8.77	6.80	7.70	6.14	6.27	7.37	5.37	14.86	7.17
Average discharge voltage (V)	3.81	3.79	3.76	3.76	3.78	3.71	3.72	3.74	3.79	3.79	3.77	3.79	3.70	3.76

A summary of the results (Table 3) shows that, in comparison, no additive improves upon the control samples. Despite this, by considering certain structurally related additives, the impact of certain features on various aspects of battery performance can be deduced.

Table 4 - A comparison of five additives with different carbonyl functional

	66	88	94	95	96
CE cycle 1 (%)	83.21	83.23	78.90	86.39	85.73
Average CE cycle 1-15 (%)	97.61	97.65	96.66	95.97	97.59
Discharge capacity 1st cycle (normalised)	0.982	0.975	0.950	0.971	0.982
Discharge capacity after 15 cycles (normalised)	0.900	0.898	0.739	0.665	0.836
Capacity retention after 15 cycles (%)	91.61	92.18	77.67	68.59	85.10
Ohmic resistance (cycled)	0.57	1.38	1.61	1.40	1.46
Internal resistance at 1khz (cycled)	7.34	7.84	8.77	6.80	7.70
Average discharge voltage (V)	3.76	3.78	3.71	3.72	3.74

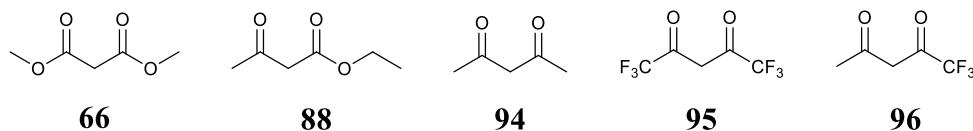**66**   **88**   **94**   **95**   **96**

Figure 84 - Structures of the additives which show different types of carbonyl functional group

Table 4 shows a comparison of values from the non-β-fluorinated di-ester, di-ketone or ketoester additives. As is evident, the symmetrical diketone systems appear to be significantly more detrimental to battery operation than the ester systems. The difference

between diester **66** and ketoester **88**, however, is small, suggesting that the preferable decomposition reaction within the cell is one involving the ester group.

Table 5 - Comparison of malonate-ester based additives on battery performance

|	62	66	102	105
CE cycle 1 (%)	85.21	83.21	82.51	86.61
Average CE cycle 1-15 (%)	97.86	97.61	97.23	98.06
Discharge capacity 1st cycle (normalised)	0.985	0.982	0.974	0.992
Discharge capacity after 15 cycles (normalised)	0.894	0.900	0.869	0.907
Capacity retention after 15 cycles (%)	90.82	91.61	89.28	91.38
Ohmic resistance (cycled)	2.51	0.57	1.41	1.51
Internal resistance at 1khz (cycled)	8.59	7.34	14.86	7.17
Average discharge voltage (V)	3.76	3.76	3.70	3.76
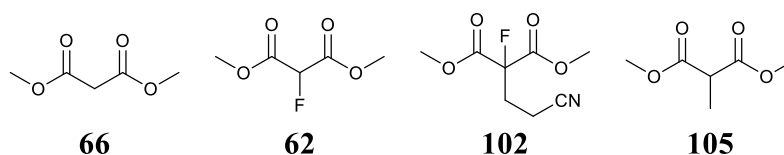
Figure 85 – Structures of additives compared in Table 5

Comparison of the β-substituted compounds show that, with the exemption of the 1st cycle tests, **62, 66** and **105** are comparable and **102** is considerably worse. This could be due to the cyano-group reacting in a detrimental manner, but this is unlikely due to the known beneficial effects of this functional group within LIBs.[55] It's possible the di-substitution is the cause of this, but definite conclusions cannot be drawn from these experiments alone.

Table 6 - Comparison of four dialkyl malonate-esters

|	27	62	98	101
CE cycle 1 (%)	87.16	85.21	84.36	88.64
Average CE cycle 1-15 (%)	98.13	97.86	97.95	98.38
Discharge capacity 1st cycle (normalised)	0.990	0.985	0.994	0.994
Discharge capacity after 15 cycles (normalised)	0.907	0.894	0.914	0.903
Capacity retention after 15 cycles (%)	91.62	90.82	91.93	90.79
Ohmic resistance (cycled)	1.29	2.51	1.34	1.38
Internal resistance at 1khz (cycled)	6.10	8.59	6.27	5.37
Average discharge voltage (V)	3.79	3.76	3.79	3.79
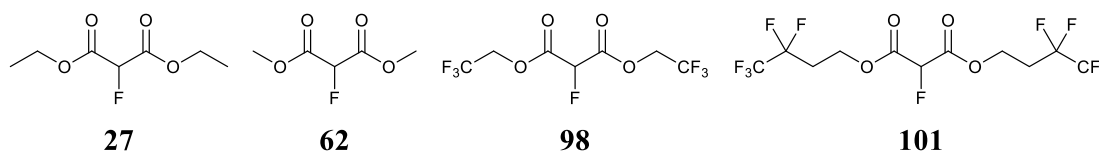
Figure 86 - Structures of the four malonate esters compared in Table 6

Comparing the different dialkyl malonate diesters gives some insight into the potential decomposition pathway for these compounds. Looking at Table 6, it can be seen that the most poorly performing additive doped battery is the battery containing **62** which is the most unsubstituted malonate (methyl). When other additives are compared, the results are largely, unaffected by electron withdrawing or donating effects.

As the only stabilising effects noted are seen are from increasing substitution on the carbon adjacent to the ester oxygen, it suggests that the decomposition mechanism is radical in nature. When this information is coupled with the observation of diketones performing worse than diesters, it suggests that a radical decomposition occurs for which the ester oxygen is important.

Figure 87 shows a possible mechanism proposed for the reduction processes of the esters within a cell. Upon accepting an electron, the carbonyl is reduced which then causes a decarboxylation reaction to form a double bond. The first step is a reasonable assumption based upon the numerous examples within the literature of reactions occurring through the single electron reduction of a carbonyl, such as the McMurry reaction.[118] It can then polymerise within the cell to form an SEI (Figure 87). This mechanism fits with the cell performance observations; it is a radical pathway that is reliant upon the ester group providing a route of elimination with an alkyl radical. It's possible that **102** is a poorer additive due to additional substitution upon the β-position causing steric hindrance, therefore, disfavouring this process.
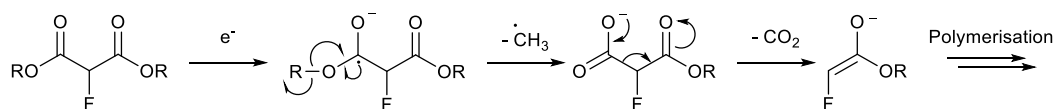

Figure 87 - Proposed mechanism for the reaction of malonates within a battery

2.5   Conclusion

A range of different dicarbonyl compounds were purified or synthesised and analysed for use as additives in LIB systems and some initial conclusions could be drawn. In general, these compounds did not improve upon the reference sample in the tests undertaken but the effect of molecular structure of additives gives some insight for developing better additives.

Diketones **94**, **95** and **96** performed markedly worse in some tests suggesting that diketones are not suitable for effective LIB additives.
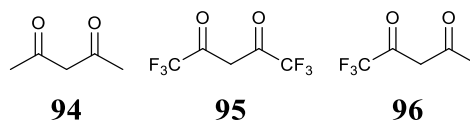
Figure 88 - Structures of **94**, **95** and **96** (left to right)

62 also performed worse than **27**, **98** and **101** which is indicative that the reduction decomposition pathway is radical in nature.
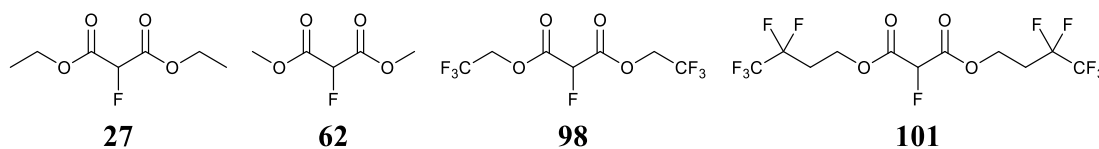
Figure 89 - Structures of **27**, **62**, **98** and **101**

Chapter 3

Synthesis of fluoroester derivatives

During the course of this project, there was a transfer of ownership of the battery division from Sony to Murata Manufacturing. Consequently, the research project shifted from battery analysis being undertaken within Sony MSL in Stuttgart, Germany, to Murata Manufacturing in Atusgi, Japan. This also resulted in access to more extensive equipment for LIB analysis whilst on placement in Japan.

The synthetic work described in this chapter was undertaken in Durham, alongside LIB analysis in Atsugi. As such, synthetic targets were developed as a result of parallel developments from LIB analysis, described in the following chapter.

Following on from the proposed mechanism of decomposition of fluoromalonate systems described in Chapter 2, our next targets were esters with more substituted alkyl chains which would provide insight into the stabilisation of the alkyl chain radical postulated to form.
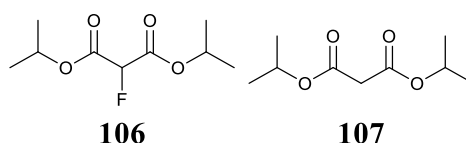

106   **107**

Figure 90 – Synthetic targets

3.1   Malonate type additives

Following on from the work described in the previous chapter, new malonate-type additives with more substituted alkyl ester groups were selected as the next targets.

3.1.1   Synthesis of di-*iso*-propyl malonates

Due to the successful transesterification with ethanol described in Chapter 2, the same reaction conditions were adapted for the synthesis of di-*iso*-propyl 2-fluoro-malonate **106.**
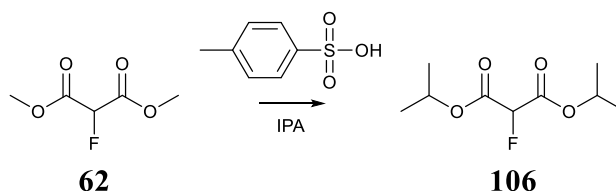

Figure 91 – Acid catalysed strategy for synthesising **106**

The increased steric bulk of the *iso*-propyl nucleophile inhibited the reaction and there were several product peaks present in the ^{19}F NMR spectrum. As such, basic reaction conditions were trialled by dissolving sodium in IPA and the reaction mixture was refluxed overnight. After work-up, the di-*iso*-propyl diester **106** was synthesised without the need for further purification in 60% yield. Due to the success of this reaction, the same conditions were repeated using dimethyl malonate to generate the non-fluorinated analogue of **106**, di-*iso*-propyl malonate **107** in 48% yield. All spectroscopic data for **107** matches literature values.[119]
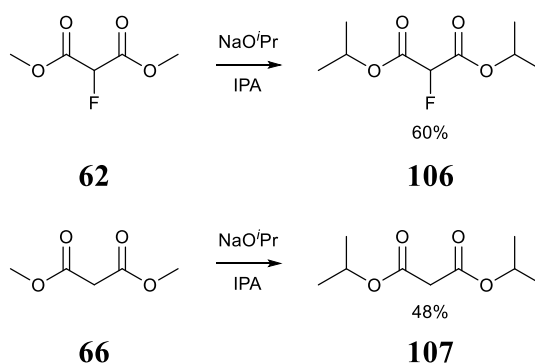

Figure 92 - Synthetic strategy for **106** and **107**

3.2   Alkylation reactions of dimethyl 2-fluoromalonate

Due to the proposed mechanism of decomposition through the elimination of CO_2, different ranges of compounds became targets. Due to the reported use of cyano-

containing compounds promoting the LIB swelling inhibition, it was thought that combination of malonate-systems with cyano containing systems could lead to beneficial LIB electrolyte additives. In addition to this, compounds with different electron withdrawing groups, such as trifluoromethyl or phenyl sulfone, were selected, to see if the CO_2 inhibition effect could be replicated or enhanced with different electron withdrawing functional groups.
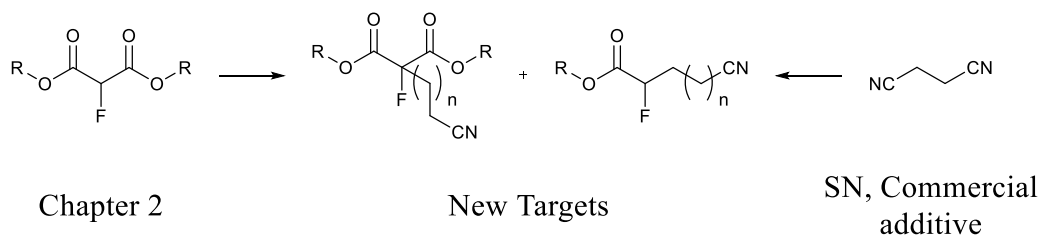

Figure 93 – Relationship of new targets to commercial additives (SN)

The first step of this synthetic strategy was alkylation of dimethyl 2-fluoromalonate to generate fluorinated diester systems which could be screened for LIB additive applicability or developed further into different potential electrolyte additives.

3.2.1   Substitution reactions of dimethyl 2-fluoromalonate with bromo-cyano-alkanes

3.2.1.1 Synthesis of compounds with varying length of alkyl chain

Whereas **102** was synthesised through a Michael addition reaction, to access longer chain-length compounds, nucleophilic substitution reactions were employed. Consequently, the use of sodium hydride with dimethyl 2-fluoromalonate generated the malonate carbanion which was reacted with bromoacetonitrile and 4-bromobutyronitrile to generate compounds **108** and **109** respectively.
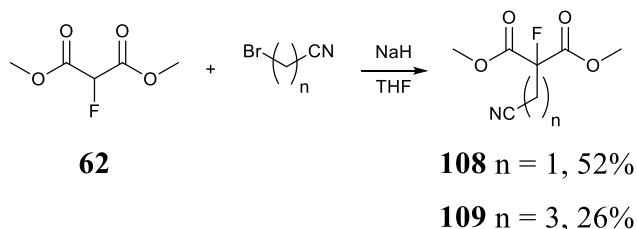

62

108 n = 1, 52%

109 n = 3, 26%

Figure 94 - Synthesis of **108** and **109**

Both reactions were followed by ^{19}F NMR spectroscopy and were rarely simple due to the often incomplete conversion of starting material to product and often, decarboxylation reactions occurred, providing several impurities. Successful purification of the desired product was complicated by the fact that these molecules are difficult to observe by TLC; the compounds and their impurities were not UV active and were not observable after testing with 10 different common TLC plate stains. Potassium permanganate proved to be the most successful but this was only visible marginally before complete bleaching of the TLC plate. Column chromatography was trialled but due to the low concentration levels of the compound through this process, compounds could not be observed clearly on the TLC plate. As such, vacuum distillation was employed to purify both compounds which, again, proved somewhat difficult due to the very similar boiling points of starting material, impurity and product, often requiring multiple distillations to isolate the desired products. However, finally, the shorter chained product, dimethyl 2-(cyanomethyl)-2-fluoromalonate **108**, was isolated in 52% yield and the longer chained product, dimethyl 2-(3-cyanopropyl)-2-fluoromalonate **109**, was isolated in a 26% yield.
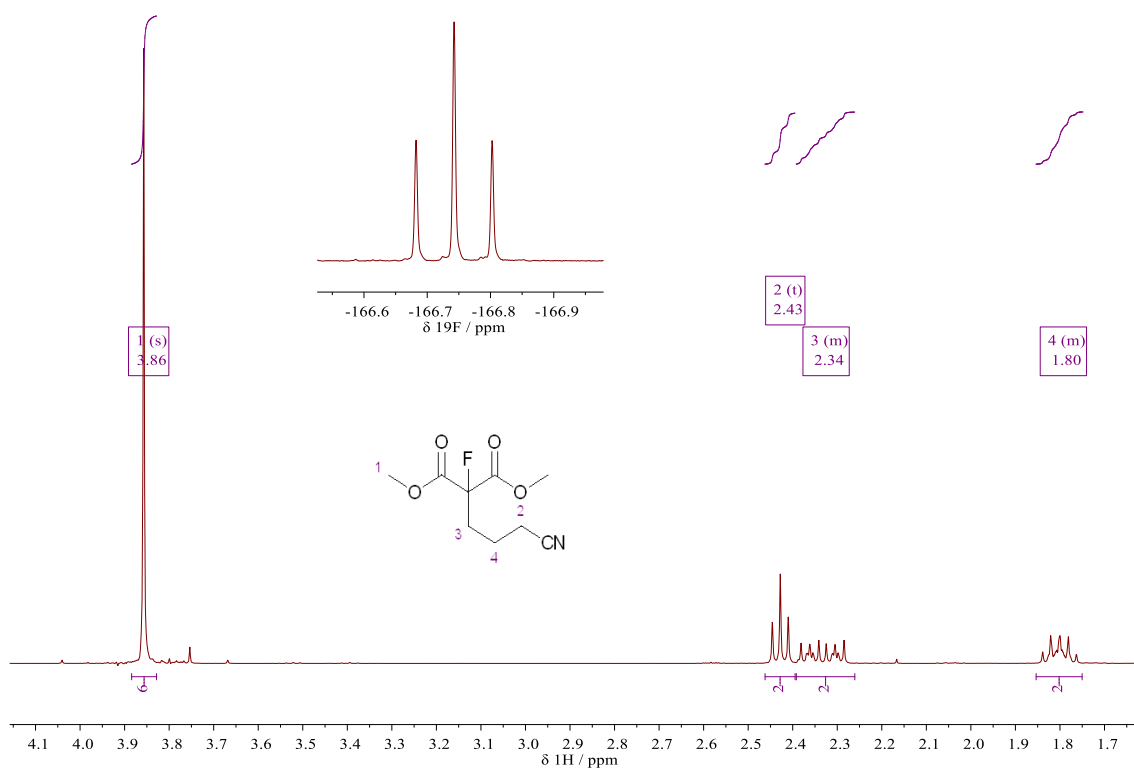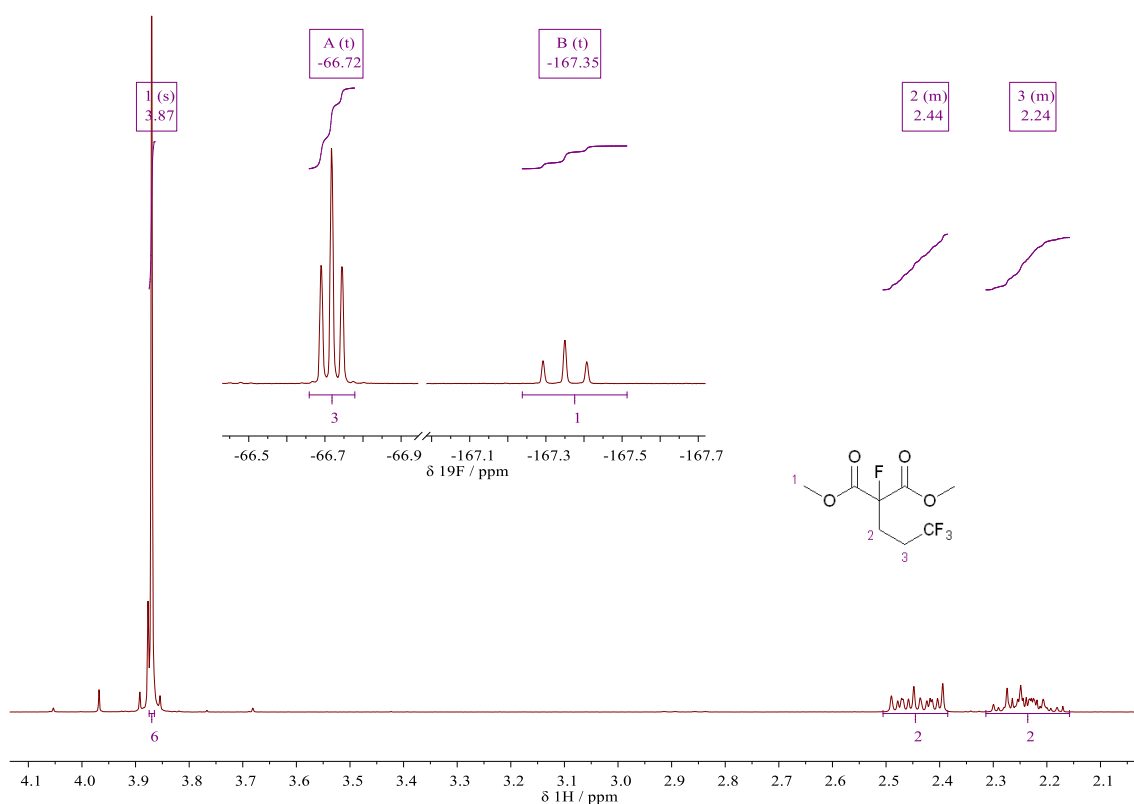

Figure 95 - ^{1}H NMR spectrum of **109**, (inset) ^{19}F NMR spectrum

3.2.1.2 Synthesis of a trifluoromethyl fluoro diester system **110**

Similarly to reactions described in the previous section, dimethyl 2-fluoromalonate was deprotonated with sodium hydride to form the carbanion salt which then reacts with 1-iodo-3,3,3-trifluoropropane substitutes through an S_N2 reaction to give **110**.

**62**   **110**
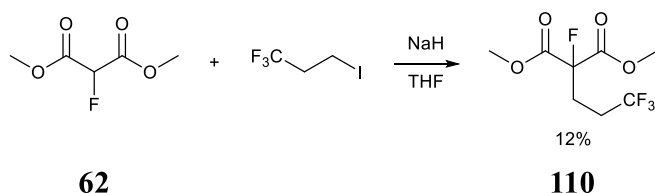
Figure 96 - Synthesis of **110**

Once again, this synthesis proved difficult, due to aforementioned isolation and purification problems. Distillation proved very difficult and, after multiple attempts, further purification could not be achieved beyond 95% purity by ^{19}F NMR spectroscopy. However, this is sufficient purity to asses LIB additive performance.

Figure 97 - ^1H NMR spectrum of **110**, (inset) ^{19}F NMR spectrum of **110**

3.2.2 Michael addition of vinyl compounds to dimethyl 2-fluoromalonate

To generate the phenyl sulfone equivalent of **102**, Michael addition of phenyl vinyl sulfone was undertaken. Using the same conditions as the previously successful Michael addition to acrylonitrile and, after 65 minutes, the ^{19}F NMR spectrum showed 85% conversion to target compound **111**.
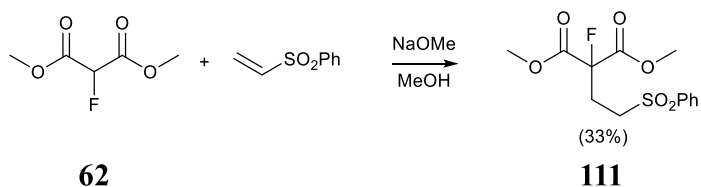
Figure 98 - Reaction scheme for **111**
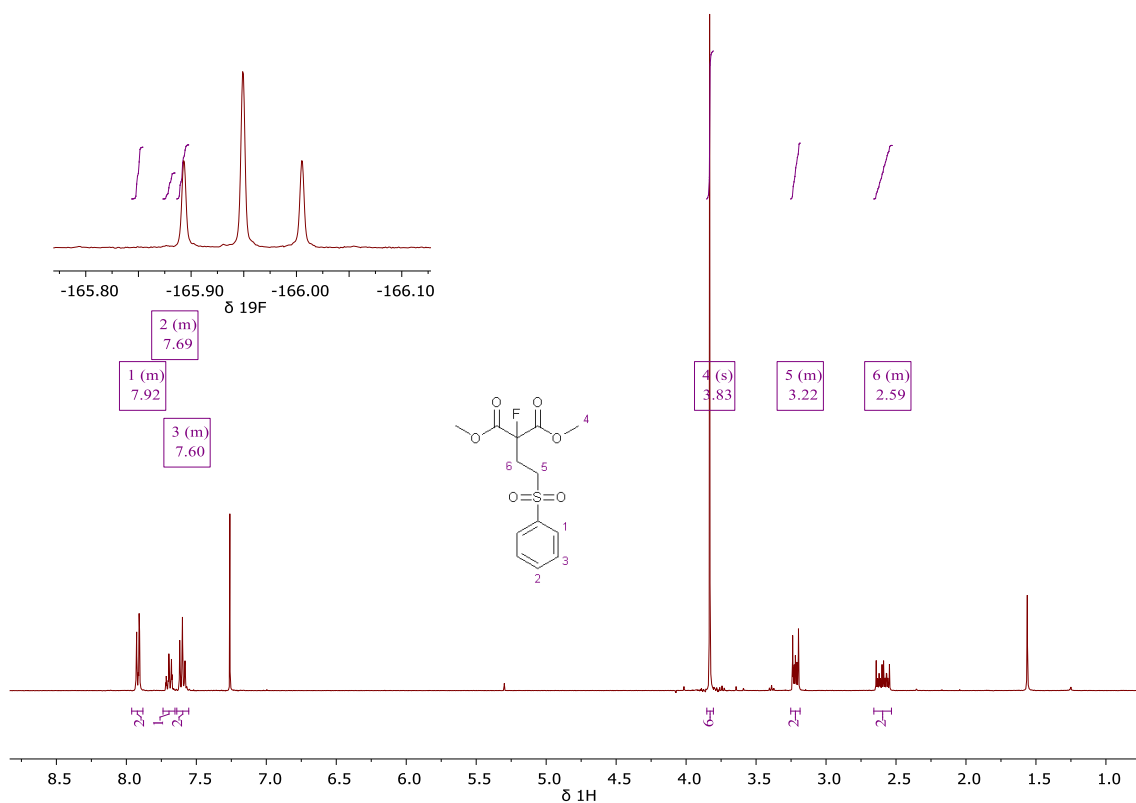
Figure 99 - ^{1}H NMR spectrum of **111**, (inset) ^{19}F NMR spectrum of **111**

Due to the presence of a phenyl ring, this compound was UV active, and was readily purified by column chromatography to give **111** in 33% yield.

3.3   Krapcho decarboxylation reactions

A useful chemical process for selectively removing one ester moiety from a dicarbonyl system, such as a dialkyl malonate, is through the use of Krapcho decarboxylation. This reaction was employed to generate the proposed fluorocyanoester products.

3.3.1   Dimethyl 2-(2-cyanoethyl)-2-fluoromalonate

The first conditions trialled for this reaction were an adaptation of literature conditions using LiCl and DMSO at reflux.[120] Decarboxylation was monitored by ^{19}F NMR spectroscopy and, after half an hour of reflux, showed little product.

The low yield was attributed towards product decomposition soon after and, as this process was going to be used to generate several more similar compounds during this project, the conditions for this reaction for these types of substrates was optimised. It was thought that the presence of fluorine may be activating the decarboxylation by strong inductive effects promoting the attack of chloride ion. As such, different temperatures were trialled and reactions monitored by ^{19}F NMR spectroscopy.
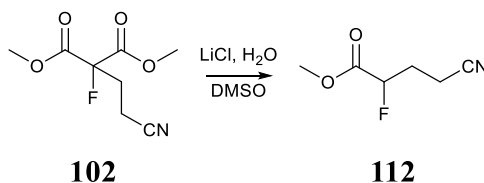

Figure 100 - Krapcho decarboxylation to generate **112**

Table 7 - Optimisation conditions for the Krapcho decarboxylation of **102**. [+] denotes crude yield, * denotes total length of reaction time

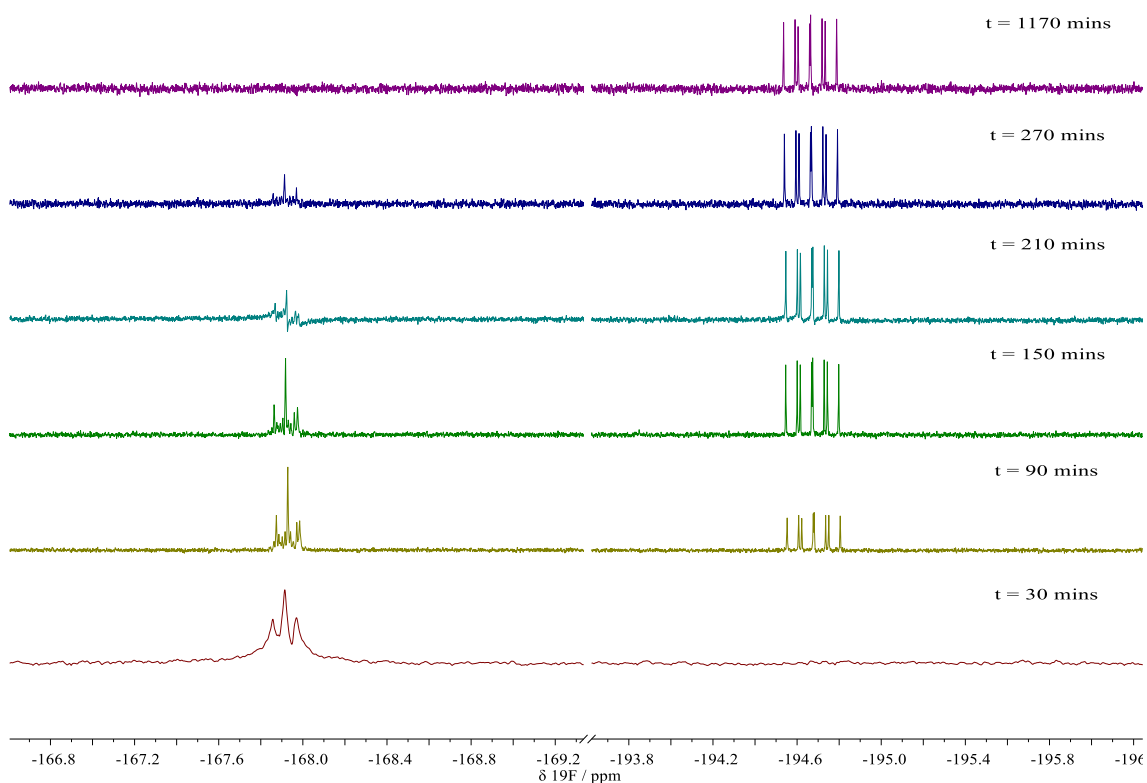| Solvent	Temperature (°C)	Conversion (%)	Yield (%)	Time (hours)
DMSO	180	100	11	0.5
DMSO	25	0	-	46
H_2O	25	0	-	46
DMSO	60	85	-	43
DMSO	100	100	66[+]	19*
DMSO	110	100	46	1.5

Figure 101 - ^{19}F NMR spectra of 100 °C reaction monitoring showing the starting material, at approximately 168 ppm, converting to the typical doublet of doublet of doublets at approximately 195 ppm of these compounds

The first set of conditions at room temperature gave no conversion. Reaction at 60 °C showed slow conversion to product, but, after 43 hours, showed only approximately 60% conversion and signs of product decomposition. By stirring the reaction at 100 °C, the

reaction progressed over 4.5 hours until 80% conversion and, after leaving the reaction overnight, showed **112** by ^{19}F NMR spectroscopy and some evidence of decomposition. Reaction at 110 °C (entry 6) proved to be much quicker, gave minimal decomposition and so these conditions were used for all subsequent Krapcho decarboxylations.
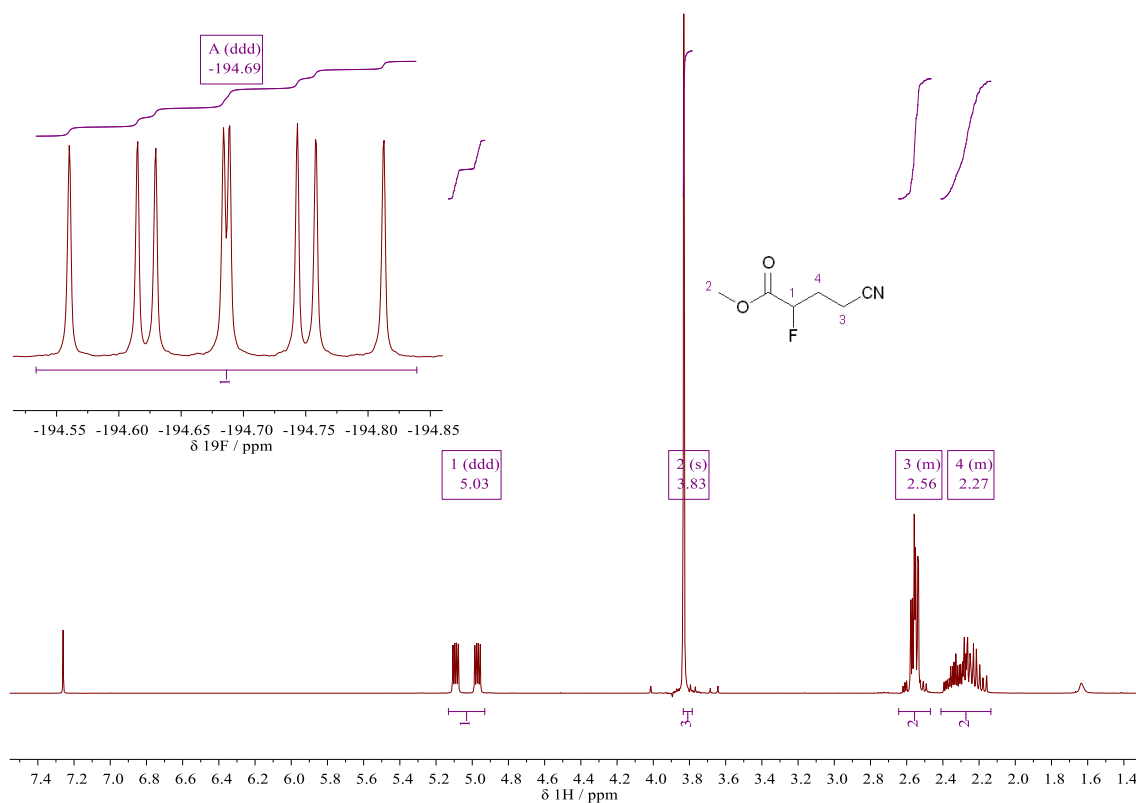

Figure 102 - ^{1}H NMR spectrum of **112**, (inset) ^{19}F NMR spectrum of **112**

3.3.2   Dimethyl 2-(3-cyanopropyl)-2-fluoromalonate

Following the optimisation of the Krapcho decarboxylation of **112**, the same conditions were used for the shorter-chained **108** substrate which was complete after 50 minutes by ^{19}F NMR spectroscopy. It's likely that the shorter alkyl chain and subsequent closer proximity of the nitrile group causes greater inductive effects which in-turn promoted the reaction.
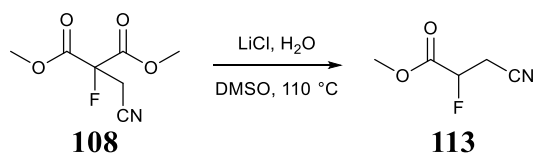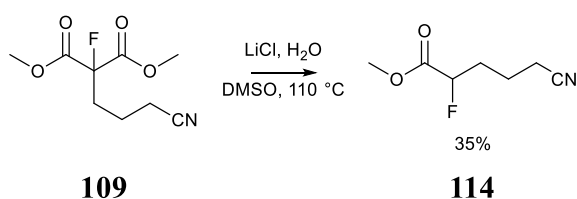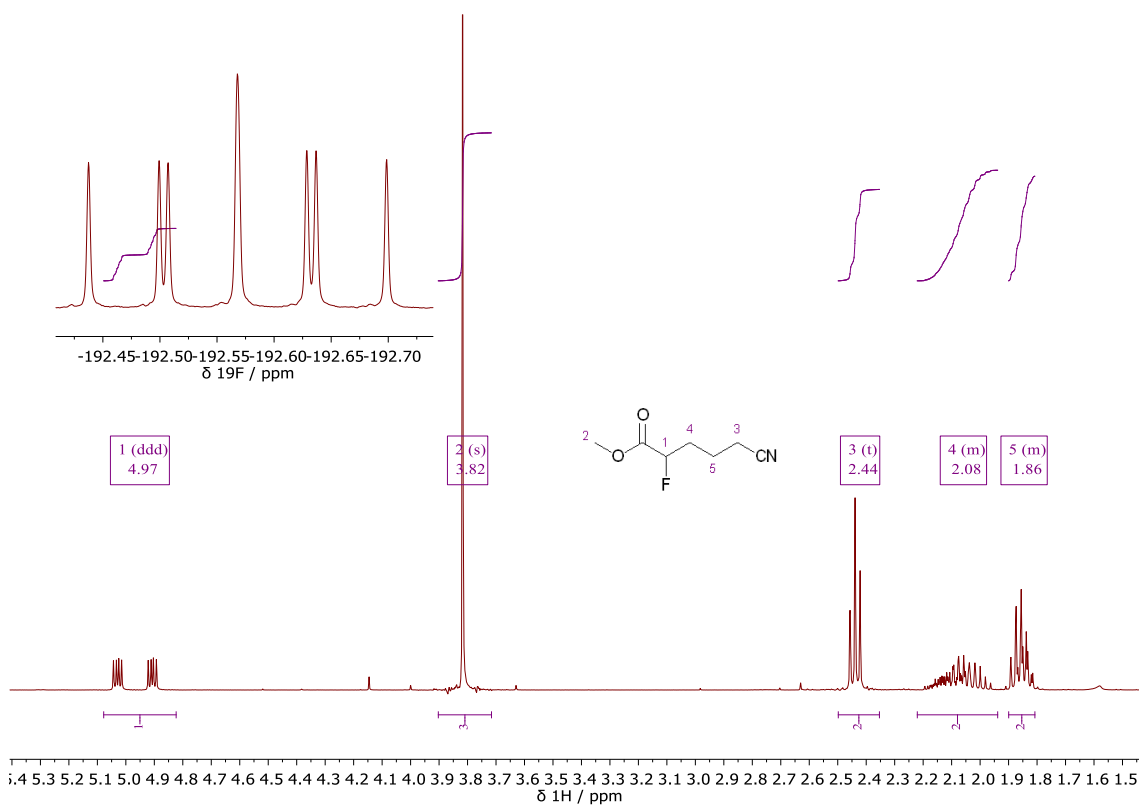
Figure 103 - Synthesis of **113**
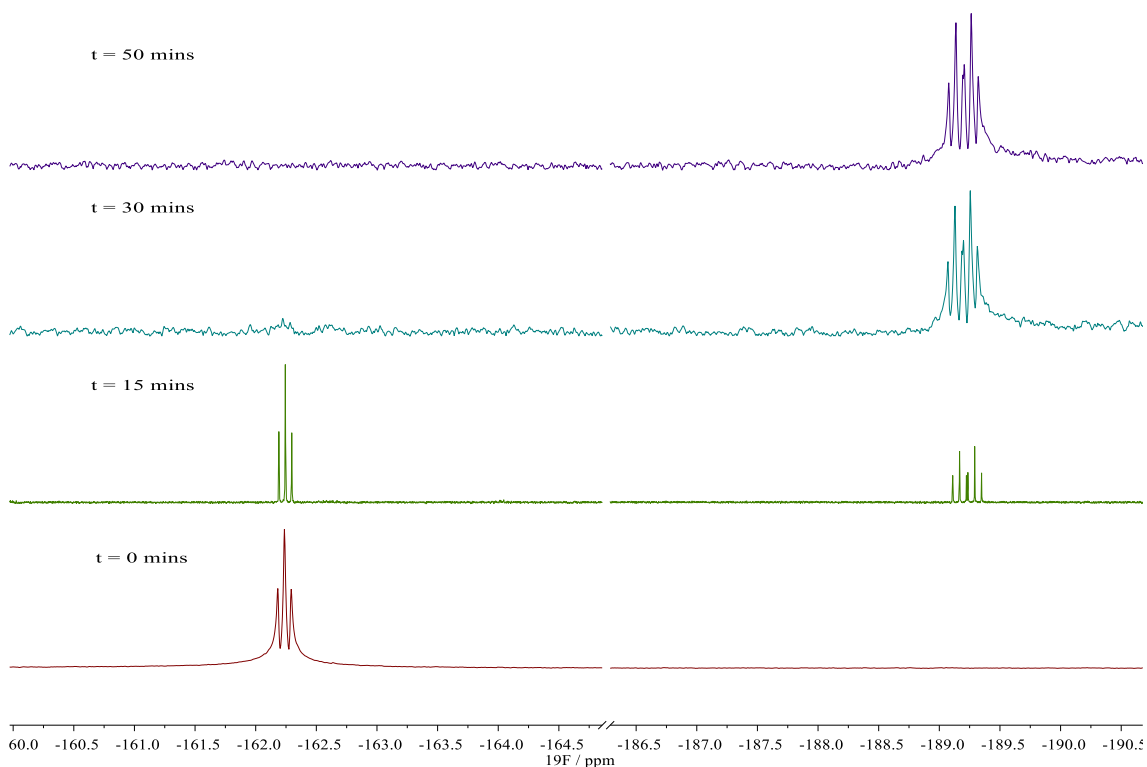
Figure 104 - ^{19}F NMR spectra of the reaction monitoring of the Krapcho decarboxylation of **108**

However, following work-up of this reaction, none of the desired compound was observed in the crude product. Repeat attempts of the reactions gave no isolated product. Presumably this is due to the shorter alkyl chain which results in a more labile proton in the γ-position causing elimination of hydrogen fluoride to form a conjugated system. Supporting this is the observation of starting material and HF in the ^{19}F NMR spectrum of the isolated product mixture and a complex mixture of side products in other analysis.
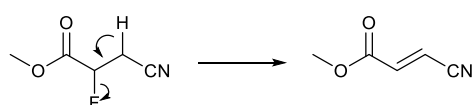
Figure 105 - Proposed decomposition pathway of **113**

### 3.3.3   Dimethyl 2-(4-cyanobutyl)-2-fluoromalonate

The Krapcho decarboxylation of dimethyl 2-(4-cyanobutyl)-2-fluoromalonate was undertaken using the same conditions and, as in the previous section, the reaction time was effected by the change in chain length. The increased distance of the nitrile reduces the inductive effects and, therefore, reaction time was increased, taking 3 hours for complete conversion by ^{19}F NMR spectroscopy.

Figure 106 - Krapcho decarboxylation for the synthesis of **114**

Figure 107 - ^{1}H NMR spectroscopy of **114**, (inset) ^{19}F NMR spectroscopy of **114**

The crude product was purified by vacuum distillation giving **114** as a clear oil in 35% yield.

3.3.4   Synthesis of methyl fluoro cyano esters with longer alkyl chains

The longer chained methyl fluoro cyano esters were prepared from dimethyl 2-fluoromalonate without the purification of the intermediate. The first reaction was undertaken using the same reaction conditions as described above. Interestingly, both of these longer chained substrates showed the presence of the mono-decarboxylated product by ^{19}F NMR spectra of the crude intermediate. Attempts were made to try push this reaction to directly synthesise the target compound in one step, but attempts were ultimately unsuccessful.

62

115 n=4
116 n=5

117 n=4, 21%
118 n=5, 19%
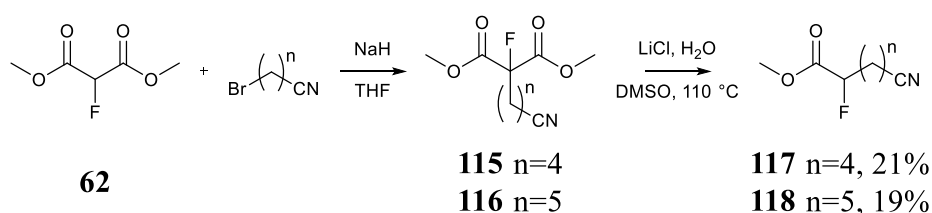
Figure 108 - Synthesis of **117** and **118**
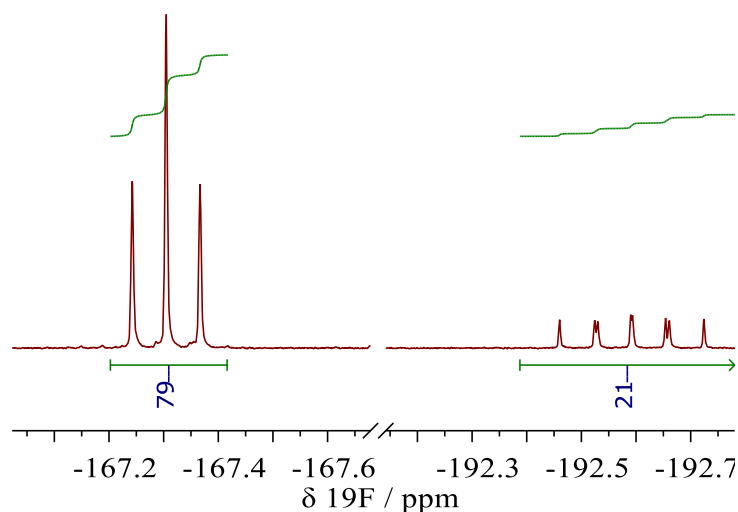
Figure 109 - ^{19}F NMR of the crude intermediate for **116**, showing 80% intermediate and 20% **118**

For each repeat of this reaction, the conversion to the intermediate was approximately 80% by ^{19}F NMR spectroscopy, with small amounts of mono-decarboxylated product present. Krapcho decarboxylation reaction time increased with increasing chain length, as with previous reactions, by taking 12 hours for **117** and 27 hours for **118**. These two compounds were purified by column chromatography, as they showed clearly by TLC

with the use of permanganate stain. Column chromatography gave the two compounds being purified to 99%+ purity in only 21% yield for **117** and 19% yield for **118** due to losses upon purification.

3.3.5   Synthesis of methyl 2,5,5,5-tetrafluoro-pentanoate

The isolation of **119** was made possible through the Krapcho decarboxylation of the previously synthesised **110**. Using the same reaction conditions, crude **119** was produced as a brown oil. Despite repeated vacuum distillations, this compound proved difficult to purify, the starting material having a very similar boiling point. After three vacuum distillations, **119** was purified to 99%+ pure by ^{19}F NMR spectroscopy in 5% yield.
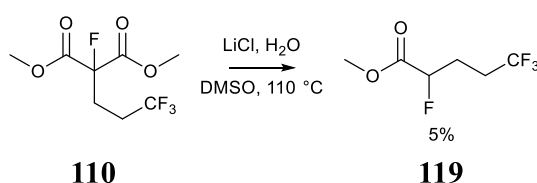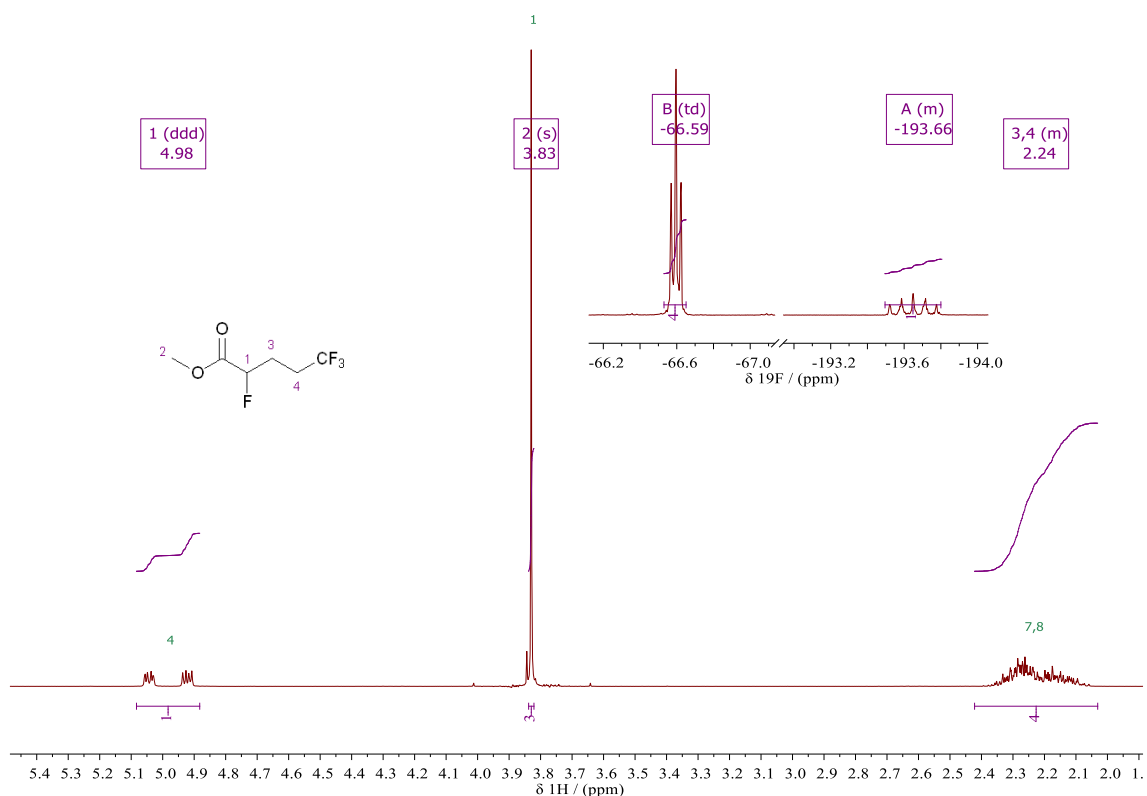

Figure 110 - Synthesis of **119**

Figure 111 - ^{1}H NMR spectrum of **119**, (inset) ^{19}F NMR spectrum of **119**

3.3.6   Synthesis of methyl 2-fluoro-4-(phenyl-sulfonyl)-butanoate

The phenyl sulfonyl derivative was synthesised from the Michael addition product of dimethyl 2-fluoromalonate and phenyl vinyl sulfone (3.2.2). Subsequent Krapcho decarboxylation reached completion after 90 minutes, roughly the same amount of time as **112**.
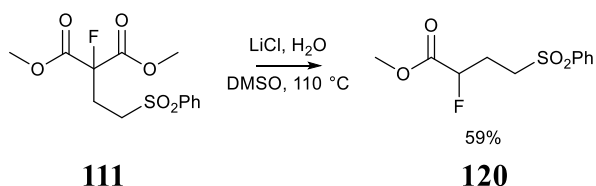
Due to the presence of an aromatic ring, the compound was UV active and therefore easily purified by column chromatography to give **120** in 59% yield. This compound was unique amongst this series of compounds due to the fact that the pure compound formed a low-melting solid. As such, alongside typical spectroscopic techniques, the structure was confirmed by x-ray crystallography.
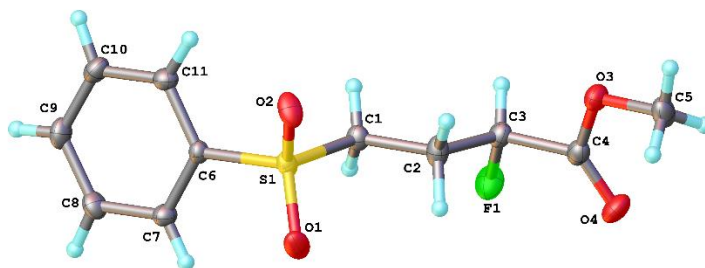

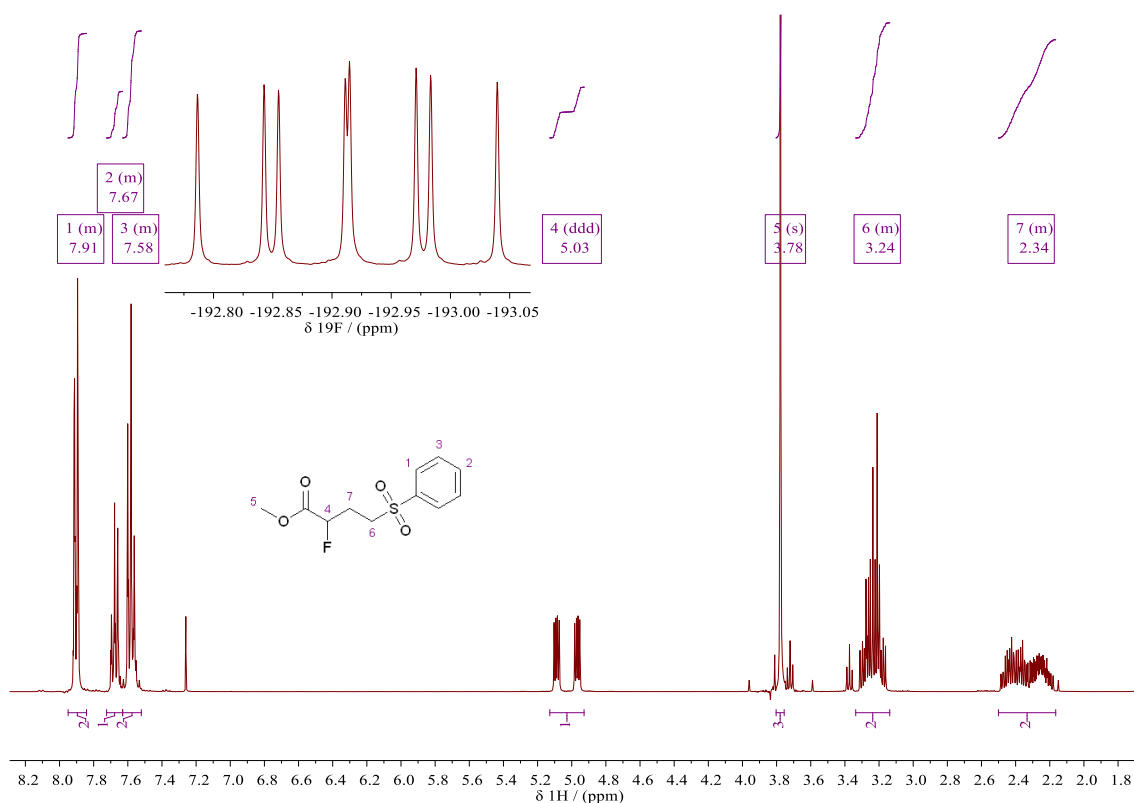Figure 112 - Structure of **120** determined by x-ray crystallography

Figure 113 - ^{1}H NMR spectrum of **120**, (inset) ^{19}F NMR spectrum of **120**

3.3.7   Synthesis of branched methyl fluoro cyano esters

To access a group of compounds that were similar to **112**, with alkyl substitution on the γ-position, substituted acrylonitriles were reacted using the same conditions as previous Michael addition reactions. The first substrates used were cinnamonitrile, the phenyl substituted vinyl-nitrile and fumaronitrile. Conversion to the intermediates was minimal, likely due to the increased steric hindrance.

Reaction with methyl substituted vinyl nitrile, crotononitrile, was much more successful. After using the same Michael addition conditions as previously, two peaks were visible in the ^{19}F NMR spectrum; one for each diastereoisomer. Attempts were not made to separate these two diastereoisomers as it was thought that the different diastereoisomers would not influence the results of any LIB analysis.
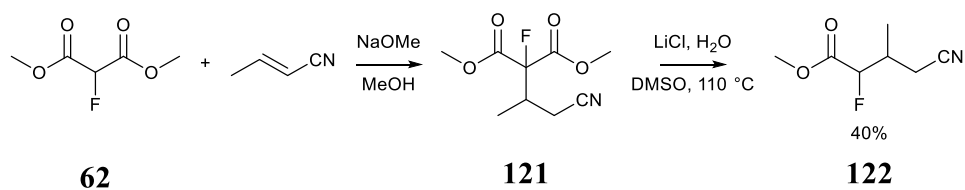
Figure 114 - Synthesis of **122**
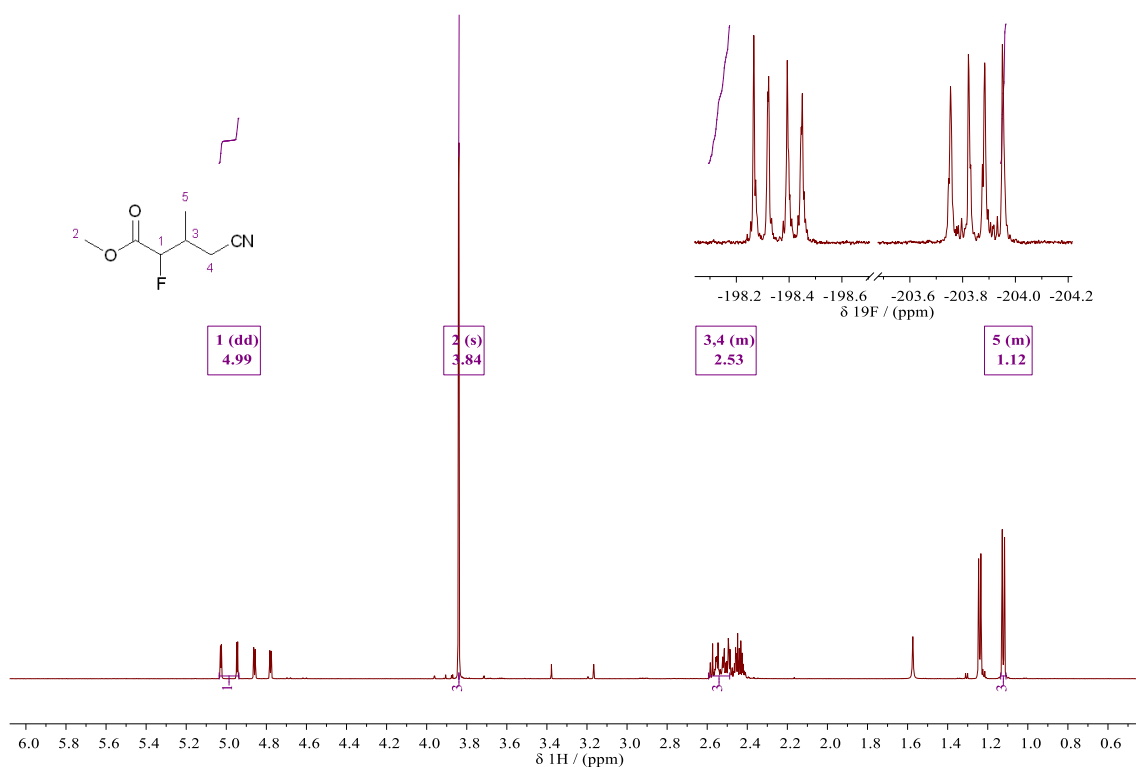
Figure 115 - ^{1}H NMR spectrum of **122**, with one diastereoisomer integrated; (inset) ^{19}F NMR spectrum of **122**

The crude reaction mixture was purified by vacuum distillation and the yield for the two-step reaction was 40%.

3.4   Free radical addition reactions for difluoro cyano ester synthesis

The di-fluorinated equivalents of **112** and **122** were realised by adapting literature conditions.[121] Ethyl 2-bromo-2,2,-difluoroacetate and metallic copper in DMSO initiates a radical addition reaction to alkenes. To generate the target compound, acrylonitrile and crotononitrile were used.
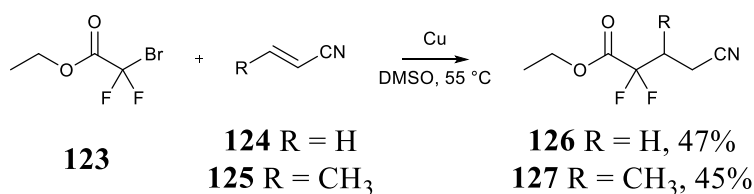
Figure 116 - Synthesis of **126** and **127**

Both reactions were undertaken in inert atmospheres and stirred for 6 hours. Both crude reaction products were pure by ^{19}F NMR spectroscopy, but were darkly coloured oils. To ensure that no impurities remained, the samples were both subjected to bulb-to-bulb vacuum distillation which gave clear oils in 47% yield for **126** and 44% yield for **127**.

3.5   Reverse Claisen condensation reaction

During the attempts to synthesise a selection of fluoro cyano ketone derivatives, the reaction of ethyl 2-fluoroacetoacetate with acrylonitrile was attempted, using the same reaction conditions as previous Michael addition reactions. The reaction was sampled and monitored by ^{19}F NMR spectroscopy, although after 30 minutes, the reaction showed no presence of the expected peak at approximately -160 ppm, but one large doublet of doublet of doublets at -195 ppm was observed instead.
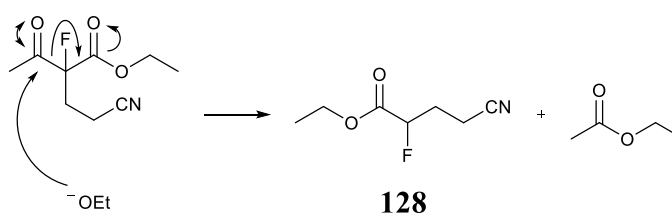
Figure 117 - Proposed mechanism of the formation of **128**

This splitting pattern was diagnostic of the fluoro cyano esters previously synthesised and the ^{1}H NMR spectrum and mass spectroscopy confirmed the synthesis of **128**. It is thought that the intermediate, once formed, undergoes a reverse-Claisen condensations reaction; ethoxide molecules attack the ketone carbonyl of the intermediate and eliminate the rest of the molecule to form **128** and ethyl acetate.
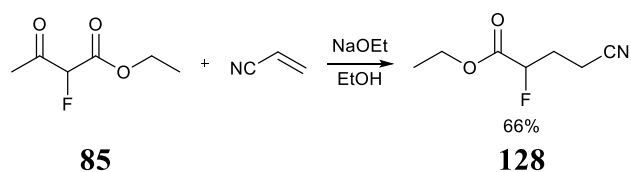
After optimisation, the reaction was repeated by stirring the reagents for 1 hour at 0 °C, which showed the conversion to the desired compound with minimal side products. The crude product was purified by vacuum distillation to provide **128** in 65% yield.

3.6   Fluoro cyano ketone derivative synthesis

Synthesis of fluoro cyano ketone derivatives were undertaken utilising similar reaction strategies to that of the malonates; Michael addition reactions and substitution reactions. Ethyl 2-fluoroacetoacetate was used as the starting material due to commercial availability.

3.6.1   Michael addition

The first strategy utilised to generate **132** was through the same process; Michael addition reaction followed by the Krapcho decarboxylation. As discussed in section 3.5, however, this lead to the direct synthesis of **128**. As a result of this, the strategy was changed to one of late-stage fluorination; the Michael addition reaction of the non-fluorinated keto-ester, followed by fluorination and then subsequent Krapcho decarboxylation.
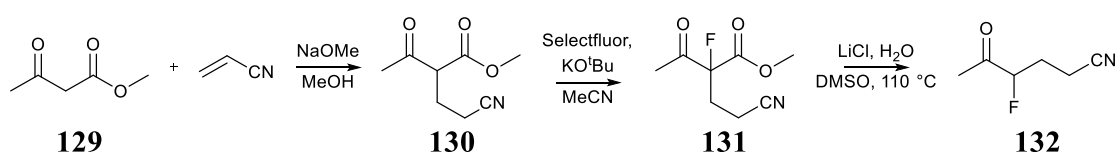

Figure 118 - Initial strategy for the synthesis of **132**

These reactions were initially undertaken on small scale without purification to scope the feasibility of the reaction. The reactions proceeded successfully; the Michael addition of **129** showed only one alkylation at reaction completion and the fluorination using Selectfluor™ showed the expected signal in the ^{19}F NMR spectra at approximately -160 ppm. Potassium *tert*-butoxide was used due to the large steric effects preventing a competing reverse Claisen condensation reaction.

It was alongside these reactions, however, the desired compound was synthesised serendipitously in a one-pot reaction starting from ethyl 2-fluoroacetoacetate. Whilst trialling reaction conditions to synthesise the carboxylic acid analogue of **112**, two peaks were observed in the ^{19}F NMR spectra. The reaction trialled was the same conditions used for the hydrolysis of dimethyl 2-fluoromalonate, 2.3 equivalents of LiOH.H$_2$O in ethanol stirred at room temperature, except with the addition of acrylonitrile. The crude mixture showed two unexpected peaks in the ^{19}F NMR spectra, one of which a doublet of doublet of doublets, much like **128**, and the other was a doublet of doublet of doublet of quartets in a ratio of approximately 1:1. After analysis by GCMS, it was found the former was the target acid, whereas the latter was the ketone product **132**.
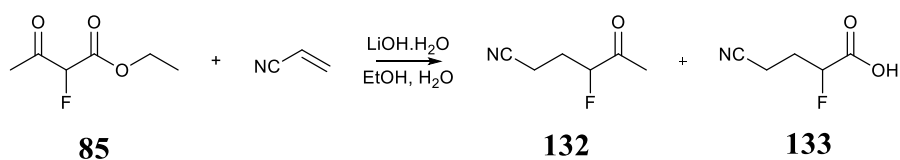

Figure 119 - The addition of acrylonitrile to the hydrolysis of dimethyl 2-fluoromalonate gave a mixture of products of **132** and **133**
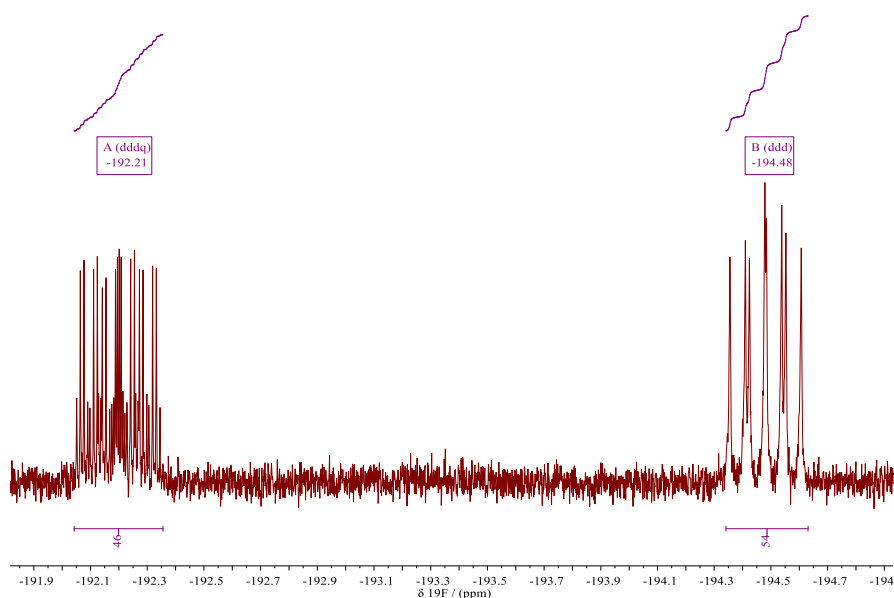

Figure 120 - ^{19}F NMR spectra of the crude product

The result was unexpected, and it was thought that the reaction proceeded by process (1) shown in Figure 121. To prove this, the reaction was repeated but without the addition of

acrylonitrile at the start of the reaction. After stirring overnight, the crude reaction mixture showed a combination of fluoroacetone and 2-fluoroacetoacetic acid derivatives by ^{19}F spectroscopy. After this time, acrylonitrile was added and the mixture was stirred for another day but no ketone product was observed, suggesting that the mechanism is that of process (1).
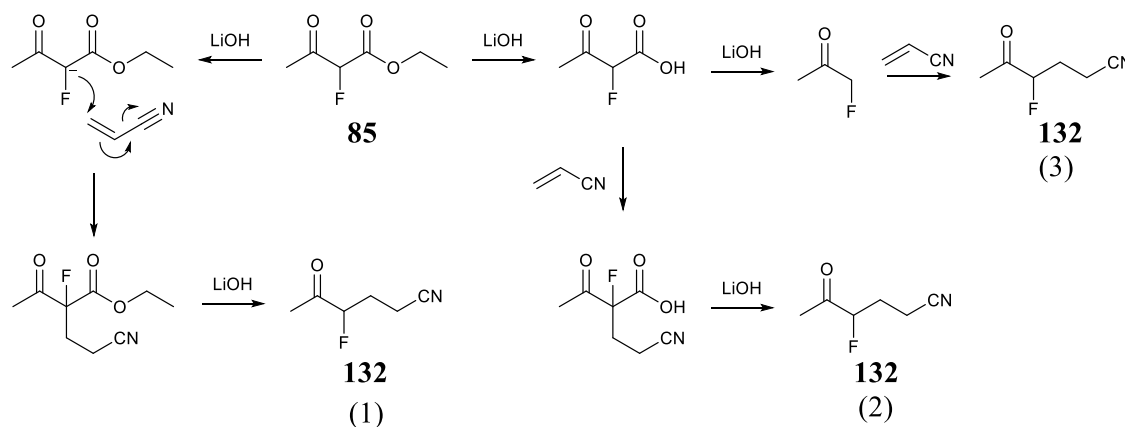

Figure 121 - Possible reaction mechanisms for the synthesis of **132**

The reaction was optimised to try to reduce the amount of acid side-product. The temperature of the reaction was trialled at both 0 °C and 60 °C and whilst the former showed no detrimental effect to the product ratios, the rate of reaction was lower. The hotter reaction conditions showed a four-fold increase in the undesirable side product. As such, the reaction temperature was kept at room temperature and the base equivalents were varied from 0.2 equivalents up to 2.2 equivalents. The optimum amount of base was found to be 1.2 equivalents; less than this caused incomplete conversion, whilst above this caused a greater degree of acid generation.
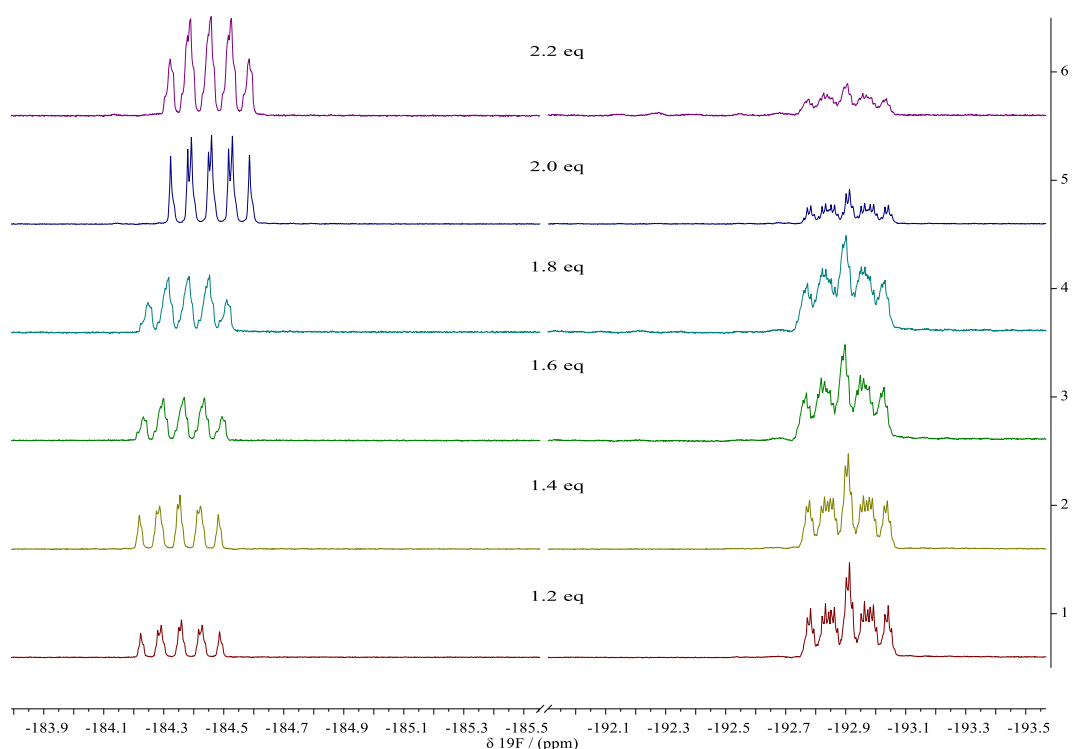
Figure 122 - ^{19}F NMR spectra of the optimisation reactions for the ketones, showing varying amounts of acid product at approximately -184 ppm and **132** at approximately 193 ppm with different equivalents of base
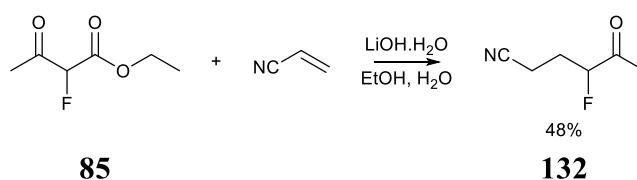
The final conditions consisted of a room temperature reaction using 1.2 equivalents of LiOH.H$_2$O and, upon work-up, the removal of the acid impurity through adjustment of reaction pH to neutral and washing with water. Crude **132** was left in approximately 97% purity but subjected to a vacuum distillation to ensure 99%+ purity for LIB analysis in a 48% yield. This experiment was also repeated several times, on 10 g scale and produced crude product pure enough for repeated use in further reactions.

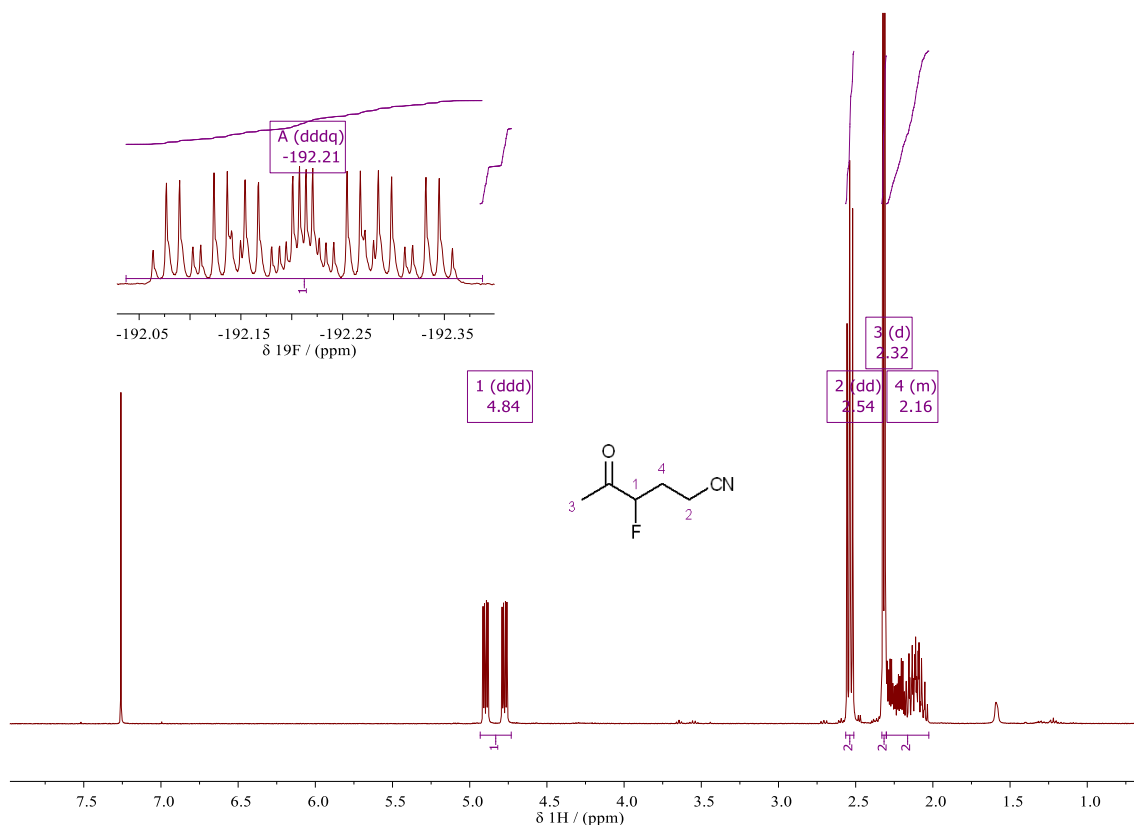Figure 123 - 1H NMR spectrum of **132**, (inset) 19F NMR spectrum of **132**

3.6.2   Substitution reactions

To generate the longer chained ketone derivatives, substitution reactions were utilised. This was first attempted using the same reaction conditions as described previously (for the synthesis of **132**) but this showed no product by ^{19}F NMR spectroscopy, only starting materials. As a result of this, numerous other conditions were trialled but no evidence of the target compound being synthesised was found.
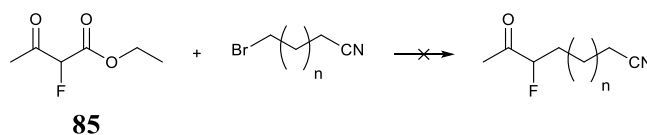

Figure 124 - Unsuccessful transformation to desired ketones from ethyl 2-fluoroacetate where n = 1 or 2

Due to these results, the strategy for the synthesis of these compounds was changed to that which was trialled first for **132**; a late stage-fluorination technique (Figure 125). Different bases were trialled for the alkylation of methyl acetoacetate, and the use of

sodium hydride produced the least amount of side products and highest degree of conversion to the desired product by GCMS. To aid in the purification of the final ketone compounds, these intermediates were purified by vacuum distillation, giving **134** in 77% yield and **135** in 72% yield.

The use of potassium *tert*-butoxide, as discussed above, allowed the deprotonation and fluorination using Selectfluor^{TM} without the competing reverse Claisen condensation reaction occurring. The crude products of these reactions were used without purification in the Krapcho decarboxylation reactions, which took 3 hours for **136** and 9 hours for **137** to reach completion respectively. The purification of these compounds proved very challenging and, after several vacuum distillations and column chromatography, the compounds were used for subsequent LIB analysis at 96%+ purity by ^{19}F NMR spectroscopy and GCMS, with yields of 36% and 30% for **136** and **137** respectively and overall yields, from methyl acetoacetate to final compounds, of 20% and 16% for **136** and **137** respectively.
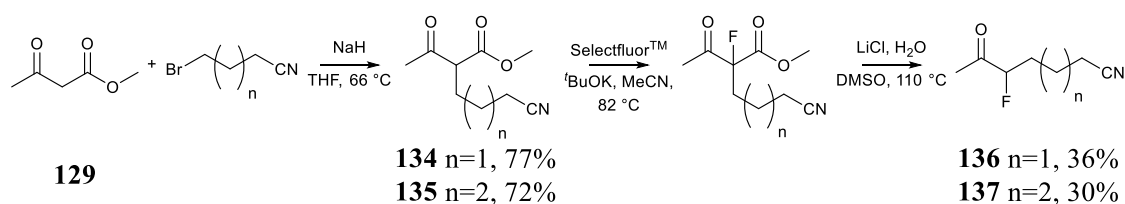

Figure 125 - Synthetic strategy for the synthesis of longer chained ketones
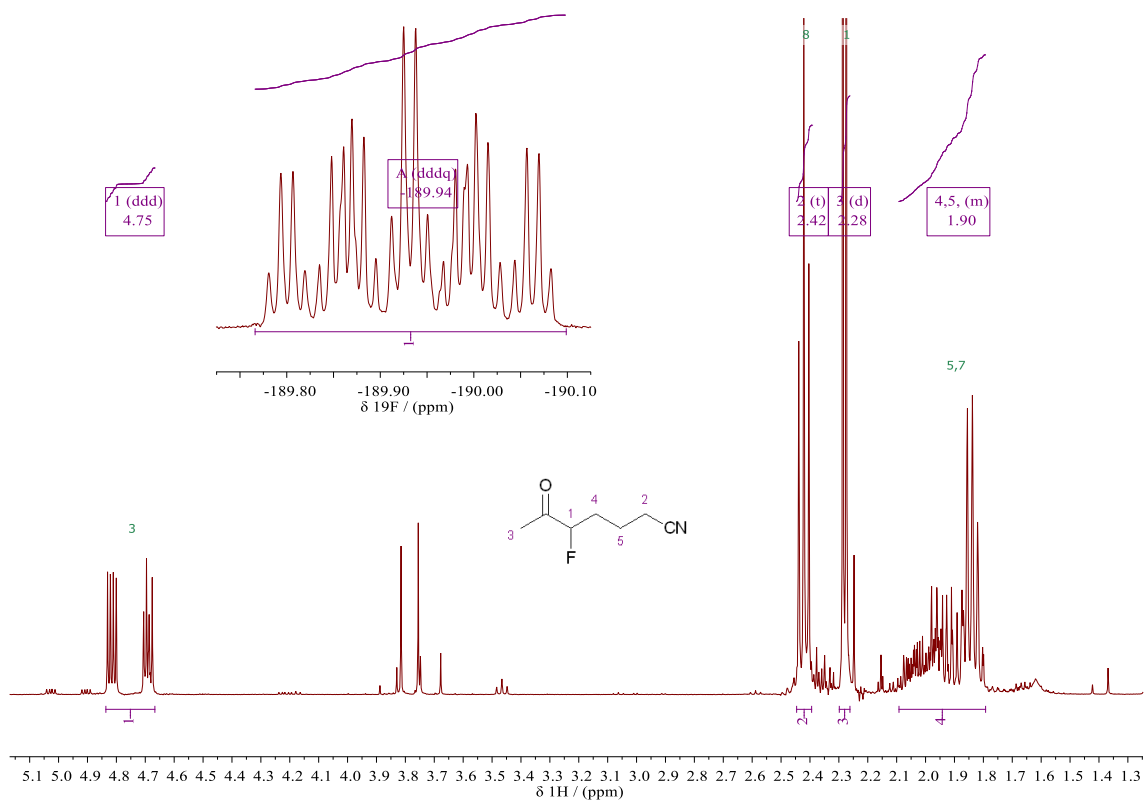
Figure 126 - ^{1}H NMR spectrum of **136**, (insert) ^{19}F NMR spectrum of **136**

3.7   Wittig reactions

Following on from the synthesis of the ketone **132**, synthesis of the alkene derivative was attempted via a Wittig reaction. The ylid was prepared by the dropwise addition of nBuLi to methyltriphenylphosphonium bromide, after which **132** was added dropwise and the reaction stirred at room temperature overnight.
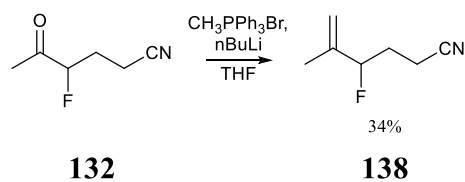
The reaction was followed by ^{19}F NMR spectroscopy and showed conversion to an apparent doublet of doublet of doublet of triplets. After an aqueous work-up, the crude product was purified using column chromatography to give the alkene **138** in 34% yield.
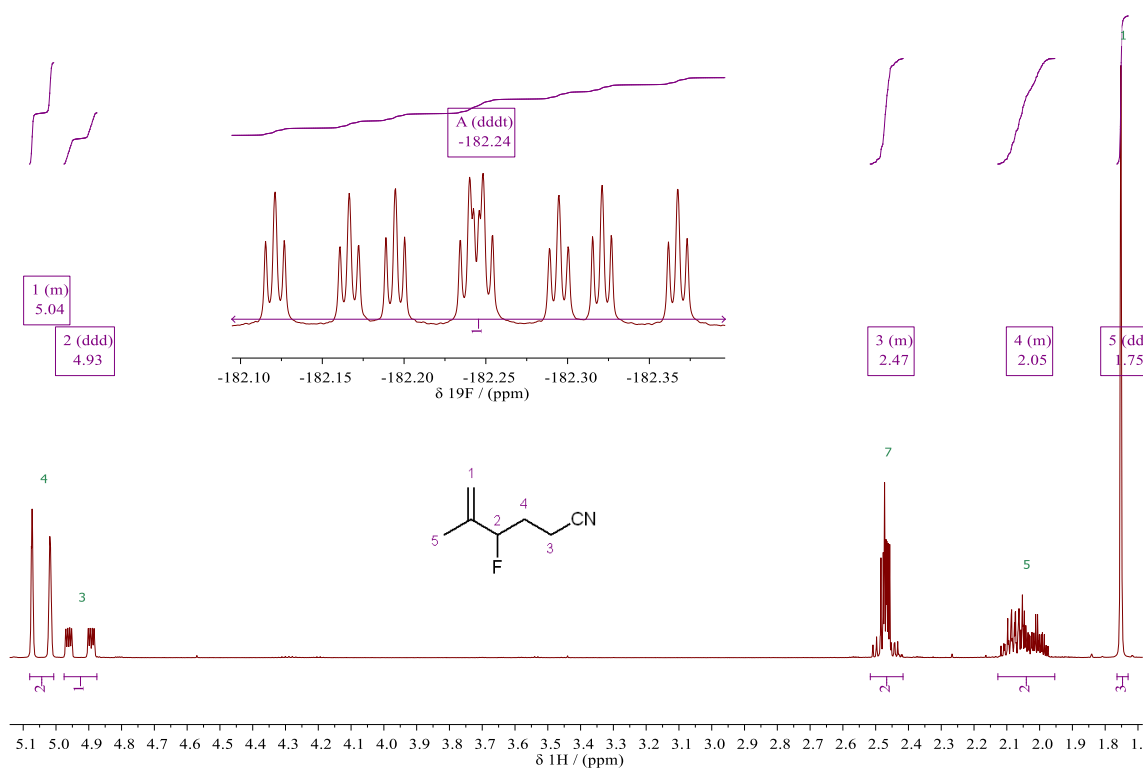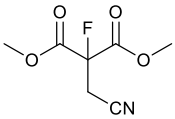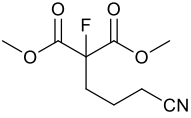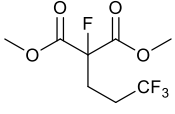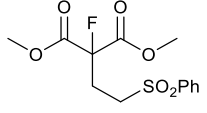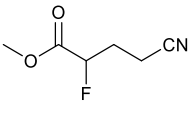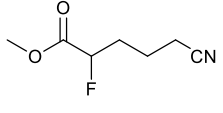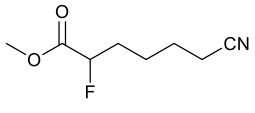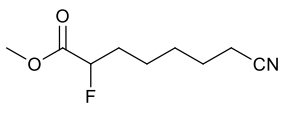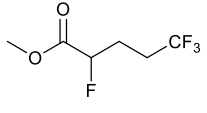
Figure 127 - ¹H NMR spectrum of **138**, (insert) 19F NMR spectrum of **138**
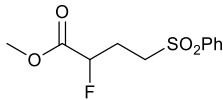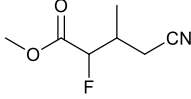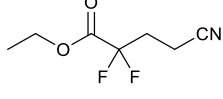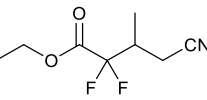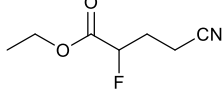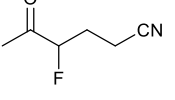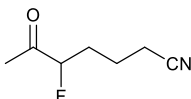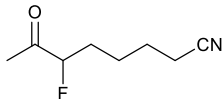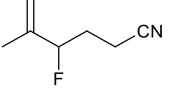
3.8 Compound list

The following compounds (Table 8) were synthesised by processes described in this chapter.

Table 8 - Compounds synthesised and purified in this chapter

Sample Name	Sample Number	Sample Structure
Di-*iso*-propyl 2-fluoromalonate	**106**	
Di-*iso*-propyl malonate	**107**	

Dimethyl 2-(cyanomethyl)-2-fluoromalonate	**108**	
Dimethyl 2-(3-cyanopropyl)-2-fluoromalonate	**109**	
Dimethyl-2-(3,3,3-trifluoropropyl)-2-fluoromalonate	**110**	
Dimethyl-2-(2-phenylsulphonyl-ethyl)-2-fluoromalonate	**111**	
Dimethyl 2-(2-cyanoethyl)-2-fluoromalonate	**112**	
Dimethyl 2-(4-cyanobutyl)-2-fluoromalonate	**114**	
Methyl 6-cyano-2-fluorohexanoate	**117**	
Methyl 7-cyano-2-fluoroheptanoate	**118**	
Methyl 2,5,5,5-tetrafluoro-pentanoate	**119**	

Methyl 2-fluoro-4-(phenyl-sulfonyl)-butanoate	**120**	
Methyl 2-fluoro-3-methyl-4-cyano-butanoate	**122**	
Ethyl 2,2-difluoro-4-cyano-butanoate	**126**	
Ethyl 2,2-difluoro-3-methyl-4-cyano-butanoate	**127**	
Ethyl 4-cyano-2-fluoro-butanoate	**128**	
3-fluoro-5-cyano-pentan-2-one	**132**	
4-fluoro-6-cyano-hexan-2-one	**136**	
5-fluoro-7-cyano-heptan-2-one	**137**	
2-methyl-3-fluoro-5-cyano-pentan-2-ene	**138**	

3.9   Conclusion

Utilising a range of different synthetic methods, a library of different compounds for use as electrolyte additives for LIB analysis were synthesised. Di-*iso*-propyl malonates (**106** and **107**) were synthesised through transesterification reactions. In addition to this, β-substituted compounds were generated through Michael addition and substitution reactions, giving compounds of varying chain lengths and varying functional groups (**108**, **109**, **110**, and **111**).

These alkylated compounds then underwent mono-decarboxylation through the application of the Krapcho decarboxylation reaction, which was found to proceed faster than literature procedures, likely due to the presence of the fluorine atom promoting the process. It was also noted that the shorter the alkyl chain, and closer the electron withdrawing group, that the shorter the Krapcho decarboxylation reaction time was.

The methyl substituted system was synthesised through the use of crotononitrile in a Michael addition reaction and subsequent Krapcho decarboxylation. Other substituted systems were trialled, but ultimately these reaction attempts were unsuccessful.

The ethyl ester equivalent of **112** was isolated through a reverse-Claisen condensation-type reaction of ethyl 2-fluoroacetoacetate, acrylonitrile and sodium ethanoate. The reaction was repeated using *iso*-propyl 2-fluoroacetoacetate but the equivalent product could not be produced, presumably due to steric effects blocking the reaction.

Ketone equivalents of the mono-ester systems were synthesised through two different means. The shortest alkyl-chained compounds, **132**, was serendipitously prepared through the use of hydrolysis conditions of ethyl 2-acetoacetate in the presence of acrylonitrile. After some optimisation, this reaction was repeatable on larger scale and gave high levels of purity as a crude reaction product without required purification.

Longer chained ketone systems had to be synthesised through a different method; starting from ethyl 2-fluoroacetoacetate resulted in no observed product forming. As such, the synthetic strategy shifted to alkylation of a non-fluorinated substrate. Ethyl acetoacetate was alkylated using sodium hydride and the corresponding bromo-alkyl nitrile and the intermediate fluorinated using Selectfluor™. The Krapcho decarboxylation reaction was

then utilised to give the final compounds, although the purification of these compounds proved challenging and could not be isolated above 96% purity.

These compounds were utilised in subsequent LIB battery analysis discussed in the following chapter.

Chapter 4

LIB analysis of fluoro cyano ester derivatives

The compounds synthesised in the previous chapter were taken forward and analysed for LIB electrolyte additive viability. As discussed at the beginning of the previous chapter, the ownership of the battery division working in collaboration with Durham passed from Sony MSL, Stuttgart, to Murata Manufacturing, Atsugi. As such, the equipment and tests undertaken were slightly different to those described in Chapter 2 due to the availability of different techniques at the different locations.

The analysis within this chapter was taken alongside the synthetic work described within Chapter 3, and provided insight into developing synthetic targets as the project moved forward. The work shall be described as a comparison of all results, as opposed to a chronological discussion, to provide an overview of all the analysis and results of the LIB testing.

The work in this Chapter was undertaken in Atsugi, Japan, in collaboration with Murata scientists during two three week placements. Partway throughout the project, the cell structure within the LIBs, such as electrode coating material, was updated by Murata and, therefore, therefore some results cannot be directly compared. However, indirect comparison is possible through the use of a reference consisting of cells containing no electrolyte additives other than 1% by weight of VC, which is also present in all doped cells. For clarity, the older battery conditions shall be referred to as battery type 1 and the newer conditions shall be referred to as battery type 2.

The types of batteries used for these tests were a mixture of coin cells and pouch cells. Coin cells allow for longer running analysis and were assembled from the constituent parts, shown in Figure 128, with the electrolyte added during assembly. For the pouch cell analysis, the cells were premade using conditions similar to that on a manufacturing plant up to the point of sealing, and the electrolyte was pipetted into the pouch before crimping.
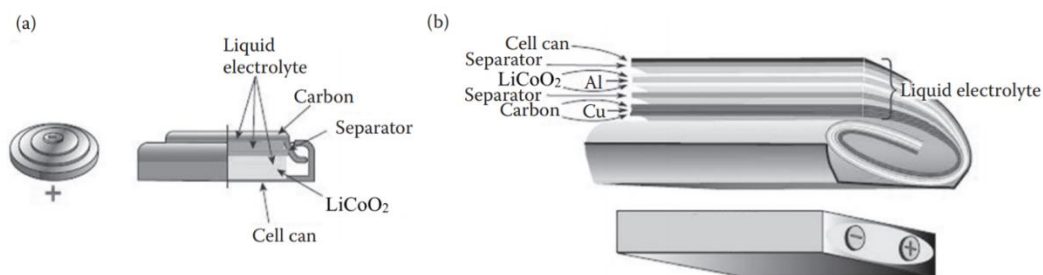
Figure 128 - Cell structures; a) coin cell; b) pouch cell

4.1   Analysis of LIB electrolyte additive

The functionality of our fluorinated additives for the use in LIBs was assessed by different metrics to that in Chapter 2; the use of more sophisticated equipment allowed longer running experiments for cyclic stability and also allowed the analysis of cell swelling and gas production.

4.1.1   Capacity retention

As discussed in Chapter 2, the cyclic stability tests are a practical assessment of the functionality of the cells and, in the following examples, were undertaken using coin cells. The charge and discharge rates were the same for each run for consistency as much as possible. The y-axis, the capacity retention, shows the ratio of discharge available after each cycle compared to the value of the first discharge.
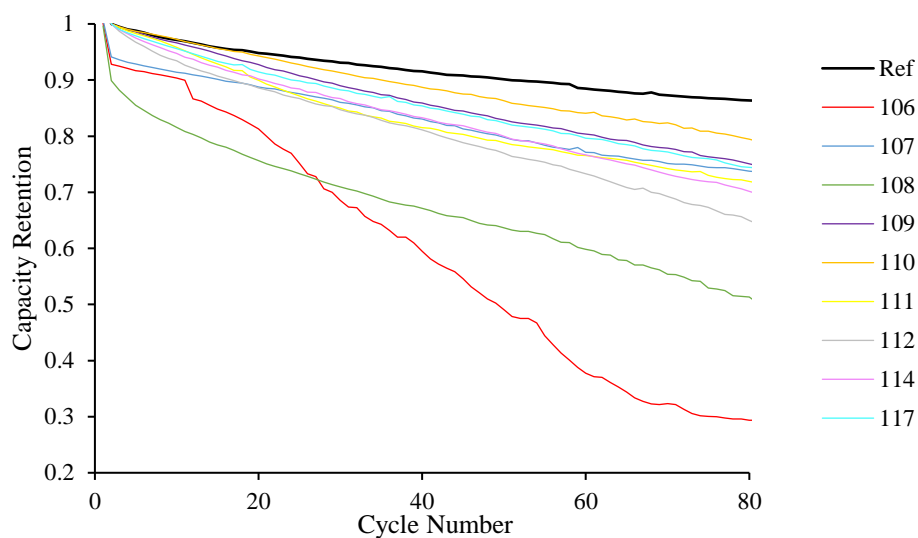
Figure 129 - Capacity retention for additives tested using battery type 1 conditions after 80 cycles
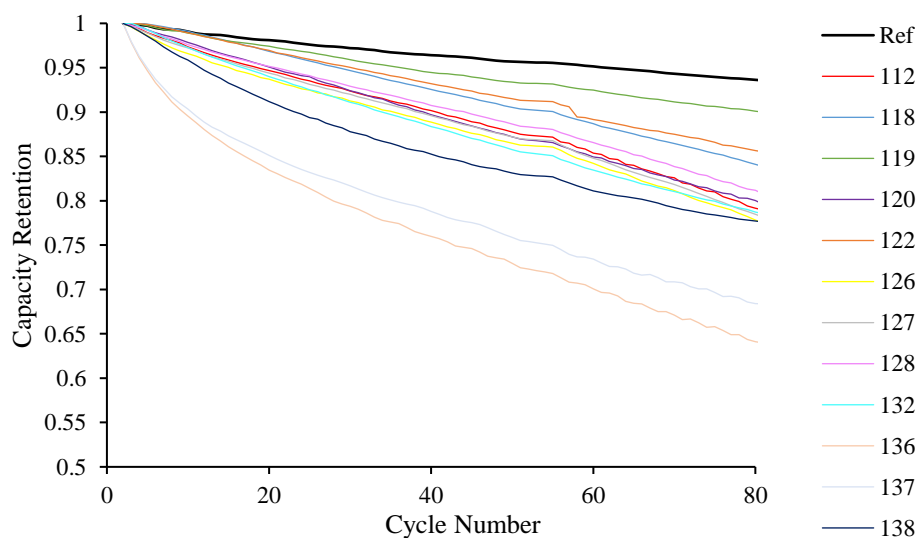
Figure 130 - Capacity retention for additives tested using battery type 2 conditions after 80 cycles

As shown in Figure 129 and Figure 130, no additive improved cell performance compared to the reference, although this is not entirely uncommon when additives are present in cells. The detrimental effect, however, should be minimal and as such, some additives were ruled out from these results; **106** and **107**, the di-*iso*-propyl malonate derivatives tested, proved comparable or much worse to other malonates previously tested and so were not taken forward for further LIB analysis.

Comparison of these electrolyte results give insight into beneficial structural elements of additives and help shine light onto which structural features are detrimental to LIB function. Comparison of **102**, **109**, **112** and **114** allows the effectiveness of diester systems to be compared to monoester systems.
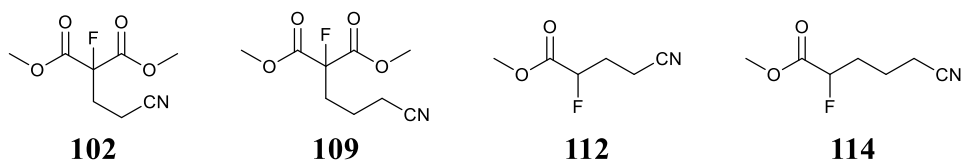
Figure 131 - Structures that allow the comparison of the effect of diesters compared to monoesters
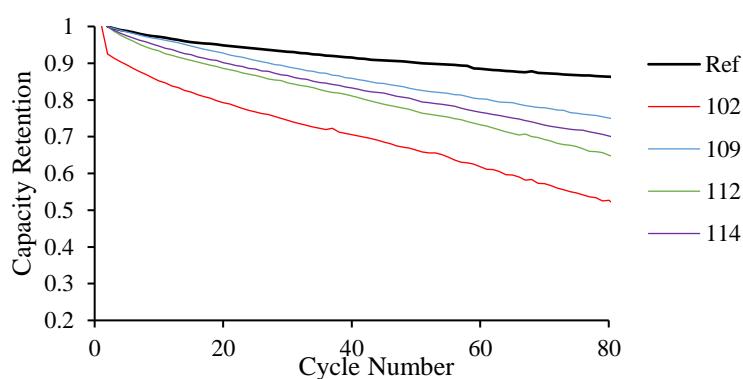
Figure 132 - Capacity retention of mono- and diester compounds

Comparing **102** with **112**, the monoester has a markedly improved capacity retention compared to the di-ester, a result which is reflected in the comparison of **109** and **114**. This clearly shows that the monoester compounds are less detrimental to LIB capacity retention than diesters or malonate-like compounds.

Despite the malonate-type compounds causing a greater reduction in capacity retention, the comparison of **102**, **108** and **109** (Figure 133) shows insight into the effect of alkyl chain length.
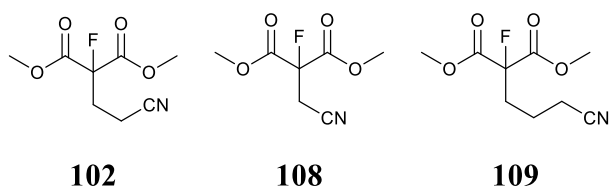
Figure 133 - Structures of malonate-like compounds that increase in length of alkyl chain
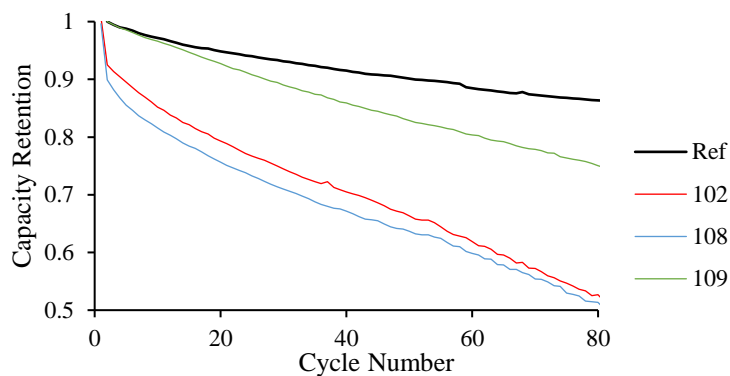
Figure 134 - Capacity retention of **102**, **108** and **109**

Looking at Figure 134, it's easy to see a simple relationship; the shorter the alkyl chain, the greater the detrimental effect upon capacity retention. The most significant improvement is observed going from **102** to **109**, an increase in one CH_2 group. Consequently, this effect can be further explored by the comparison of the methyl fluoro cyano ester additives, shown in Figure 136.
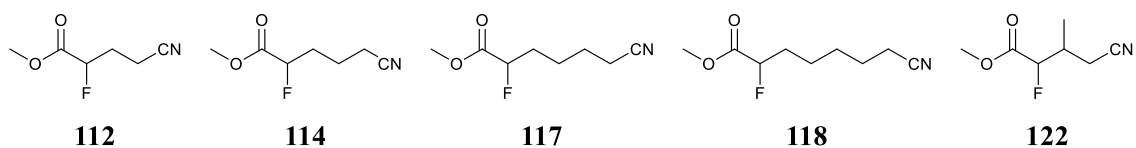
Figure 135 – Structure of methyl fluoro cyano esters
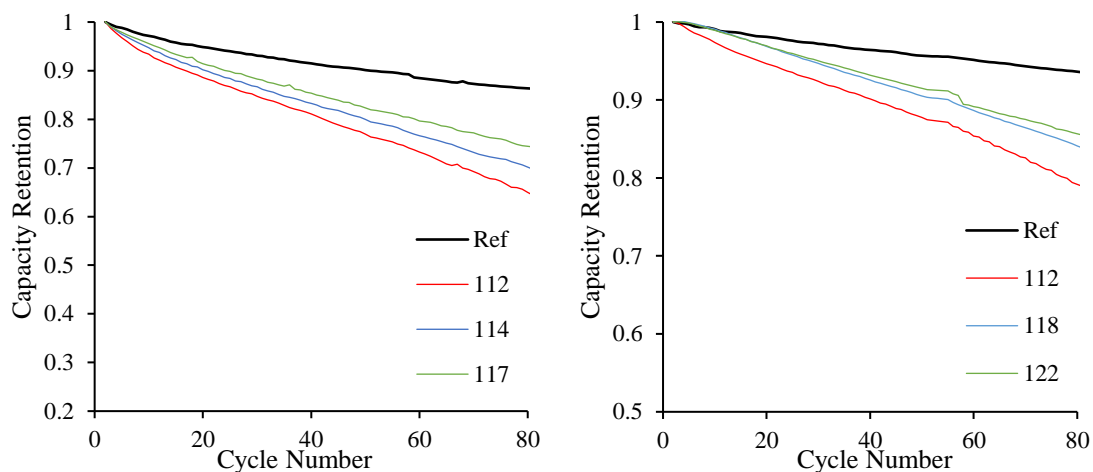
Figure 136 - Capacity retentions for methyl fluoro cyano ester additives with varying alkyl chain length, (left) battery type 1 conditions; (right) battery type 2 conditions

These results are also in agreement with those of the malonate-type compounds. Whilst direct comparison of **114** and **117,** and **118** cannot be done due to different conditions, they both show markedly improved capacity retentions compared to **112**. It is possible, however, that the change of effect between **117** and **118** (an increase of one CH_2 group) is minimal. Interestingly, **122**, which is a branched isomer of **114**, shows a similar effect to that of **118**. It is possible that the electron donating effect of the methyl group is providing a similar effect as a longer chain within the additive.

The effect of the cyano-group upon capacity retention was also probed through the comparison of the results of **102**, **110** and **111**. These functional groups were chosen as they were all electron withdrawing, but with the potential to react differently within the cell.
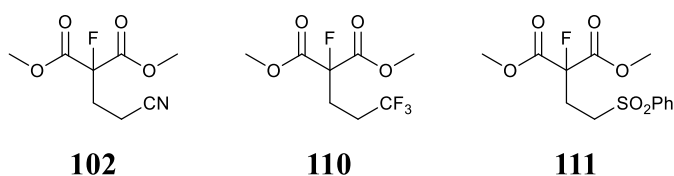
Figure 137 – Malonate-type additives with varying functional groups at the end of the alkyl chain
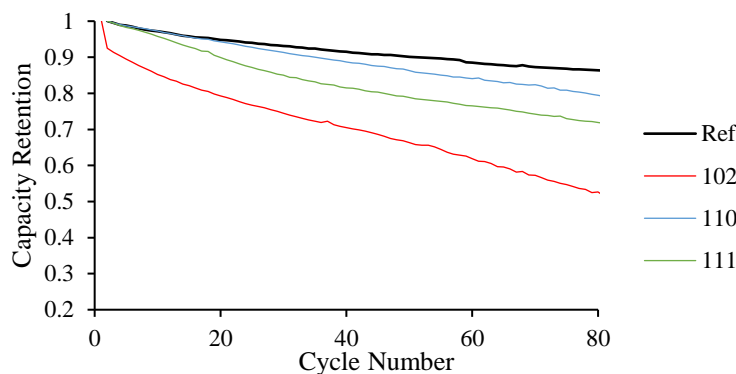
Figure 138 - Capacity retention of malonate-type additives with different functional groups at the end of the alkyl chain

Interestingly, the additive that caused the most dramatic detrimental effect in the LIB over 80 cycles was the cyano-containing additive, with the trifluoromethylated additive performing best of the three. This holds true when comparing the different functional groups within the methyl fluoro cyano ester system (Figure 140), although the phenyl sulfonyl additive performs similar to the cyano containing compound.

112   **119**   **120**
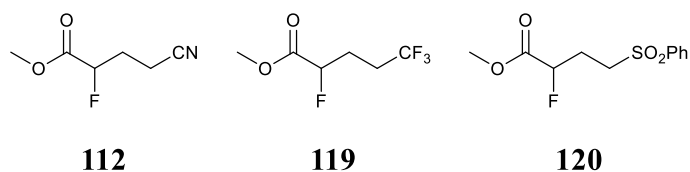
Figure 139 – Methyl fluoro cyano ester additives with differing functional group at the end of the chain
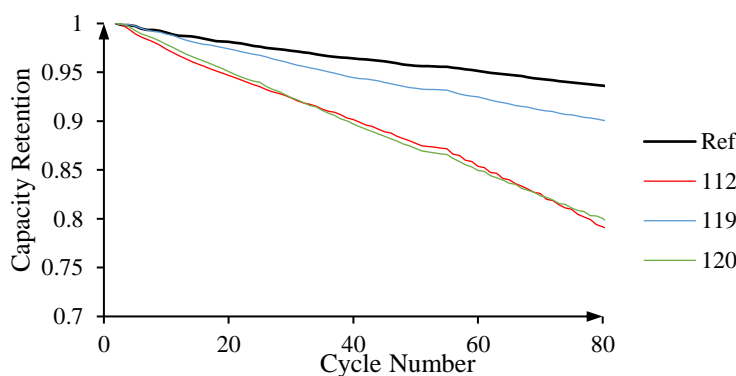
Figure 140 – Capacity retention of methyl fluoro cyano ester additives with differing functional group at the end of the chain

The effect of changing the ester alkyl group of the fluoro cyano ester can also be seen from comparing **112** (methyl ester) and **128** (ethyl ester); the effect is minimal (Figure

142), suggesting chain length at this position has little effect on capacity retention, although the small sample size means this conclusion has to be drawn with some degree of caution.
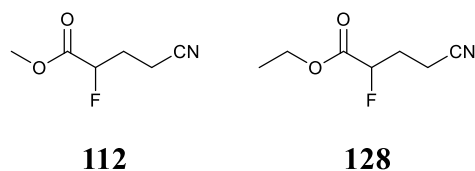
Figure 141 - Additives with different alkyl esters
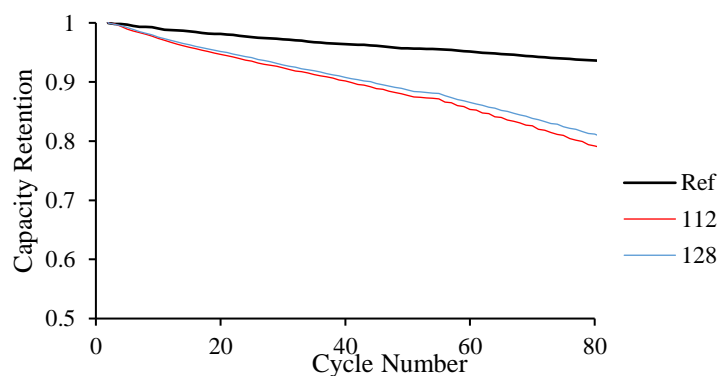
Figure 142 - Capacity retention of additives with different alkyl esters

The effects of fluorination was also probed through the comparison of **112**, **126,** and the commercially available **139**, as well as the comparison of **122** to **127**. The di-fluorinated compounds, due to the synthetic strategy used for the synthesis of these compounds and commercial availability, are ethyl esters but following on from previous results (Figure 142), this should have minimal effect upon LIB performance.
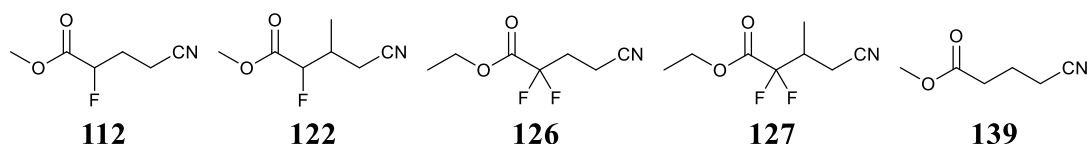
Figure 143 - Structures of additives that allow the investigation of the effect of fluorination upon battery performance
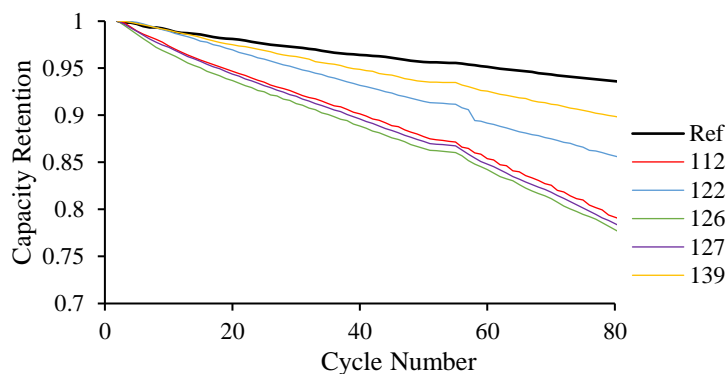
Figure 144 – Capacity retention comparing the effect of fluorination

From Figure 144, it can be seen that the effect of di-fluorination compared to mono-fluorination is minimal with regards to **112** and **126**, although **122** is significantly improved when compared to **127**. In addition to this, the non-fluorinated compound, **139,** performed significantly better than all of the fluorinated additives. It's difficult to draw a definite trend from this, and more experiments would be needed for confirmation, but there is a weak correlation between a lower degree of β-fluorination and improved capacity retention.

The use of alternative functional groups was investigated, through the use of ketone and alkene groups' *beta* to the fluorine group.
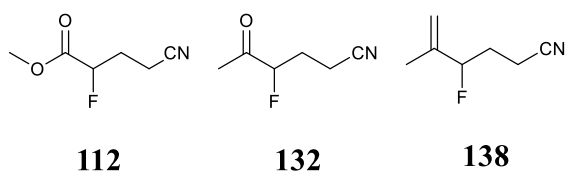
Figure 145 - Structures of additives that vary the functional group adjacent to the fluorine to carbon bond
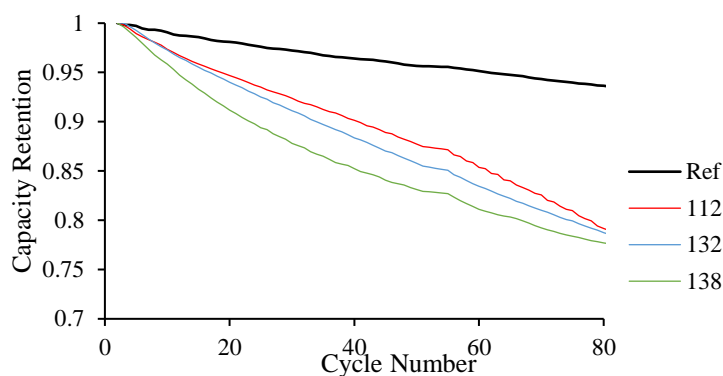
Figure 146 - Capacity retention of additives with different functional groups adjacent to the fluorine to carbon bond

Altering the functional group adjacent to the fluorine atom results in small changes in capacity retention, with all showing similar degradation after 80 cycles.

The ketone derivatives were further investigated, and compounds of varying alkyl chain lengths were synthesised (Chapter 3) to determine the alkyl chain in the ketone derivative has on capacity retention.
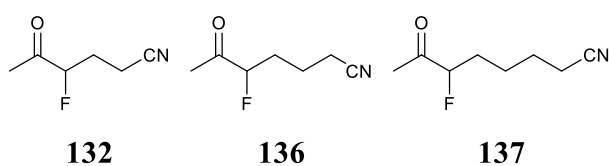
Figure 147 - Structure of ketone additives with varying alkyl chain lengths
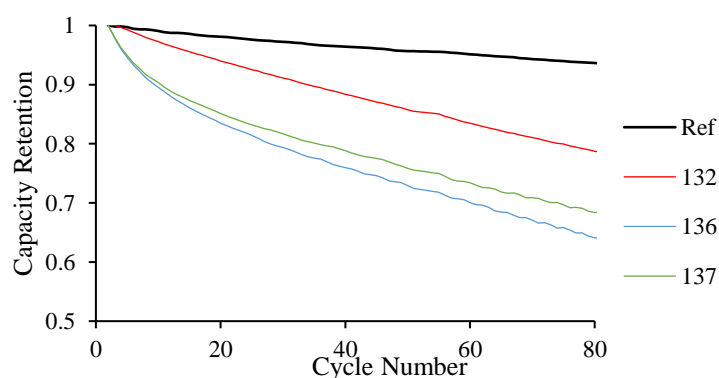
Figure 148 - Capacity retention of different ketone additives

Interestingly, the effect of chain length upon capacity retention for ketone additives follows a weak correlation that is opposite to that shown for the ester compounds

described above. The least detrimental to battery performance is found to be **132**, the shortest alkyl chain. Despite **136** performing marginally better than **137**, these two are comparable.

Whilst providing data into the long-term use as additives, capacity retention is only one facet of LIB performance which need to be considered alongside further data.

4.1.2   Float test

The float test behaves as a stress test for LIBs and results in artificial aging of the cells. This is achieved by charging and holding the cells at a constant voltage of 4.45 V at 60 °C for several hours. As these are at the most extreme and reactive conditions, degradation within the battery leads to gas production and, therefore, swelling within the cell. The results of these tests are measured by monitoring the thickness of the cells. The swelling of LIBs is of significant interest, due to notable recent examples of batteries bursting making headline news[122] and is, therefore, of significant interest to the development of new additives.
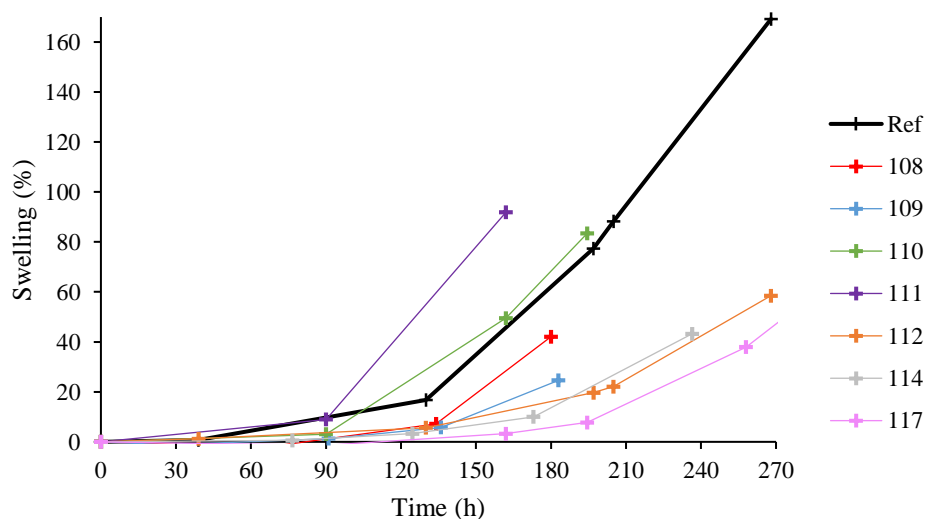
Figure 149 - Float test results for additives tested with battery type 1 conditions
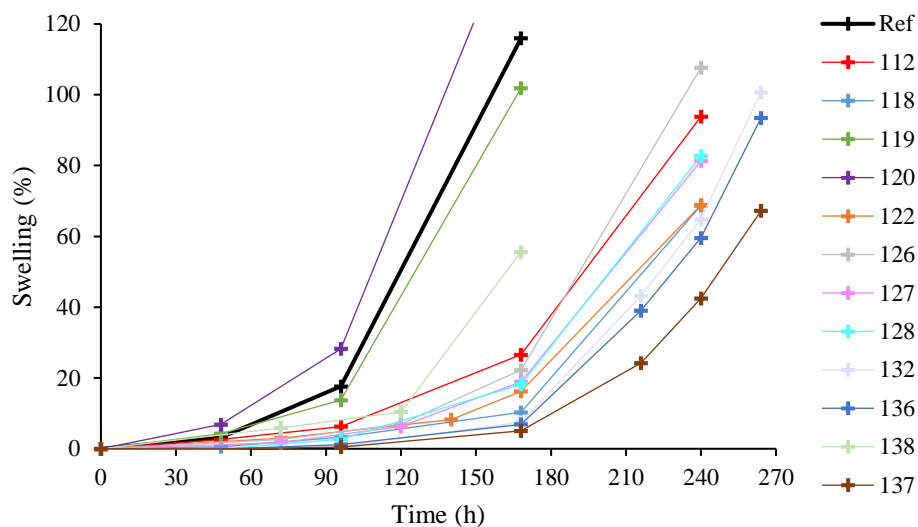
Figure 150 - Float test results for additives tested with battery type 2 conditions

The results of the float tests showed that most additives investigated decreased cell swelling in comparison to the reference electrolyte. Notably, **110**, **111**, **119** and **120** all performed comparably or worse than the reference sample. These samples differ from the other additives as they lack a cyano functional group. Due to the poor performance of these additives they would not be viable LIB electrolyte additives.

Similarly to the capacity retention tests, comparison of certain related structures allows the probing of the effect of certain functional groups upon the cause of swelling within LIBs. The comparison of **102**, **109**, **112** and **114** can show the effect of diester compounds compared to monoester compounds.
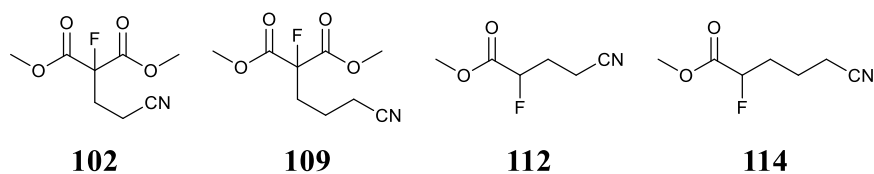
Figure 151 - Structures that allow the comparison of the effect of diesters compared to monoesters
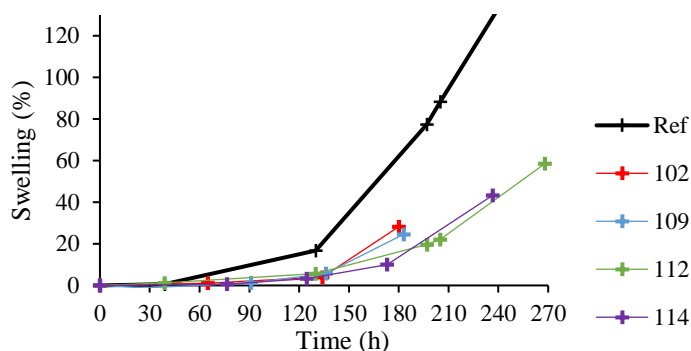
Figure 152 – Float test analysis comparing monoester to diester LIB additives

The monoester additives perform markedly better than the malonate-like compounds, with both **112** and **114** showing improved swelling performances over **102** and **109**. This is in agreement with the cyclic stability data, suggesting that the malonate-type systems are inferior to monoesters for use as LIB electrolyte additives.
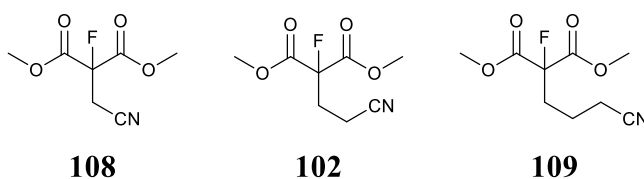
Figure 153 - Structures of malonate-like compounds that increase in length of alkyl chain
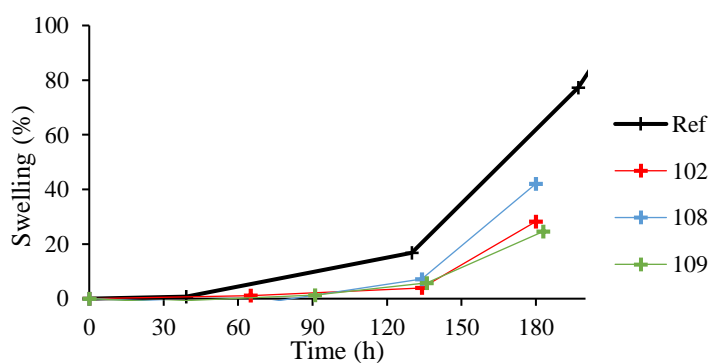
Figure 154 – Float test analysis showing the effect of chain length upon malonate-type additives

Comparison of **102**, **108,** and **109** probes the effect of chain length upon cell swelling and, as shown in Figure 154, highlights that the longer the chain length between fluoroester and cyano functionality, the more the swelling is inhibited. This result is in agreement

with the comparison of different chain lengths for methyl fluoro-cyano ester compounds, although it's difficult to say whether the effect of increasing the chain length has tapered off due to the inability to directly compare **117** and **118**. Interestingly, the substituted **122** compound also shows swelling inhibition similar to that of **118**.
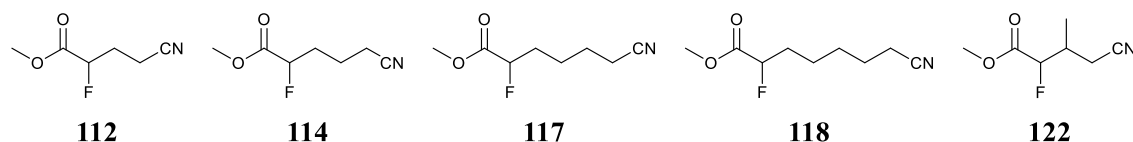
Figure 155 – Structures of monoester additives with varying structures of the alkyl backbone
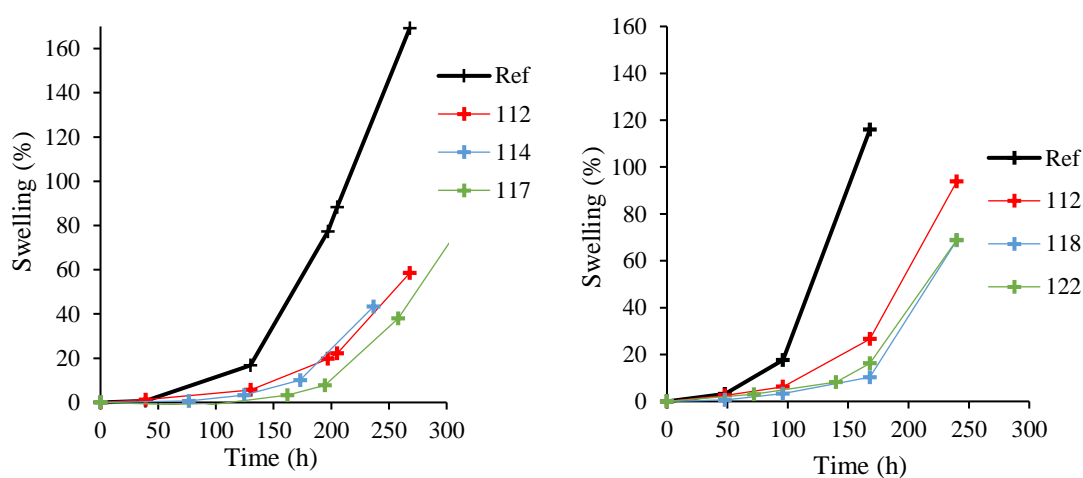
Figure 156 - Float tests comparing the effect of chain length and structure on cell swelling, (left) battery type 1 conditions; (right) battery type 2 conditions
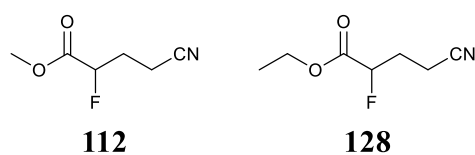
Figure 157 – Structures of additives that vary only by the alkyl ester group
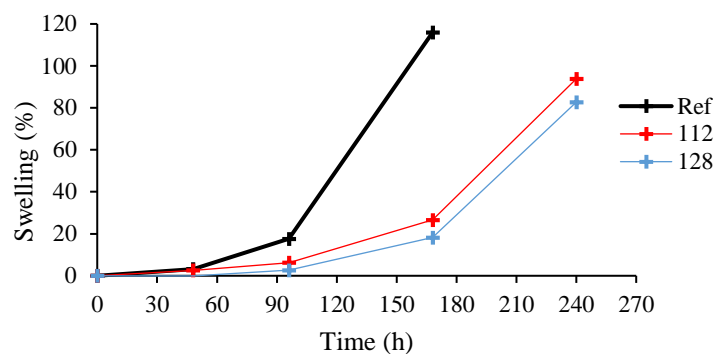
Figure 158 – Float test probing the effect of changing the ester alkyl upon cell swelling

Comparing **112** and **128**, suggests that the ethyl group (**128**) is marginally better at swelling inhibition than the methyl ester (**112**). This effect is not significant however, and as the results are comparable, allows for the reasonable cross examination of the ethyl ester difluorinated species **126** and **127** with the methyl ester monofluorinated species **112** and **122**.

| **112** | **122** | **126** | **127** | **139** |
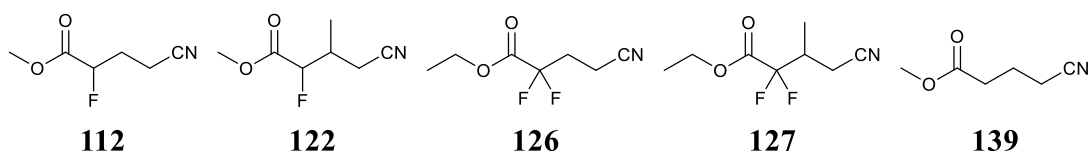
Figure 159 – Additives which vary in degree of β-fluorination
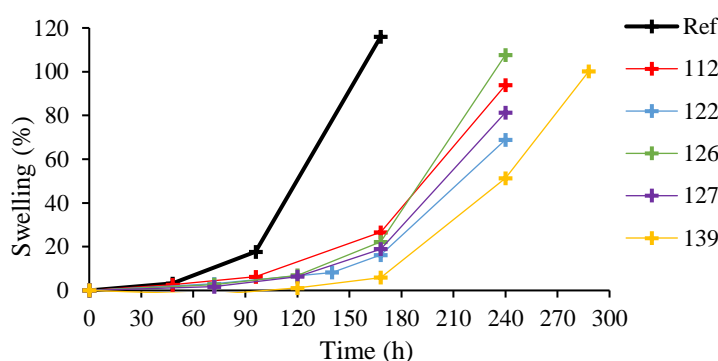
Figure 160 – Float test probing the effect of fluorination upon LIB swelling

Comparing the results of the float tests of mono- and di- β-fluorination, the effect of the fluorine atom is quite clear; decreasing the degree of β-fluorination results in greater inhibition of swelling of the LIB cell. The difference between **112** and **126** is comparable

to that of **122** and **127**, and the non-fluorinated additive shows significantly increased levels of inhibition.
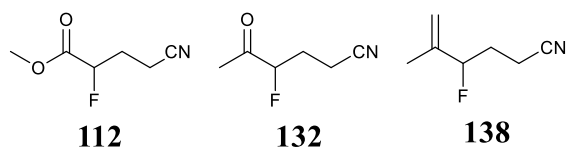
Figure 161 – Structures of additives that vary the functional group adjacent to the fluorine to carbon bond
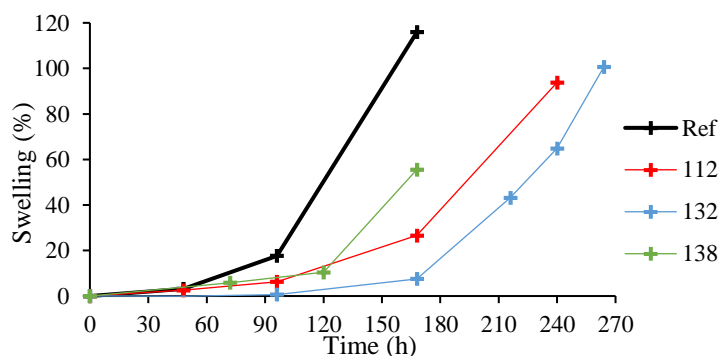
Figure 162 – Float test comparing the effects of different functional groups adjacent to the fluorine to carbon bond on LIB swelling

Changing the functional group *beta* to the carbon-fluorine bond also shows dramatic changes to the swelling within the cell. The alkene based additive shows poor swelling inhibition, whilst the ketone derivative shows increased improvement to the prevention of swelling. This is somewhat surprising due to the similar behaviour shown by these compounds in the capacity retention tests, but is possibly due to different additive degradation pathways within the cell.
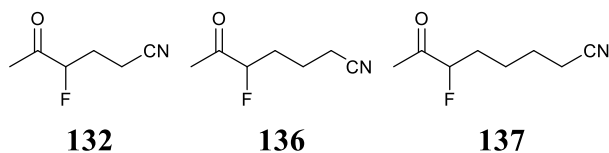
Figure 163 – Structures of ketone additives with different chain lengths
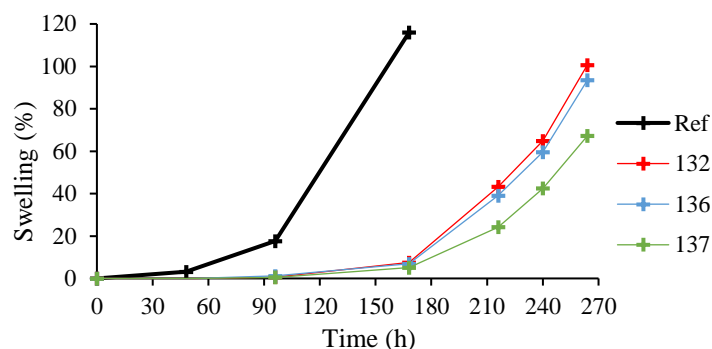
Figure 164 – Float test analysing the effect of ketone alkyl chain length upon cell swelling

The comparison of fluoro cyano ketone derivatives of different chain lengths shows a similar trend to that observed for the methyl fluoro cyano esters above; the longer the alkyl chain between functional groups the more inhibited the swelling. Interestingly, this effect seems to be much larger between **136** and **137** than **132** and **136**.

4.1.3   Conclusions drawn from capacity retention and float test data

The combined results of the capacity retention and float tests show that many of the fluorinated compounds synthesised are not viable electrolyte additives for LIBs. It was shown that the monoester systems are more beneficial to both swelling prevention and lifetime stability than the malonate like systems.

It was observed that the cyano functional group is much more beneficial to cell swelling inhibition than the phenyl sulfonyl and trifluoromethyl functional groups. The latter two families of additives performed comparable or worse than the reference sample with regards to swelling of the cell.

Varying the alkyl group bonded to the ester results in minimal change to battery properties, although this must be taken with some caution due to the comparison of only two compounds. Similarly, the use of alkene over ketone or ester functional groups results in more detrimental effects to battery operation.

From these experiments, it was shown that the lower degree of β-fluorination improves cell performance; that is monofluorinated are more effective than difluorinated analogues.

For all compounds, increasing the alkyl backbone chain length between the fluoroester and cyano functional group increased the degree to which swelling was inhibited, although for the ketone additives this also caused a decrease in capacity retention. For the methyl fluoro cyano esters, the longer alkyl chain resulted in improved capacity retention. Interestingly, the branched backbone compound showed improvement to cell swelling inhibition similar to that of the longer chained compound.
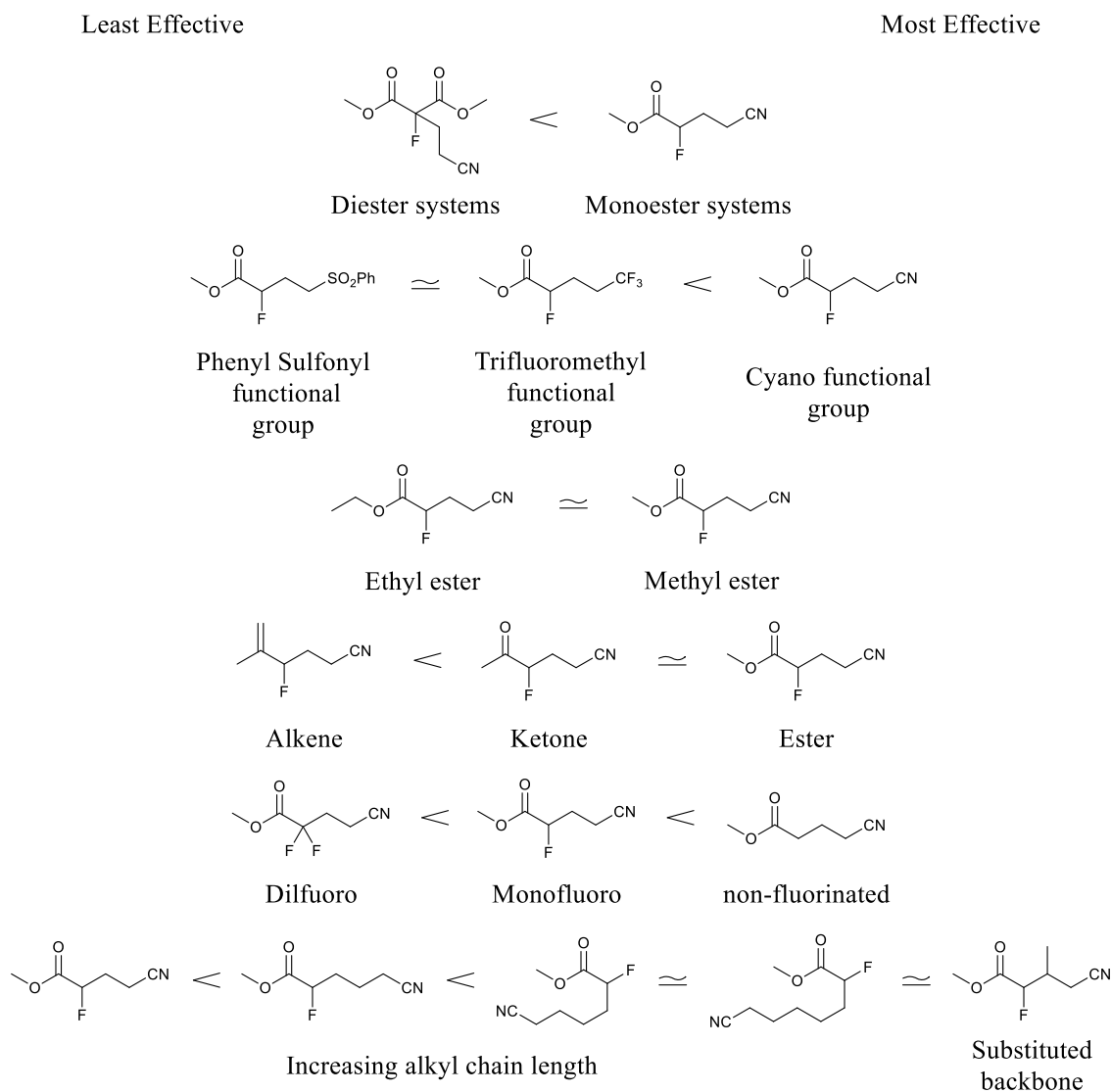
Figure 165 - Conclusions from capacity retention and float test data

Overall, the additive that inhibited cell swelling the most was **137**, the longest chained ketone, although this additive also gave rise to a large detrimental effect to capacity

retention. The compound that performs most strongly in both of these two tests is arguably **118**, the longest chained methyl fluoro cyano ester.

In addition to this, interesting trends have been observed, specifically with the correlation between the swelling prevention dependence on alkyl backbone chain length of the fluoro cyano esters and the mode of action is explored in the remainder of this chapter.

4.2   Insight into additive decomposition of fluorocyanoesters within LIBs

Extensive evaluation of possible additive decomposition pathways was explored for the methyl fluoro cyano esters, with the aim of understanding why alkyl chain length has such a dominant effect upon battery properties when using these additives. It's hypothesised that the first reduction of all these compounds places an electron into the π* orbital on the carbonyl to form a radical anion which then reacts further which may be rationalised using a range of different techniques. Due to processes, such as the McMurry reaction, this is thought to be a fair suggestion.[118]
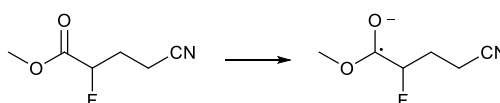
Figure 166 - Proposed first step of additive decomposition

4.2.1   Linear swep voltammetry

Since these electrolyte additives react to form part of the SEI, cyclic voltammetry can give information upon the processes that are undertaken within the cell upon first charge. For these tests, half cells were made using graphite and metallic lithium electrodes, effectively showing only the reactions that occur upon the anode.
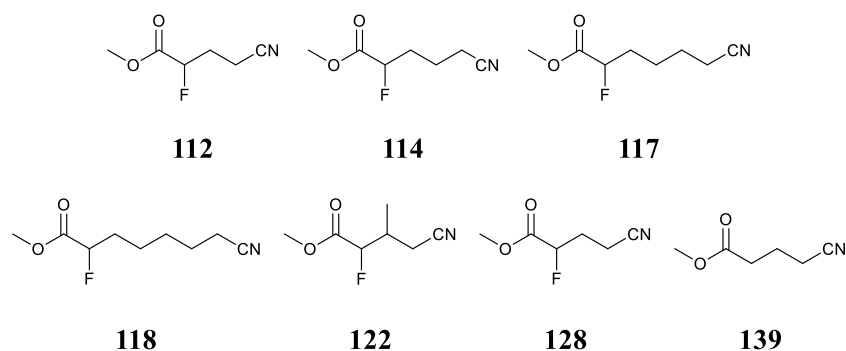
Figure 167 - Structures of the fluoro cyano esters
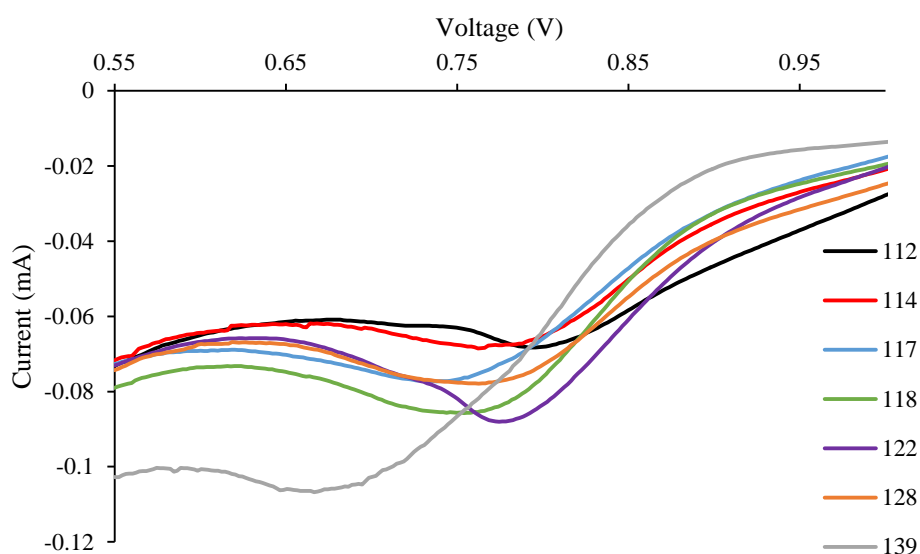
Figure 168 – linear sweep data of the cyano esters, V vs Li/Li⁺

As can be seen, comparing the reduction peak of **112** to **139**, the presence of the β-fluorination results in a more reactive compound, due to reduction occurring at a higher voltage. Similarly, the increasing of the chain length, through the reduction of inductive effects, decreases the reactivity of the additives, and is seen through the shifting of the reduction peak to lower voltages, although this is a small change going from **117** to **118**.

This trend is also observed through examination of the substituted compounds **122** and **128**. The methyl group on the alkyl chain in **122** is electron donating which reduces the inductive effects of the fluorine and results in a shifted reduction peak. The ethyl ester on **128**, compared to the methyl ester in **112**, results in less electron withdrawing effects

observed in the carbon of the carbonyl and therefore reduces reactivity of the compound marginally, resulting in a shift in the reductive peak.

These observations support the conclusion that the carbonyl is reduced first and also points towards trends in battery properties with regards to chain length and reduction potential.

4.2.2   Consumption data

This test consists of one charge then discharge of coin cells which are then opened and the electrolyte extracted with dimethyl carbonate. The exact quantity of components present in the extracted electrolyte was found by GCMS analysis and the use of a calibration curve.

It can be seen in Table 9 that after the first charge and discharge cycle that similar levels of VC and EC consumption occur across all cells, but the amount of additive consumed varies. It can be seen from the relative amounts of additive present that they have been consumed to form the SEI, whereas **139** remained unreacted, supporting the suggestion that β-fluorination increases reactivity due to easier reduction.

Table 9 - Consumption data for cells, reference cells and cells doped with methyl cyano esters

Retention after 1st cycle (%)				
Component	**Ref**	**112**	**114**	**139**
EC	97	99	97	97
VC	27	24	30	26
Additive	-	47	58	101

Also noteworthy is that the degree of consumption of **112** is higher than **114**, supporting the data from the CV measurements that the longer alkyl chains results in a decrease of reactivity.

4.2.3   Electrode surface analysis

Probing of the electrode surface layer was undertaken using ^{1}H NMR spectroscopy. This was achieved through disassembling coin cells within an Ar atmosphere and washing the anode with dimethyl carbonate. This was left to evaporate before the residue was taken up in D_2O. The anode was selected to be the focus of NMR analysis due to previous experiments suggesting the reactions were reductive in nature and, therefore, taking place upon that electrode.

To aid with the analysis of these compounds, the electrolyte solvents used were the deuterated equivalents; EC-d_4 and PC-d_6, which led to much clearer spectra where the peaks observed arise from the additives alone.

Through the use of 2D COSY NMR, the unconsumed native additives were observed clearly within the D_2O wash, along with numerous other complex peaks, many of which are attributed to complex reactions of the additive with electrolyte solvent. Other components were also observed in the NMR spectra however, such as the non-fluorinated equivalents of the additives as well as some fragmentation.

The presence of native and non-fluorinated compounds in the D_2O washings suggests that some of these materials were adsorbed upon the surface, as opposed to reacted into further SEI products. If the latter was true, it would be expected to observe hydrolysis products which is not the case.
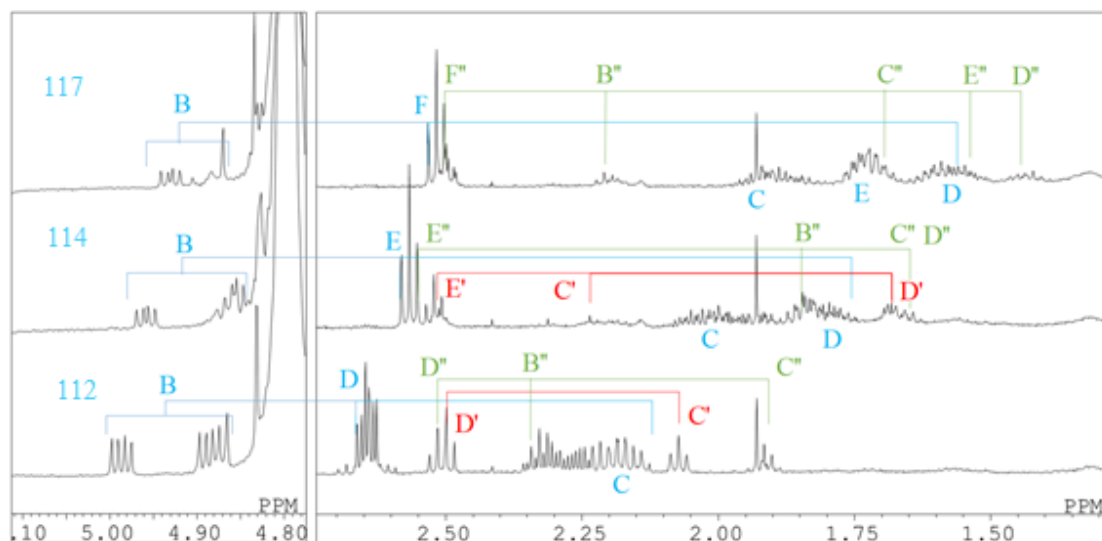
Figure 169 - ^{1}H NMR spectra of the D$_2$O wash of the extracted anodes of test cells
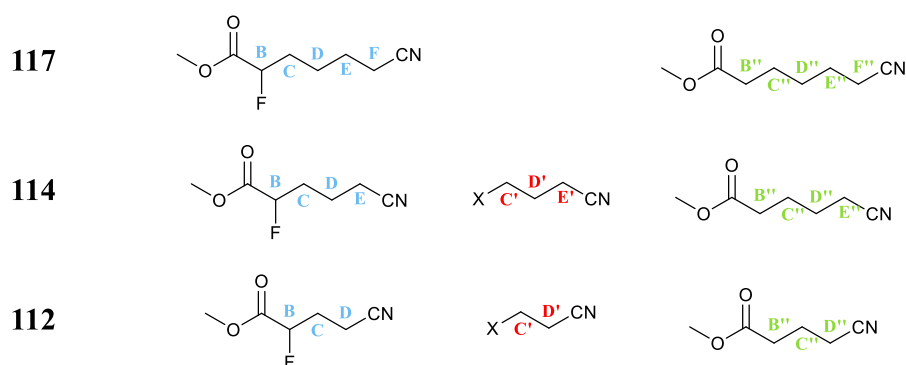
Figure 170 - Structures of samples and detected decomposition products from ^{1}H NMR spectroscopy

The peaks for the unconsumed products were easy to assign by comparison to known ^{1}H NMR spectra. Also the non-fluorinated analogues could be assigned similarly. The positions of C', D' and E' (Figure 170) were assigned and identified using relationships observed in 2D ^{1}H COSY NMR spectroscopy and the relative positions in the spectrum. The identity of X however cannot be definitively assigned, due to a lack of protons on this functional group, but is assumed to be a carbonyl group resulting from the reaction of the fragment with electrolyte solvent. Interestingly, the peaks for the cyano-alkyl fragment were much subdued in **114** compared to **112** and not observed at all for the longer chained **117**.

The analysis of ^{19}F NMR spectroscopy showed only the presence of the native fluorinated additive and additional LiF. When the ^{19}F NMR spectra was obtained for **139**, no fluorine peak for LiF was observed so it can be assumed that LiF resonances are produced by the fluorinated additives.

Bringing all this data together, some information of reactions that occur within the cell can be determined as discussed later (4.2.5). The presence of unreacted additive after cycling is confirmed, as suggested by the consumption data. In addition to this, the presence of non-fluorinated equivalents of each compound suggests that fluorine is lost during the charging process and there is an additional process that produces cyano alkyl fragmentation. It is not known whether these processes are sequential or competing but it can be seen that the latter process is inhibited in longer chained compounds when compared to shorter chained compounds.

4.2.4 Analysis of LIB gas composition

The swelling that occurs within a cell is due to the production of gases throughout the lifespan of the cell and is mostly the production of CO_2 through reactions of the carbonate solvents. The analysis of gas composition was undertaken by injecting Ar into the assembled pouch cells before subjecting the cells to float test conditions. After a set time, the cells were removed from these conditions and the gas extracted carefully using a syringe and analysed using gas chromatography. The use of known standards and a calibration curve allowed determination of relative composition. It's important to note that these values are relative and are not definitive values of the gases present within the cells.

112   **139**   **140**
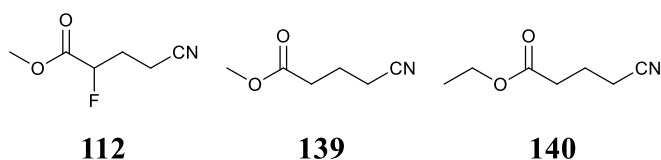
Figure 171 - Compounds compared in the gas analysis
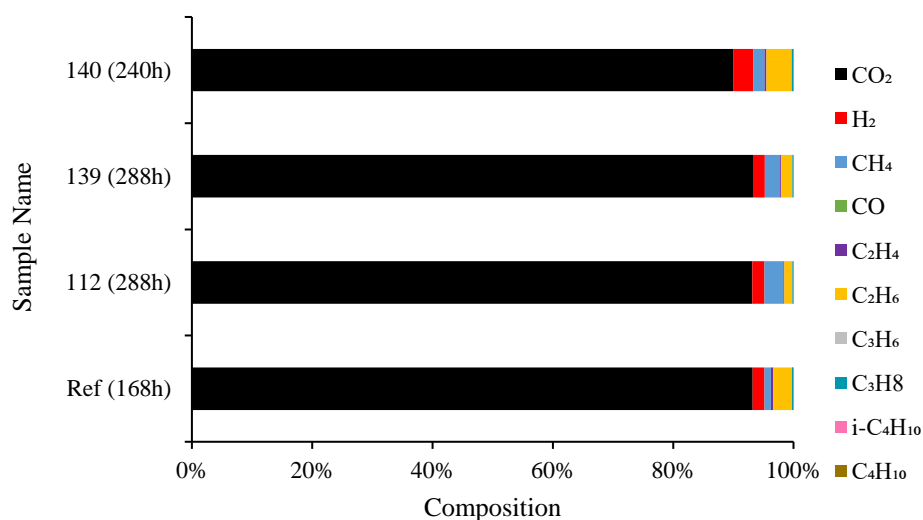
Figure 172 - Relative compositions of gases extracted from cells after float test conditions

It can be seen clearly in Figure 172 that the major component of the gas produced is CO_2 which, as discussed before, is the major product of solvent decomposition. As shown in the float tests, additives prevent swelling of the cells, believed to be by mainly reacting before the solvent to form an SEI and inhibiting decomposition reactions. The relative compositions of the remaining gases present may give insight into the reactions that are taking place within the cell.
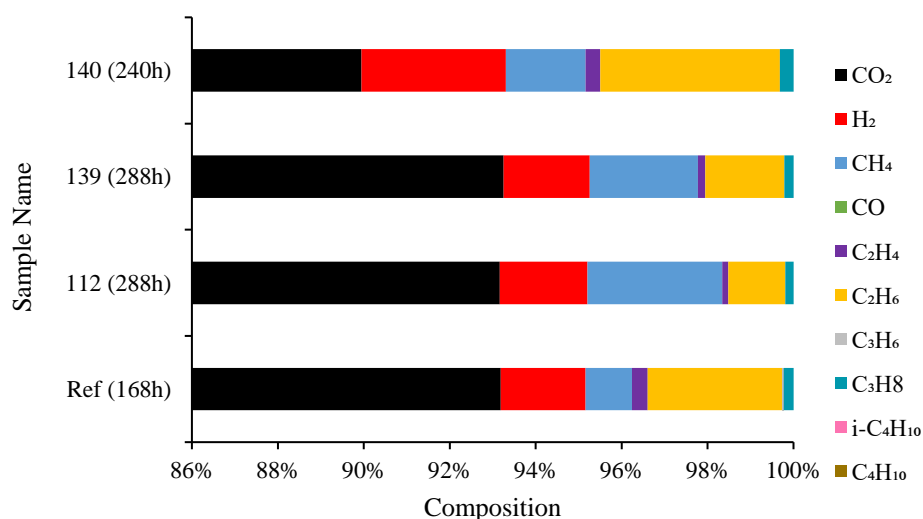
Figure 173 – 'Zoomed in' Relative compositions of gases extracted from cells after float test conditions

Examination of the smaller quantities of different gases shows the production of ethylene and hydrogen gas by fluorinated, non-fluorinated and reference samples and this has been shown to be commonly produced by ethylene carbonate decomposition.[123] What is interesting to note, is the increased proportion of methane produced from both **112** and **139** compared to the reference. When this information is considered alongside the increased amount of ethane produced from **140**, it provides evidence to support a mechanism similar to that which was proposed in Chapter 2; after reduction of the carbonyl peak in these systems, there may be a process which causes the elimination of the alkyl group bonded in the ester. As such, this mechanism needs to be considered when final mechanisms of how additives react within the cell are proposed.

4.2.5   Mechanisms of decomposition

Compiling the information deduced from all of these tests gives three distinct mechanisms for possible decomposition pathways. The presence of the non-fluorinated analogues of the additives in the ^{1}H NMR spectrum, after cycling, shows clear evidence of a defluorination process taking place within the cell. This is further confirmed by the presence of LiF in the ^{19}F NMR spectra of the fluorinated additives. As the first electron transfer is the reduction of the carbonyl from the CV measurements, the subsequent loss of fluorine would likely follow through the addition of another electron and elimination to form the enolate, which could then tautomerise to the non-fluorinated analogue (process (1)).

$$(1)$$
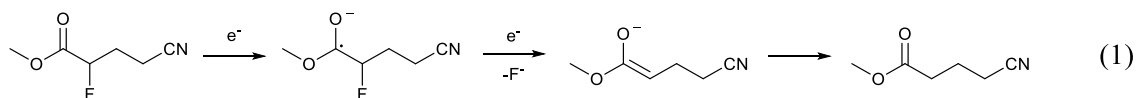
Figure 174 - Mechanism of process (1)

In addition to this, the NMR analysis shows the presence of an alkyl fragment, likely containing a cyano group. This fragment increases in length with the increasing alkyl chain backbone of the additives, and so can be shown to originate from decomposition of the additive. The splitting of the NMR analysis suggests that this fragment is bonded to a carbonyl, most likely that of solvent. As such, this process likely involves the homolytic cleavage of a carbon to carbon bond, after the reduction of the carbonyl, and the radical

fragment produced then reacts further with the solvent to form part of the SEI on the anode (process (2)).

$$\text{(2)}$$
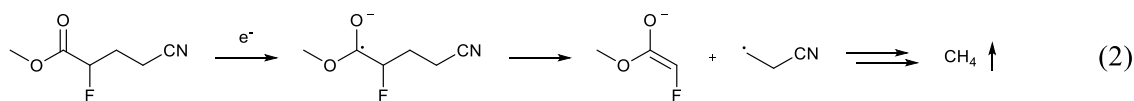
Figure 175 - Mechanism of process (2)

The gas analysis suggested a third decomposition pathway; the increased amount of methane generated in the cells of the methyl fluoro cyano esters suggests that the gas is produced from decomposition of the additives. This is further confirmed through the gas analysis of **140**, the ethyl cyano ester, which showed an increased amount of ethane as opposed to methane. This process is most likely due to elimination of methane after the reduction of the carbonyl (process (3)).

$$\text{(3)}$$
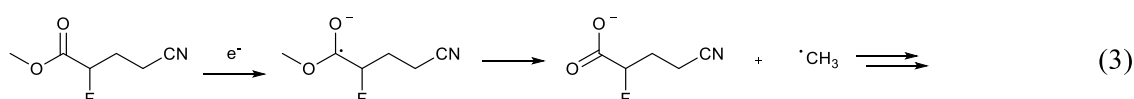
Figure 176 - Mechanisms of process (3)

The longer chain compounds possibly inhibit process (2) through the increased distance of the cyano functional group from the bonds that homolytically cleave. This would result in less electron withdrawing inductive effects that would stabilise a radical or charged species produced.

Due to the observation that process (1) occurs more than (2), when comparing the ^{1}H NMR spectra, and the results of the float test and capacity retention analysis, it can be seen that the former process is beneficial to LIB operation. It's likely that the non-fluorinated analogue and the LiF produced on the anode are layering onto the surface of the cathode and provide protection, similar to the way succinonitrile and other cyano-containing additives perform.[58, 57]

As process (2) is more common in the poorer performing additives, it's likely that these radical reduction reactions occurring on the anode and being incorporated into the SEI, including process (3), offset the beneficial effects of process (1). As such, it is likely that

finding the best additive is based upon optimisation of process (1) and minimisation of the other processes.

4.2.6 Application of mechanism to explain performance of other additives

The fact that process (1) has been attributed to beneficial effects observed within the LIBs analysis can explain why some additives performed poorly. There are beneficial interactions of the cyano group upon the cathode[54-58] and, therefore, additives tested that lack this functional group would be expected to only undergo reductive anodic processes (2) and (3), and be much more detrimental to LIB operation.
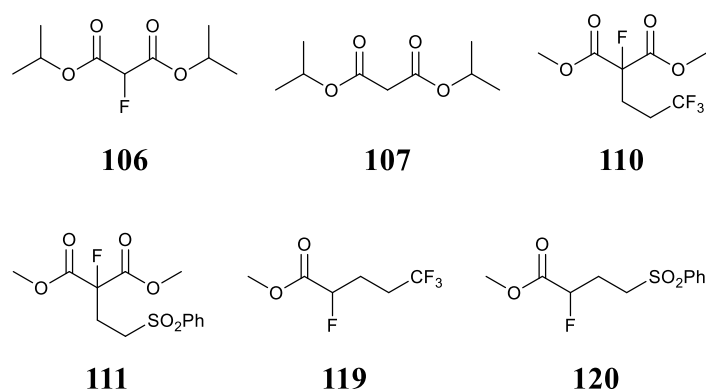
Figure 177 – Non-cyano additives

106 and **107**, and the malonate additives tested in Chapter 2, did not perform as well as the other additives tested due to the lack of a cyano group and possibly undergoing detrimental anodic radical based decomposition reactions. Similarly, **110**, **111**, **119** and **120** all lack the cyano group, and the reason for **111** and **120** performing notably poor is the presence of the sulfonyl functional group which would open the possibility for further reduction processes.
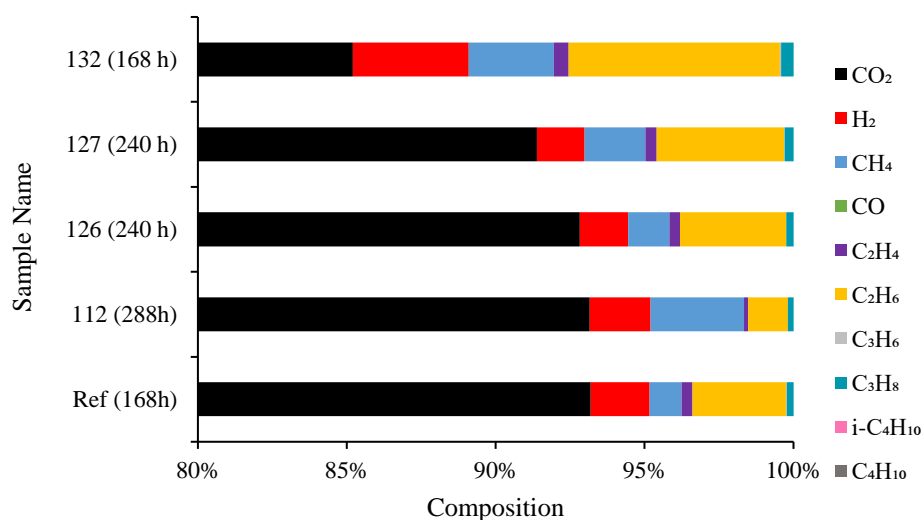
Figure 178 – Comparison of gas composition of ketone additives and **112**

The behaviour of the ketone additives is interesting due to the much improved swelling properties despite poor capacity retention. It would be expected that, due to the change of functional group preventing process (3), that perhaps process (1) would be enhanced and better functionality within all aspects of a LIB would be observed. The gas composition of these ketone additives, however, are interesting due to the much larger amount of ethane gas produced. This is somewhat surprising and is indicative of different mechanism of decomposition occurring involving fragmentation of the alkyl chain.
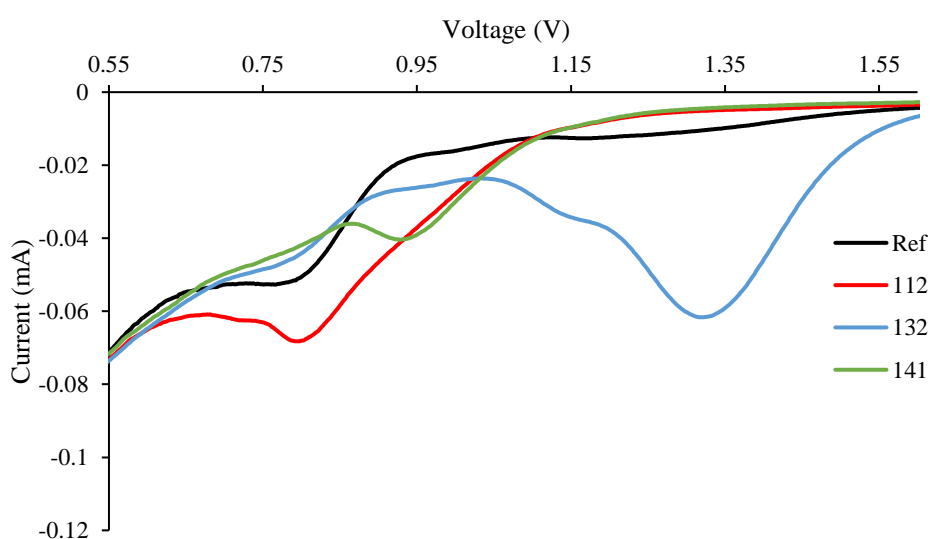
Figure 179 – Linear sweep voltammograms of **112**, **132** and **141**, V vs Li/Li$^+$
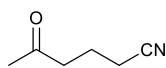
141

The CV data of the ketone compounds suggest that these are very reactive compounds; the reduction peak for the non-fluorinated additive, **141**, is at a higher voltage than that of **112**. This information alone does not prove otherwise, but could be indicative of a different reaction mechanism, through the much lower potentials required to reduce the ketone additives.

4.3   Conclusions

The compounds synthesised in Chapter 3 were subject to capacity retention and float test analysis using coin cells and pouch cells respectively. The former test behaves as a life time test, to assess electrolyte and additive functionality of the battery over 80 cycles, whilst the latter is akin to a stress test and probes into the swelling that occurs within cells.

The substituted malonate systems, **106** and **107**, were quickly dismissed due to their poor performance in the capacity retention tests. Following this, **110**, **111**, **119** and **120** were also dismissed due to poor results in the float test. No additive improved upon the reference sample throughout the capacity retention test, but all the samples, with exception to those noted, improved upon the reference cell with regards to swelling inhibition.

Interestingly, trends were observed in the methyl fluoro cyano ester additives - the longer the alkyl chain backbone, the greater degree of swelling inhibition. This trend also included one compound (**122**) that was tested with a substituted backbone which had comparable swelling inhibition as the longer chained compounds. In addition to this, ethyl esters were tested, although this seemed to have minimal effect upon LIB properties compared to analogous methyl esters.

β-difluorinated systems were also analysed and contrasted with β-monofluorinated and non-fluorinated systems. A weak correlation was found between less fluorination and improved capacity retention and a strong link found between less fluorination and improved swelling inhibition.

Different functional groups were also compared, with alkene, ketone and ester behaving similarly in capacity retention tests. In the float tests, the ketone was superior in swelling prevention. A trend was also observed for the increased alkyl backbone chain length of ketones and the increased amount of swelling inhibition. In addition to this, a weak trend was observed for the capacity retention, the longer chain ketones appear to have a negative effect upon this property.

The mechanism of the methyl fluoro cyano ester was probed using CV, data on the rate of consumption, NMR spectroscopy and analysis of the gas generated during testing. These combined techniques allows us to propose three possible mechanism for the decomposition of this family of additives.
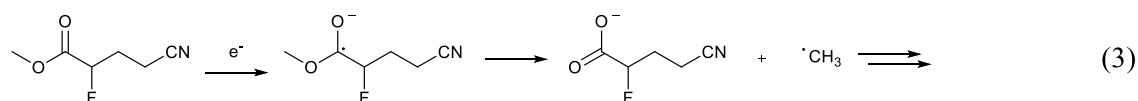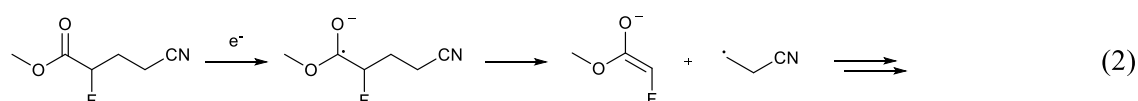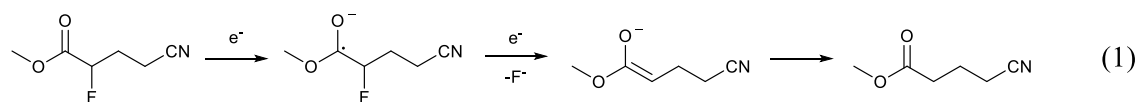
Process (1) is assumed to be beneficial to battery output, as it is the process that is promoted in the more promising longer chained additives. It is reasonable to think that the LiF and non-fluorinated analogues produced a layer on the cathode surface as a protecting agent, similar to that of other cyano containing compounds.

It is thought that processes (2) and (3) are detrimental to battery performance, as these are promoted in the longer chained compounds which could lead to further reactions upon the anode and further solvent degredation.

Comparisons were made between these mechanisms and other additives, and further findings were determined. The different decomposition pathway of the phenyl sulfonyl containing compounds and malonate type compounds explain the detrimental effects they had upon battery performance. The lack of a cyano group in the trifluoromethylated compounds also results in the deficiency of beneficial interactions produced by nitrile groups on the cathode surface. Some conclusions drawn from the ketone additive

analysis, including CV and gas analysis, suggest that alternative reaction mechanisms are available to these additives due to their much higher reactivities. More data is required on these compounds before any definitive conclusions can be drawn upon their decomposition pathways.

Overall, due to the minimal amount of process (2) and process (3), and the increased amount of process (1), the additive that performed consistently the highest is **118**. The longest alkyl chain promoted LiF formation and, with the resulting non-fluorinated compound, layered onto the cathode preventing CO_2 generation.

Conclusion

The aims of this project were to synthesise a range of fluorinated carbonyl compounds and probe their applicability as electrolyte additives for the formation of a beneficial SEI. To this end, dimethyl 2-fluoromalonate was chosen as a starting point due to recent literature suggesting this similar derivatives can be used within LIBs.

A range of different fluorinated dicarbonyl systems were synthesised or purified and subjected to LIB analysis. The results of these tests were contrasted to find relationships between battery performance and compound structure. The results showed that none of the additives prepared here improved upon the reference cell, a cell with no additive other than VC, and indicated that diketones were unsuitable for use as LIB additives. In addition to this, the results suggested that a more substituted alkyl ester resulted in higher performing additives. The data put together was used to propose a radical decomposition pathway for the malonate compounds.
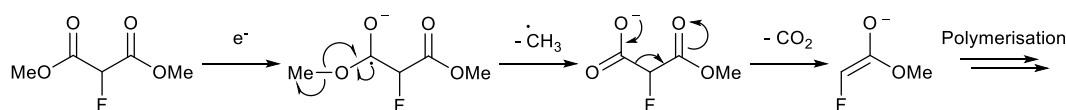
Figure 180 - Proposed mechanism of malonate compounds decomposition

These results lead to the design of new compounds; dialkyl malonates with a higher degree of substitution, to stabilise alkyl radical formation, and cyano-monoester compounds which would combine the benefits of dialkyl fluoromalonate and succinonitrile. Di-*iso*-propyl malonate derivatives were synthesised through transesterification reactions of dimethyl malonate and dimethyl 2-fluoromalonate. Alkylation reactions of dimethyl 2-fluoromalonate were undertaken using substitution reactions and Michael addition reactions.
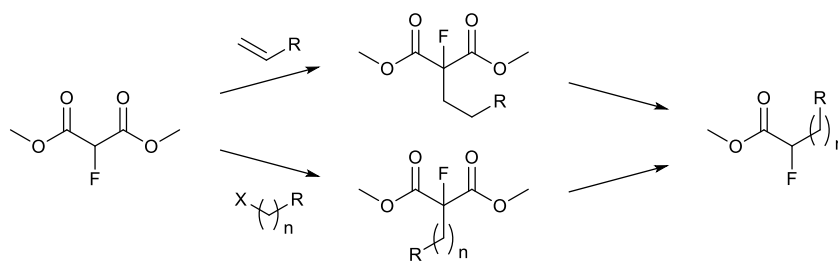
Figure 181 - Synthetic strategy for the synthesis of methyl fluoro ester additives; n = 1 to 5, X = Br or I, R = CN, SO$_2$Ph, CF$_3$

The alkylated systems were monodecarboxylated to generate methyl fluoro cyano esters through the Krapcho decarboxylation reaction. This reaction was optimised due to the presence of fluorine in the β-position promoting the reaction and increasing the reaction rate when compared to literature. The ethyl fluoro cyano ester was synthesised from methyl 2-fluoroacetoacetate through a reverse Claisen condensation reaction. A couple of difluorinated compounds were synthesised through the free radical addition reactions of Michael acceptors to ethyl 2-bromo-2,2-difluoroacetate.
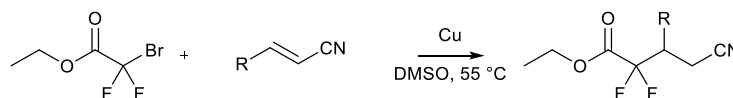
Figure 182 - Synthesis of ethyl difluoro cyano ester additives; R = H or CH$_3$

A synthetic strategy to a fluorinated cyano ketone additive was serendipitously discovered through the use of hydrolysis conditions of methyl 2-acetoacetate in the presence of acrylonitrile. The synthesis of longer chained fluoro cyano ketone additives was achieved by substitution reactions of methyl acetoacetate to the corresponding bromo alkyl cyano compounds. Following this, intermediates were fluorinated using Selectfluor^{TM} and decarboxylated using the Krapcho conditions. The Wittig reaction was utilised on the fluoro cyano ketone to synthesise the corresponding alkene.
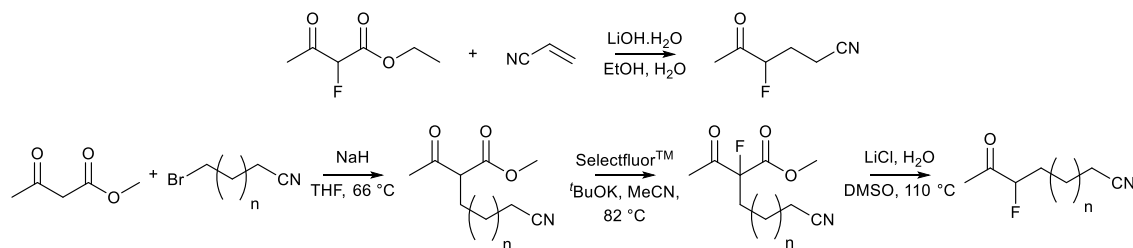
Figure 183 - Synthesis of fluoro cyano ketone additives

These synthesised additives were subjected to LIB analysis and were analysed for the effect upon the capacity retention and swelling prevention of LIBs. The di-*iso*-propyl malonates and trifluoromethyl and phenyl sulfonyl containing compounds were quickly dismissed due to the poor performance. Little change was observed in LIB operation changing between ketone, ester or alkene functional groups, also in varying the alkyl ester from methyl to ethyl.

Fluoro cyano ketone additives showed lower performance in capacity retention with increased alkyl backbone chain length, but increased swelling inhibition. The methyl fluoro cyano esters showed a similar trend; the longer the alkyl backbone chain, the higher cell performance in float and swelling tests.

The mechanism of the methyl fluoro cyano ester was probed using CV, data on the rate of consumption, NMR spectroscopy and analysis of the gas generated during testing. These combined techniques provided information to propose three possible mechanism for the decomposition of this family of additives.
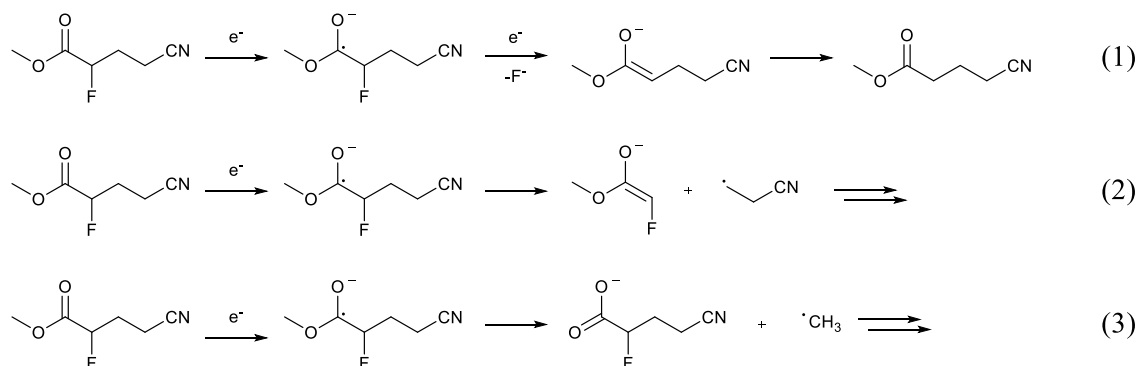
Figure 184 - Mechanisms of methyl fluoro cyano ester additive decomposition

Process (1) was found to be the beneficial process due to it being the process promoted the most in longer alkyl-chained compounds, whereas processes (2) and (3) were more prominent in the shorter alkyl-chained compounds and so are thought to be detrimental to battery performance.
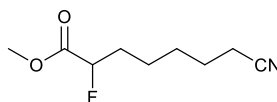
118

Overall, due to the minimal amount of process (2) and process (3), and the increased amount of process (1), the additive that performed consistently the highest is **118**. The longest alkyl chain promoted LiF formation and, with the resulting non-fluorinated compound, layered onto the cathode preventing CO_2 generation.

Due to the very complicated nature of conditions within a LIB system, it's difficult to explore the inner reactions and workings of these cells. The control and manipulation of such reactions within a cell is difficult due to the many possible competing reactions of solvents and salts within the battery. Through the use of multifaceted analysis and chemical tuning, a rare example of understanding and control of mechanistic additive decomposition has been shown.

Experimental

General

NMR spectroscopy

Proton, Fluorine and carbon nuclear magnetic resonance spectra (^{1}H, ^{13}C and ^{19}F NMR) were obtained from a Bruker 400 Ultrashield spectrometer (^{1}H NMR at 400 MHz, ^{13}C NMR at 101 MHz and ^{19}F at 376 MHz) and a Varian VNMRS 600 (^{1}H NMR at 700 MHz) using residual solvent peaks as the internal standard (^{1}H NMR; CDCl3 at 7.26 ppm, ^{13}C NMR; 77.16 ppm) and an external standard (^{19}F NMR; CFCl$_3$). NMR spectroscopic data are reported as follows: chemical shift (ppm), integration, multiplicity (s = singlet, d = doublet, t = triplet, q = quartet, m =multiplet), coupling constant (Hz) and assignment.

Mass Spectrometry

ESI data were obtained from a TQD mass spectrometer (Waters Ltd, UK), and accurate mass EI data were obtained from a QtoF Premier mass spectrometer (Waters, UK). Any GCMS data obtained were from a Trace GCMS (Thermo-Finnigan Corporation).

Infra-red Spectroscopy

Infra-red (IR) spectra were recorded on a Perkin Elmer FTIR Spectrum Two^{TM} fitted with and ATR diamond probe.

X-Ray Analysis

Crystollographic data were recorded with a Bruker D* venture or Agilent Xcalibur diffractometer equipped with Cryostream (Oxford Cryosystems) low temperature device at 120 K with graphite-monochromated MoKα-radiation (λ = 0.71073 Å).

Chemicals and solvents

Unless otherwise stated, commercially available solvents were used without purification. Dry solvents were obtained using an Innovative Technology Inc. Solvent Purification System. All column chromatography was carried out using Silicagel LC60A (40 – 63 micron) purchased from Fluorochem. All other reagents or solvents were purchased from Fluorochem, Sigma Aldrich, Apollo or TCI.

Chapter 2

Synthesis

Diethyl 2-fluoromalonate (**27**)
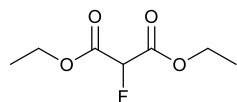
Dimethyl 2-fluoromalonate (0.6 g, 4 mmol) was dissolved in ethanol (30 mL) with *p*-Toluenesulfonic acid (0.2 g, 1.2 mmol) and heated to reflux for six hours. Afterwards, the solvent was removed *in vacuo* and ethanol (20 mL) was added and the reaction mixture was brought to reflux for a further 6 hours. The solvent was removed *in vacuo*, the remaining residue taken up in water (30 mL), extracted with ethyl acetate (3 x 30 mL), dried with brine (3 x 30 mL) and $MgSO_4$ and concentrated *in vacuo* to give a crude product as a yellow oil. The crude product was purified using kugel rohr distillation to yield *diethyl 2-fluoromalonate* as a clear oil (0.41 g, 58%). δ_H (CDCl$_3$, 400 MHz) 5.27 (1H, d, $^2J_{CF}$ 48.3 Hz, CFH), 4.33 (4H, q, $^3J_{HH}$ 7.1 Hz, CH$_2$), 1.33 (6H, t, $^3J_{HH}$ 7.1 Hz, CH$_3$); δ_F (CDCl$_3$, 376 MHz) -195.05 (d, $^2J_{HF}$ 48.3 Hz); δ_C (CDCl$_3$, 101 MHz) 164.11 (d, $^3J_{CF}$ 24.1 Hz, C=O), 85.47 (d, $^2J_{CF}$ 196.7 Hz, CHF), 62.88 (s, CH$_2$), 14.13 (s, CH$_3$); m/z (GC-EI$^+$) 179.1 [M + H]$^+$, 133.1 [M − CH$_3$CH$_2$O]$^+$, 106.1 [M + H − C$_3$H$_5$O$_2$]$^+$. All spectroscopic data matches literature values.[110]

Dimethyl 2-fluoromalonate (**62**)
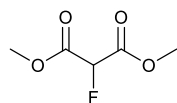
Following a reported procedure,[99] dimethyl malonate (19.8 g, 150 mmol, 17.22 mL) and copper nitrate hydrate (3.50 g, 15 mmol) were dissolved in acetonitrile (85 mL) and placed in a 250 mL fluorinate vessel. The reaction mixture was cooled to 0 - 5 °C, stirred at 650 rpm using an overhead stirrer and, after purging the systems with N$_2$ for 5 minutes, fluorine gas (20% v/v in N$_2$, 50 mL min^{-1}, 170 mmol) was introduced into the solution for 7 hours. The reactor was purged with N$_2$ for 10 minutes, the solvent removed *in vacuo*, the residue portioned between water (50 mL) and ethyl acetate (50 mL) and the aqueous layer was extracted with ethyl acetate (2 x 50 mL). The combined organic layers were

washed with saturated $NaHCO_3$ (3 x 20 mL) and brine (3 x 20 mL) and then dried over $MgSO_4$. The solvent was removed *in vacuo* leaving crude product. The crude product was purified via vacuum distillation to give *dimethyl 2-fluoromalonate* (16.92 g, 75% yield, 99% purity) as a clear, transparent oil. δ_H NMR (CDCl$_3$, 400 MHz) 5.32 (1H, d, $^2J_{CF}$ = 48.1 Hz, CFH), 3.88 (6H, s, CH$_3$); δ_F (CDCl$_3$, 376 MHz) -195.21 (d, $^2J_{HF}$ = 48.1 Hz, CHF); δ_C (CDCl$_3$, 101 MHz) 164.42 (d, $^3J_{CF}$ = 24.1 Hz, C=O), 85.27 (d, $^2J_{CF}$ = 197.3 Hz, CF), 53.54 (CH$_3$); m/z (GC-EI$^+$) 151 (9%, [M + H]$^+$), 119 (36%, [M – CH$_3$O]$^+$), 91 (51%, [M – CO$_2$CH$_3$]$^+$), 59 (100%, [M – CHFCO$_2$CH$_3$]$^+$. Spectroscopic data agreed with those previously reported.[99]

Meldrum's Acid (2,2-Dimethyl-1,3-dioxane-4,6-dione) (**69**)
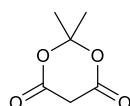
Following a literature method,[115] malonic acid (1 g, 9.61 mmol) was suspended in acetic anhydride (0.70 g, 12.0 mmol) in the presence of 2 drops of catalytic concentrated sulphuric acid and cooled to 0 ºC. Acetone (1.47 g, 15.4 mmol) was added dropwise and the reaction was allowed to stir for 2.5 hours, after which the reaction mixture was allowed to cool overnight at 5 ºC to precipitate *2,2-Dimethyl-1,3-dioxane-4,6-dione* (0.69, 50% yield) as white needles. δ_H (CDCl$_3$, 400 MHz) 3.62 (2H, s, CH$_2$), 1.79 (6H, s, CH$_3$); δ_C (CDCl$_3$, 101 MHz) 163.04 (s, C=O), 106.35 (s, CH$_2$), 36.25 (s, C(CH$_3$)$_2$), 27.65 (s, CH$_3$); m/z (GC-EI) 129 (10%, [M-CH$_3$]); all spectroscopic data match literature values.[116]

Bis(3,3,3-trifluoroethyl) malonate (**97**)
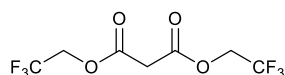
Adapting a reported procedure,[111] malonic acid (0.42 g, 4 mmol, 1 eq) and 3,3,3-trifluoroethanol (2.16 g, 22 mmol, 5.4 eq) were dissolved in toluene (30 mL) and H_2SO_4 (0.07 g, 0.8 mmol) was added dropwise and the temperature raised to 85 °C. After six hours, the reaction mixture was diluted with more toluene (80 mL) and washed with a

concentrated bicarbonate solution (4 x 30 mL), water (3 x 30 mL) and brine (3 x 30 mL) and dried over $MgSO_4$. The reaction mixture was then concentrated *in vacuo* to give bis(3,3,3-trifluoroethyl) 2-fluoromalonate (0.31 g, 29% yield) as a clear oil. ($[M + H]^+$, 269.0262, $C_7H_6O_4F_6$ requires: $[M + H]^+$, 269.0249); IR (neat, cm-1) 1757, 1413, 1348, 1280, 1256, 1159, 1133, 1060, 981, 842, 665, 646, 549, 446; δ_H (CDCl$_3$, 400 MHz) 4.55 (4H, q, $^3J_{HF}$ = 8.3 Hz, CH2-CF3), 3.61 (2H, s, CH$_2$); δ_F (CDCl$_3$, 376 MHz) -73.82 (t, $^3J_{HF}$ = 8.2 Hz, CF$_3$); δ_C (CDCl$_3$, 101 MHz) 164.17 (s, C=O), 122.64 (q, $^1J_{CF}$ = 277.1 Hz, CF$_3$), 61.36 (q, $^2J_{CF}$ = 37.3 Hz, CH$_2$CF$_3$), 40.31 (s, CH$_2$); m/z (ASAP) 269 (33%, [M+H]).

Bis(trifluoroethyl) 2-fluoromalonate (**98**)
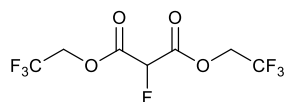
Adapting a reported procedure,[111] fluoromalonic acid (3 g, 24.6 mmol, 1 eq) and trifluoroethanol (15.6 g, 156 mmol, 6.3 eq) were dissolved in toluene (30 mL) and H_2SO_4 (0.71 g,7.2 mmol) was added dropwise and the temperature raised to 85 °C. After six hours, the reaction mixture was diluted with more toluene (80 mL) and washed with a concentrated bicarbonate solution (4 x 30 mL), water (3 x 30 mL) and brine (3 x 30 mL) and dried over $MgSO_4$. The reaction mixture was then concentrated *in vacuo* and purified via vacuum distillation to give *bis(trifluoroethyl) 2-fluoromalonate* as a clear oil. ($[M + H]^+$, 287.0151, $C_7H_5F_7O_4$ requires: $[M]^+$, 287.0154); IR (neat, cm^{-1}) 1775, 1415, 1283, 1234, 1159, 1053, 979, 842, 649, 567; δ_H (CDCl$_3$, 400 MHz) 5.52 (1H, d, $^2J_{HF}$ = 47.2 Hz, CFH), 4.76 – 4.50 (4H, m, CH$_2$); δ_F (CDCl$_3$, 376 MHz) -73.82 – -73.92 (6F, m, CF$_3$), -196.30 (1F, d, $^2J_{HF}$ = 47.3 Hz, CFH); δ_C (CDCl3, 101 MHz) 161.86 (d, $^2J_{CF}$ = 25.2 Hz, C=O), 122.23 (q, $^1J_{CF}$ 277.4 = Hz, CF$_3$), 84.29 (d, $^1J_{CF}$ 199.5 = Hz, CHF), 61.94 (q, $^2J_{CF}$ = 38.0 Hz, CH$_2$); m/z (ASAP) 287.0 (99.9%, $[M + H]^+$), 267.0 (7%, $[M – F]^+$), 159.0 (100%, $[M – C_3H_2F_2O_2]^+$).

Bis-(4,4,4,3,3-pentafluorobutyl)-malonate (**100**)

Adapting a reported procedure,[111] malonic acid (0.31 g, 3 mmol, 1 eq) and 4,4,4,3,3-pentafluorobutanol (1.97 g, 12 mmol, 4 eq) were dissolved in toluene (30 mL) and H_2SO_4 (0.07 g, 0.8 mmol) was added dropwise and the temperature raised to 85 °C. After six hours, the reaction mixture was diluted with more toluene (80 mL) and washed with a concentrated bicarbonate solution (4 x 30 mL), water (3 x 30 mL) and brine (3 x 30 mL) and dried over $MgSO_4$. The reaction mixture was then concentrated *in vacuo* to give *bis(4,4,4,3,3-pentafluorobutyl) 2-fluoromalonate* (0.98 g, 82% yield) as a clear oil. ([M + H]$^+$, 397.0495, $C_{11}H_{10}F_{10}O_4$ requires: [M + H]$^+$, 397.0498); IR (neat, cm^{-1}) 1743, 1339, 1312, 1187, 1133, 1076, 1006, 767, 720, 696, 589, 524, 456; δ_H (CDCl$_3$, 400 MHz) 4.43 (4H, t, $^3J_{HF}$ = 6.5 Hz, CH$_2$-O), 3.42 (2H, s, CH$_2$-CO), 2.54 – 2.35 (4H, m, CH$_2$-CF$_2$); δ_F (CDCl$_3$, 376 MHz) -85.86 (6F, s, CF$_3$), -117.72 (4F, t, $^3J_{HF}$ = 17.6 Hz, CF$_2$); δ_C (CDCl$_3$, 101 MHz) 165.62 (s, C=O), 123.91 – 110.58 (m, CF$_3$, CF$_2$), 57.42 (t, $^3J_{CF}$ = 4.6 Hz, CH$_2$O), 41.02 (s, CH$_2$-CO), 30.08 (t, $^2J_{CF}$ = 21.9 Hz, CH$_2$-CF$_2$); m/z (ASAP) 397 (100%, [M+H]$^+$).

Bis-(4,4,4,3,3-pentafluorobutyl)-2-fluoromaloante (**101**)
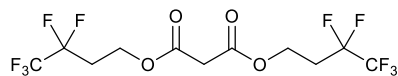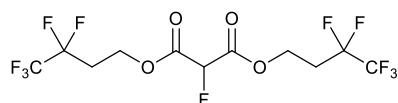

Adapting a reported procedure, fluoromalonic acid (0.37 g, 3 mmol, 1 eq) and 4,4,4,3,3-pentafluorobutanol (2 g, 12 mmol, 4 eq) were dissolved in toluene (30 mL) and H_2SO_4 (0.07 g, 0.8 mmol) was added dropwise and the temperature raised to 85 °C. After six hours, the reaction mixture was diluted with more toluene (80 mL) and washed with a concentrated bicarbonate solution (4 x 30 mL), water (3 x 30 mL) and brine (3 x 30 mL) and dried over $MgSO_4$. The reaction mixture was then concentrated *in vacuo* to give *bis(4,4,4,3,3-pentafluorobutyl) 2-fluoromalonate* (0.97 g, 95% yield) as a clear oil. ([M

+ H]$^+$, 415.0409, C$_{11}$H$_{10}$F$_{11}$O$_4$ requires: [M + H]$^+$, 287.0154); IR (neat, cm^{-1}) 1783, 1761, 1349, 1290, 1187, 1130, 1076, 1008, 769, 721, 694, 590, 523, 493; δ_H (CDCl$_3$, 400 MHz) 5.33 (1H, d, $^2J_{HF}$ = 47.8 Hz, CFH), 4.55 (4H, td, $^3J_{HH}$ = 6.5 Hz, $^4J_{HF}$ = 1.0 Hz, CO-CH$_2$), 2.58 – 2.38 (4H, m, CH$_2$-CF$_2$); δ_F (CDCl$_3$, 376 MHz) -85.81 (6F, s, CF$_3$), -117.74 (4F, t, $^3J_{HF}$ = 17.5 Hz, CF$_2$), -195.72 (1F, d, $^2J_{HF}$ = 47.8 Hz, CHF), δ_C (CDCl$_3$, 101 MHz) 163.22 (d, $^2J_{CF}$ = 24.6 Hz, C=O), 124.74 – 109.98 (m, CF$_3$, CF$_2$), 84.93 (d, $^1J_{CF}$ = 198.0 Hz, CFH), 58.59 (t, $^3J_{CF}$ = 4.5 Hz, CH$_2$O), 30.09 (t, $^2J_{CF}$ = 22.0 Hz, CH$_2$); m/z (ASAP) 415.0 (100%, [M +H]$^+$), 397.1 (23%, [M + H$_2$ – F]$^+$), 295 (3%, [M – CF$_2$CF$_3$]$^+$.

Dimethyl 2-(2-cyanethyl)-2-fluoromalonate (**102**)
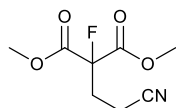
Following a reported procedure,[113] dimethyl fluoromalonate (0.3 g, 2 mmol) was added to a solution of sodium methoxide in methanol (0.01 g sodium, 0.4 mmol, in 20 mL methanol) and before acrylonitrile (0.52 g, 10 mmol) was added and the solution stirred for an hour at 60 °C. Afterwards the solvent was removed in vacuo, the residue taken up in water (3 x 30 mL), extracted with ethyl acetate (3 x 30 mL), washed with brine (3 x 30 mL) and dried over MgSO4. The remaining solution is concentrated *in vacuo* to yield a yellow oil which is purified via vacuum distillation (b.p 150 °C, 5 mbar) to yield dimethyl 2-(2-cyanoethyl)-2-fluoromalonate (0.13 g, 32%) as a clear oil. δ_H (CDCl$_3$, 400 MHz) 3.88 (1H, s, CH$_3$), 2.64 – 2.50 (4H, m, CH$_2$); δ_F (CDCl3, 376 MHz) -167.78 – -168.05 (m); δ_C (CDCl$_3$, 101 MHz) 165.50 (d, $^2J_{CF}$ = 25.3, C=O), 117.87 (s, CN), 92.79 (d, $^1J_{CF}$ = 201.2 Hz, C-F), 53.97 (s, CH$_3$), 30.30 (d, $^2J_{CF}$ = 21.5 Hz, CH$_2$), 11.62 (d, $^3J_{CF}$ = 5.5 Hz, CH$_2$); m/z (GC-EI+) 204.1 (3%, [M+H]+), 144.1 (11.21%, [M – C2H3O2]+), 59.1 (47%, [C2H3O2]+). All spectroscopy data matches literature values.[113]

Dimethyl 2-methyl-malonate (**105**)
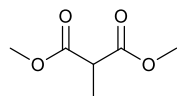
2,2,5-trimethyl-1,3-dioxane-4,6-dione (1g, 6.3 mmol) was added to methanol (30 mL) and HCl (0.25 mL, 6.9 mmol) and refluxed for 6 hours. Afterwards the solvent was removed *in vacuo*, the residue taken up in ethyl acetate (30 mL) and washed with sodium bicarbonate (3 x 30 mL), water (3 x 30 mL) and brine (3 x 30 mL). The ethyl acetate was then removed *in vacuo* to yield a yellow oil which was purified by kugel rohr distillation to yield *dimethyl 2-methylmalonate* (0.57 g, 62%) as a clear oil. δ_H (CDCl$_3$, 400 MHz) 3.73 (6H, s, OCH$_3$), 3.46 (1H, q, $^3J_{HH}$ = 7.3 Hz, CH), 1.42 (3H, d, $^3J_{HH}$ = 7.3 Hz, CCH$_3$); δ_C (CDCl$_3$, 101 MHz) 170.51 (s, C=O), 52.52 (s, OCH$_3$, 45.83 (s, CH), 13.65 (s, CCH$_3$); m/z (GC-EI$^+$) 146 (7%, [M]$^+$), 115 (97%, [M − OCH$_3$]$^+$, 87 (36%, [M − O$_2$CH$_3$]$^+$, 72 (30%, [M − O$_2$(CH$_3$)$_2$]$^+$, 59 (100%, [CO$_2$CH$_3$]$^+$). Spectroscopic data agrees with those previously reported.[124]

Battery Analysis (Sony)

Battery tests were performed in three-electrode split cells from EL-CELL. An amount of 100 µl of electrolyte was used for each test cell. Test cell assembly and electrolyte preparation was performed in an argon filled glovebox.

The following table summarizes parameters of the tests:

Anode	Cathode	Electrolyte	Temp.	Additives	Volt. range
Sony A13155TGE (**graphite**)	Sony A35155TGB (LCO)	1M LiPF$_6$ EC-DMC	23 °C	1vol% malonate	3- 4.45 V

For the split cell tests glass fibre separators with integrated Li-reference electrode (EL-CELL, Germany) were used. The diameter of both electrodes was 18 mm. Cells were placed into a climate chamber from Binder to maintain a temperature of 23±0.1°C during electrochemical characterization. The measurements were performed using a VMP-3 from Biologic applying a constant-current – constant-voltage cycling profile including EIS measurements after 12 h rest, first charge, first discharge and after the test, respectively. EIS measurements were performed using 10mV excitation amplitude and a frequency range of 500 khz to 5 mHz.

The following test schedule was used for the split cell tests:

Step #	Description	C-rate charge	C-rate discharge	Upper-cut-off voltage [V]	Lower-cut-off voltage [V]	Cut-off current C-rate	Rest time [min]
1	12h rest @ OCV						
2	EIS measurement						
3	Charge	0.1		4.45		0.01	10
4	EIS measurement						410
5	Discharge		0.1		3		10
6	EIS measurement						410
7	Charge/discharge	0.2	0.2	4.45	3	0.05	10
8	Charge/discharge	0.2	0.5	4.45	3	0.05	10
9	Charge/discharge	0.2	1	4.45	3	0.05	10
10	Charge/discharge	0.5	0.5	4.45	3	0.05	10
11	10 times charge/discharge	1	1	4.45	3	0.05	10
12	EIS measurement						410

Chapter 3

Di-*iso*-propyl 2-fluoromalonate (**106**)
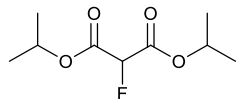
Sodium (0.03 g, 1.4 mmol) was dissolved in *iso*-propanol (30 mL) and diethyl 2-fluoromalonate (0.5 g, 2.8 mmol) was added and heated to reflux for 19 hours. The solvent was removed *in vacuo*, the remaining residue taken up in water (30 mL), extracted with diethyl ether (3 x 30 mL), dried with brine (3 x 30 mL) and MgSO$_4$ and concentrated *in vacuo* to yield *di-iso-propyl 2-fluoromalonate* as a pale yellow oil (0.35 g, 60%). δ_H (CDCl$_3$, 400 MHz) 5.19 (1H, d, $^2J_{HF}$ = 48.4 Hz), 5.17 (2H, hept, $^3J_{HH}$ = 6.3 Hz), 1.30 (12H, dd, $^3J_{HH}$ = 7.5 Hz, $^3J_{HH}$ = 6.3 Hz); δ_F (CDCl$_3$, 376 MHz) -194.92 (d, $^2J_{HF}$ = 48.5 Hz); δ_C (CDCl$_3$, 101 MHz) 163.72 (d, $^2J_{CF}$ = 24.0 Hz, C=O), 85.61 (d, $^1J_{CF}$ = 195.4 Hz, CFH), 70.89 (s, CHMe$_2$), 21.72 (s, Me), 21.66 (s, Me); m/s (GC-EI$^+$) 191 (1.3%, [M – CH$_3$]$^+$), 163 (1%, [M – *i*Pr]$^+$, 147 (4%, [M – O*i*Pr]$^+$), 87 (2%, [M – CFHCO$_2$*i*Pr]$^+$), 43 (100, [*i*PR]$^+$).

Di-*iso*-propyl malonate (**107**)
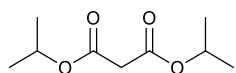
Sodium (0.01 g, 0.6 mmol) was dissolved in *iso*-propanol (30 mL) and di,ethyl 2-malonate (0.3 g, 2.3 mmol) was added and heated to reflux for 19 hours. The solvent was removed *in vacuo*, the remaining residue taken up in water (30 mL), extracted with diethyl ether (3 x 30 mL), dried with brine (3 x 30 mL) and MgSO$_4$ and concentrated *in vacuo* to yield *di-iso-propyl malonate* as a pale yellow oil (0.32 g, 91%). δ_H (CDCl$_3$, 400 MHz) 5.06 (2H, hept, $^3J_{HH}$ = 6.3 Hz, C*H*(CH$_3$)$_2$), 3.30 (2H, s, CH$_2$), 1.26 (12H, d, $^3J_{HH}$ = 6.2 Hz, CH$_3$); δ_C (CDCl$_3$, 101 MHz) 166.39 (s, C=O), 69.16 (s, CHMe$_2$), 42.50 (s, CH$_2$), 21.81 (s, CH$_3$); m/s (GC-EIMS) 189 (2%, [M + H]$^+$), 173 (2%, [M – CH$_3$]$^+$), 129 (89%, [M –

O^{i}Pr]$^+$), 87 (91%, [CO$_2$^{i}Pr]$^+$), 59 (43%, [O^{i}Pr]$^+$). All spectroscopic data matches literature matches literature values.[119]

Dimethyl 2-(cyanomethyl)-2-fluoromalonate (**108**)
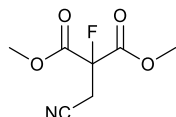
Dimethyl 2-fluoromalonate (4 g, 26.65 mmol) was added to a suspension of sodium hydride (0.83 g, 34.64 mmol [1.39 g of 60% sodium in mineral oil, washed with hexane]) in THF (100 mL) and left to stir for 15 minutes. After this time, bromoacetonitrile (3.52 g, 29.31 mmol) was added dropwise and left to stir for 19 hours. After this time, 200 mL of water was added to the reaction mixture and extracted with ethyl acetate (3 x 30 mL). The organic layers were combined and washed with water (3 x 30 mL), brine (3 x 30 mL) and dried over MgSO$_4$. The solvent was removed *in vacuo* and the crude product purified by vacuum distillation (140 ^{o}C, 3 mbar) to give *dimethyl 2-(cyanomethyl)-2-fluoromalonate* (2.62 g, 52% yield) as a clear oil. ([M + H]+, 190.0519, C$_7$H$_9$FNO$_4$ requires: [M + H]+,190.0516); IR (neat, cm^{-1}) 2963, 2261, 1754, 1438, 1410, 1313, 1259, 1221, 1151, 1087, 1055, 950, 888, 828, 803, 783, 696, 619;δ_H (CDCl$_3$, 400 MHz) 3.91 (3H, s, CH$_3$), 3.26 (1H, d, $^3J_{HF}$ = 20.1 Hz, CH$_2$); δ_F (CDCl$_3$, 376 MHz) -162.28 (t, $^3J_{HF}$ = 20.1 Hz); δ_C (CDCl$_3$, 101 MHz) 164.09 (d, $^2J_{CF}$ = 24.6 Hz, C=O), 113.35 (d, $^3J_{CF}$ = 2.6 Hz, CN), 90.39 (d, $^1J_{CF}$ = 208.7 Hz, CF), 54.33 (s, CH$_3$), 24.25 (d, $^2J_{CF}$ = 23.1 Hz, CH$_2$); m/s (GC-EIMS$^+$) 188 (1%, [M − H]$^+$), 149 (1%, [M − CH$_2$CN]$^+$), 130 (2%, [M − CO$_2$Me]$^+$).

Dimethyl 2-(3-cyanopropyl)-2-fluoromalonate (**109**)
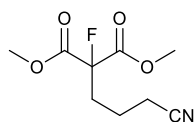
Dimethyl 2-fluoromalonate (2 g, 13.3 mmol) was added to a suspension of sodium hydride (0.58 g, 24 mmol [0.96 g of 60% sodium in mineral oil, washed with hexane]) in THF (50 mL) and allowed to stir for 15 minutes. After this time, 4-bromobutyronitrile (2.17 g, 14.66) and left to stir for 19 hours. After this time, 100 mL of water was added to the reaction mixture and extracted with ethyl acetate (3 x 30 mL). The organic layers were combined and washed with water (3 x 30 mL), brine (3 x 30 mL) and dried over MgSO$_4$. The solvent was removed *in vacuo* and the crude product purified by kugel rohr distillation (150 °C, 2.5 mbar) to give *dimethyl 2-(3-cyanopropyl)-2-fluoromalonate* (0.75 g, 26% yield) as a clear oil. ([M + H]+, 218.0820, C$_9$H$_{13}$FNO$_4$ requires: [M + H]$^+$, 218.0829); IR (neat, cm^{-1}) 2961, 2248, 1750, 1474, 1281, 1247, 1226, 1200, 1184, 1150, 1104, 1079, 993, 953, 924, 826, 799, 785, 696, 614, 544; δ_H (CDCl$_3$, 400 MHz) 3.86 (6H, s, **CH$_3$**), 2.43 (2H, t, $^3J_{HH}$ = 7.2 Hz, **CH$_2$**-CN), 2.40 – 2.28 (2H, m, CF-**CH$_2$**), 1.85 – 1.75 (1H, m, CH$_2$-**CH$_2$**-CH$_2$); δ_F (CDCl$_3$, 376 MHz) -166.75 (t, $^3J_{HF}$ = 22.6 Hz); δ_C (CDCl$_3$, 101 MHz) 166.04 (d, $^2J_{CF}$ = 25.5 Hz, C=O), 118.63 (s, CN), 94.16 (d, $^1J_{CF}$ = 199.7 Hz, CF), 53.61 (s, CH$_3$), 33.04 (d, $^2J_{CF}$ = 21.5 Hz, **CH$_2$**-CF), 19.43 (d, $^3J_{CF}$ = 3.4 Hz, CH$_2$-**CH$_2$**-CH$_2$), 16.99 (s, **CH$_2$**-CN).

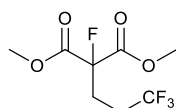Dimethyl 2-(3,3,3-trifluoropropyl)-2-fluoromalonate (**110**)

Dimethyl 2-fluoromalonate (10 g, 66.6 mmol) was added to a suspension of sodium hydride (1.68 g, 70.0 mmol [2.80 g of 60% sodium in mineral oil, washed with hexane]) in THF (100 mL) and left to stir for 15 minutes. To this suspension, 1-iodo-3,3,3-trifluoropropane (16.4 g, 73.3 mmol) was added dropwise and the mixture allowed to stir for 100 minutes. After this time, 200 mL of water was added to the reaction mixture and extracted with ethyl acetate (4 x 50 mL). The organic layers were combined and washed with water (3 x 50 mL), brine (3 x 30 mL) and dried over MgSO$_4$. The solvent was removed *in vacuo* and the crude product purified by vacuum distillation (50 °C, 2.5 mbar) to give *dimethyl 2-(3,3,3-trifluoropropyl)-2-fluoromalonate* (1.95 g, 12% yield) as a pale

pink oil. IR (neat, cm^{-1}) 2965, 1753, 1451, 1440, 1403, 1331, 1297, 1256, 1229, 1136, 1077, 1049, 1027, 922, 851, 827, 793, 700, 569, 416; δ_H (CDCl$_3$, 400 MHz) 3.87 (6H, s, CH$_3$), 2.51 – 2.38 (2H, m, CH$_2$CF), 2.31 – 2.16 (2H, m, CH$_2$CF$_3$); δ_F (CDCl$_3$, 376 MHz) -66.72 (t, $^3J_{HF}$ = 10.0 Hz, CF$_3$), -167.35 (t, $^3J_{HF}$ = 21.6 Hz, CF); δ_C (CDCl$_3$, 101 MHz) 165.75 (d, $^2J_{CF}$ = 25.3 Hz, C=O), 124.91 (q, $^1J_{CF}$ = 276.8, CF$_3$), 93.11 (d, $^1J_{CF}$ = 200.7 Hz, CF), 53.70 (s, CH$_3$), 27.96 (qd, $^2J_{CF}$ = 30.2 Hz, $^3J_{CF}$ = 4.3 Hz, **CH$_2$CF$_3$**), 27.19 (dq, $^2J_{CF}$ = 21.7 Hz, $^3J_{CF}$ = 3.5 Hz, **CH$_2$CF**); 247 (1%, [M + H]$^+$), 215 (1%, [M – OMe]$^+$), 187 (8%, [M – CO$_2$Me]$^+$), 150 (2%, [M – CH$_2$CH$_2$CF$_3$]$^+$), 97 (7%, [CH$_2$CH$_2$CF$_3$]$^+$, 59 (90%, [CO$_2$Me]$^+$).

Dimethyl 2-(2-phenylsulfonylethyl)-2-fluoromalonate (**111**)
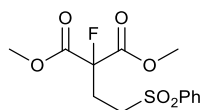
Dimethyl 2-fluoromalonate (1 g, 6.7 mmol) was added to a solution of sodium methoxide (0.03 g, 1.7 mmol sodium in 30 mL methanol) and allowed to stir for 15 minutes. After this time, phenyl vinyl sulfone (1.23 g, 7.3 mmol) was added and heated to 60 ^{o}C for 2 hours. After this time, the solvent was removed *in vacuo* and the residue taken up in water. The product was then extracted with ethyl acetate (3 30 mL), the organic layers were combined and washed with water (3 x 30 mL), brine (3 x 30 mL) and dried over MgSO$_4$. The solvent was removed *in vacuo* and the crude product purified by column chromatography (gradient neat toluene to 1:1 toluene:ethyl acetate) to give *Dimethyl 2-(2-phenylsulfonylethyl)-2-fluoromalonate* (0.70 g, 33% yield) as a clear oil. ([M + H]$^+$, 319.0648, C$_{13}$H$_{16}$FO$_6$S requires: [M + H]$^+$, 319.0652); IR (neat, cm^{-1}) 2961, 1751, 1439, 1307, 1281, 1234, 1196, 1176, 1143, 1084, 1061, 1019, 1000, 967, 917, 831, 817, 788, 741, 688, 613, 555, 527, 457; δ_H (CDCl$_3$, 400 MHz) 7.94 – 7.89 (2H, m, Ar-H), 7.73 – 7.67 (1H, m, Ar-H), 7.63 – 7.56 (2H, m, Ar-H), 3.83 (6H, s, CH$_3$), 3.25 – 3.18 (2H, m, CH$_2$-CN), 2.66 – 2.54 (2H, m, CH$_2$CF); δ_F (CDCl$_3$, 376 MHz) -165.94 (t, $^3J_{HF}$ = 21.1 Hz); δ_C (CDCl$_3$, 101 MHz) 165.58 (d, $^2J_{CF}$ = 25.4 Hz, C=O), 138.57 (s, Ar), 134.29 (s, Ar), 129.66 (s, Ar), 128.23 (s, Ar), 92.80 (d, $^1J_{CF}$ = 200.8 Hz, CF), 53.93 (s, CH$_3$), 50.27 (d,

$^3J_{CF}$ = 3.5 Hz, CH$_2$SO$_2$Ph), 27.87 (d, $^2J_{CF}$ = 21.8 Hz, CH$_2$CF); m/s (GC-EI$^+$) 287 (2%, [M – MeO]$^+$), 259 (4%, [M – CO$_2$Me]$^+$), 177 (100, [M – SO$_2$Ph]$^+$), 141 (4%, [SO$_2$Ph]$^+$), 77 (30%, [Ph]$^+$), 59 (28%, [CO$_2$Me]$^+$).

Methyl 4-cyano-2-fluoro-butanoate (**112**)
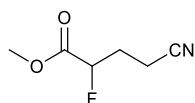
Dimethyl 2-(2-cyanoethyl)-2-fluoromalonate (5 g, 24.6 mmol) was dissolved in DMSO (100 mL) with lithium chloride (2.09 g, 49.2 mmol) and water (0.58 g, 32 mmol) and the reaction mixture was heated to 110 °C and left for 1.5 hours. After this time, water (300 mL) was added to the reaction mixture and extracted with diethyl ether (6 x 50 mL) and the organic layers combined. The organic layer was then washed with water (3 x 30 mL), brine (3 x 30 mL), dried over MgSO$_4$ and the solvent was removed *in vacuo*. The crude product was then purified by vacuum distillation (88 °C, 2.9 mbar) to give *methyl 4-cyano-2-fluoro-butanoate* (1.64 g, 46% yield) as a clear oil. ([M + H]$^+$, 146.0626, C$_6$H$_9$FO$_2$N requires: [M + H]$^+$, 146.0617); IR (neat, cm^{-1}) 2961, 2250, 1744, 1441, 1363, 1283, 1224, 1200, 1078, 1012, 926, 798, 400; δ_H (CDCl$_3$, 400 MHz) 5.04 (1H, ddd, $^2J_{HF}$ = 48.3 Hz, $^3J_{HH}$ = 7.9 Hz, $^3J_{HH}$ = 4.0 Hz, CF*H*), 3.84 (3H, s, C*H*$_3$), 2.64 – 2.49 (2H, m, CFHC*H*$_2$), 2.42 – 2.18 (2 H, m, C*H*$_2$CN); δ_F (CDCl$_3$, 376 MHz) -194.70 (ddd, $^2J_{HF}$ = 48.4 Hz, $^3J_{HF}$ = 26.1 Hz, $^3J_{HF}$ = 20.5 Hz); δ_C (CDCl$_3$, 101 MHz) 168.66 (d, $^2J_{CF}$ = 23.3 Hz, C=O), 118.02 (s, CN), 86.56 (d, $^1J_{CF}$ = 187.0 Hz, CF), 52.79 (s, CH$_3$), 28.32 (d, $^2J_{CF}$ = 21.3 Hz, CHF-**C**H$_2$), 12.74 (d, $^3J_{CF}$ = 4.7 Hz, **C**H$_2$-CN); m/s (GC-EI$^+$) 146.1 (1%, [M + H]$^+$), 114.1 (5%, [M – OCH$_3$]$^+$), 86.1 (21%, [M – O$_2$CH$_3$]$^+$).

Methyl 5-cyano-2-fluoro-pentanoate (**114**)
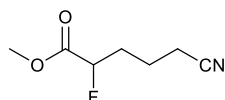
Dimethyl 2-(3-cyanopropyl)-2-fluoromalonate (3 g, 24.6 mmol) was dissolved in DMSO (100 mL) with lithium chloride (1.17 g, 27.6 mmol) and water (0.37 g, 20.7 mmol) and the reaction mixture was heated to 110 °C and left for 3 hours. After this time, water (200 mL) was added to the reaction mixture and extracted with ethyl acetate (4 x 50 mL) and the organic layers combined. The organic layer was then washed with water (5 x 30 mL), brine (3 x 30 mL), dried over MgSO$_4$ and the solvent was removed *in vacuo*. The crude product was then purified by vacuum distillation (62 °C, 2.5 mbar) to give *methyl 5-cyano-2-fluoro-pentanoate* (0.78 g, 35% yield) as a clear oil. ([M + H]$^+$, 160.0776, C$_7$H$_{11}$FNO$_2$ requires: [M + H]$^+$, 160.0774); IR (neat, cm^{-1}) 2960, 2248, 1758, 1743, 1440, 1364, 1285, 1219, 1178, 1093, 1044, 1021, 991, 943, 856, 766, 654, 571, 513; δ_H (CDCl$_3$, 400 MHz) 4.97 (ddd, $^2J_{HF}$ = 48.8 Hz, $^3J_{HH}$ = 7.4 Hz, $^3J_{HH}$ = 4.1 Hz, CFH), 3.82 (s, CH$_3$), 2.44 (t, $^3J_{HH}$ = 6.9 Hz, CH$_2$CN), 2.22 – 1.94 (m, CHF-CH_2), 1.90 – 1.81 (m, CH$_2$-CH_2-CH$_2$); δ_F (CDCl$_3$, 376 MHz) -192.42 – -192.71 (ddd, $^2J_{HF}$ = 48.8 Hz, $^3J_{HF}$ = 23.2 Hz, $^3J_{HF}$ = 22.9 Hz); δ_C (CDCl$_3$, 101 MHz) 169.63 (d, $^2J_{CF}$ = 23.7 Hz, C=O), 118.97 (s, CN), 88.17 (d, $^1J_{CF}$ = 185.4 Hz, CHF), 52.70 (s, CH$_3$), 31.19 (d, $^2J_{CF}$ = 21.0, CHFCH$_2$), 20.88 (d, $^4J_{CF}$ = 3.2 Hz, CH$_2$-CH$_2$-CH$_2$), 17.02 (s, CH$_2$-CN); m/s (GC-EIMS$^+$) 160 (1%, [M + H]$^+$), 128 (1%, [M − OMe]$^+$), 100 (28%, [M − CO$_2$Me]$^+$), 92 (31%, [M − CHFCO$_2$Me + H]$^+$), 68 (100%, [CHFCO$_2$Me]$^+$), 59 (65%, [CO$_2$Me]$^+$).

Methyl 2-cyano-6-fluorohexanoate (**117**)
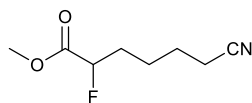
Dimethyl 2-fluoromalonate (4 g, 26.7 mmol) was added dropwise to a suspension of sodium hydride (1.34 g, 70 mmol) in THF (100 mL) and allowed to stir for 1 hour at room temperature before adding bromovaleronitrile (6.5 g, 40 mmol, 4.7 mL) and allowed to stir for 19 hours. The reaction mixture was then quenched by addition of 50 mL of concentrated ammonium chloride and 50 mL of water. The product was extracted by ethyl acetate (3 x 50 mL), dried with brine (3 x 30 mL) and over MgSO$_4$ and reduced *in vacuo*. The crude reaction mixture was then taken up in DMSO (100 mL) and lithium chloride

(0.77 g, 18 mmol) and water (0.21 g, 12 mmol, 0.21 mL) were added and the reaction mixture heated to 110 ºC for 12 hours. After this time, water was added (200 mL) and the product extracted with ethyl acetate (4 x 50 mL), washed with water (4 x 50 mL) and dried with brine (3 x 30 mL) and over MgSO4. The solvent was reduced *in vacuo* and the crude product was purified by column chromatography (gradient from neat hexane to 1:3 ethyl acetate:hexane) to give *Methyl 2-cyano-6-fluorohexanoate* (0.98 g, 21% yield, 99%+ purity) as a clear oil. ([M + H]$^+$, 174.0929, $C_8H_{13}FNO_2$ requires: [M + H]$^+$, 174.0930);); IR (neat, cm^{-1}) 2957, 2873, 2247, 1759, 1743, 1440, 1358, 1287, 1167, 1219, 1167, 1100, 1050, 1003, 868, 736, 653, 513, 482, 466, 434, 418; δ_H (CDCl$_3$, 599 MHz) 4.91 (1H, ddd, $^2J_{HF}$ = 48.9 Hz, $^3J_{HH}$ = 7.4 Hz, $^3J_{HH}$ = 4.3 Hz), 3.78 (3H, s, CH$_3$), 2.35 (2H, t, $^3J_{HH}$ = 7.0 Hz, CH$_2$CN), 2.00 – 1.84 (2H, m, CH$_2$CF), 1.70 (2H, m, **CH$_2$**CH$_2$CN), 1.65 – 1.57 (2H, m, **CH$_2$**CH$_2$CF); , δ_F (CDCl3, 376 MHz) -192.25 (ddd, $^2J_{HF}$ = 48.9 Hz, $^3J_{HF}$ = 26.6 Hz, $^3J_{HF}$ = 23.8 Hz).; δ_C (CDCl$_3$, 151 MHz) 170.04 (d, $^2J_{CF}$ = 23.7 Hz, C=O), 119.36 (s, CN), 88.59 (d, $^1J_{CF}$ = 185.0 Hz, CF), 52.52 (s, CH$_3$), 31.57 (d, $^3J_{CF}$ = 21.1 Hz, CH$_2$CF), 25.01 (s, **CH$_2$**CH$_2$CN), 23.78 (d, $^4J_{CF}$ = 3.1 Hz, **CH$_2$**CH$_2$CF), 17.11 (s, **CH$_2$**CN).; m/s (GC-EI$^+$) 174 (1%, [M+H]$^+$), 133 (13%, [M – CH$_2$CN]$^+$), 114 (29%, [M – CO$_2$Me]$^+$), 105 (6%, [M – C$_3$H$_6$CN]$^+$), 82 (32%, [M – C$_3$H$_4$FO$_2$]$^+$), 68 (100, [M – C$_4$H$_6$FO$_2$]$^+$), 59 (75%, [M – C$_6$H$_9$FN]$^+$).
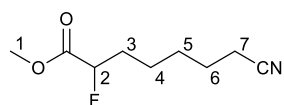
Methyl 2-cyano-7-fluoroheptanoate (**118**)

Dimethyl 2-fluoromalonate (6.5 g, 43.3 mmol) was added dropwise to a suspension of sodium hydride (2.18 g, 91 mmol) in THF (100 mL) and allowed to stir for 1 hour at room temperature before adding 7-Bromoheptanenitrile (9.9 g, 56 mmol, 7.5 mL) and allowed to stir for 19 hours. The reaction mixture was then quenched by addition of 50 mL of concentrated ammonium chloride and 50 mL of water. The product was extracted by ethyl acetate (3 x 50 mL), dried with brine (3 x 30 mL) and over MgSO4 and reduced *in vacuo*. The crude reaction mixture was then taken up in DMSO (100 mL) and lithium chloride

(3.67 g, 87 mmol) and water (1.01 g, 56 mmol, 0.21 mL) were added and the reaction mixture headed to 110 °C for 27 hours. After this time, water was added (200 mL) and the product extracted with ethyl acetate (4 x 50 mL), washed with water (4 x 50 mL) and dried with brine (3 x 30 mL) and over $MgSO_4$. The solvent was reduced *in vacuo* and the crude product was purified by column chromatography (gradient from neat hexane to 1:3 ethyl acetate:hexane) to give *Methyl 2-cyano-7-fluoroheptanoate* (1.51 g, 19% yield, 99%+ purity) as a clear oil. ([M + H]$^+$, 188.1087, $C_9H_{15}FNO_2$ requires: [M + H]$^+$, 188.1087);); IR (neat, cm^{-1}) 2955, 2246, 1760, 1440, 1281, 1217, 1097, 1010, 730; δ_H (CDCl$_3$, 599 MHz) 4.90 (1H, ddd, $^2J_{HF}$ = 49.0 Hz, $^3J_{HH}$ = 7.2 Hz, $^3J_{HH}$ = 4.6 Hz, H^2), 3.78 (3H, s, H^1), 2.34 (2H, t, $^3J_{HF}$ = 7.1 Hz, H^7), 1.97 – 1.79 (2H, m, H^3), 1.66 (2H, p, $^3J_{HH}$ = 7.1 Hz, H^6), 1.54 – 1.43 (4H, m, H^4, H^5).; , δ_F (CDCl3, 376 MHz) -192.36 (ddd, $^2J_{HF}$ = 49.0 Hz, $^3J_{HF}$ = 26.5 Hz, $^3J_{HF}$ = 24.2 Hz).; δ_C (CDCl$_3$, 151 MHz) 170.27 (d, $^2J_{CF}$ = 23.8 Hz, C=O), 119.61 (s, CN), 88.75 (d, $^1J_{CF}$ = 184.5 Hz, C^2), 52.42 (s CH$_3$), 32.09 (d, $^2J_{CF}$ = 21.1 Hz, C^3), 28.17 (s, C^5), 25.20 (s, C^6), 23.72 (d, $^3J_{CF}$ = 3.1 Hz, C^4), 17.11 (s, C^7).; *m/z* (GC-EIMS) 188 (2%, [M + H]$^+$), 156 (1%, [M – OMe]$^+$), 147 (4%, [M – CH$_2$CN]$^+$), 128 (17%, [M – CO$_2$Me]$^+$), 96 (70%, [M – CHFCO$_2$Me]$^+$), 82 (48%, [C$_4$H$_8$CN]$^+$), 68 (100, [C$_3$H$_6$CN]$^+$), 59 (73%, [CO$_2$Me]$^+$).

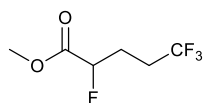Methyl 2,5,5,5-tetrafluoro-pentanoate (**119**)

Dimethyl 2-fluoromalonate (10 g, 66.6 mmol) was added dropwise to a suspension of sodium hydride (3.36 g, 140 mmol) in THF (100 mL) and stirred for fifteen minutes. After this time, 1-iodo-2,2,2-trifluoro-ethane was added and the reaction mixture stirred for 22 hours at room temperature. The reaction mixture was then added to concentrated ammonium chloride solution (50 mL) and water (50 mL) and extracted with Ethyl acetate (3 x 50 mL). The organic layers were combined and dried with brine (3 x 30 mL) and over $MgSO_4$ before concentrating *in vacuo*. The crude intermediate was added to DMSO (100 mL), lithium chloride (3.67 g, 86.5 mmol) and water (1.01 g, 56.2 mmol, 1.01 mL)

and the reaction mixture was heated to 110 °C for 90 minutes. After this time, water (200 mL) was added to the reaction mixture and the product extracted with ethyl acetate (5 x 50 mL), dried with brine (3 x 30 mL) and over MgSO$_4$, then the solvent removed *in vacuo* to give the crude product. The product was purified by successive vacuum distillations to give *methyl 2,5,5,5-tetrafluoro-pentanoate* (0.366 g, 5% yield, 99%+) as a clear oil. IR (neat, cm^{-1}) 2961, 1762, 1515, 1442, 1405, 1345, 1285, 1258, 1241, 1221, 1144, 1124, 1093, 1056, 1025, 1014, 869, 821, 801; δ_H (CDCl$_3$, 400 MHz) 4.98 (1H, ddd, $^2J_{HF}$ = 48.3 Hz, $^3J_{HF}$ = 8.0 hz, $^3J_{HF}$ = 3.9 Hz, CHF), 3.83 (3H, s, CH$_3$), 2.42 – 2.03 (4H, m, CH$_0$); δ_F (CDCl$_3$, 376 MHz) -66.59 (3F, t, $^3J_{FH}$ = 10.1 Hz, CF$_3$), -193.50 – -193.80 (1F, m, CHF); δ_C (CDCl$_3$, 101 MHz) 169.13 (d, $^2J_{CF}$ = 23.5 Hz, C=O), 126.50 (q, $^1J_{CF}$ = 275.9 Hz, CF$_3$), 87.07 (d, $^1J_{CF}$ = 186.4 Hz, CHF), 52.65 (s, CH$_3$), 29.05 (qd, $^2J_{CF}$ = 30.0 Hz, $^3J_{CF}$ = 4.1 Hz, **CH**$_2$CF$_3$), 25.24 (dq, $^2J_{CF}$ = 21.4 Hz, $^3J_{CF}$ = 3.2 Hz, **CH**$_2$CHF); m/s (GC-EIMS) 189 (57%, [M + H]$^+$).

Methyl 2-fluoro-4-(phenyl-sulfonyl)-butanoate (**120**)
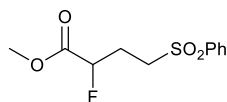
Dimethyl 2-(phenyl-sulfonyl-ethyl)-2-fluoro-malonate (6.02 g, 18.91 mol) was added to DMSO (100 mL) with lithium chloride (1.6 g, 37.82 mmol) and water (0.44 g, 24.59 mmol) and heated at 110 °C for 90 minutes. After this time water was added (200 mL) and the mixture extracted with ethyl acetate (4 x 50 mL) and washed with brine (3 x 30 mL) and dried over MgSO$_4$. The solvent was removed *in vacuo* and the crude product was purified by column chromatography (gradient neat toluene to 1:3 ethyl acetate:toluene) to give *methyl 2-fluoro-4-(phenyl-sulfonyl)-butanoate* (2.91 g, 59% yield) as a white crystalline solid. ([M + H]$^+$, 261.0595, C$_{11}$H$_{14}$FO$_4$S requires: [M + H]$^+$, 261.0597); δ_H (CDCl$_3$, 400 MHz) 7.93 – 7.88 (2H, m, Ar), 7.71 – 7.65 (1H, m, Ar), 7.61 – 7.55 (2H, m, Ar), 5.03 (1H, ddd, $^2J_{HF}$ = 48.3 Hz, $^3J_{HH}$ = 7.8 Hz, $^3J_{HH}$ = 4.2 Hz, CHF), 3.78 (3H, s, CH$_3$), 3.33 – 3.15 (2H, m, CH$_2$SO$_2$), 2.51 – 2.13 (2H, m, CH$_2$CF); δ_F (CDCl$_3$, 376 MHz) -192.91 (ddd, $^2J_{HF}$ = 48.3 Hz, $^3J_{HF}$ = 25.8 Hz, $^3J_{HF}$ = 21.2 Hz); δ_C (CDCl$_3$, 101

MHz) 168.86 (d, $^2J_{CF}$ = 23.5 Hz, C=O), 138.64 (s, Ar), 134.20 (s, Ar), 129.60 (s, Ar), 128.14 (s, Ar), 86.63 (d, $^1J_{CF}$ = 186.6 Hz, CFH), 52.83 (s, CH₃), 51.25 (d, $^3J_{CF}$ = 3.3 Hz, C**H**₂SO₂Ph), 25.95 (d, $^2J_{CF}$ = 21.5 Hz, **CH₂**CFH); *m/z* (GC-EI-MS) 260 (0.1%, [M]⁺), 229 (3%, [M – OMe]⁺), 201 (5%, [M – CO₂Me]⁺), 169 (4%, [M – CHFCO₂Me]⁺), 141 (10%, [M – CH₂CH₂CHFCO₂Me]⁺), 119 (100, [M - SO₂Ph]⁺), 91 (5%, [M – CH₂CH₂SO₂Ph]⁺), 77 (59%, [Ph]⁺), 59 (46, [CO₂Me]⁺).

Methyl 2-fluoro-3-methyl-4-cyano-butanoate (**122**)
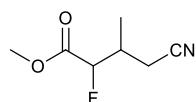
Dimethyl 2-fluoromalonate (3.00 g, 20.0 mmol) was added to a solution of sodium methoxide (0.09 g of sodium in 50 mL of methanol) with crotononitrile (2.68 g, 40.0 mmol, 3.25 mL) and stirred at 60 °C for 2 hours. After this time, the solvent was removed *in situ* and added to DMSO (50 mL) with lithium chloride (1.69 g, 42.4 mmol) and water (0.47 g, 26 mmol) and heated to 110 °C for 90 minutes. After this time, water (100 mL) was added and the solution was extracted with ethyl acetate (5 x 30 mL), washed with water (3 x 30 mL) and brine (3 x 30 mL) before drying with MgSO₄. The resulting residue was purified by vacuum distillation to give *methyl 2-fluoro-3-methyl-4-cyano-butanoate* (1.26 g, 40% yield) as a clear oil and mixture of diastereomers. IR (neat, cm⁻¹) 2961, 2250, 1759, 1744, 1688, 1459, 1440, 1369, 1297, 1222, 1132, 1100, 1012, 998, 957, 867, 775, 585; δ_H (CDCl₃, 600 MHz) 4.99 (1H, dd, $^2J_{HF}$ = 48.6 Hz, $^3J_{HH}$ = 2.9 Hz, CHF), 3.84 (3H, s, OCH₃), 2.59 – 2.49 (3H, m, CH, CH₂), 1.14 – 1.11 (3H, m, CHC**H**₃), δ_F (CDCl₃, 376 MHz) -198.20 – -198.51 (m, CHF), -203.72 – -204.01 (m, CHF*); δ_C (CDCl₃, 151 MHz) 168.61 (d, $^2J_{CF}$ = 11.7 Hz, C=O), 117.72 (s, CN), 89.73 (d, $^1J_{CF}$ = 190.1 Hz, CHF), 52.80 (s, OCH₃), 33.84 (d, $^2J_{CF}$ = 20.7 Hz, CH), 20.89 (d, $^3J_{CF}$ = 3.7 Hz, CH₂), 13.57 (d, ^3J = 4.8 Hz, CHC**H**₃); m/s (GC-EIMS) 160 (1%, [M + H]⁺), 128 (2%, [M – OMe]⁺), 100 (10%, [M – CO2Me]⁺), 92 (32%, [CH₂FCO₂Me]⁺), 59 (63%, [CO₂Me]⁺)

Ethyl 2,2-difluoro-4-cyano-butanoate (**126**)
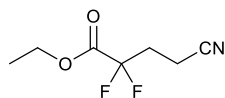
Following literature conditions[121], In an atmosphere of argon, ethyl bromodifluoroacetate (2 g, 9.85 mmol, 1.26 mL) was added to a suspension of copper (1.41 g, 22.17 mmol) in DMSO (50 mL) after which acrylonitrile (0.52 g, 9.85 mmol, 0.65 mL) was added dropwise and the reaction mixture was allowed to stir for 6 hours at 55 °C. After this time, the reaction mixture was poured onto a mixture of saturated ammonium chloride solution and ice and extracted with diethyl ether (3 x 50 mL). The combined organic extracts were washed with brine and dried over MgSO$_4$. The crude product was purified by vacuum distillation (16 mbar, 175 °C) to give *ethyl 2,2-difluoro-4-cyano-butanoate* (0.82 g, 47%) as a clear oil. δ_H (CDCl$_3$, 400 MHz) 4.37 (q, 2H, $^3J_{HH}$ = 7.1 Hz, CH$_2$), 2.62 (m, 2H, CH$_2$CN), 2.57 – 2.40 (m, 2H, CF$_2$CH$_2$), 1.38 (t, 3H, $^3J_{HH}$ = 7.2 Hz, CH$_3$); δ_F (CDCl$_3$, 376 MHz) -107.42 (t, $^3J_{HF}$ = 15.8 Hz); *m/z* (GC-EIMS) 178 ([M+H]$^+$, 1%), 104 ([M-CO$_2$Et]$^+$, 39%), 73 ([CO$_2$Et]$^+$, 3%), 54 ([CH$_2$CH$_2$CN]$^+$, 28%) all spectroscopic values match literature values.[121]

Ethyl 2,2-difluoro-3-methyl-4-cyano-butanoate (**127**)
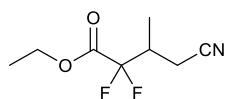
Adapting literature conditions[121], In an atmosphere of argon, ethyl bromodifluoroacetate (2 g, 9.85 mmol, 1.26 mL) was added to a suspension of copper (1.41 g, 22.17 mmol) in DMSO (50 mL) after which crotonitrile (0.66 g, 9.85 mmol, 0.80 mL) was added dropwise and the reaction mixture was allowed to stir for 6 hours at 55 °C. After this time, the reaction mixture was poured onto a mixture of saturated ammonium chloride solution and ice and extracted with diethyl ether (3 x 50 mL). The combined organic extracts were washed with brine and dried over MgSO$_4$. The crude product was purified by vacuum distillation (16 mbar, 175 °C) to give *ethyl 2,2-difluoro-3-methyl-4-cyano-*

butanoate (0.76 g, 44%) as a clear oil. ([M + H]+, 192.0835, $C_8H_{12}F_2O_2N$ requires: [M + H]+, 192.0836); IR (neat, cm-1) 2988, 2254, 1760, 1466, 1428, 1375, 1314, 1282, 1194, 1136, 1113, 1100, 1054, 1011, 951, 856, 839, 760, 714, 656, 571; δ_H (CDCl$_3$, 400 MHz) 4.37 (1, 2H, $^3J_{HH}$ = 7.1 Hz, CH$_2$), 2.77 – 2.58 (m, 2H, CH$_2$CN), 2.51 – 2.37 (m, 1H, C*H*CH$_3$), 1.37 (t, 3H, $^3J_{HH}$ = 7.1 Hz, CH$_2$C*H$_3$*), 1.29 – 1.17 (m, 3H, C*H$_3$*CH); δ_F (CDCl$_3$, 376 MHz) -109.87 (dd, $^2J_{FF}$ = 260 Hz, $^3J_{HF}$ = 1.7 Hz), -116.26 (dd, $^2J_{FF}$ = 260 Hz, $^3J_{HF}$ = 4.7 Hz); δ_C (CDCl$_3$= 101 MHz) 162.96 (t, $^2J_{CF}$ = 32.2 Hz, C=O), 117.24 (s, CN), 115.76 (dd, $^1J_{CF}$ = 256.0 Hz, $^1J_{CF}$ = 253.8 Hz, CF$_2$), 63.58 (s, *C*H$_2$CH$_3$), 35.68 (t, $^2J_{CF}$ = 22.8 Hz, CH), 18.09 (t, $^3J_{CF}$ = 5.5 Hz, *C*H$_2$CN), 14.09 (s, CH$_2$*C*H$_3$), 12.90 – 12.65 (m, CH$_3$). *m/z* (GC-EIMS) 192 ([M+H]$^+$, 0.44%), 151 ([M-CH$_2$CN]$^+$, 0.82%), 123 ([M-CH$_3$CHCH$_2$CN]$^+$, 3%), 118 ([M-CO$_2$Et]$^+$, 20%), 73 ([CO$_2$Et]$^+$, 3%), 69 ([CH$_3$CH$_2$CH$_2$CN]$^+$, 26%), 68 ([CH$_3$CHCH$_2$CN]$^+$, 10%), 45 ([CH$_3$CH$_2$O]$^+$, 4%).

Ethyl 4-cyano-2-fluoro-butanoate (**128**)
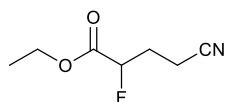
Ethyl 2-fluoroacetoacetate (3 g, 20.3 mmol, 2.54 mL) was added to a solution of sodium ethoxide (0.09 g sodium, 4 mmol) in ethanol (30 mL) after which acrylonitrile (5.37 g, 101 mmol) was added and the solution stirred for an hour at 0 °C. Afterwards the solvent was removed in vacuo, the residue taken up in water (50 mL), extracted with ethyl acetate (3 x 30 mL), washed with brine (3 x 30 mL) and dried over MgSO$_4$. The remaining solution is concentrated in vacuo and purified by vacuum distillation (70 °C, 2.4 mbar) to yield ethyl 4-cyano-2-fluorobutanoate (2.08 g, 65% yield, 99%+ purity) as a yellow oil. ([M + H]$^+$, 160.0777, $C_7H_{11}FNO_2$ requires: [M + H]$^+$, 160.0774); IR (neat, cm^{-1}) 2987, 2250, 1756, 1443, 1376, 1278, 1219, 1196, 1093, 1077, 1020, 940, 858, 752; δ_H (CDCl$_3$, 400 MHz) 5.01 (1H, ddd, $^2J_{HF}$ = 48.5 Hz, $^3J_{HH}$ = 8.0 Hz, $^3J_{HH}$ = 4.0 Hz, CHF), 4.29 (2H, q, $^3J_{HH}$ = 7.2 Hz, **CH$_2$**CH$_3$), 2.67 – 2.46 (2H, m, CH$_2$CN), 2.41 – 2.13 (2H, m, CHFC**H$_2$**), 1.33 (3H, t, $^3J_{HH}$ = 7.1 Hz, CH$_2$C**H$_3$**); δ_F (CDCl$_3$, 376 MHz) -194.57 (ddd, $^2J_{HH}$ = 48.5 Hz, $^3J_{HF}$ = 26.4 Hz, $^3J_{HF}$ = 20.2 Hz); δ_C (CDCl$_3$, 101 MHz) 168.34 (d, $^2J_{CF}$ = 23.2 Hz,

C=O), 118.19 (s, CN), 86.70 (d, $^{1}J_{CF}$ = 186.9 Hz, CHF), 62.28 (s, O-CH$_2$), 28.47 (d, $^{2}J_{CF}$ = 21.5 Hz, **CH$_2$**CHF), 14.22 (s, CH$_3$), 12.90 (d, $^{3}J_{CF}$ = 4.5 Hz, **CH$_2$**CN).; m/s (GC-EIMS) 160 (1%, [M + H]$^{+}$), 132 (114, [M − OC$_2$H$_5$]$^{+}$), 86 (36%, [M − CO$_2$Et]$^{+}$), 73 (2%, [CO$_2$Et]$^{+}$), 54 (5%, [C$_3$H$_4$N]$^{+}$), 45 (11%, [OC$_2$H$_5$]$^{+}$).

3-fluoro-5-cyano-pentan-2-one (**132**)
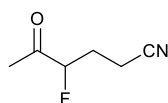
Ethyl 2-fluoro-acetoacetate (3 g, 20.3 mmol, 2.54 mL) was added to a solution of lithium hdroxide monohydrate (1.02 g, 24.3 mmol) in ethanol (76.8 mL) and water (13.2 mL) with acrylonitrile (1.61 g, 30.4 mmol, 1.99 mL) and left to stir at room temperature for 19 hours. After this time, the ethanol was removed *in vacuo* and the remaining solution was added to water (100 mL) and the pH adjusted to neutral using hydrochloric acid (1 M). The solution was extracted using ethyl acetate (3 x 50 mL), washed using brine (3 x 30 mL) and dried over MgSO$_4$. The solvent was removed *in vacuo* to give the crude product as a yellow oil. The product was purified by vacuum distillation (2.4 mbar, 100 °C) to give *3-fluoro-5-cyano-pentan-2-one* as a clear oil (1.27 g, 48% yield). ([M + H]+, 130.0652, C$_6$H$_9$FNO requires: [M + H]+, 130.0668); IR (neat, cm^{-1}) 2945, 2249, 1724, 1424, 1360, 1239, 1177, 1090, 1066, 963, 935, 619, 548, 519; δ_H (CDCl$_3$, 400 MHz) 4.84 (1H, ddd, $^{2}J_{HF}$ = 49.3 Hz, $^{3}J_{HH}$ = 8.8 Hz, $^{3}J_{HH}$ = 3.9 Hz, CHF), 2.54 (2H, dd, $^{3}J_{HH}$ = 7.8 Hz, $^{3}J_{HH}$ = 6.7 Hz, CH$_2$CN), 2.32 (3H, d, $^{4}J_{HF}$ = 4.9 Hz, CH$_3$), 2.30 – 2.03 (2H, m, CHFC**H$_2$**); δ_F (CDCl$_3$, 376 MHz) -192.21 (dddq, $^{2}J_{HF}$ = 49.3 Hz, $^{3}J_{HF}$ = 29.3, $^{3}J_{HF}$ = 17.5 Hz, $^{4}J_{HF}$ = 4.9 Hz); δ_C (CDCl$_3$, 101 MHz) 206.40 (d, $^{2}J_{CF}$ = 25.3 Hz), 118.24 (s, CN), 93.50 (d, $^{1}J_{CF}$ = 186.4 Hz, CHF), 27.54 (d, $^{2}J_{CF}$ = 20.9 Hz, CHF**CH$_2$**), 26.20 (s, **CH$_2$**CN), 13.13 (d, $^{3}J_{CF}$ = 4.7 Hz, CH$_3$); *m/z* (GC-EIMS) 129 ([M]$^{+}$, 3%), 86 ([M-OCCH$_3$]$^{+}$, 2%), 43 ([CH$_3$CO]$^{+}$, 100%).

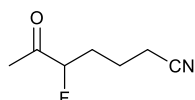Methyl 2-(3-cyanopropyl)-acetoacetate (**134**)
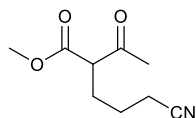
Methyl acetoacetate (10 g, 86.12 mmol, 9.80 mL) was added dropwise to a suspension of sodium hydride (2.17 g, 90.42 mmol) in THF (250 mL) and, after stirring at room temperature for one hour, 4-bromobutyronitrile (14.02 g, 94.73 mmol) was added and then heated to reflux for 19 hours. After this time, concentrated ammonium chloride solution (100 mL) and water (300 mL) was added and the mixture extracted with ethyl acetate (3 x 100 mL), the organics combined and washed with brine (3 x 30 mL) and dried over MgSO$_4$. The solvent was removed *in vacuo* and the impurity removed by vacuum distillation to leave behind *Methyl 2-(3-cyanopropyl)-acetoacetate* (12.11 g, 77%) as a clear oil. ([M + H]$^+$, 184.0978, C$_9$H$_{14}$O$_3$N requires: [M + H]$^+$, 184.0974); IR (neat, cm-1) 2957, 2248, 2160, 2033, 1743, 1716, 1436, 1361, 1208, 1154, 1059, 984, 750; δ_H (CDCl$_3$, 600 MHz) 3.75 (3H, s, C*H$_3$*O), 3.46 (1H, t, $^3J_{HH}$ = 7.2 Hz, C*H*), 2.37 (2H, t, $^3J_{HH}$ = 7.1 Hz, C*H$_2$*CN), 2.24 (1H, s, C*H$_3$*C=O), 2.01 – 1.94 (2H, m, CHC*H$_2$*), 1.72 – 1.60 (2H, m, CH$_2$C*H$_2$*CH$_2$); δ_C (CDCl$_3$, 101 MHz) 202.02 (s, CH$_3$*C*=O), 169.70 (s, CH$_3$O*C*=O), 119.13 (s, *C*N), 58.66 (s, *C*HCH$_2$), 52.79 (s, *C*H$_3$O), 29.18 (s, *C*H$_3$C=O), 26.98 (s, CH*C*H$_2$), 23.39 (s, CH$_2$*C*H$_2$CH$_2$), 17.24 (s, *C*H$_2$CN); *m/z* (LC-ESIMS) 184 (100, [M + H]$^+$), 152 (4%, [M – OCH$_3$]$^+$), 142 (1%, [M – CH$_3$CN]$^+$), 112 (1%, [M – C$_3$O$_2$H$_5$]$^+$).

Methyl 2-(4-cyanobutyl)-acetoacetate (**135**)
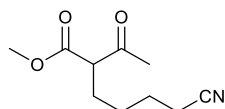
Methyl acetoacetate (10 g, 86.12 mmol, 9.80 mL) was added dropwise to a suspension of sodium hydride (2.17 g, 90.42 mmol) in THF (250 mL) and, after stirring at room temperature for one hour, 5-bromovaleronitrile (15.35 g, 94.73 mmol) was added and heated to reflux for 19 hours. After this time, concentrated ammonium chloride solution

(100 mL) and water (300 mL) was added and the mixture extracted with ethyl acetate (3 x 100 mL), the organics combined and washed with brine (3 x 30 mL) and dried over MgSO$_4$. The solvent was removed *in vacuo* and the impurity removed by vacuum distillation to leave behind *Methyl 2-(4-cyanobutyl)-acetoacetate* (12.23 g, 72%) as a clear oil. ([M + H]$^+$, 198.1127, C$_{10}$H$_{16}$O$_3$N requires: [M + H]$^+$, 198.1130); IR (neat, cm-1) 2956, 2248, 2159, 2028, 1743, 1716, 1436, 1361, 1207, 1151, 1059, 991; δ_H (CDCl$_3$, 700 MHz) 3.74 (3H, s, OCH_3), 3.43 (1H, t, $^3J_{HH}$ = 7.1 Hz, CH), 2.34 (2H, t, $^3J_{HH}$ = 7.1 Hz, CH_2CN), 2.23 (3H, s, COCH_3), 1.86 (2H, m, CHCH_2), 1.67 (2H, m, CH_2CH$_2$CN), 1.47 – 1.39 (2H, m, CHCH$_2$CH_2); δ_C (CDCl$_3$, 176 MHz) 202.54 (s, CH$_3$$C$=O), 170.05 (s, CH$_3OC$=O) , 119.45 (s, CN), 59.25 (s, CHCO), 52.65 (s, OCH$_3$), 29.16 (s, CH$_3$C=O), 27.24 (s, CHCH$_2$), 26.54 (s, CHCH$_2$$CH_2$), 25.26 (s, CH$_2CH_2$CN), 17.05 (s, CH$_2$CN); *m/z* (GC-EIMS) 198 (1%, [M + H]$^+$), 166 (6%, [M – OMe]$^+$), 155 (21%, [M + H – COCH$_3$]$^+$), 116 (16%, [M + H – (CH$_2$)$_4$CN]$^+$), 81 (11%, [CH(CH$_2$)$_3$CN]$^+$), 59 (3%, [CO$_2$Me]$^+$), 55 (26%, [CH$_3$CH$_2$CN]$^+$), 43 (100, [COMe]$^+$).

4-fluoro-6-cyano-hexan-2-one (**136**)

Methyl 2-(3-cyanopropyl)-acetoacetate (12.11 g, 66.10 mmol) was added to a suspension of potassium *tert*-butoxide (1.48 g, 13.22 mmol) in acetonitrile (250 mL) and stirred for 15 minutes before Selectfluor^{TM} (23.42 g, 66.10 mmol) was added and heated to 85 °C for 43 hours. After this time, the solvent was removed *in vacuo* and the residue taken up in water (200 mL), extracted with ethyl acetate (3 x 50 mL), the organics combined and washed with brine (3 x 30 mL) and dried over MgSO$_4$. The solvent was removed *in vacuo* giving crude Methyl 2-fluoro-2-(3-cyanopropyl)-acetoacetate. This was added to DMSO (200 mL) with water (1.16 g, 64.42 mmol) and lithium chloride (4.20 g, 99.11 mmol) and heated to 110 °C for 3 hours. After this time, water (300 mL) was added to the solution and extracted with ethyl acetate (5 x 100 mL). The combined organics were washed with water (3 x 100 mL), brine (3 x 50 mL) and dried over MgSO$_4$. The solvent was removed

in vacuo and the residue purified by vacuum distillation (2.5 mbar, 82 °C) and column chromatography (neat ether, RF = 0.55) to give *4-fluoro-6-cyano-hexan-2-one* (2.58 g, 36% yield, 97% purity) as a clear oil. ([M + H]+, 144.0827, $C_7H_{11}FNO$ requires: [M + H]+, 144.0825); IR (neat, cm^{-1}) 2957, 2247, 1723, 1458, 1426, 1361, 1233, 1176, 975, 945, 800, 619, 580, 525; δ_H (CDCl$_3$, 400 MHz) 4.75 (1H, ddd, $^2J_{HF}$ = 49.7 Hz, $^3J_{HF}$ = 7.9 Hz, $^4J_{HF}$ = 4.1 Hz, C*H*F), 2.42 (2H, t, $^3J_{HH}$ = 6.9 Hz, C*H*$_2$CN), 2.28 (3H, d, $^4J_{HF}$ = 4.8 Hz, C*H*$_3$), 2.09 – 1.79 (4H, m, CHFC*H*$_2$C*H*$_2$CH$_2$CN); δ_F (CDCl$_3$, 376 MHz) -189.94 (dddq, $^2J_{HF}$ = 49.7 Hz, $^3J_{HF}$ = 28.5, $^3J_{HF}$ = 20.4 Hz, $^4J_{HF}$ = 4.8 Hz); δ_C (CDCl$_3$, 101 MHz) 207.34 (d, $^2J_{CF}$ = 25.6 Hz, *C*=O), 118.98 (S, *C*N), 95.02 (d, $^1J_{CF}$ = 185.2, *C*HF), 30.55 (d, ^2J = 20.8 Hz, CHF*C*H$_2$), 26.08 (s, CH$_2$*C*H$_2$CH$_2$), 21.04 (d, ^3J = 3.5 Hz, *C*H$_3$), 17.08 (s, *C*H$_2$CN); *m/z* (GC-EIMS) 144 (0.1%, [M + H]$^+$), 123 (1%, [M – HF]$^+$), 101 (4%, [M – CH$_3$CO]$^+$), 68 (0.6%, [M – CH$_3$COCHF]$^+$), 54 (6%, [CH$_2$CH$_2$CN]$^+$), 43 (100%, [CH$_3$CO]$^+$).

5-fluoro-7-cyano-heptan-2-one (**137**)
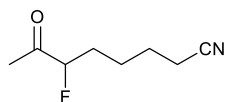
Methyl 2-(4-cyanobutyl)-acetoacetate (12.23 g, 62.01 mmol) was added to a suspension of potassium *tert*-butoxide (1.39 g, 12.40 mmol) in acetonitrile (250 mL) and stirred for 15 minutes before Selectfluor^{TM} (21.97 g, 62.01 mmol) was added and heated to 85 °C for 43 hours. After this time, the solvent was removed *in vacuo* and the residue taken up in water (200 mL), extracted with ethyl acetate (3 x 50 mL), the organics combined and washed with brine (3 x 30 mL) and dried over MgSO$_4$. The solvent was removed *in vacuo* giving crude methyl 2-fluoro-2-(4-cyanobutyl)-acetoacetate. This was added to DMSO (200 mL) with water (1.09 g, 60.58 mmol) and lithium chloride (3.95 g, 93.21 mmol) and heated to 110 °C for 9 hours. After this time, water (300 mL) was added to the solution and extracted with ethyl acetate (5 x 100 mL). The combined organics were washed with water (3 x 100 mL), brine (3 x 50 mL) and dried over MgSO$_4$. The solvent was removed *in vacuo* and the residue purified by column chromatography (1:1 ether:hexane, RF = 0.3)

to give *5-fluoro-7-cyano-heptan-2-one* (2.21 g, 30% yield, 98% purity) as a clear oil. ([M + H]$^+$, 158.0988, $C_8H_{13}FNO$ requires: [M + H]$^+$, 158.0981); IR (neat, cm^{-1}) 2956, 2247, 1725, 1427, 1360, 1225, 1090, 982, 947, 734, 619, 540; δ_H (CDCl$_3$, 400 MHz) 4.72 (1H, ddd, $^2J_{HF}$ = 50.0 Hz, $^3J_{HH}$ = 7.9 Hz, $^3J_{HH}$ = 4.2 Hz, C*H*F), 2.37 (2H, t, $^3J_{HH}$ = 6.9 Hz, C*H*$_2$CN), 2.26 (3H, d, $^4J_{HF}$ = 4.8 Hz, CH$_3$), 1.96 – 1.56 (6H, m, CHFCH$_2$C*H*$_2$C*H*$_2$C*H*$_2$CN); δ_F (CDCl$_3$, 376 MHz) -189.78 (dddq, $^2J_{HF}$ = 50.0, $^3J_{HF}$ = 28.7 Hz, $^3J_{HF}$ = 21.8 Hz, $^4J_{HF}$ = 4.9 Hz); δ_C (CDCl$_3$, 101 MHz) 207.99 (d, $^2J_{CF}$ = 25.9 Hz, *C*=O), 119.38 (s, *C*N), 95.49 (d, $^1J_{CF}$ = 184.6 Hz, *C*HF), 30.97 (d, $^2J_{CF}$ = 20.8 Hz, *C*H$_2$CHF), 26.08 (s, CHF*C*H$_2$CH$_2$), 25.12 (s, *C*H$_2$CH$_2$CN), 23.91 (d, $^3J_{CF}$ = 3.3 Hz, *C*H$_3$), 17.17 (s, *C*H$_2$CN); *m/s* (GC-EIMS) 158 (0.2%, [M+H]$^+$), 142 (0.4%, [M-CH$_3$]$^+$), 115 (9%, [M+H-COCH$_3$]$^+$), 82 (2%, [M-CH$_3$COCHF]$^+$), 76 (4%, [CH$_3$COCHF + H]$^+$), 54 (9%, [CH$_2$CH$_2$CN]$^+$), 43 (100%, [COCH$_3$]$^+$).

2-methyl-3-fluoro-5-cyano-pentan-2-ene (**138**)
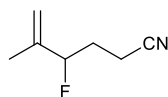
1 molar nBuLi (1.92 g, 29.97 mmol, 11.99 mL) was added to a suspension of methyltriphenylphosphonium bromide (10.71 g, 29.97 mmol) in THF (100 mL) at -78 °C and stirred for two hours. After this, 3-fluoro-5-cyano-pentan-2-one (3 g, 23.2 mmol) was added dropwise and left to warm to room temperature and stir overnight. After confirming reaction completion by ^{19}F NMR, saturated ammonium chloride (100 mL) was added until the pH was neutral, water was added (100 mL) and extracted with ethyl acetate (3 x 50 mL). The organic extracts were combined and washed with brine (3 x 30 mL) and a dried over MgSO$_4$. The crude reaction product was purified by column chromatography (gradient hexane to 30% ethyl acetate in hexane) to give 2-methyl-3-fluoro-5-cyano-pentan-2-ene (1.01 g, 7.9 mmol, 34% yield) as a clear oil. ([M + H]+, 128.0876, $C_7H_{11}FN$ requires: [M + H]+, 128.0876); IR (neat, cm-1) 2947, 2249, 1439, 1381, 1027, 910, 583, 541; δ_H (CDCl$_3$,400 MHz) 5.09 – 5.00 (m, 2H, C*H*$_2$CCH$_3$), 4.93 (ddd, 1H, $^2J_{HH}$ = 47.9 Hz, $^3J_{HH}$ = 8.2 Hz, $^3J_{HH}$ = 4.5 Hz, C*H*F), 2.47 (ddd, 2H, $^3J_{HH}$ = 7.8 Hz, $^3J_{HH}$ = 6.8 Hz, $^4J_{HF}$

= 1.5 Hz, CH_2CN), 2.17 – 1.92 (m, 2H, CHFCH_2), 1.75 (t, 3H, $^4J_{HF}$ 1.3, CH_3); δ_F (CDCl$_3$, 376 MHz) -182.24 (dddt, $^2J_{HF}$ = 47.9 Hz, $^3J_{HF}$ = 27.4 Hz, $^3J_{HF}$ = 17.4 Hz, $^4J_{HF}$ = 2.2 Hz); δ_C (CDCl$_3$, 101 MHz) 141.47 (d, $^3J_{CF}$ = 17.6 Hz, H$_2$C=C), 119.05 (s, CN), 114.01 (d, $^3J_{CF}$ = 10.1 Hz, H$_2$$C$=C), 93.36 (d, $^1J_{CF}$ = 173.3 Hz, CF), 29.46 (d, $^2J_{CF}$ = 23.8 Hz, CHFCH$_2$), 17.47 (d, $^3J_{CF}$ = 3.4 Hz, CH$_3$), 13.17 (d, $^3J_{CF}$ = 5.3 Hz, CH$_2$CN); m/z (GC-EIMS) 127 ([M]$^+$, 2%), 112 ([M-CH$_3$]$^+$, 42%), 87 ([M-CH$_2$CN]$^+$, 71%), 73 ([M-CH$_2$CH$_2$CN]$^+$, 100%), 54 ([CH$_2$CH$_2$CN]$^+$, 61%), 41 ([CH$_3$CCH$_2$]$^+$, 89%).

Chapter 4

LIB cell evaluation

The base electrolyte solution (EL) was prepared by dissolving 1 mol/kg of the LiPF6 salt into the solvent that consisted of a mixture of ethylene carbonate (EC) and propylene carbonate (PC) in a 1:1 weight ratio, followed by the addition of 1 wt% of vinylene carbonate (VC). Materials were battery grade and obtained from Tomiyama Pure Chemicals Industries (Japan) and used without further purification.

Battery investigations were carried out using coin-type cell and pouch-type cells depending on the experiment. Cathode electrodes were prepared by mixing lithium cobaltoxide (LiCoO2; LCO) with a small amount of conductive carbon additive and poly-vinylidenefluoride (PVDF) binder dispersed in N-methyl pyrrolidinone (NMP), and the resulting paste was applied to an aluminum foil current-collector and then dried at 120 °C under vacuum overnight. Anode electrodes were prepared by mixing graphite as the active material by the same way, and the resulting paste was applied to a copper foil current-collector and dried at 200 °C under vacuum overnight. The cells were assembled where a polyethylene separator of 20um thickness was placed between the two electrodes, and each EL containing the additive was injected into the assembled cell.

Cell performance was evaluated using a commercial battery tester (TOSCAT, Toyo System Co., Ltd.). The cells were first charged at a constant current density 0.1C to 4.45V and constant voltage until the current reached 1/50C at room temperature. The cells were

discharged at a constant current density 0.2C to 3.0V to determine the initial capacity of the cell. Then the cell was charged to 4.45V again and charged at constant voltage at 4.45V at 60 oC. After 240 hours of constant voltage charging, some cells were discharged to 3.0V and then the same charge-discharge test as the 1st cycle was performed to determine the capacity retention after aging.

Linear sweep voltammetry was performed using a multichannel potentio-galvanostat (Bio-Logic Science Instrument VMP3), and Impedance measurements were conducted using a frequency response analyzer (Solartron 1260) with an electrochemical interface (Solartron SI 1287) in the frequency range of 0.1 Hz to 1 MHz. Z-plot software was employed for data analysis.

Nuclear Magnetic Resonance (NMR)

NMR analysis was carried out to determine the SEI and electrolyte components that resulted from additive reactions. Electrodes were collected as mentioned above, rinsed with acetone-d6, and soaked in deuterated water to extract SEI components by hydrolysis. The resulted deuterated aqueous and acetone-d6 solutions were transferred to NMR tubes and 1H and 19F-NMR analysis was carried out (Bruker 400 MHz). Resonances were callibrated with sodium 3-(trimethylsilyl)-[2,2,3,3-d4]-propanoate (TPS) and lithium bis(trifluoromethanesulfonyl)imide (LiTFSI), respectively. The acquired data was processed by commercial software (ALICE2).

Electrolyte composition

The tested cells was immersed in sufficient DMC to extract electrolyte and the composition of the extracted solution was determined using gas chromatography (Shimadzu GC-20), coupled to a single quadrupole mass spectrometer (Shimadzu QP2020). One drop of extracted electrolyte was added to a 20 mL glass vial and placed on the head-space sampler (Shimadzu HP-20) heated to 250 ℃. The GC used a split injection with helium as the carrier gas and equipped with a carbowax-type column (Stabilwax, 30 m, internal diameter 0.35 mm, internal coating 1 μm). The oven temperature ramped from 40 ◦C to 250 ◦C at a rate of 20 ◦C/min. Total ion mass scan was performed to identify and quantify each electrolyte component by retention time and ion

ratios of mass spectrum except DMC for extraction. A calibration curve was used to determine the relative amounts of each components, performed using commercial software (Shimadzu LabSolutions).

Gas Analysis

Gas generated during the continuous charging test was collected with a syringe directly from the pouch type cell, and was analyzed using an accumulated microGC system (Agilent MicroGC490) equipped with two parallel columns; Molsieve 5A for separation of hydrogen, carbon monoxide, methane, and PoraPLOT Q for separation of carbon dioxide and other volatile hydrocarbons (under C4). A calibration curve was calculated with a standard gas of each component and was used to determine the relative composition of the generated gas mixture.

References

1   A. Volta, *Phil. Trans. R. Soc. Lond.*, 1800, **90**, 403–431.

2   *https//www.marketresearchengine.com/lithium-ion-battery-market1 (accessed May 2019).*

3   *https//www.spglobal.com/marketintelligence/en/news-insights/trending/V6HGmjhVv_syEM065qM-fw2 (accessed May 2019).*

4   W. Wang, D. Choi and Z. Yang, in *Lithium-Ion Batteries: Advanced Materials and Technologies*, eds. X. Yuan, H. Liu and J. Zhang, CRC Press, Boca Raton, 2011, pp. 21–22.

5   *https//www.nytimes.com/2006/08/15/technology/15battery.html (accessed May 2019).*

6   *https//www.cnet.com/news/samsung-galaxy-note-7-explosion-battery-manufacturing-error/ (accessed May 2019).*

7   E. Turner, *Elements of Chemistry: Including the Actual State and Prevalent Doctrines of the Science*, 1841.

8   *https//ingeniumcanada.org/ingenium/collection-research/collection-item.php?id=2010.0087.001 (accessed May 2019).*

9   H. Davy, *Phil. Trans. R. Soc. Lond.*, 1807, **1**, 1–44.

10   H. Davy, *Phil. Trans. R. Soc. Lond.*, 1808, **98**, 333–370.

11   G. Planté, *Comptes Rend us l'Académie des Sci.*, 1860, **55**, 640.

12   C. A. Faure, U.S. Pat., US552425A, 1895.

13   R. M. Dell and D. A. J. Rand, *Understanding Batteries*, Royal Society of Chemistry, 2001.

14   K. Mallion, R. Turner and A. Todd, U.S. Pat., US3824131A, 1974.

15   S. Herman, *Delmar's Standard Textbook of Electricity*, Cengage Learning, 2008.

16   J. B. Goodenough and K. S. Park, *J. Am. Chem. Soc.*, 2013, **135**, 1167–1176.

17   M. S. Whittingham, *Science*, 1976, **192**, 1126–1127.

18   K. Mizushima, P. C. Jones, P. J. Wiseman and J. B. Goodenough, *Mater. Res. Bull.*, 1980, **15**, 783–789.

19   R. Yazami and P. Touzain, *J. Power Sources*, 1983, **9**, 365–371.

20   A. Yoshino, K. Sanechika and T. Nakajima, EP Pat., 0205856 B1, 1985.

21   S. S. Zhang, *J. Power Sources*, 2006, **162**, 1379–1394.

22   E. Wang, W. Bowden, D. Ofer, N. Iltchev, R. Moses and K. Brandt, *J. Electrochem. Soc.*, 2000, **147**, 4023–4028.

23   M. Y. Saidi, F. Gao, J. Barker and C. Scordilis-Kelley, U.S. Pat., 5,846,673, 1998.

24   T. Shiga and K. Takechi, U.S. Pat. US 6,235,431 B1, 2001.

25   O. Hiroi, K. Hamano, Y. Yoshida, S. Yoshioka, H. Shiota, J. Aragane, S. Aihara, D. Takemura, T. Nishimura, M. Kise, H. Urushibata and H. Adachi, U.S. Pat. US 6,306,540 B1, 2003.

26   S. S. Zhang, K. Xu and T. R. Jow, *Electrochem. Solid-State Lett.*, 2002, **5**, A206–A208.

27   C. S. Cha, X. P. Ai and H. X. Yang, *J. Power Sources*, 1995, **54**, 255–258.

28   X. M. Feng, X. P. Ai and H. X. Yang, *J. Appl. Electrochem.*, 2004, **34**, 1199–1203.

29   J. Prakash, C. W. Lee and K. Amine, U.S. Pat. US 6,455,200 B1, 2002.

30   P. Verma, P. Maire and P. Novák, *Electrochim. Acta*, 2010, **55**, 6332–6341.

31   K. Zaghib, G. Nadeau and K. Kinoshita, *J. Electrochem. Soc.*, 2000, **147**, 2110–2115.

32   R. Yazami and Y. F. Reynier, *Electrochim. Acta*, 2002, **47**, 1217–1223.

33   J. O. Besenhard, M. Winter, J. Yang and W. Biberacher, *J. Power Sources*, 1995, **54**, 228–231.

34   G.-C. Chung, H.-J. Kim, S.-I. Yu, S.-H. Jun, J. Choi and M.-H. Kim, *J. Electrochem. Soc.*, 2002, **147**, 4391.

35   D. Aurbach, E. Zinigrad, Y. Cohen and H. Teller, *Solid State Ionics*, 2002, **148**, 405–416.

36   E. Peled, D. Golodnitsky, A. Ulus and V. Yufit, *Electrochim. Acta*, 2004, **50**, 391–395.

37   D. Aurbach, M. D. Levi, E. Levi and A. Schechter, *J. Phys. Chem. B*, 1997, **101**, 2195–2206.

38   Y. Ein-Eli and V. R. Koch, *J. Electrochem. Soc.*, 1997, **144**, 2968–2973.

39   M. G. Scott, A. H. Whitehead and J. R. Owen, *J. Electrochem. Soc.*, 1998, **145**, 1506–1510.

40   Y. Ein-Eli, B. Markovsky, D. Aurbach, Y. Carmeli, H. Yamin and S. Luski, *Electrochim. Acta*, 1994, **39**, 2559–2569.

41   D. Bar-Tow, E. Peled and L. Burstein, *J. Electrochem. Soc.*, 1999, **146**, 824–832.

42   E. Peled, D. Bar Tow, A. Merson, A. Gladkich, L. Burstein and D. Golodnitsky, *J. Power Sources*, 2001, **97**–**98**, 52–57.

43   H. S. Lee, J. Mcbreen and S. Choi, *J. Electrochem. Soc.*, 1998, **145**, 2813–2818.

44   S. Komaba, T. Itabashi, B. Kaplan, H. Groult and N. Kumagai, *Electrochem. commun.*, 2003, **5**, 962–966.

45   M. Nie, J. Demeaux, B. T. Young, D. R. Heskett, Y. Chen, A. Bose, J. C. Woicik and B. L. Lucht, 2015, **162**, 7008–7014.

46   D. Aurbach, K. Gamolsky, B. Markovsky, Y. Gofer, M. Schmidt and U. Heider, *Electrochim. Acta*, 2002, **47**, 1423–1439.

47   M. W. Wagner, C. Liebenow and J. O. Besenhard, *J. Power Sources*, 1997, **68**, 328–332.

48   R. McMillan, H. Slegr, Z. . Shu and W. Wang, *J. Power Sources*, 1999, **81**–**82**, 20–26.

49   K. Kanamura, S. Shiraishi and Z. Takehara, *J. Electrochem. Soc.*, 1994, **141**, L108–L110.

50   G. V Zhuang, H. Yang, B. Blizanac and P. N. Ross Jr., *Electrochem. Solid-State Lett.*, 2005, **8**, A441–A445.

51   M. D. Levi, E. Markevich, C. Wang, M. Koltypin and D. Aurbach, *J. Electrochem. Soc.*, 2004, **151**, A848–A856.

52   R. T. Jow, S. Zhang, K. Zu and M. S. Ding, U.S. Pat, US 6,905,762 B1, 2005.

53   S. S. Zhang, K. Xu and T. R. Jow, *J. Power Sources*, 2004, **129**, 275–279.

54   T. Yong, J. Wang and Y. Mai, *Ionics (Kiel).*, 2013, **6**, 1099–1103.

55   G. Kim and J. R. Dahn, *J. Electrochem. Soc.*, 2015, **162**, 437–447.

56   Y. Abu-lebdeh and I. Davidson, *J. Power Sources*, 2009, **189**, 576–579.

57   Y. Abu-lebdeh and I. Davidson, *J. Electrochem. Soc.*, 2009, 60–65.

58   H. Zhi, L. Xing, X. Zheng, K. Xu and W. Li, *J. Phys. Chem. Lett.*, 2017, 8–12.

59   M. Koh, A. Yamauchi, M. Tomita and A. Tani, U.S. Pat US 2011/0009644, 2011.

60   M. Kobayashi, T. Inoguchi, T. Iida, T. Tanioka, H. Kumase and Y. Fukai, *J. Fluorine Chem.*, 2003, **120**, 105–110.

61   Q. Huang, T. Wang, M. Yan and Z. Jiang, *J. Electrochem. Soc.*, 2006, **153**, A2363.

62   X. Zuo, M. Xu, W. Li, D. Su and J. Liu, 2006, 196–199.

63   B. Zhang, M. Metzger, S. Solchenbach, M. Payne, S. Meini, H. A. Gasteiger, A. Garsuch and B. L. Lucht, *J. Phys. Chem. C*, 2015, **119**, 11337–11348.

64   H. M. Jung, S. Park, J. Jeon, Y. Choi and S. Yoon, *J. Mat. Chem. A*, 2013, 11975–11981.

65   J. Hyung-Min, KR Pat., 1020070022968, 2007.

66   X.-G. Sun, C. Liao, L. Baggetto, B. Guo, R. R. Unocic, G. M. Veith and S. Dai, *J. Mater. Chem. A*, 2014, **2**, 7606–7614.

67   S. Wan, X. Jiang, B. Guo, S. Dai and X.-G. Sun, *Chem. Commun.*, 2015, 9817–9820.

68   H. Lyu, Y. Li, C. J. Jafta, C. A. Bridges, H. M. Meyer, A. Borisevich, M. P. Paranthaman, S. Dai and X. G. Sun, *J. Power Sources*, 2019, **412**, 527–535.

69   D. O'Hagan and D. B. Harper, *J. Fluorine Chem.*, 1999, **100**, 127–133.

70   H. Moissan, *Comptes Rendus l'Académie des Sci.*, 1886, 1544–1545.

71   *https//www.nobelprize.org/prizes/chemistry/1906/summary/ (accessed May 2019).*

72   K. O. Christe, *Inorg. Chem.*, 1986, **25**, 3721–3722.

73   J. Wang, M. Sánchez-Roselló, J. L. Aceña, C. del Pozo, A. E. Sorochinsky, S. Fustero, V. A. Soloshonok and H. Liu, *Chem. Rev.*, 2014, **114**, 2432–2506.

74   E. Lück and G. von R. Lipinski, in *Ulmann's Encyclopedia of industrial chemistry*, eds. B. Elvers, G. Bellussi, J. Bus, K. Drauz, H. Griem, V. Hessel, A. Kleeman, B. Kutscher, S. Moran, J. Mukherjee, R. Palkovits, G. Qiao, M. Roper, K. Sundmacher, J. H. Teles, R. Ulber, K. Wagemann and U. Wietelmann, Wiley-VCH, Weinheim, 2000, vol. 7, pp. 381–395.

75   H. Mei, J. Han, S. Fustero, M. Medio-Simon, D. M. Sedgwick, C. Santi, R. Ruzziconi and V. A. Soloshonok, *Chem. – A Eur. J.*, 2019, 10.1002/chem.201901840.

76   D. O'Hagan, *Chem. Soc. Rev.*, 2008, **37**, 308–19.

77   L. Pauling, *The Nature of a Chemical Bond and the Structore of Molecules and Crystals; An Introduction to Modern Structure Chemistry*, Cornell University Press, New York, 1939.

78   K. B. Wiberg and P. R. Rablen, *J. Am. Chem. Soc.*, 1993, **115**, 614–625.

79   A. Bondi, *J. Phys. Chem.*, 1964, **68**, 441–451.

80   A. G. Orpen, L. Brammer, F. H. Allen, O. Kennard, D. G. Watson and R. Taylor, *J. Chem. Soc. Dalt. Trans.*, 1989, S1–S83.

81   L. E. X. Leong, S. Khan, C. K. Davis, S. E. Denman and C. S. McSweeney, *J. Anim. Sci. Biotechnol.*, 2017, **8**, 1–11.

82   E. V. Anslyn and D. A. Dougherty, *Modern Physical Organic Chemistry*,
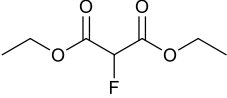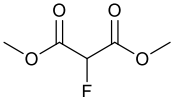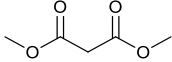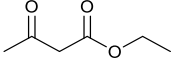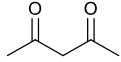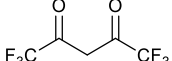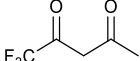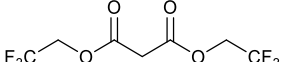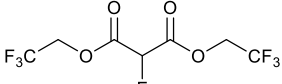
University Science Books, 2006.

83   I. Ojima, *Fluorine in Medicinal Chemistry and Chemical Biology*, John Wiley & Sons, 2009.

84   S. Purser, P. R. Moor, S. Swallow and V. Gouverneur, *Prog. Med. Chem.*, 2015, **54**, 65–133.

85   A. Harsanyi and G. Sandford, *Green Chem.*, 2015, **17**, 2081–2086.

86   M. G. Campbell and T. Ritter, *Org. Process Res. Dev.*, 2014, **18**, 474–480.

87   *https//emergency.cdc.gov/agent/hydrofluoricacid/basics/facts.asp (accesed May 2019).*

88   A. E. Feiring, *J. Fluorine Chem.*, 1979, **13**, 7–18.

89   G. A. Olah, J. T. Welch, Y. D. Vankar, M. Nojima, I. Kerekes and J. A. Olah, *J. Org. Chem.*, 1979, **44**, 3872–3881.

90   P. Singh, *Synthesis*, 2002, **17**, 2561–2578.

91   R. E. Banks and R. G. Syvretb, *J. Chem. Soc. Chem. Commun.*, 1992, 595–596.

92   K. L. Kirk, *Org. Process Res. Dev.*, 2008, **12**, 305–321.

93   A. Harsanyi and G. Sandford, *Org. Process Res. Dev.*, 2014, **18**, 981–992.

94   E. D. Bergmann, S. Cohen and I. Shahak, *J. Chem. Soc.*, 1956, 3286–3289.

95   Binhai Kangjie Chemical Co. Ltd, Jiangsu Weier Chemical Co. Ltd, J. Gu, H. Li, Y. Yunglong, D. Youxing, China Pat. CN107935853A, 2018.

96   A. Günter, H. Weintritt and S. Böhm, U.S. Pat, US 7,807,851 B2, 2012.

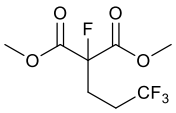97   E. T. Satumov, J. J. Medvedev, D. I. Nilov, M. A. Sandzhieva, I. A. Boyarskaya,
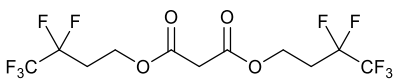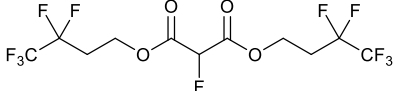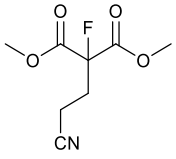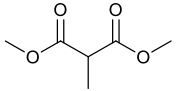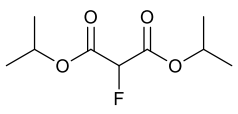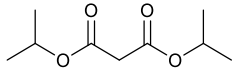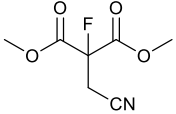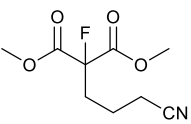
V. A. Nikolaev and A. V. Vasilyev, *Tetrahedron*, 2016, **72**, 4835–4844.

98   S. T. Purrington and D. L. Woodard, *J. Org. Chem.*, 1990, **55**, 3423–3424.

99   A. Harsanyi and G. Sandford, *Green Chem.*, 2015, **17**, 3000–3009.

100   R. D. Chambers, M. A. Fox, D. Holling, T. Nakano, T. Okazoe and G. Sandford, *Chem. Eng. Technol.*, 2005, **28**, 344–352.

101   B. Huang, C. Li, H. Wang, C. Wang, L. Liu and J. Zhang, *Org. Lett.*, 2017, **19**, 5102–5105.

102   M. Sambaiah, P. Mallesham, K. Shiva Kumar, Y. Bobde, P. K. Hota, S. Yennam, B. Ghosh and M. Behera, *Synlett*, 2019, **30**, 586–592.

103   E. Lisse and G. Sandford, *J. Fluorine Chem.*, 2018, **206**, 117–124.

104   C. A. Fisher, A. Harsanyi, G. Sandford, D. S. Yufit and J. A. K. Howard, *Chimia*, 2014, **68**, 425–429.

105   S. T. Purrington, C. L. Bumgardner, N. V. Lazaridis and P. Singh, *J. Org. Chem.*, 1987, **52**, 4307–4310.

106   R. D. Chambers and R. C. H. Spink, *Chem. Commun.*, 1999, **2**, 883–884.

107   T. J. Nash and G. Pattison, *Eur. J. Org. Chem.*, 2015, **2015**, 3779–3786.

108   P. Reszka, R. Schulz, K. Methling, M. Lalk and P. J. Bednarski, *ChemMedChem*, 2010, **5**, 103–117.

109   X. Huang, W. Zhao, X. Zhang, M. Liu, S. N. S. Vasconcelos and W. Zhang, *Molecules*, 2018, **23**, 1-7.

110   R. D. Chambers and J. Hutchinson, *J. Fluorine Chem.*, 1998, **92**, 45–52.

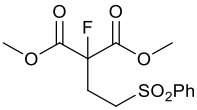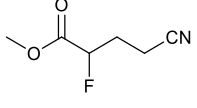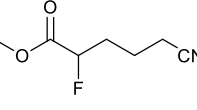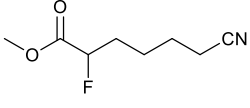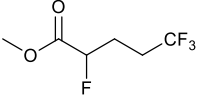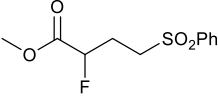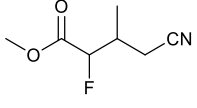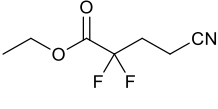111   J. M. Takacs, Z. Xu, X. T. Jiang, A. P. Leonov and G. C. Theriot, *Org. Lett.*,
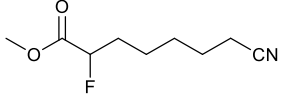
2002, **4**, 3843–3845.

112   K. Matsuo and M. Shindo, *Org. Lett.*, 2011, **13**, 4406–4409.

113   N. J. Willis, C. A. Fisher, C. M. Alder, A. Harsanyi, L. Shukla, J. P. Adams and
       G. Sandford, *Green Chem.*, 2016, **18**, 1313–1318.

114   T. Umemoto and S. Ishihara, *J. Am. Chem. Soc.*, 1993, **115**, 2156–2164.

115   I. N. Nesterova, A. K. Shanazarov, A. M. Poznyak, M. I. Lakoza, B. V
       Shemeryankin and V. G. Granik, *Pharm. Chem. J.*, 1994, **28**, 41–43.

116   ETH Zurich, WO Pat., WO2016/075085, 2016.

117   J.-M. Atebamba, J. Moskon, S. Pejovnik and M. Gaberscek, *J. Electrochem. Soc.*,
       2010, **157**, A1218.

118   J. Clayden, N. Greeves, S. Warren and P. Wothers, *Organic Chemistry*, Oxford
       University Press, Oxford, 2nd edn., 2001.

119   F. Hou, X. C. Wang and Z. J. Quan, *Org. Biomol. Chem.*, 2018, **16**, 9472–9476.

120   A. P. Krapcho, J. F. Weimaster, J. M. Eldridge, E. G. E. Jahngen, A. J. Lovey
       and W. P. Stephens, *J. Org. Chem.*, 1978, **43**, 138–147.

121   K. Sato, M. Tamura, K. Tamoto, M. Omote, A. Ando and I. Kumadaki, *Chem.
       Pharm. Bull.*, 2000, **48**, 1023–1025.

122   *https://www.ft.com/content/13abbe62-70db-11e6-a0c9-1365ce54b926 (accessed
       August 2019).*

123   K. Tasaki, K. Kanda, T. Kobayashi, S. Nakamura and M. Ue, *J. Electrochem.
       Soc.*, 2006, **153**, A2192.

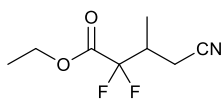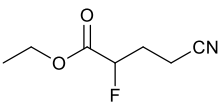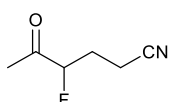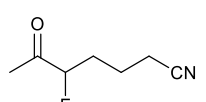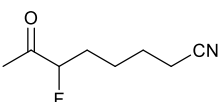124   E. N. Gutierrez and R. C. Reardon Jr., U.S. Pat., 3892787, 1975, .
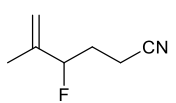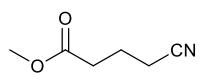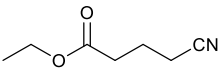
Appendix

List of compounds subjected to LIB analysis

Sample Name	Sample Number	Sample Structure
Diethyl 2-fluoromalonate	**27**	
Dimethyl 2-fluoromalonate	**62**	
Dimethyl malonate	**66**	
Ethyl acetoacetate	**88**	
Acetylacetone	**94**	
Hexafluoro-acetylacetone	**95**	
1,1,1-trifluoro-2,4,-pentadione	**96**	
Bis(2,2,2-trifluoroethyl) malonate	**97**	
Bis(2,2,2-trifluoroethyl) 2-fluoromalonate	**98**	

Bis(4,4,4,3,3-pentafluorobutyl) malonate	**100**	
Bis(4,4,4,3,3-pentafluorobutyl) 2-fluoromalonate	**101**	
Dimethyl 2-(2-cyanoethyl)-2-fluoromalonate	**102**	
Dimethyl 2-methyl malonate	**105**	
Di-*iso*-propyl 2-fluoromalonate	**106**	
Di-*iso*-propyl malonate	**107**	
Dimethyl 2-(cyanomethyl)-2-fluoromalonate	**108**	
Dimethyl 2-(3-cyanopropyl)-2-fluoromalonate	**109**	
Dimethyl-2-(3,3,3-trifluoropropyl)-2-fluoromalonate	**110**	

Dimethyl-2-(2-phenylsulphonyl-ethyl)-2-fluoromalonate	**111**	
Dimethyl 2-(2-cyanoethyl)-2-fluoromalonate	**112**	
Dimethyl 2-(4-cyanobutyl)-2-fluoromalonate	**114**	
Methyl 6-cyano-2-fluorohexanoate	**117**	
Methyl 7-cyano-2-fluoroheptanoate	**118**	
Methyl 2,5,5,5-tetrafluoro-pentanoate	**119**	
Methyl 2-fluoro-4-(phenyl-sulfonyl)-butanoate	**120**	
Methyl 2-fluoro-3-methyl-4-cyano-butanoate	**122**	
Ethyl 2,2-difluoro-4-cyano-butanoate	**126**	

Ethyl 2,2-difluoro-3-methyl-4-cyano-butanoate	**127**	
Ethyl 4-cyano-2-fluoro-butanoate	**128**	
3-Fluoro-5-cyano-pentan-2-one	**132**	
4-Fluoro-6-cyano-hexan-2-one	**136**	
5-Fluoro-7-cyano-heptan-2-one	**137**	
2-Methyl-3-fluoro-5-cyano-pentan-2-ene	**138**	
Methyl 4-cyanobutanoate	**139**	
Ethyl 4-cyanobutanoate	**140**	
5-cyano-pentan-2-one	**141**	